



Microwave Electronics

**DEVELOPMENT OF FREE SPACE METHOD FOR
MATERIAL CHARACTERISATION AND GPR STUDY
& A CASE STUDY ON BIOLOGICAL SAMPLES**

*Thesis submitted to the
Cochin University of Science and Technology
in partial fulfilment of the
requirements for the degree of
Doctor of Philosophy
under the Faculty of Technology*

By

BIJU KUMAR S.

**DEPARTMENT OF ELECTRONICS
FACULTY OF TECHNOLOGY
COCHIN UNIVERSITY OF SCIENCE AND TECHNOLOGY
COCHIN 682 022, INDIA**

MARCH 2002

CERTIFICATE

This is to certify that this thesis entitled "**DEVELOPMENT OF FREE SPACE METHOD FOR MATERIAL CHARACTERISATION AND GPR STUDY & A CASE STUDY ON BIOLOGICAL SAMPLES**" is a bona fide record of the research work carried out by Mr. Biju Kumar S., under my supervision in the Department of Electronics, Cochin University of Science and Technology. The results presented in this thesis or parts of it have not been presented for any other degree.



Dr. K. T. MATHEW
(Supervising Teacher)
Professor

Department of Electronics
Cochin University of Science and Technology

Cochin 682 022
18th March 2002

DECLARATION

I hereby declare that the work presented in this thesis entitled "**DEVELOPMENT OF FREE SPACE METHOD FOR MATERIAL CHARACTERISATION AND GPR STUDY & A CASE STUDY ON BIOLOGICAL SAMPLES**" is based on the original work done by me under the supervision of **Dr. K. T. Mathew** in the Department of Electronics, Cochin University of Science and Technology, and that no part thereof has been presented for any other degree.

Cochin 682 022
18th March 2002


BIJU KUMAR. S

Acknowledgements

I would like to score my deepest sense of gratitude to my research guide, Dr. K. T. Mathew, Professor, Dept. of Electronics, Cochin University of Science and Technology, Kerala, India for his excellent guidance, constant and incessant encouragement. It has been really a great pleasure and privilege to work under him.

I am grateful to Dr. K. G. Balakrishnan, Professor & Head, Dept. of Electronics, Cochin University of Science and Technology, Kerala, India for his keen interest and persistent support during the progress of the research work.

I am much indebted to the wholehearted support extended by the formerly heads of the Department of Electronics, Prof. P. R. S. Pillai and Prof. C. S. Sridhar (presently Principal, SBMS Institute of Technology, Bangalore).

Let me express my heartfelt thanks to the founder head of the department, Prof. K. G. Nair (presently Director, STIC, CUSAT) for his timely suggestions and encouragement during the tenure of my research work.

It is with great pleasure, I record my sincere thanks to Dr. P. Mohanan, Professor, Department of Electronics, Cochin University of Science and Technology for the constant encouragement and the fruitful discussions with him, throughout the period of research.

Sincere thanks are due to Dr. C. K. Aanandan, Reader, Department of Electronics for his valuable suggestions and encouragement.

I would like to express my sincere thanks to Prof. K. Vasudevan, Dr. Deepu Rajan, Mr. James Kurian and Mr. D. Rajaveerapa, faculty of this department for the constant encouragement rendered to me.

I take this opportunity to place on record the help received from Dr. Philip Augustine, Director, Digestive Disease Centre, PVS hospital, Cochin and other staff during a collaborative work with them.

During the period of research, I was financially supported by Cochin University of Science and Technology by providing Junior Research Fellowship. Also, Technical University of Delft, The Netherlands supported the research through their Fellowship for a period of one year. Finally I received financial support from Council of Scientific and Industrial Research (CSIR) through Senior Research Fellowship. I sincerely acknowledge all these help.

I also would like to acknowledge the financial support from International Center for Theoretical Physics (ICTP), Italy by sanctioning the Young Collaborator Programme, Department of Science and Technology (DST), Govt. of India for providing the Young Scientist Award to visit Germany to attend the Nobel Laureates meeting and DFG, Germany for their support during my visit to Germany for a week.

May I express my deep felt indebtedness to Dr. U. Raveendranath, Scientist, NAL, Bangalore, Dr. Joe Jacob, Research Associate, Dept. of Electronics, CUSAT and Dr. Jacob George, Corning Inc., USA for their memorable service throughout my period of research.

I thankfully bear in mind the sincere cooperation and the enthusiastic words by Dr. Sebastian Mathew, Sl. Grade Lecturer, K.E College, Mannanam, Dr. V. P. Joseph, Sr. Lecturer, Christ College, Irinjalakuda, Mr. V. M. Ananda Kumar, Lecturer, VTMNSS College, Dhanuvachapuram, Prof. V. P. Devassia, Model Engg. College, Thrikkakara, Dr. Thomaskutty Mathew, Lecturer, MG University Regional Center, Edapally, Mr. Cyriac M. Odackal, Lecturer, Dept. of Electronics, Mr. Girish. G, R & D Engineer, IBM, Bangalore and Mr. Girish Kumar. C, Lecturer, College of Appl. Science, Peerumedu.

The encouragement and cooperation received from Dr. K. K. Narayanan, Lecturer, SD College Alapuzha, Dr. Ratheesh, Scientist, CMET, Thrissur, Dr. Jagannath Bhatt, Scientist, STIC, and Mr. Paul. V. John, Scientist, STIC are also thankfully acknowledged.

I would like to give a special word of thanks to my colleagues in the department, Mr. Mani. T. K., Ms. Mini. M. G., Mr. G. S Binoy, Ms. Sona. O. Kundukulam, Ms. Manju Paulson, Ms. Mridula. M., Ms. Binu Paul, Mr. Anil Lonappan, Mr. Shabeer Ali, Ms. Sree Devi, Dr. C. P. Anil Kumar, Mr. Sajith N. Pai, Mr. Prakash Kumar, Mr. Binu George, Ms. Latha Kumary and Dr. Jaimon Yohannan.

I take this opportunity to thank Dr. Beena. C, Librarian, Dept. of Physics, Mr. Suresh, Librarian, Dept. of Electronics, Ms. Jayanthi, STIC and Mr. Ibrahimkutty, Dept. of Electronics for their help and co-operation.

I would like to thank the office and technical staff of Dept. of Electronics, friends at the Dept. of Physics, CUSAT, RRL, Trivandrum and Siberia & Savanna Hostels for their interest in promoting my research.

BIJU KUMAR S.

CHAPTER 1	1
Introduction	1
1.1 Industrial Scientific and Medical (ISM) Applications of Microwaves:.....	3
1.1.1 Industrial Applications	3
1.1.2 Biological effects & medical application:.....	5
1.1.3 Scientific applications	6
1.2 Material Characterisation	6
1.2.1 Characterisation using guided waves	9
1.2.1.1 waveguides.....	9
1.2.1.2 Resonant cavities.....	10
1.2.2 Dielectric measurements using swept frequency techniques	12
1.2.3 Free waves.....	12
1.2.4 Accuracy conditions.....	13
1.3 Brief sketch of present study.....	13
CHAPTER 2	15
Free Space Measurements.....	15
2.1 Introduction	15
2.1 Introduction	16
2.2 Review of the past work.....	18
2.3 Complex Permittivity measurements of solids	23
2.3.1 Theoretical formulation.....	23
2.3.1.1 Single Layer Medium.....	23
2.3.1.2 Compound Materials.....	26
2.3.2 Experimental set-up	27
2.3.3 Measurement technique and Procedure	32
2.3.3 Measurement technique and Procedure	33
2.3.4 Experimental results for solid samples	35
2.3.4.1 Results from reflection measurements	35
2.3.4.2 Limitations and Accuracy Conditions.....	38
2.3.4.3 Results from Transmission measurements.....	39
2.3.4.4 Limitations and Accuracy Conditions.....	40
2.3.5 Measurement and Results of NID compounds.....	42
2.3.5.1 Verification of Results with Theory.....	44
2.4 Complex permittivity measurements of liquids	48
2.4.1 Theoretical formulation.....	48
2.4.2 Experimental set-up and method of measurement	53
2.4.3 Experimental Results	54
2.5 Summary	56
References	57
Appendix 2.1: Implementation of TRL calibration method.....	60

Requirements for TRL standards	60
Selection of Optimal LINE Length	61
Performing the calibration.....	61
Checking the Performance	62
CHAPTER 3	63
GPR technique for Buried Object Detection	63
3.1 Introduction	63
3.1 Introduction	64
3.2 Review of the past work.....	66
3.3 Theoretical Analysis.....	70
3.3.1 Response from a Void.....	78
3.3.2 Extraction of object details from the range profiles.....	83
3.4 Experimental Results	86
3.4.1 Detection of Dielectrics.....	86
3.4.2 Root detection	90
3.4.3. Void Detection	99
3.4.4 Leak Detection	99
3.5 Summary	101
References	102
CHAPTER 4	105
Biological Study	105
4.1 Introduction	105
4.1 Introduction	106
4.2 Review of the past work.....	107
4.3 Sample collection and method of measurement.....	110
4.4 Theoretical considerations	115
4.5 Measurement Procedure.....	118
4.6 Accuracy conditions.....	118
4.7 Experimental Results	119
4.7.1 Bile	119
4.7.2 Bile Stone	125
4.7.3 Gastric Juice	127
4.7.4 Saliva.....	129
4.7.5 Pancreatic Stone	131
4.7.6 Pancreatic Juice	133
4.7.7 Sweat	135
4.7.8 Chicken Bile.....	137
4.8 Dielectric contrast of fluids with water	139
4.9 Summary	143
References	144

CHAPTER 5	148
Conclusions and Future Scope	148
APPENDIX:REPRINTS OF PUBLISHED PAPERS	151
Subject Index	152

Chapter 1

Introduction

The unending quest of man to know more and more about the secrets of nature starts from his very existence. This is a natural consequence of his superior status of intelligence, which makes him different from animals. The growth of science results from his pursuit for novelty.

Electricity and Magnetism originated from the manifestations of nature through certain phenomena. In 1269, Magnetism was initiated by Pierre de Maricourt who identified the north and south poles of a magnet. Electricity began with Stephen Gray and it is Jean-Theophile Desaguliers who showed that there are two types of materials: conductors and insulators. Following, George Simon Ohm, Joseph Henry, James Prestcott Joule, Benjamin Franklin, Joseph Priestly, Henry Cavendish, Augustin de Coulomb, Karl-Friedrich Gauss and many others contributed to the growth of Electricity.

Electricity and Magnetism developed as two independent branches of science till the first half of the 19th century. It was in 1819, with the observation of Christian Oersted that the magnetic needle oriented itself perpendicular to a wire carrying electric current, the relationship between these two was revealed. The famous Ampere's law, formulated by Andre-Marie Ampere based on Oesterd's work is considered as a milestone in electromagnetism. In 1831, Micheal Faraday demonstrated the existence of an induced current in a circuit. This was a significant development in strengthening the relationship between the two branches of Electricity and Magnetism.

James Clerk Maxwell, known as the founder of Electromagnetism, in 1860, developed a theory consolidating the four laws viz. Faraday's law, Gauss' laws for electric and magnetic fields and Ampere's law. He removed the inconsistency of Ampere's law by adding the new factor called displacement current density. This revolutionary suggestion paved the way for the prediction of the existence of electromagnetic waves. These waves were suggested to propagate in dielectric media and their speed in vacuum is that of light. Maxwell's equations were published in 1873 in his "*Treatise on electricity and magnetism*" and are considered as the pillars of electromagnetism. The world was kept waiting for years for the practical demonstration of this theory until Heinrich-Rudolf Hertz first produced, broadcasted and received radio waves in his laboratory at Technical Institute, Karlsruhe, Germany. The use of electromagnetic waves for long distance transfer of information was first demonstrated by young Italian scientist Guglielmo Marconi in the year 1901. The broadcast of the first ever long distance message through air from Cornwall and its reception at the distant place Newfoundland was a startling event for the world.

Meanwhile, electromagnetic waves of smaller wavelength than those developed by Hertz was produced and studied by the eminent Indian scientist Jagadish Chandra Bose. He experimented in the millimeter wave range and developed many important components and detection devices. It was scientist Arrora who christened the waves of shorter wavelength as 'microwaves' in the year 1932. Tremendous strides in microwave technology were achieved during World War II through the developments in the field of radar.

Three decades of electromagnetic spectrum consisting of UHF, SHF and EHF constitute microwaves. Characteristic features of microwaves can be summarised as follows.

Parameters	Values
Frequency	300 MHz – 300 GHz
Wavelength	1m – 1mm
Period of oscillation	3 ns – 3 ps
Energy of microwave photon	1.2 μ eV – 1.2 meV

Applications of Microwaves can be mainly classified into two domains: information and power. Information domain deals with applications in the field of radar and communications. Power domain includes industrial, scientific and medical (ISM) applications. A chart of the applications of microwaves in various fields is shown in *figure 1.1*.

1.1 Industrial Scientific and Medical (ISM) Applications of Microwaves:

1.1.1 Industrial Applications

The processes in many industries involve drying in one or more stages. Since microwave drying offers the best efficiency, it is a best substitute for other conventional methods. The frequencies employed for this purpose are 434, 915 and 2450 MHz. Microwave drying is adopted during the manufacturing of paper and cardboard, printing inks, bulk processing of bags, drying web materials etc. Drying of wood using microwaves got much attention due to the loss rate of only 2% as compared with that of 22% in hot-air drying. It is also used in drying of plaster tiles, ceramics, foundry moulds and concrete. In the pharmaceutical industry, drying of granules can be performed using microwaves. These waves can be irradiated during the copolymerisation process, polyurethane reaction process and thermosetting resins reticulation. They can be used during dewaxing of casting moulds and backing are carried out simultaneously. Purification of sandy oil and coals, pyrolyzation of shales, gasification of coal, liquification of heavy oil, hardening of foundry mouldings, sintering of ferrites and ceramics, crushing rocks and concrete, drying potato chips, pasta and cigarette, soil treatment, opening of oyster shells, vulcanisation and devulcanisation of rubbers can be performed using microwaves. Microwave drying offers wide application in nuclear waste management by solidifying droplets of radioactive waste in solution. The preservation of food by the elimination of proliferating parasitic micro-organisms such as bacteria, yeasts and mildew, enzymatic inactivation, sterilization and pasteurization and disinfestation of stored grain are performed with microwaves.

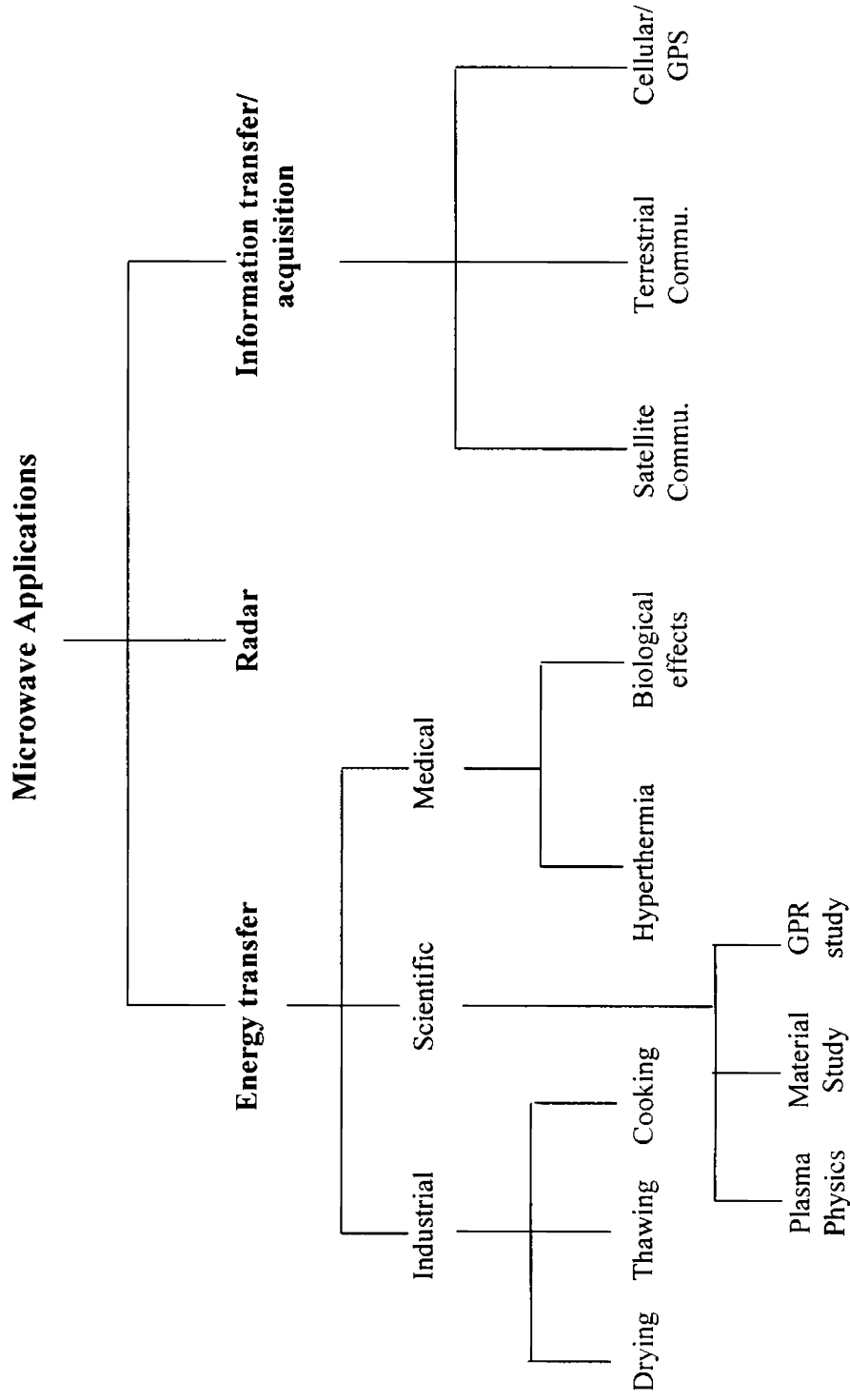


Figure 1.1 Classification chart of the applications of microwaves

Microwave heating can save time and energy. Other advantages of microwave drying are: three-dimensional uniformity of humidity distribution, avoidance of overheating, selective microwave heating of the water component and a reduction in the length of the dryers. Microwaves give a better-finished product as compared with the conventional treatment. There are also other advantages such as fast start up and shut down speed, ease of access and control, and economy of space.

Microwaves are very well used for thawing and tempering. The lower ISM frequencies (434 & 896/915 MHz) are better suited to the thawing process because they allow better penetration. Another main application of Microwaves is in cooking. Microwave oven, which is a common household item now, is designed employing the thermal applications of microwaves. The advantages of microwave cooking are: the finished product is of much higher qualities with respect to color, appearance, taste, nutritional properties and the remarkable absence of curling. This method of cooking provides a considerable saving of energy.

1.1.2 Biological effects & medical application:

Microwave offers many therapeutic applications. Diathermy and hyperthermia are the major areas that involve heating of the tissue by some means of energy deposition. Diathermy treatment is applied for patients with arthritis, rheumatism etc. The hyperthermia finds its use in the treatment of cancer. This technique seems to have no side effects. It has been reported that there is an increase in the antigenicity of malignant cells treated with microwaves. In the clinical side, microwave hyperthermia is effective in relieving neurologic or arthritic pain. It has been reported that the pregnant women suffering from chronic inflammation of the pelvis could be treated with 2.45 GHz radiation without adverse effects.

Recently, many scientists are concentrating their work on developing new methods of microwave imaging of biological systems by mapping the complex permittivity of the organs. A sudden change observed in the permittivity map may indicate a pathological condition. The conventional imaging methods are the X-ray and the Magnetic Resonance (MR) Imaging. The main practical disadvantage of the MR Imaging is that the equipment is too costly. In X-ray imaging, the method of

density imaging employed is observed not to be much effective in the case of detection of tumors and swellings. This is due to the fact that the densities of malignant and normal tissues are nearly the same. But, as the complex permittivity of tumour cells differ considerably, the microwave complex permittivity imaging when developed, may prove to be best suited for the detection.

1.1.3 Scientific applications

The interaction of electromagnetic waves of small amplitude with plasma in the solid state may be successfully used for determining basic semiconductor parameters such as resistivity, mobility of charge carriers and relaxation time. Microwaves can be used as the alternating voltage to accelerate electrons in the accelerators like the linear accelerator (linac), the cyclotron, the microton and the synchrotron.

Material characterization is another important scientific application. Since the topic of research in the thesis is material characterization, different techniques and their accuracy conditions are discussed in detail below.

1.2 Material Characterisation

The relation between the electromagnetic field quantities and the properties of a material medium is described by the permittivity and permeability of the medium. Both these quantities represent the electromagnetic properties of matter.

The study of the electromagnetic properties of matter lies in solving Maxwell's equations with necessary boundary conditions and in determining the properties of electromagnetic wave propagation in medium. This problem can be approached in both ways. We can either determine the properties of wave propagation in a given medium by knowing the permittivity and the permeability of the medium or establish the electromagnetic properties of matter from the character of wave propagation. In electrodynamics, solution of both problems is of considerable practical use.

The complex permittivity or permeability of material medium can be evaluated either from measurements of the propagation constant ' γ ' of a plane electromagnetic wave propagating through that medium or from the measured impedance ' Z ' of the medium. Determination of the propagation constant of a plane wave forms the basis of the microwave measurements of the complex permittivity by the free-space method. The fundamental concept in the complex permittivity measurements in a guided wave structure is the measurement of the impedance of material medium.

The knowledge of electromagnetic properties of matter, obtained by studying the interaction of the wave with matter can be used for influencing the properties of matter during its irradiation by stronger electromagnetic fields or for a permanent change of its internal structure after application of strong electromagnetic fields. Strong interaction of an electromagnetic wave with matter can be used for attaining irreversible processes such as dielectric heating, microwave discharge formation, microwave plasma heating and microwave diathermy. Further the structure modification of organic matter and biological materials can also be resulted through the interaction with e.m. waves.

The knowledge from the microwave measurements contributes not only to our information about structure of the matter but also influences the development and production of new materials and devices based on new principles. There has been immense interest in the microwave properties of dielectric and magnetic materials since they are widely used in the microwave circuits, devices, quasi-optical components such as substrates, dielectric waveguides, radiation absorbing materials (RAM) and telecommunication. The design of these components needs the electric and magnetic response of the materials at the operating frequencies. The quality requirements are more demanding for the materials used for fabrication of MICs than for the low frequency circuits. In contrast to the low frequency circuits, the dielectric substrates in the high frequency operation not only provides a support to the circuit but also actively participate in the functioning of the circuit. This is the main reason why electromagnetic waves are very important and efficient diagnostic tools. The dielectric constant and thickness of the substrate decide the impedance of the

transmission lines. The materials used in the fabrication of MICs are very wide, involving materials ranging from polymers, ceramics, special high purity metals and alloys.

Dielectric resonators are widely used for MIC application. They are made of low loss, high dielectric constant ($\epsilon_r = 20-100$) ceramic mixtures such as the titanates, zirconates, tantalates, niobates etc. The conventional range of loss tangent, $\tan\delta$ is between 0.00004 and 0.0004 and of Q-factor is from 2000 to 50000. Because of the many application of ferrites in microwave frequency range, a designer of the ferrite devices has to know the detailed characteristics of the material. Ferrites are extensively used as phase shifters for switching and control of microwave signals and in communication systems like phased array antenna. Lithium ferrites are used in the fabrication industry of memory devices and latching microwave devices. The frequency range of its use extends even to millimeter wave bands. Ferrites have dielectric constant in the range 9 – 20 and $\tan\delta$ less than 0.001. For lithium ferrites ϵ_r is in the range 14-20 and typical $\tan\delta$ of the range of 0.00025. Rare earth Iron Garnets (ReIG) are used for realization of microwave components such as band pass and band stop filters. They also find application in harmonic generators, limiters and programmable frequency sources/counters for high-resolution radar systems. YIG (Yttrium-Iron Garnets) tuned oscillators have found wide application in modern electronic instrumentation system due to their broad tuning range, excellent tuning linearity and clean spectrum.

Radome is an enclosure for protecting an antenna from changing environment conditions, generally intended to leave the electrical performance of the antenna unaffected. ie, radome is a housing for an antenna. Materials used for fabrication of radomes are primarily selected for adequate physical strength and good electrical characterisation. Radomes are expected to have large electromagnetic transmission coefficient. Best radome performance is obtained by choosing low loss and low dielectric constant material. Variation of these values over the range of frequency of interest dictates the performance of the radome's bandwidth. These electrical properties together with mechanical strength characteristics form the basis of the selection of materials for radome design.

The methods available for measuring electrical properties such as (complex permittivity ϵ , loss tangent $\tan\delta$, conductivity σ and permeability μ) fall into two categories according to the nature of the wave: (1) guided waves and (2) Free waves.

1.2.1 Characterisation using guided waves

1.2.1.1 waveguides

The characterization using waveguides has got much attention owing to the relative simplicity in the measurement setup and procedure. The sample can be placed directly into a waveguide or resonator in which the electromagnetic field is strictly defined.

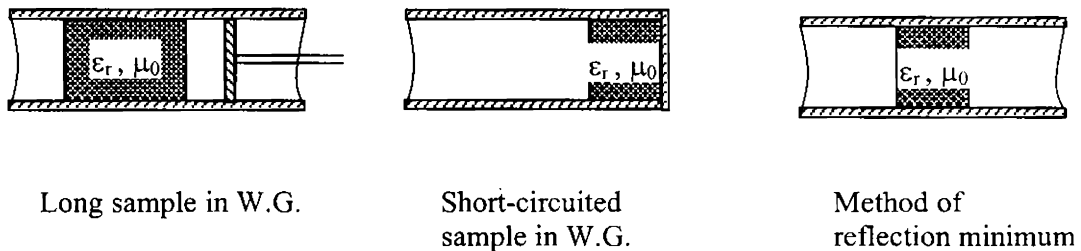


Figure 1.2 Different waveguide methods of material characterization

These methods may be considered nowadays as classical, but in many practical cases they are not applicable. Measurement in coaxial lines and waveguides is destructive in principle. Though the specimen is not destroyed during measurement, it must be accurately machine-worked to fit the coaxial line or waveguide or closed resonator shapes. The specimens inserted into the coaxial lines or waveguides must fit perfectly so that between the sample and the coaxial line or waveguide walls no gap that would heavily influence the accuracy of measurement should appear. Resonators seem to be rather more advantageous from this point of view since they are filled by the specimen only partially.

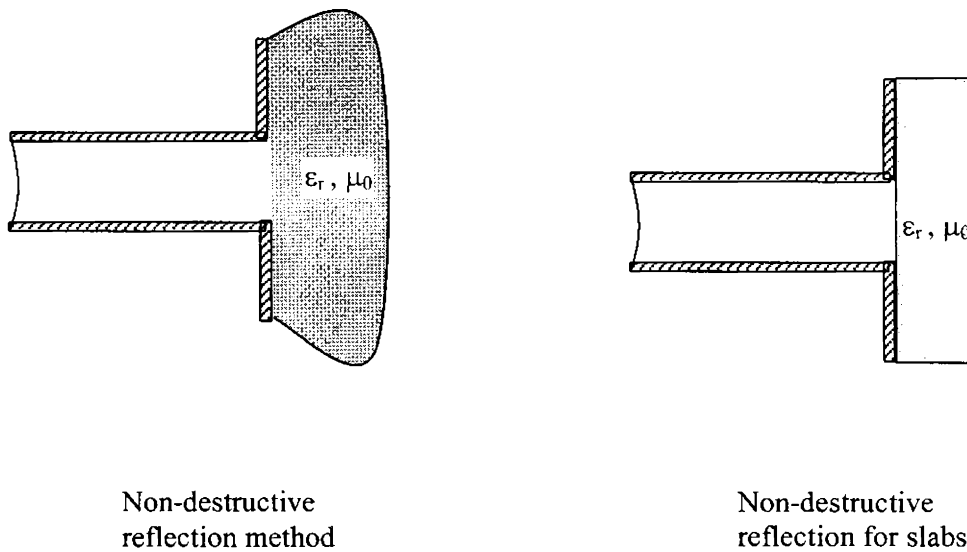


Figure 1.3 Different waveguide probing methods

1.2.1.2 Resonant cavities

Mainly there are two types of waveguide cavities: Rectangular Waveguide cavities and Circular Waveguide cavities. Resonators are constructed from closed section of the corresponding waveguide. Electromagnetic energy is stored within the cavity, and power can be dissipated in the metallic walls of the cavity as well as in the dielectric filling the cavity. Coupling to the resonator can be by a small aperture or a small probe or loop. In the rectangular cavity resonator, TE_{101} mode is the dominant resonant mode corresponding to the TE_{10} dominant waveguide mode. Since the dominant circular waveguide mode is TE_{11} mode, the dominant cylindrical cavity mode is the TE_{111} mode. Corresponding to a resonant frequency, there will be two parameters namely resonant frequency and quality factor. The unloaded and loaded parameters will be employed to determine the dielectric properties of the sample placed.

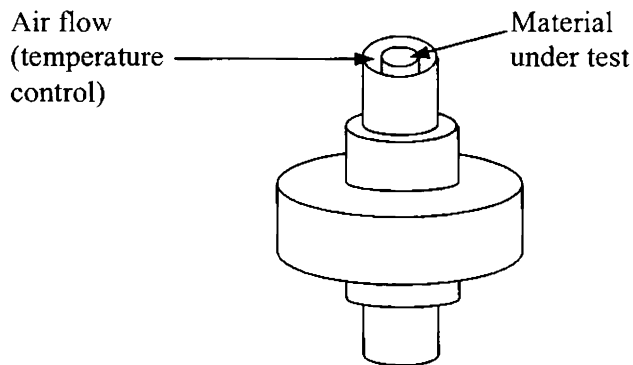


Figure 1.4 Circular cavity loaded with tubes

The dielectric constant of the dielectric resonators in the pellet form can be measured by the method suggested by Hakki and Coleman. The short-circuited resonator is operated as a transmission resonator with small coupling antennas used to couple the power. These antennas are connected to the network analyser.

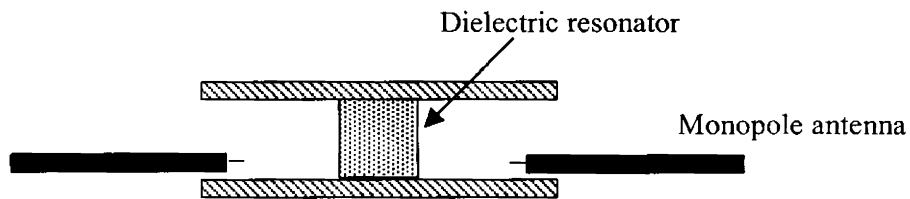


Figure 1.5 Hakki-Coleman method for measurement of dielectric resonators under end-shortened condition

The general geometry of the open resonator is shown in *figure 1.6*. There are two spherical mirrors having radii of curvature R_1 and R_2 , separated by a distance 'd'. Depending on the focusing properties of these mirrors, the energy in the resonator may be confined to a narrow region about the axis of the mirrors.

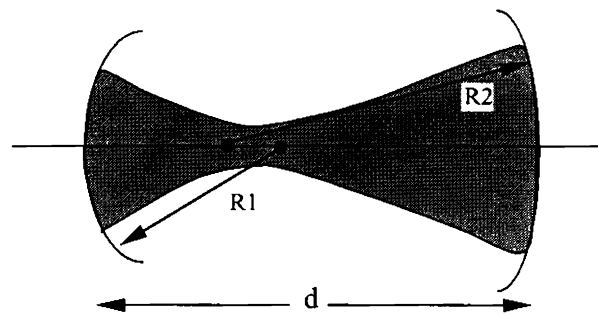


Figure 1.6 Open resonator method

1.2.2 Dielectric measurements using swept frequency techniques

Swept frequency dielectric measurement has advantages over conventional techniques. It becomes quite obvious that for measuring dielectric constant, a very desirable condition is to have a sample length of one quarter wavelength or multiple thereof. It is rather difficult to change the physical dimensions of the sample in a continuous manner. Instead the electrical length of the sample can be varied by changing the frequency. In this way it is possible to create conditions such as a quarter wavelength, which makes it relatively easy to calculate the complex dielectric wavelength. This approach forms the basis for the swept frequency method.

1.2.3 Free waves

Free-space microwave measurement of the complex permittivity of dielectric materials and media is fully contactless and non-destructive. It can be carried out at high and even at low temperatures, in strong magnetic and electric fields. Above all, the method is useful for the measurement of materials in planar form. It can be applied in industry for continuous control of properties of planar materials in series production of dielectric and semiconductor devices. The method can also be successfully used in the chemical industry, biology, medicine and many other fields. But these types of applications of free-space method are not yet fully developed due to many accuracy constraints. The free space method of characterizing the radome materials is shown in *figure 1.7*.

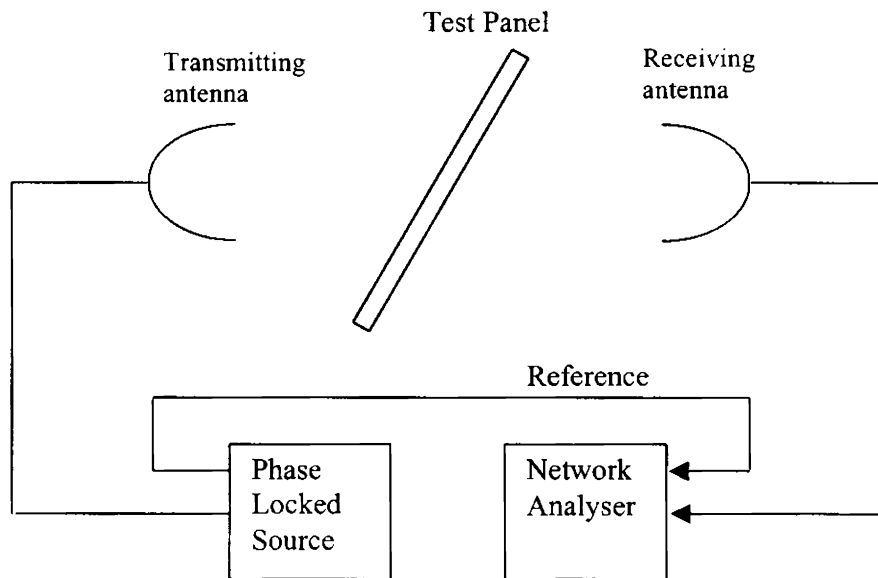


Figure 1.7 Free space method for characterization of radome materials

1.2.4 Accuracy conditions

The accurate determination of complex permittivity assumes that the probing wave will not affect the material or medium being studied. In order to satisfy this, the output power used in microwave measurements must be sufficiently low. Its magnitude is so adjusted that it should not change the characteristics such as plasma ionization degree and the specimen temperature. Only then, it is possible to attain easily interpretable information about electromagnetic properties of the material or medium under study.

1.3 Brief sketch of present study

Development of different methodologies appropriate for the characterization based on the dielectric properties of materials under different state and environment is presented in this thesis.

The materials and the corresponding methods applied for the study are detailed below.

- (1) materials that are available in planar form - free space method
- (2) buried materials - time domain analysis of the reflected signal
- (3) biological samples - cavity perturbation technique

Chapter 2 gives in detail the development of free space method for the characterization of planar samples. Solid materials like polystyrene, glass, glass epoxy and cement and liquids like oil, methanol, ethanol, and water are considered. Their dielectric parameters are calculated from the reflected and transmitted data and are compared with the standard values available.

Chapter 3 deals with the application of free waves for buried object detection. A pyramidal horn antenna of nominal gain kept in free space is employed for the measurement. Necessary theoretical support using Finite Difference Time Domain method is given. Amplitude of reflected signal using a simulated wave from different objects placed at different depths is evaluated. It is compared with the values obtained from the real situation.

Chapter 4 deals with the characterization of biological samples using cavity perturbation method. Since biological samples are available only in small quantity, the cavity perturbation method is best suited for the study. Different samples of bile, gastric juice, pancreatic juice, bile stone, pancreatic stone, chicken bile, sweat and saliva are taken for the study. The dielectric parameters obtained for these samples are tabulated.

Chapters 5 gives the conclusions derived from the study and future scope of the work.

Chapter 2

Free Space Measurements

Free space measurement method is implemented with ordinary pyramidal horn antennas and specially designed microwave test bench. The design of the microwave test bench and the THRU-REFLECT-LINE (TRL) calibration are discussed. The planar samples are characterized using this method. Complex permittivity of Non-Interactive Distributive (NID) dielectric compounds is also determined and verified with the theoretically calculated values. Theoretical formulation is modified for measurement of liquids and experimental results are tabulated.

2.1 Introduction

Dielectric study of materials has got wide applications in science and technology [1]. The technological applications span over the areas like communication, remote sensing, radar, design of circuit components [2-5] etc. Wireless communication uses free waves and naturally the performance may be degraded due to the reflection from surroundings. So, while installing the indoor wireless communication networks like WLAN and Bluetooth, one needs the characterization of different indoor items, thereby enabling the optimization of the network [2,3]. A number of methods have been employed for the dielectric characterization of the materials. Main methods of characterization are: Time-Domain methods, Frequency-Domain Transmission Line techniques, Two-Terminal Measurements, Closed Cavity methods, Open Resonators, Free-Space methods, microstrip methods etc. Each method is characterized by its frequency of operation, area of applications and the nature of the sample. Measurements in two-terminal cells are limited up to 100 MHz. Time-domain methods at microwave frequencies offer broad bandwidth, but at the cost of resolution. Most accurate measurement of dielectric properties is offered by frequency-domain measurements. Closed cavities are operational up to 40 GHz and open resonators are commonly used in the frequency range of 30-200 GHz.

An attractive feature of the free space method is that it has got a wide operational frequency range extending up to millimeter range. Component dimension limits the operational frequency in the case of other methods. This versatile method facilitates measurements in the whole microwave spectrum. Another important feature of free-space measurement of the complex permittivity of dielectric materials is that it is fully contactless and non-destructive. Also, measurements can be carried out at wide range of temperatures, in strong magnetic and electric fields. It enables the determination of dielectric parameters at any frequency in the operating band whereas other methods such as resonator methods provide the properties only at discrete frequencies determined by their dimensions.

In spite of having much potential in the field of material characterisation, many aspects of this technique remain to be studied. For example, the extent of influence of several parameters affecting the accuracy of the method has not yet been fully understood. The necessary requirements for an ideal system to ensure accuracy are the following:

1. an antenna system that would transmit a plane electromagnetic wave into a limited volume
2. the plane electromagnetic wave should pass through the sample specimen completely with negligible edge diffraction of incident energy.

In the measurement of complex permittivity in free space, we place a planar specimen of unknown material in the space between the transmitting and receiving antennas and a plane electromagnetic wave is incident on it. The measurement is based on the fact that the variation of the phase and amplitude of the plane electromagnetic wave passing through or reflecting from a dielectric specimen, depend on the dielectric and magnetic properties.

Following are the steps involved in development of a technique for the measurement of dielectric properties of materials.

1. the choice of a suitable theoretical model which represents the best real physical situation in the measurement
2. the choice of such an experimental arrangement which satisfies in the best possible way the assumptions of the theoretical model, and
3. suitable calibration technique and accuracy of the experimental method

The correctness of the results depends on the fulfillment of these conditions

This chapter deals in detail with the choice of the suitable theoretical model, design of experimental equipment, method of measurement, calibration procedure and evaluation of experimental data in the case of the free space measurement. The method is novel in the sense that it has been implemented using ordinary pyramidal horn of approximately 15dBi gain. The theoretical model for measuring the complex

permittivity in free space considers a plane electromagnetic wave incident normally on an infinite plane-parallel plate of a homogeneous dielectric medium. Its complex permittivity is determined from the measured values of the reflection coefficient and/or transmission coefficient of the plane electromagnetic wave reflected from or transmitted through the plate. The theory is developed assuming that the materials are perfect dielectrics. In the experimental side, the design of the test bench built in house satisfying the theoretical model, is discussed. The measurement is done after proper calibration – THRU-REFLECT-LINE (TRL) calibration.

Dielectric constant of different solid materials and Non-Interacting Dielectric (NID) mixtures is determined at different microwave frequency bands. The work is also extended to characterization of liquids with the modification of the theory. Accuracy conditions for the improvement of results are also discussed.

2.2 Review of the past work

Glaz et al [7] developed the microwave systems for moisture sensing, which measured the reflection coefficient and/ or transmission coefficient. The study is performed at 2.45 GHz. The free space reflection coefficient of a metal-backed material is collected to determine its moisture content from the dielectric properties retrieved. They have compared the results with spot focusing antenna and ordinary pyramidal horn antenna.

Musil and Zacek [8] extensively describe principles and methods of the complex permittivity measurements using free space methods. Different methods of focusing microwave power are also described.

Huang et al. [9] characterised the layered dielectric medium using reflection coefficient. They demonstrated that the complex permittivity and the thickness of a single-layer medium can be obtained by the use of reflection coefficient at two slightly different frequencies. The assumption made in the development of the theory is that the dielectric properties of a medium change slowly with the frequency, but the reflection coefficient is very sensitive to it.

Ghodgaonkar et al. [10] developed a free space measurement system for the determination of dielectric properties of planar slabs of ceramic and composite materials in the frequency range 14.5 – 17.5 GHz. They employed a pair of spot – focussing horn lens antennas connected to the network analyser. The size of the sample to be measured, calibration methods, time domain gating etc were mentioned for the better accuracies. Complex permittivity was calculated iteratively from the equation. They characterised teflon and PVC and the results from free space method are then compared with that from the waveguide measurements. They also described the characterization of dielectric sheets in the 8.2-40 GHz frequency range [11], which measures the reflection and transmission coefficients. They argued that the diffraction effects are negligible if the minimum transverse dimension of the sample is greater than three times the E-plane 3-dB beamwidth of the antenna at its focus. Samples like teflon, sodium borosilicate glass and some microwave absorbing materials were studied. Different accuracy conditions and measurement procedure were extensively described in this paper.

Gerhard L. Friedsam and Erwin M. Biebl [12] developed a free-space system operating in the 75 GHz to 95 GHz range for measurement of the complex permittivity. Transmission coefficient through the sample while the collimated gaussian beam passing through the sample is measured at different angles. The complex permittivity is subsequently calculated from the measured data by applying a nonlinear least-squares method. The measured 3-dB beamwidth of the antennas in the frequency range 75-95 GHz was in between 1 and 2 degrees. In order to minimise the influence of the reflected from the sample and the diffraction effects at the edges of the sample holder on the measured data, the measurements have been limited to angles of incidence within the range 10^0 and 40^0 .

Characterisation of small pellet samples of electrolytes such as AgI at microwave frequencies is done by free space method [13]. Unlike the transmission-line and/or cavity methods, which need elaborate sample heating arrangements and also have restricted applications to low-loss materials, the present technique offers simpler and direct measurement. They made the measurement in the frequency range 7-12 GHz.

Juan Munoz et al. [14] developed a free-space method for determining the dielectric and magnetic properties of materials from reflection measurements made at normal incidence and transmission measurements made at normal and oblique incidence is proposed. Their method combines both frequency domain measurements and time domain analysis. Measurements are made in the X-band. A focussing assembly for the incident beam using ellipsoidal concave mirror is also incorporated for better results. They characterised the low-loss materials like teflon, nylon and polymethyl methacrylate and some microwave absorbing materials and it was compared with the results using other established methods.

Lasri et al. [15] tried to build systems which can, in some cases, be used as an alternative to the automatic network analyser, to improve the development of microwave characterisation of materials in an industrial context. They have proposed and devised the systems which can be used to obtain the S-parameters of a material under test. The sample was placed on the metal plate and reflected data was collected using the horn antenna.

The effect of microwaves on mountain pine beetle and the pupae of darkling beetle in the waveguide and in free space method with the wide range of doses of low-level radiation at 10 GHz, 35 GHz and 74 GHz was studied [16]. In the free space measurement method, the irradiation was performed after the insects placed on a shallow styrofoam tray which was in turn, placed on a microwave absorber using the horn antenna placed at the near field.

D. T. Fralick [17] designed a free space set-up for the characterisation of the permittivity of the radome materials in W-band. The transmission loss through the radome at the operating frequencies, 84 GHz – 94 GHz, was done. The measurement was performed using HP 85106 millimeter wave system.

In a paper, Volgyi [18] introduced a microwave monitoring system that can be applied for quality forecast of particle-boards using the free-space measurement methods. This system operating at 5.8 GHz measures the complex permittivity. Multifrequency operation is introduced, minimizing the errors caused by distance-

variation between material under test and backscatter. They also tried to compare the real mechanical properties to the measured microwave parameters.

The metal backed planar samples are characterized by the free-space bistatic measurement set up operating in the frequency range of 5.85-40 GHz [19]. Two spot focusing horn lens antennas are used as transmitter and receiver and they avoid diffraction effects. Two samples, Teflon and Eccogel 1365-90 were characterized for both parallel and perpendicular polarizations.

Friederich and Moore [20] generated Gaussian beam profile with lenses consisting of two plano-convex pieces with flat faces next to each other. They set up an arrangement called “boom arch”, which allows one to characterize the reflectivity of materials at various incident and reflected angles which in turn gives the material properties such as complex permittivity, permeability and other parameters such as reflectivity, transmissivity etc. This facility has been used at frequencies from 2 to 100 GHz and the measurement is possible at very high temperature.

Bistatic frequency diversity microwave imaging technique has been demonstrated by Lin and Chu [21] as a tool for the applications of remote sensing, imaging radar, and non-destructive evaluation.

Kaida Bin Khalid [22] discusses the development of a moisture meter for lossy liquids which is based on the reflection method. He describes the dielectric properties of various lossy liquids at different percentage of moist content. The moisture meter consists of a transmitter which transmits microwave signal towards the sample holder which is backed by a metallic reflector and the reflected signal is picked by a receiver and the received signal is monitored by a meter.

Varadan and Varadan characterized the artificial chiral composites by the free space set up in the frequency range 5.8-40 GHz [23]. The parameters such as complex permittivity, permeability and chirality factor are measured.

The signature of gram at 9.5 GHz using the indigenously developed set-up and the principle adopted is bistatic method is mentioned by Sharma et al [24]. They

have taken the observations at several growth stages of gram, which found change in the parameters like brightness temperature and scattering coefficient.

The relative complex permittivity measurements for five different kind of wheat samples and the improvements in the free-space measuring systems has been described by Kraszewski et al [25]. The operating frequency band is 3-13 GHz.

Okamura and Zhang [26] describe a method to find out the moisture content of materials based on the phase shift changes in the transmitted signal at two different frequencies. They used two rectangular horn antennas operating in the X-band for the characterization. They compared the experimentally obtained moisture content with that from the oven moisture content measurement.

Jose et al. [27] describe the characterization of liquids using free space methods. They employed spot-focussed lens antennas and characterized the liquids in the range of 5-110 GHz. The results include characterization of water and methanol using this method.

In-situ dielectric characterization of materials in the wide band of frequencies for a wide range of temperature using the free space methods and spot-focussing lens antennas is discussed in this paper [28].

2.3 Complex Permittivity measurements of solids

2.3.1 Theoretical formulation

2.3.1.1 Single Layer Medium

Considering a single dielectric slab of thickness 'd', the e.m. wave falling on it undergoes multiple reflection and transmission generating a resultant reflected signal and a transmitted signal. *Figure 2.1* illustrates the path of e.m. wave through different media, multiple reflection and transmission [29]. S_{11} and S_{21} are the resultant reflection and transmission coefficients.

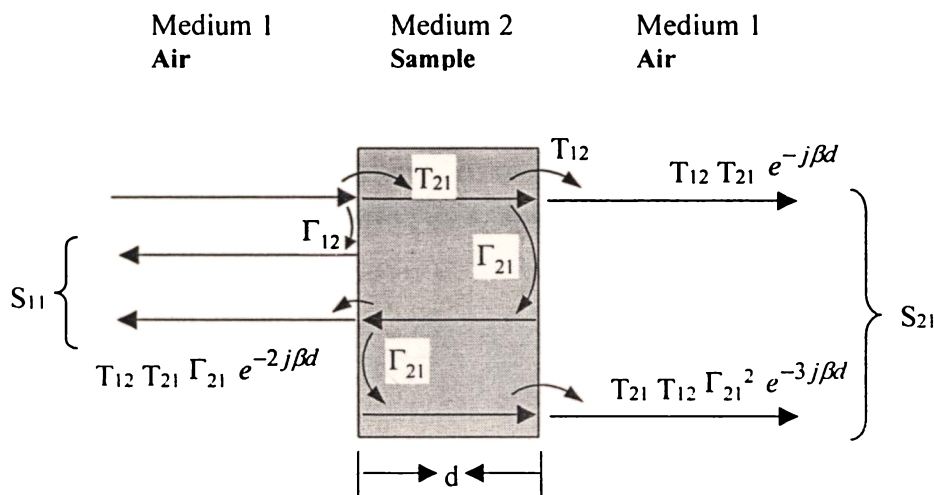


Figure 2.1 Wave propagating through a dielectric slab

The propagation constant through the medium is

$$\gamma = j\omega \sqrt{\mu_0 \epsilon_0 \left(\epsilon_r' - \frac{j\sigma}{\omega \epsilon_0} \right)} \quad (2.1)$$

$$= \frac{j\omega x}{c}, \text{ where } x = \sqrt{\epsilon_r^*} = \sqrt{\epsilon_r' - j\epsilon_r''} \text{ and 'c' is the}$$

velocity of light.

Γ_{mn} and T_{mn} are the reflection and transmission coefficients at different boundaries, where 'm' and 'n' are the different media.

Reflection coefficient from medium 1 (air) to medium 2 (dielectric) is given by

$$\Gamma_{12} = \left(\frac{Z_1 - Z_0}{Z_1 + Z_0} \right) \quad (2.2)$$

But $Z_1 = \frac{Z_0}{\sqrt{\epsilon_r^*}}$, impedance of the medium, and $Z_0 = 120\pi$, free space impedance.

Using the ray-tracing model, the total input reflection coefficient can be written as

$$\Gamma_{in} = \Gamma_{12} + T_{12}T_{21}\Gamma_{21}e^{-2j\beta d} + T_{12}T_{21}\Gamma_{21}^3e^{-4j\beta d} + \dots \quad (2.3)$$

Rearranging the above equation, we get

$$\Gamma_{in} = \Gamma_{12} + \frac{T_{12}T_{21}\Gamma_{21}e^{-2j\beta d}}{1 - \Gamma_{21}^2e^{-2j\beta d}} \quad (2.4)$$

Γ_{12} is the intrinsic reflection coefficient of the initial reflection and $(T_{12}T_{21}\Gamma_{21}e^{-2j\beta d})$ the contribution due to the first bounce within the slab.

$$\beta d = \frac{2\pi d}{\lambda} = \frac{2\pi d\sqrt{\mu_r\epsilon_r}}{\lambda_0} = \frac{\omega d}{c}x \quad (2.5)$$

where λ is the wavelength in the medium, λ_0 is the free space wavelength, μ_r and ϵ_r are the complex relative permeability and permittivity of the medium respectively. We also know $\Gamma_{21} = -\Gamma_{12}$, $T_{12} = 1 + \Gamma_{12}$ and

$T_{21} = 1 + \Gamma_{21} = 1 - \Gamma_{12}$. Indices 1 and 2 represent the air and the medium respectively. Substituting equation (2.5) in (2.4) and rearranging

$$\Gamma_{in} = S_{11} = \frac{\left[1 - e^{-2j\frac{\omega d}{c}x} \right]}{\left[1 - \Gamma_{12}^2 e^{-2j\frac{\omega d}{c}x} \right]} \Gamma_{12} \quad (2.6)$$

Usually for a dielectric medium μ_r is taken as unity and $\sqrt{\mu_r \epsilon_r}$ is reduced to

$$\sqrt{\epsilon_r} = \sqrt{\epsilon_r' - j\epsilon_r''} = x$$

$$\tan \delta = \frac{\epsilon_r''}{\epsilon_r'} \quad (2.7)$$

For the transmitted signal, total transmission coefficient S_{21} is evaluated as

$$S_{21} = \frac{\left[(1 - \Gamma_{12}^2) e^{-j\frac{\omega d}{c}x} \right]}{\left[1 - \Gamma_{12}^2 e^{-2j\frac{\omega d}{c}x} \right]} \quad (2.8)$$

The reflection coefficient, Γ_{12} at the air-medium interface is related to the impedance Z_0 and Z_1 of the air and dielectric slab respectively as, $\Gamma_{12} = (Z_1 - Z_0)/(Z_1 + Z_0)$. But $Z_0 = 120\pi$ and $Z_1 = \frac{Z_0}{x}$. Solving S_{11} and S_{21} independently, x can be found out and hence complex dielectric constant, ϵ_r . The exponentials in the equations (2.6) and (2.8) should be expanded to enough number of terms for the convergence of the required solution.

2.3.1.2 Compound Materials

Combination of two or more dielectric materials is called compound material. For a non-interactive and distributive mixture of two dielectrics (see *figure 2.2*), any property P of the dielectric material is given by [30]

$$P = v_1 P_1 + v_2 P_2 \quad (2.9)$$

Here v_1 and v_2 are the volume fraction of the individual components. If the parameter considered is dielectric constant, the effective dielectric constant of the compound will be

$$\begin{aligned} \varepsilon_{r\text{eff}} &= v_1 \varepsilon_{r1} + v_2 \varepsilon_{r2} \\ \varepsilon_{r\text{eff}} &= \frac{\varepsilon_{r1} V_1 + \varepsilon_{r2} V_2}{V_1 + V_2} \end{aligned} \quad (2.10)$$

where ε_{r1} and ε_{r2} are the dielectric constants and V_1 and V_2 are the volumes of the two samples respectively. It can be extended to any number of samples. Since the two sample sheets have the same cross sectional area compared to the span of illumination of the electromagnetic wave, the volume fraction can be replaced by the thickness fraction.

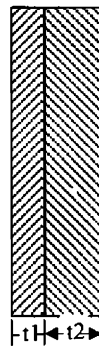


Figure 2.2 Configuration of NID compound

Volume fractions take the form as

$$\frac{V_1}{V_1 + V_2} = \frac{t_1}{t_1 + t_2} \quad (2.11)$$

$$\frac{V_2}{V_1 + V_2} = \frac{t_2}{t_1 + t_2} \quad (2.12)$$

If 't₁' and 't₂' are thickness of the two samples, then (2.10) can be written as

$$\varepsilon_{r\text{eff}} = \frac{\varepsilon_{r1} t_1 + \varepsilon_{r2} t_2}{t_1 + t_2} \quad (2.13)$$

The effective dielectric constant can be employed for determining the complex permittivity of a constituent in a compound provided their volume fraction or thicknesses are given.

2.3.2 Experimental set-up

The experimental set up consists of Vector Network Analyser (VNA) HP 8510C, S-parameter test set HP 8514B, sweep oscillator HP 83651B, interfacing computer and microwave test bench. The schematic diagram of the experimental set-up is shown in *figure 2.3*. Two identical antennas are mounted on the test bench and the sample material in the form of flat sheet is kept positioned at the reference plane. The measurements are carried out in J and X bands. For J band measurement, pyramidal horns of Half Power Beam Width (HPBW) 22.5° (E-plane) and 21.5° (H-plane) and aperture dimension 14 cm x 10.5 cm are employed. For X-band, the antennas have HPBW 18° (E-plane) and 15.5° (H-plane) and aperture dimension 9.8 cm x 7.5 cm. The radiation patterns of the horn antennas are given in the *figures 2.4 & 2.5*.

The test bench is specially designed for the free space measurement. It is constructed with low loss polystyrene materials so that the reflection is minimised. The need of a test bench is to move precisely the antenna at the time of LINE calibration, to position the metal plate for REFLECT calibration and the samples for the measurement after calibration. The transmitter and receiver mounts can be very

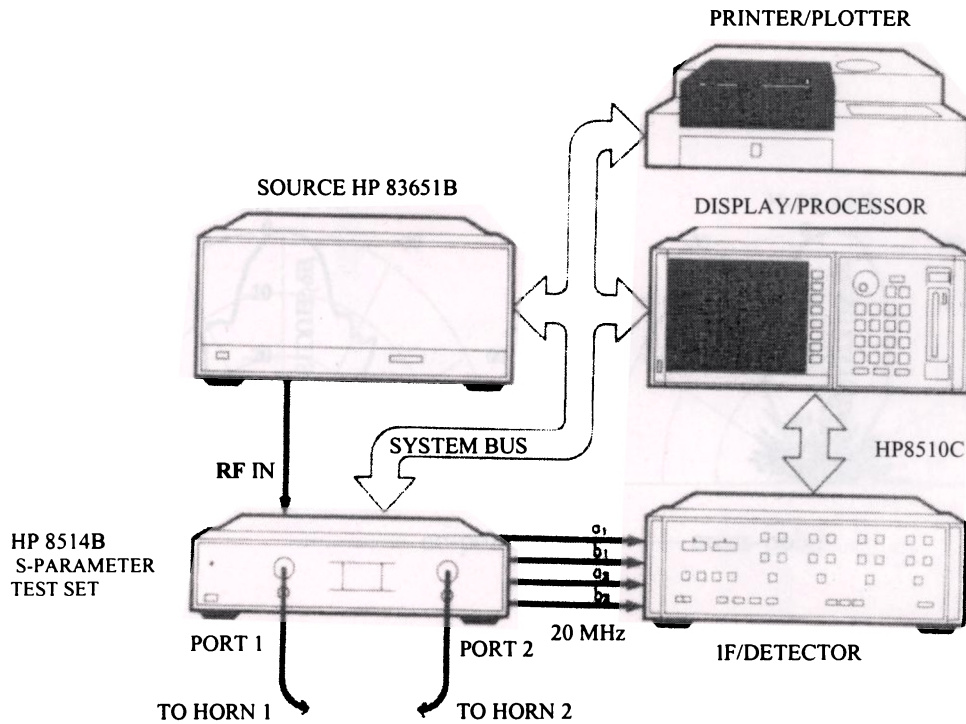


Figure 2.3 Schematic diagram of the experimental set-up

precisely set at any position with accuracy of <1 mm. The antennas are moved through a distance to which the network analyser is set for LINE calibration. This accuracy is very essential for better calibration. The schematic diagram of the test bench is shown in *figure 2.6*. Two antenna axes are held in the on-axis position and ensured that they are at the same height from the base of the bench. Antennas can be moved along the test bench channel by rotating the pedal. For one complete rotation of the pedal, antenna moves by 1 mm. The sample materials in the form of flat sheet are placed in between two identical antennas. To minimise unwanted reflection from the surroundings, the test bench is placed in an anechoic chamber and measurements are performed. The schematic diagram of convertible anechoic chamber is shown in *figure 2.7*.

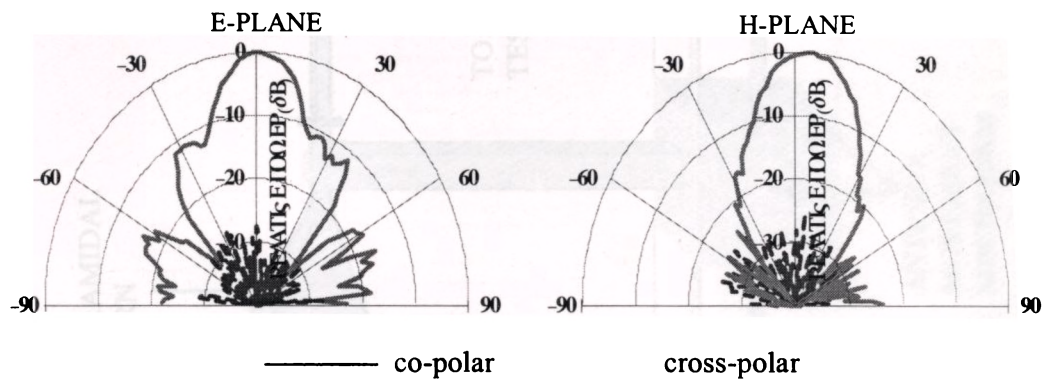


Figure 2.4 Radiation pattern of J-band pyramidal horn antenna

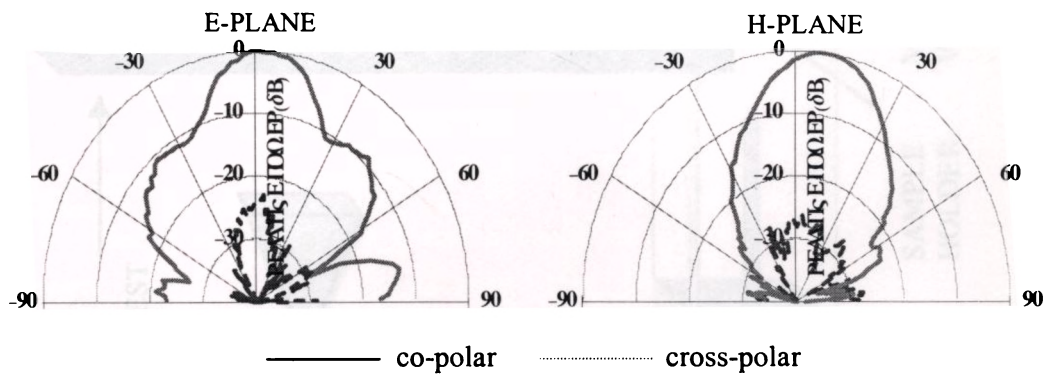


Figure 2.5 Radiation pattern of X-band pyramidal horn antenna

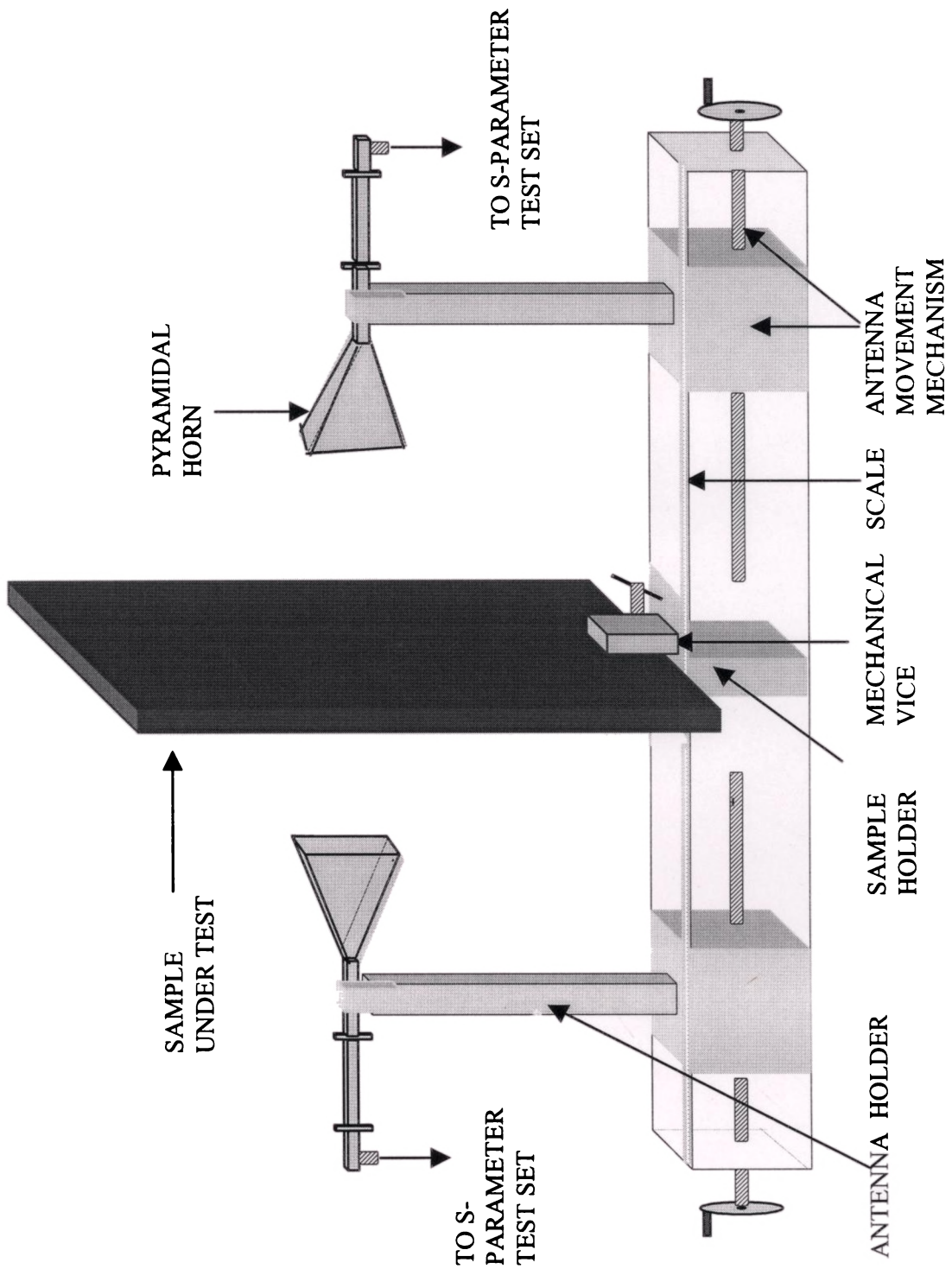


Figure 2.6 Schematic diagram of the test bench

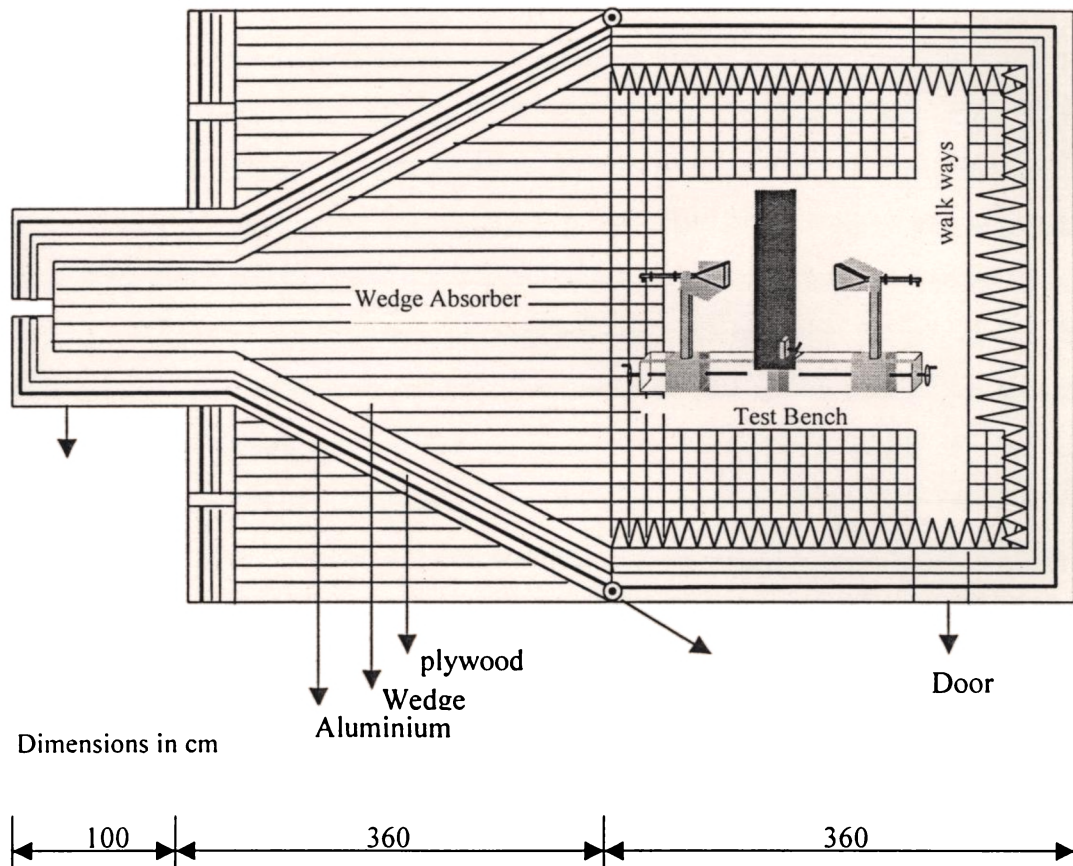


Figure 2.7 The schematic diagram of the anechoic chamber

2.3.3 Measurement technique and Procedure

To begin with, the system is calibrated using THRU-REFLECT-LINE (TRL) calibration. Two horn antennas of the same band are mounted on the two antenna holders of the test bench. The antennas are positioned nearly at a distance of 1 m (greater than the far field distance of the horn antennas, $\frac{2D^2}{\lambda}$ where D is the large dimension of the antenna) from the sample holder so that the wave impinging on the sample will be plane wave. During THRU calibration, the antennas are kept on-axis and the network analyser system performs a series of measurements (S_{11} , S_{22} , S_{21} , S_{12} etc) and then it waits for the next calibration. For REFLECT calibration, we place a metal plate at the sample holder of the test bench and give the keyboard entry for S_{11} and S_{22} . After this calibration, LINE calibration is to be done. Before giving the entry for this calibration, antennas are to be moved for the distance set in the network analyser. The distance set in the analyser is to be taken carefully so that the necessary conditions are satisfied. The detailed description of TRL calibration, criteria of selecting LINE length and accuracy conditions are given in the *appendix 2.1*. After completing the calibration, the whole calibration can be stored in any one of the Cal set available in the network analyser. The antennas are then moved to the original position (THRU position) from the LINE position and the system is now ready for measurement. A metal sheet is placed at the sample holder and the time domain band pass response is taken to verify the calibration. If the calibration is correct, the maximum of the time domain response will be at zero seconds both for S_{11} and S_{22} as shown in the *figure 2.8*. The maximum at zero second indicates that the reference position is set at the position of the metallic plate. The response of transmission coefficient in the THRU position without any sample is shown in *figure 2.9*. After checking the performance of calibration, the sample materials in the form of sheets are kept at the sample holder and S_{11} or S_{22} and/or S_{12} or S_{21} whichever is needed, is saved in the computer.

For each band, TRL calibration should be separately done. Accordingly, the LINE lengths are to be changed. While taking the measurement with the sample placed at the sample holder, gating can also be applied for better accuracy. It is noted

that gating span from the centre to both the sides should be the same. Otherwise it would make a considerable error in the phase data, which in effect affects the final result. In order to minimise the edge diffraction, the sample size should be more than 5λ . S_{11} and S_{21} are measured after fixing sample sheet at the reference plane.

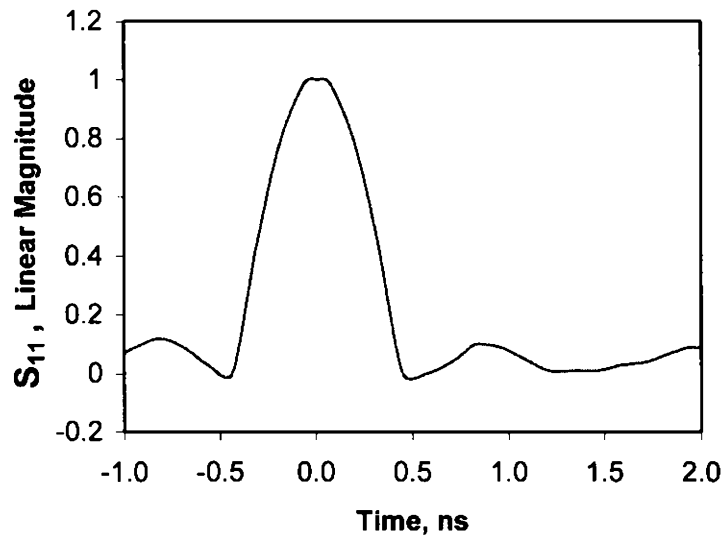


Figure 2.8 Time domain response of S_{11} with a metal plate at the sample holder

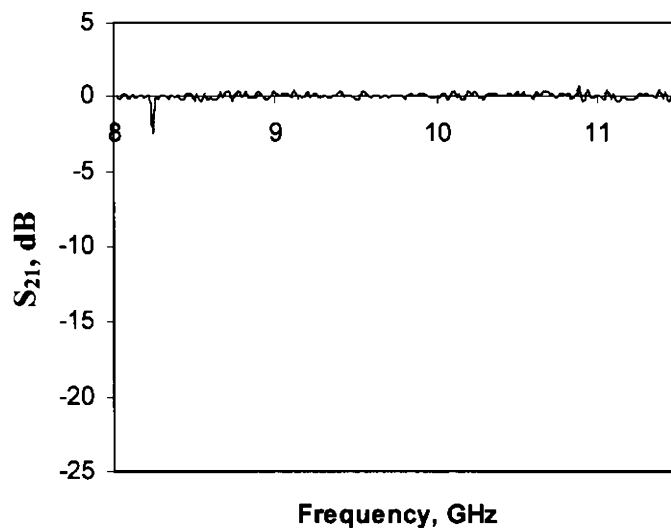


Figure 2.9 Transmission coefficient after TRL calibration

Effective dielectric constant of Non-Interactive Distributive (NID) mixture of dielectrics can also be found from the S-parameter measurements. For that, sample sheets are kept together at the sample holder for the measurement. This method can be extended to any number of samples of known thickness.

The samples considered for the study are polystyrene (thickness 4 mm), glass (thickness 4.76 mm), glass epoxy (thickness 1.56 mm), cement (thickness 5.8 mm). The compound samples are polystyrene-glass (thickness 8.76 mm), polystyrene-glass epoxy (thickness 5.56 mm), polystyrene-cement (thickness 9.8 mm).

2.3.4 Experimental results for solid samples

2.3.4.1 Results from reflection measurements

The samples are clamped at the sample holder of the microwave test bench as shown in *figure 2.6* and reflected data are taken and stored in the computer. Then equation (2.6) is solved to get 'x', which in turn gives complex permittivity. The results obtained in J and X bands are shown in *tables 2.1 and 2.2*.

Table 2.1 Complex permittivity of different materials in J-band calculated from the reflection coefficient

Frequency (GHz)	Material							
	Polystyrene (thickness 4 mm)		Glass (thickness 4.76 mm)		Glass Epoxy (thickness 1.56 mm)		Cement (thickness 5.8 mm)	
	ϵ_r	$\tan \delta$	ϵ_r	$\tan \delta$	ϵ_r	$\tan \delta$	ϵ_r	$\tan \delta$
5.20	2.69	0.070	5.000	0.153	3.50	0.288	3.13	0.255
5.30	2.64	0.066	4.95	0.152	3.52	0.290	3.07	0.254
5.40	2.65	0.064	4.85	0.147	3.49	0.272	3.02	0.253
5.50	2.62	0.067	4.73	0.150	3.47	0.269	2.97	0.254
5.60	2.60	0.057	4.66	0.143	3.47	0.256	2.93	0.254
5.70	2.58	0.055	4.60	0.140	3.46	0.245	2.88	0.257
5.80	2.55	0.050	4.56	0.144	3.44	0.238	2.84	0.259
5.90	2.53	0.046	4.51	0.154	3.42	0.241	2.80	0.262
6.00	2.51	0.045	4.47	0.149	3.4	0.223	2.77	0.265
6.10	2.49	0.043	4.44	0.158	3.37	0.216	2.74	0.270
6.20	2.47	0.040	4.41	0.156	3.36	0.208	2.71	0.273
6.30	2.46	0.037	4.38	0.162	3.33	0.211	2.687	0.277
6.40	2.43	0.036	4.36	0.167	3.31	0.199	2.662	0.282
6.50	2.50	0.035	4.35	0.177	3.21	0.201	2.64	0.286
6.60	2.40	0.033	4.32	0.178	3.26	0.193	2.62	0.291
6.70	2.35	0.039	4.26	0.183	3.27	0.186	2.60	0.296
6.80	2.37	0.030	4.28	0.191	3.22	0.193	2.58	0.301
6.90	2.39	0.032	4.20	0.189	3.19	0.192	2.56	0.304

Table 2.2 Complex permittivity of different materials in X-band calculated from the reflection coefficient

Frequency (GHz)	Material							
	Polystyrene (thickness 4 mm)		Glass (thickness 4.76 mm)		Glass Epoxy (thickness 1.56 mm)		Cement (thickness 5.8 mm)	
	ϵ_r	$\tan \delta$	ϵ_r	$\tan \delta$	ϵ_r	$\tan \delta$	ϵ_r	$\tan \delta$
8.0	2.60	0.029	5.50	0.010	3.61	0.211	2.41	0.254
8.2	2.49	0.035	5.45	0.006	3.73	0.167	2.41	0.300
8.4	2.60	0.115	5.31	0.003	3.55	0.251	2.34	0.346
8.6	2.66	0.078	5.17	0.011	3.68	0.148	2.56	0.295
8.8	2.62	0.037	5.04	0.021	3.89	0.177	2.67	0.379
9.0	2.67	0.010	4.94	0.269	3.57	0.188	2.22	0.402
9.2	2.56	0.018	4.76	0.031	3.51	0.206	2.18	0.387
9.4	2.63	0.003	4.67	0.035	3.60	0.204	2.01	0.437
9.6	2.64	0.007	4.59	0.040	3.58	0.208	2.15	0.414
9.8	2.68	0.029	4.46	0.040	3.44	0.240	2.29	0.364
10.0	2.67	0.009	4.34	0.046	3.19	0.271	2.11	0.439
10.2	2.55	0.012	4.23	0.046	3.35	0.206	2.26	0.492
10.4	2.58	0.050	4.16	0.046	3.47	0.260	2.02	0.448
10.6	2.88	0.011	4.12	0.047	3.36	0.273	2.19	0.371
10.8	2.68	0.059	4.02	0.042	3.29	0.281	2.03	0.650
11.0	2.60	0.027	3.96	0.040	3.22	0.301	2.45	0.324
11.2	2.63	0.022	3.87	0.036	3.47	0.295	1.98	0.926
11.4	2.40	0.110	3.83	0.034	3.14	0.304	2.00	0.563
11.6	2.64	0.079	3.81	0.027	3.08	0.316	1.89	0.588
11.8	2.64	0.120	3.78	0.025	2.98	0.337	1.96	0.623

Results show that the real part of complex permittivity agrees well with the results from other methods [8]. But the imaginary part shows a difference in comparison with the standard values. Also the real and imaginary parts don't show a monotonic variation, which is the inherent property of free space method.

2.3.4.2 Limitations and Accuracy Conditions

It is noted that the accuracy is reduced when we take measurements in higher frequency bands. In the present study on J and X bands, X band measurements have lesser accuracy. The accuracy can be increased by using highly focussed beams. The inherent limitation of all free space methods is that the accuracy in the loss tangent of the materials is poor [11]. Another major drawback of free space methods is that, very thick samples in comparison with the wavelength when used, will create an ambiguity in the phase values. The following precautions have been taken care of in the experiment to ensure better results.

1. The positions of sample holder and antenna mount are well fixed. Slight change in its position while calibration and measurement will be a source of error in the data especially in the phase. The phase is very critical in the permittivity measurements. Also, it is ensured that the angle of incidence is normal.
2. The distance moved for LINE calibration (corresponding to delay time set in the line standard 15 of the network analyser) is accurate.
3. The number of points is set to maximum and sweep is in step mode. Averaging can also be applied for more accuracy.
4. The calibrating metal plate (used for Reflection calibration in TRL calibration) and samples are uniform and kept vertical. Bending of samples or metal plate will make considerable error.
5. Sample is placed exactly at the reference plane (the position of metal sheet in the Reflect Calibration). A small change in the position can cause a major error. To avoid the error, sample holding mechanism in the sample holder should be firm.
6. In order to minimise the edge diffraction, samples of size more than 5λ are taken.
7. The exponential term in the equation (2.6) is expanded upto a maximum power of 10 for convergence with an accuracy of the order of 0.001 for all samples. It is found that the convergence is faster for low loss materials.

2.3.4.3 Results from Transmission measurements

After calibrating the set up, the accuracy of calibration is verified. Measurement can be performed as explained in the reflection part. After placing the sample in the sample holder S_{21} is noted/stored for the whole frequency range of the calibrated band. The data can be stored in any of the formats Real-Imaginary or Real-Phase or both the parameters separately. The results are derived after the data obtained is substituted in the MATHEMATICA program and it gives the result. The results obtained are tabulated in the following *tables 2.3 and 2.4*.

Table 2.3 Complex permittivity of different materials in J-band calculated from the transmission coefficient

Frequency (GHz)	Material							
	Polystyrene (thickness 4 mm)		Glass (thickness 4.76 mm)		Glass Epoxy (thickness 1.56 mm)		Cement (thickness 5.8 mm)	
	ϵ_r	$\tan \delta$	ϵ_r	$\tan \delta$	ϵ_r	$\tan \delta$	ϵ_r	$\tan \delta$
5.1	2.65	0.084	5.33	0.303	3.91	0.077	3.75	0.253
5.2	2.55	0.101	5.25	0.314	3.80	0.087	3.82	0.137
5.3	2.54	0.097	5.29	0.286	3.79	0.079	3.71	0.208
5.4	2.64	0.081	5.26	0.296	3.77	0.082	3.70	0.235
5.5	2.65	0.085	5.19	0.272	3.71	0.068	3.20	0.247
5.6	2.7	0.065	5.26	0.291	3.73	0.080	3.27	0.288
5.7	2.74	0.043	5.12	0.271	3.67	0.077	3.13	0.272
5.8	2.76	0.047	5.24	0.288	3.7	0.078	3.09	0.280
5.9	2.78	0.070	5.11	0.217	3.60	0.110	3.06	0.285
6.0	2.8	0.034	5.2	0.290	3.68	0.076	2.99	0.238
6.1	2.63	0.067	5.08	0.317	2.95	0.127	2.88	0.301
6.2	2.43	0.020	5.15	0.295	3.65	0.074	2.75	0.333
6.3	2.84	0.096	5.17	0.193	3.55	0.104	2.74	0.408
6.4	2.74	0.003	5.08	0.297	3.63	0.074	2.70	0.415
6.5	2.72	0.035	5.017	0.314	3.51	0.066	2.87	0.334
6.6	2.85	0.015	5.01	0.297	3.61	0.078	2.72	0.363
6.7	2.55	0.052	4.90	0.353	3.49	0.114	2.61	0.430
6.8	2.86	0.034	4.96	0.288	3.59	0.081	2.55	0.488

Table 2.4 Complex permittivity of different materials in X-band
from the transmission coefficient

Frequency (GHz)	Material							
	Polystyrene (thickness 4 mm)		Glass (thickness 4.76 mm)		Glass Epoxy (thickness 1.56 mm)		Cement (thickness 5.8 mm)	
	ϵ_r'	$\tan \delta$	ϵ_r'	$\tan \delta$	ϵ_r'	$\tan \delta$	ϵ_r'	$\tan \delta$
8.0	2.38	0.120	5.42	0.023	3.69	0.079	2.71	0.363
8.2	2.59	0.115	5.40	0.020	3.68	0.078	2.66	0.359
8.4	2.10	0.110	5.36	0.014	3.71	0.087	2.82	0.394
8.6	2.66	0.010	5.33	0.010	3.66	0.087	2.52	0.490
8.8	2.12	0.122	5.29	0.004	3.58	0.079	2.41	0.367
9.0	2.61	0.069	5.28	0.002	3.44	0.097	2.69	0.288
9.2	2.42	0.113	5.26	0.0002	3.71	0.096	2.32	0.566
9.4	2.36	0.046	5.26	0.0004	3.51	0.109	2.15	0.514
9.6	2.63	0.112	5.25	0.0002	3.37	0.093	2.49	0.452
9.8	2.45	0.077	5.25	0.001	3.39	0.118	2.16	0.569
10.0	2.64	0.038	5.25	0.004	3.26	0.127	2.24	0.556
10.2	2.15	0.120	5.25	0.007	3.30	0.123	2.09	0.601
10.4	2.64	0.068	5.25	0.011	3.28	0.118	2.18	0.583
10.6	2.61	0.034	5.24	0.018	3.27	0.120	2.26	0.550
10.8	2.26	0.106	5.24	0.026	3.22	0.132	2.15	0.469
11.0	2.55	0.019	5.23	0.030	3.35	0.125	2.03	0.542
11.2	2.66	0.098	5.21	0.040	3.37	0.082	2.01	0.624
11.4	2.59	0.066	5.20	0.045	3.12	0.111	1.98	0.650
11.6	2.64	0.018	5.19	0.050	3.01	0.152	2.03	0.654
11.8	2.59	0.004	5.18	0.050	3.17	0.150	1.92	0.753

2.3.4.4 Limitations and Accuracy Conditions

The accuracy conditions mentioned in the section 2.3.4.2 (Nos. 1,2,3,6 & 7) are valid for the transmission measurements also and are hence not mentioned here.

The conditions other than these are

1. After calibration, a low loss sample is placed at the sample holder and the sum of the reflected and transmitted power is noted. If the sum is not unity, that indicates that there is some error in the calibration. Then the system needs re-calibration to avoid error in the results.
2. The thickness of the calibrating metal sheet causes a constant phase error in the transmission data. Therefore a phase difference corresponding to the thickness of the sheet is added to the data for the evaluation of the dielectric parameters.
3. The exponential term in the equation (2.8) is expanded to higher terms so that it makes the exponent to converge to a fixed value. Normally, a power of 10 is sufficient for all types of materials. It is observed that an accuracy level of the order of 0.001 is achieved for various samples.

Complex permittivity is also calculated by the simultaneous solution of equations (2.6) and (2.8) ie, S_{11} and S_{21} values. It is found that the computational time is high and the accuracy is more or less the same as individual solutions from S_{11} and S_{21} . Dielectric parameters of certain materials for selected frequencies are given in table 2.4a

Table 2.4a Complex Permittivity of samples from simultaneous solution of S_{11} and S_{21}

Frequency (GHz)	Material					
	Polystyrene (thickness 4 mm)		Glass (thickness 4.76 mm)		Glass Epoxy (thickness 1.56 mm)	
	ϵ_r'	$\tan \delta$	ϵ_r'	$\tan \delta$	ϵ_r'	$\tan \delta$
5	2.90	0.051	6.00	0.007	3.97	0.091
5.2	2.83	0.040	5.88	0.026	3.83	0.075
5.4	2.78	0.031	5.70	0.058	3.71	0.061
5.6	2.72	0.024	5.61	0.085	3.59	0.046
5.8	2.67	0.018	5.55	0.110	3.48	0.031
6	2.62	0.013	5.56	0.131	3.37	0.016
6.2	2.56	0.007	5.63	0.153	3.27	0.008
6.4	2.52	0.002	5.75	0.175	3.18	0.018
6.6	2.47	0.005	5.85	0.207	3.10	0.037
6.8	2.44	0.013	5.91	0.258	3.04	0.058

2.3.5 Measurement and Results of NID compounds

Compound materials are generally formed by combining two or more dielectric sheets. In the present study compounds considered are constructed from two sheets kept together (polystyrene-glass, polystyrene-glass epoxy, polystyrene-cement) at the sample holder. S_{11} and S_{21} corresponding to these compounds are stored and permittivity is found out from these data using the equations (2.6) and (2.8) for the two bands of frequencies. The results are given in the following tables 2.5 & 2.6.

Table 2.5 Complex permittivity of different NID compounds in J and X-bands calculated from the reflection coefficient

Frequency (GHz)	Polystyrene-Glass (thickness 8.76 mm)		Polystyrene-Glass Epoxy (thickness 5.56 mm)		Polystyrene-Cement (thickness 9.8 mm)	
	ϵ'_r	$\tan \delta$	ϵ'_r	$\tan \delta$	ϵ'_r	$\tan \delta$
5.2	4.10	0.151	2.98	0.256	2.820	0.276
5.4	3.90	0.174	2.93	0.239	2.892	0.196
5.6	3.70	0.194	2.89	0.225	2.615	0.209
5.8	3.52	0.210	2.83	0.208	2.700	0.164
6.0	3.35	0.224	2.79	0.197	2.573	0.153
6.4	3.40	0.094	2.72	0.176	2.007	0.173
6.6	3.26	0.082	2.68	0.168	2.406	0.421
6.8	3.13	0.073	2.66	0.158	2.467	0.306
8.2	3.190	0.121	2.661	0.124	2.567	0.182
8.6	3.813	0.081	2.423	0.215	2.128	0.338
9.0	3.001	0.097	2.772	0.101	2.821	0.145
9.4	3.522	0.033	2.838	0.075	2.131	0.265
9.8	3.647	0.056	2.670	0.089	2.451	0.214
10.2	3.673	0.125	2.504	0.065	2.323	0.220
10.6	3.924	0.054	2.916	0.100	2.555	0.256
11.0	3.309	0.068	2.725	0.145	2.011	0.143
11.4	3.257	0.065	2.008	0.160	2.274	0.108
11.8	3.190	0.111	2.506	0.119	2.222	0.219

Table 2.6 Complex permittivity of different NID compounds in J and X-bands calculated from the transmission coefficient

Frequency (GHz)	Polystyrene-Glass (thickness 8.76 mm)		Polystyrene-Glass Epoxy (thickness 5.56 mm)		Polystyrene-Cement (thickness 9.8 mm)	
	ϵ_r'	$\tan \delta$	ϵ_r'	$\tan \delta$	ϵ_r'	$\tan \delta$
5.2	3.913	0.444	2.97	0.024	2.876	0.098
5.4	3.997	0.139	2.94	0.024	2.673	0.243
5.6	3.914	0.256	2.92	0.024	3.001	0.307
5.8	3.823	0.200	2.90	0.021	3.265	0.126
6.0	3.899	0.389	2.89	0.021	2.844	0.180
6.2	4.008	0.276	2.88	0.017	2.603	0.258
6.4	4.126	0.216	2.91	0.019	2.886	0.253
6.6	4.249	0.196	2.85	0.014	2.640	0.304
6.8	3.991	0.222	2.991	0.093	2.656	0.209
8.2	4.127	0.211	2.689	0.103	2.312	0.287
8.6	4.086	0.165	2.934	0.075	2.610	0.181
9.0	3.930	0.157	2.816	0.070	3.004	0.114
9.4	3.671	0.099	2.243	0.081	3.090	0.201
9.8	3.407	0.001	2.003	0.209	2.999	0.324
10.2	3.435	0.197	2.704	0.174	2.385	0.269
10.6	3.225	0.124	3.126	0.066	2.442	0.217
11.0	3.219	0.225	2.954	0.123	2.681	0.188
11.4	3.188	0.144	2.827	0.188	2.284	0.296
11.8	3.261	0.066	2.713	0.106	2.008	0.333

2.3.5.1 Verification of Results with Theory

The complex permittivity of the constituents of the compound has already been measured from reflection and transmission coefficient for two bands of frequencies (*tables 2.1, 2.2, 2.3 & 2.4*) and their values are in good agreement with the standard values. Substituting these values in (2.13), the theoretical values for the compound can be obtained. The obtained values given in *tables 2.7 and 2.8* can be compared with the measured values of the compounds given in *tables 2.5 and 2.6*.

Table 2.7 Complex permittivity of different NID compounds calculated theoretically from reflection measurements

Frequency (GHz)	Polystyrene-Glass		Polystyrene-Glass Epoxy		Polystyrene-Cement	
	ϵ'_r	$\tan \delta$	ϵ'_r	$\tan \delta$	ϵ'_r	$\tan \delta$
5.2	3.945	0.127	2.917	0.143	2.950	0.186
5.4	3.845	0.121	2.886	0.135	2.869	0.182
5.6	3.719	0.116	2.844	0.125	2.795	0.179
5.8	3.642	0.114	2.800	0.115	2.722	0.179
6.0	3.575	0.116	2.760	0.107	2.664	0.180
6.2	3.524	0.119	2.720	0.098	2.612	0.183
6.4	3.479	0.125	2.677	0.093	2.567	0.187
6.6	3.443	0.132	2.641	0.088	2.530	0.191
6.8	3.408	0.140	2.608	0.086	2.494	0.196
8.2	4.098	0.014	2.838	0.084	2.443	0.190
8.6	4.024	0.031	2.946	0.103	2.601	0.204
9.0	3.903	0.188	2.923	0.071	2.404	0.224
9.4	3.738	0.025	2.902	0.073	2.263	0.231
9.8	3.647	0.036	2.893	0.099	2.449	0.214
10.2	3.463	0.035	2.774	0.078	2.378	0.282
10.6	3.554	0.034	3.015	0.093	2.472	0.200
11.0	3.339	0.035	2.774	0.116	2.511	0.198
11.4	3.177	0.060	2.608	0.176	2.163	0.358
11.8	3.259	0.060	2.735	0.186	2.238	0.381

Table 2.9 Difference between experimental and theoretical values for reflection measurements

Frequency (GHz)	Polystyrene-Glass		Polystyrene-Glass Epoxy		Polystyrene-Cement	
	$\Delta \epsilon_r'$	$\Delta \tan \delta$	$\Delta \epsilon_r'$	$\Delta \tan \delta$	$\Delta \epsilon_r'$	$\Delta \tan \delta$
5.2	0.155	0.024	0.063	0.113	-0.130	0.090
5.4	0.055	0.053	0.044	0.104	0.023	0.014
5.6	-0.019	0.078	0.046	0.100	-0.180	0.030
5.8	-0.122	0.096	0.030	0.093	-0.022	-0.015
6.0	-0.225	0.108	0.030	0.090	-0.091	-0.027
6.2	0.016	-0.015	0.030	0.087	0.211	-0.026
6.4	-0.079	-0.031	0.043	0.083	-0.560	-0.014
6.6	-0.183	-0.050	0.039	0.080	-0.124	0.230
6.8	-0.278	-0.067	0.052	0.072	-0.027	0.110
8.2	-0.908	0.107	-0.177	0.040	0.124	-0.008
8.6	-0.211	0.050	-0.523	0.112	-0.473	0.134
9.0	-0.902	-0.091	-0.151	0.030	0.417	-0.079
9.4	-0.216	0.008	-0.064	0.002	-0.132	0.034
9.8	0	0.020	-0.223	-0.010	0.002	0
10.2	0.210	0.090	-0.270	-0.013	-0.055	-0.062
10.6	0.370	0.020	-0.099	0.007	0.083	0.056
11.0	-0.030	0.033	-0.049	0.029	-0.500	-0.055
11.4	0.080	0.005	-0.600	-0.016	0.111	-0.250
11.8	-0.069	0.051	-0.229	-0.067	-0.016	-0.162

Table 2.10 Difference between experimental and theoretical values for transmission measurements

Frequency (GHz)	Polystyrene-Glass		Polystyrene-Glass Epoxy		Polystyrene-Cement	
	$\Delta \epsilon_r'$	$\Delta \tan \delta$	$\Delta \epsilon_r'$	$\Delta \tan \delta$	$\Delta \epsilon_r'$	$\Delta \tan \delta$
5.2	-0.104	0.192	0.069	-0.072	-0.426	-0.028
5.4	-0.067	-0.093	-0.017	-0.057	-0.594	0.059
5.6	-0.177	0.033	-0.069	-0.046	-0.036	0.100
5.8	-0.285	-0.014	-0.124	-0.037	0.310	-0.065
6.0	-0.205	0.179	-0.157	-0.027	-0.068	0.022
6.2	0.100	0.059	0.108	-0.023	-0.016	0.044
6.4	0.114	0.011	-0.080	-0.008	0.170	0.008
6.6	0.225	-0.010	-0.213	-0.022	-0.133	0.087
6.8	-0.010	0.017	-0.074	0.044	-0.021	-0.081
8.2	0.029	0.197	-0.149	0.019	-0.131	0.097
8.6	0.062	0.134	-0.012	-0.028	0.009	-0.023
9.0	0.027	-0.031	-0.107	-0.001	0.600	-0.110
9.4	-0.067	0.074	-0.659	0.008	0.827	-0.030
9.8	-0.240	-0.035	-0.890	0.110	0.550	0.110
10.2	-0.028	0.162	-0.070	0.096	0.007	-0.013
10.6	-0.329	0.090	0.111	-0.027	-0.030	0.017
11.0	-0.120	0.190	0.180	0.007	0.170	-0.010
11.4	0.011	0.084	0.219	0.012	0.121	-0.062
11.8	0.002	0.006	-0.022	-0.080	-0.230	-0.048

Great care should be taken not to trap air between the samples when they are placed together at the sample holder for taking measurement on the compound. The air trap will deteriorate the accuracy of the complex permittivity.

2.4 Complex permittivity measurements of liquids

2.4.1 Theoretical formulation

In the case of the measurement of dielectric properties of liquids, a container for the experimental liquid is unavoidable. So, the propagation of waves through five media, medium 1 to medium 5, should be considered as shown in *figure 2.10*. The problem is complex due to the presence of four dielectric interfaces. As many of the liquid samples are lossy, development of theory necessitates the inclusion of loss terms also.

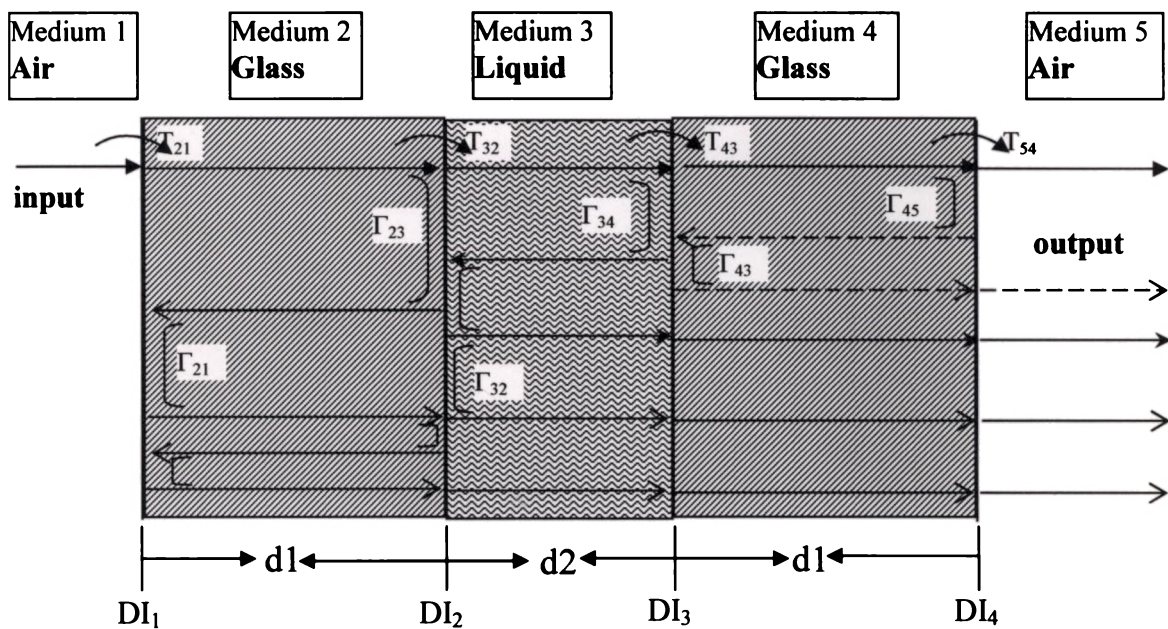


Figure 2.10 Propagation of an e.m. wave through a liquid in a container

Let the thickness of the glass plate be 'd1' and the thickness of the liquid column is 'd2'. The parameters defining the system such as impedance, phase change, transmission and reflection coefficients are given as

$$\text{impedance of medium 1 (air), } \eta_1 = 377 \, \Omega$$

$$\text{impedance of medium 2 (glass), } \eta_2 = \frac{\eta_1}{\sqrt{x}} \Omega,$$

x is relative the complex permittivity of glass (known)

$$\text{impedance of medium 3 (liquid), } \eta_3 = \frac{\eta_1}{\sqrt{y}} \Omega,$$

y is the complex permittivity of liquid (to be found out)

Reflection coefficients and transmission coefficients at different interfaces as shown in *figure 2.10* are given below.

Transmission coefficients

$$T_{21} = \frac{2\eta_2}{\eta_1 + \eta_2}$$

$$T_{32} = \frac{2\eta_3}{\eta_2 + \eta_3}$$

$$T_{43} = \frac{2\eta_4}{\eta_3 + \eta_4}$$

$$T_{54} = \frac{2\eta_5}{\eta_4 + \eta_5}$$

Reflection coefficients

$$\Gamma_{21} = \frac{\eta_1 - \eta_2}{\eta_1 + \eta_2}$$

$$\Gamma_{32} = \frac{\eta_2 - \eta_3}{\eta_2 + \eta_3}$$

$$\Gamma_{43} = \frac{\eta_3 - \eta_4}{\eta_3 + \eta_4}$$

$$\Gamma_{54} = \frac{\eta_4 - \eta_5}{\eta_4 + \eta_5}$$

θ_1 , θ_2 and θ_3 are the phase changes occurring at the media, medium 2 (glass), medium 3 (liquid) and medium 4 (glass) respectively. Since many of the liquids are medium loss or high loss, attenuation factor should also be considered while calculating the phase factor.

$$\theta_1 = \gamma_1 d_1 = (\alpha_1 + j\beta_1)d_1 \quad (2.14)$$

$$\theta_2 = \gamma_2 d_2 = (\alpha_2 + j\beta_2)d_2 \quad (2.15)$$

$$\theta_3 = \gamma_1 d_1 = (\alpha_1 + j\beta_1)d_1 \quad (2.16)$$

where ' γ ' is the propagation constant defined as $\gamma = \alpha + j\beta$, where ' α ' represents the attenuation term and ' β ' represents the phase constant. The values of ' α ' and ' β ' are defined as

$$\alpha = \frac{\omega\sqrt{\mu\epsilon}}{\sqrt{2}} \sqrt{\sqrt{1 + \left(\frac{\sigma}{\omega\epsilon}\right)^2} - 1} \quad (2.17)$$

$$\beta = \frac{\omega\sqrt{\mu\epsilon}}{\sqrt{2}} \sqrt{\sqrt{1 + \left(\frac{\sigma}{\omega\epsilon}\right)^2} + 1} \quad (2.18)$$

Definition of operators

Defining appropriate operators for multiple reflection and transmission will make the theoretical treatment easy. The operator should facilitate the signature (percentage of the available input) of a signal at the output port. The multiple reflections between the dielectric interfaces should be effectively incorporated into the theory through the use of the operator.

The output (through the interface DI_4) of a signal considered at any interface could be facilitated by operator 'O'.

The emerging signal from the interface DI₄ due to a signal just inside the interface DI₁ is given by the operating that signal by the operator O₁, given by

$$O_1 = T_{54}T_{43}T_{32}e^{-j(\theta_1+\theta_2+\theta_3)} \quad (2.19)$$

The emerging signal from the interface DI₄ due to a signal just inside the interface DI₂ is given by operating that signal by the operator O₂, given by

$$O_2 = T_{54}T_{43}e^{-j(\theta_2+\theta_3)} \quad (2.20)$$

Similarly, the emerging signal from the interface DI₄ due to a signal just inside DI₃ is given by operating that signal by the operator O₃, given by

$$O_3 = T_{54}e^{-j(\theta_3)} \quad (2.21)$$

Different terms contributing the power at the output

Considering the dielectric interface DI₁, the amplitude of the wave just inside the medium 2 is given by T₂₁. The effect of this wave at the output is O₁• T₂₁. A part of T₂₁, (Γ₂₃T₂₁e^{-j(θ₁)}) will be reflected back from DI₂ towards DI₁. This will be again reflected at DI₁ and this term is defined by (Γ₂₃Γ₂₁T₂₁e^{-j(2θ₁)}). The effect of this wave at the output is given by O₁• (Γ₂₃Γ₂₁T₂₁e^{-j(2θ₁)}). Thus defining all the reflections occurring inside the medium 2, we will get a series term which is represented below.

$$\text{set 1} = O_1 T_{21} [1 + \Gamma_{23}\Gamma_{21}e^{-j(2\theta_1)} + \Gamma_{23}^2\Gamma_{21}^2e^{-j(4\theta_1)} + \dots]$$

$$= O_1 T_{21} \frac{1}{1 - \Gamma_{21} \Gamma_{23} e^{-j2\theta_1}} \quad (2.22)$$

Multiple reflections in the third medium and their effect at the output is given by

$$\begin{aligned} \text{set 2} &= T_{54} T_{43} e^{-j(\theta_2 + \theta_3)} \times T_{21} T_{32} \Gamma_{34} \Gamma_{32} e^{-j(\theta_1 + 2\theta_2)} [1 + \Gamma_{34} \Gamma_{32} e^{-j(2\theta_2)} + \\ &\Gamma_{34}^2 \Gamma_{32}^2 e^{-j(4\theta_2)} + \dots] \\ &= O_2 T_{21} T_{32} \Gamma_{34} \Gamma_{32} e^{-j(\theta_1 + 2\theta_2)} \frac{1}{1 - \Gamma_{34} \Gamma_{32} e^{-j2\theta_2}} \quad (2.23) \end{aligned}$$

Multiple reflections in the fourth medium and their effect at the output is given by

$$\text{set3} = O_3 T_{43} \Gamma_{45} \Gamma_{43} T_{32} T_{21} e^{-j(\theta_1 + \theta_2 + 2\theta_3)} \frac{1}{1 - \Gamma_{45} \Gamma_{43} e^{-j2\theta_3}} \quad (2.24)$$

The same procedure is applied to get the following terms, which contribute power to the output.

$$\text{set4} = O_2 T_{32} \Gamma_{21} \Gamma_{23} T_{21} e^{-j(3\theta_1)} \frac{1}{1 - \Gamma_{34} \Gamma_{32} e^{-j2\theta_2}} \quad (2.25)$$

$$\text{set5} = O_2 T_{32} \Gamma_{21}^2 \Gamma_{23}^2 T_{21} e^{-j(5\theta_1)} \frac{1}{1 - \Gamma_{34} \Gamma_{32} e^{-j2\theta_2}} \quad (2.26)$$

$$\text{set6} = O_2 T_{32} \Gamma_{21}^3 \Gamma_{23}^3 T_{21} e^{-j(7\theta_1)} \frac{1}{1 - \Gamma_{34} \Gamma_{32} e^{-j2\theta_2}} \quad (2.27)$$

$$\text{set7} = O_1 \Gamma_{21} T_{23} T_{21} T_{32} \Gamma_{34} e^{-j(2\theta_1 + 2\theta_3)} \frac{1}{1 - \Gamma_{21} \Gamma_{23} e^{-j2\theta_1}} \quad (2.28)$$

$$\text{set8} = O_2 \Gamma_{34} \Gamma_{32} T_{32} \Gamma_{21} T_{23} T_{21} T_{32} \Gamma_{34} e^{-j(3\theta_1+4\theta_2)} \quad (2.29)$$

$$\text{set9} = O_2 \Gamma_{32} T_{34} \Gamma_{45} T_{43} T_{32} T_{21} e^{-j(\theta_1+2\theta_2+2\theta_3)} \quad (2.30)$$

$$\text{set10} = O_1 \Gamma_{21} T_{23} T_{34} \Gamma_{45} T_{43} T_{32} T_{21} e^{-j(2\theta_1+2\theta_2+2\theta_3)} \quad (2.31)$$

There are infinite numbers of such reflected signals. For ease of computation, contributions from terms less than 1% of the incident signal is neglected.

$$S_{\text{total}} = \text{set1} + \text{set2} + \text{set3} + \text{set4} + \text{set5} + \text{set6} + \text{set7} + \text{set8} + \text{set9} + \text{set10} \quad (2.32)$$

The transmission coefficient obtained from the network analyzer is approximated as S_{total} and substituted in to the above equation.

Equation (2.32) is solved to get the value of complex permittivity of liquid. MATHEMATICA 3.0 is used for the calculation.

2.4.2 Experimental set-up and method of measurement

The set-up is the same as that discussed in the case of dielectric sheets with the only change of addition of a container. Schematic cross sectional view of the container with liquid is shown in the *figure 2.11*.

Table 2.12 Complex permittivity of oil and methanol at X-band

Frequency (GHz)	Oil at X-band		Methanol at X-band	
	ϵ_r'	$\tan \delta$	ϵ_r'	Tan δ
8.56	3.18	0.283	7.35	1.480
8.88	2.24	0.134	6.89	1.485
9.20	2.55	0.125	6.44	1.491
9.52	2.55	0.125	6.01	1.496
9.84	2.55	0.125	5.59	1.503
10.16	2.55	0.125	5.74	1.415
10.48	2.55	0.125	5.88	1.333
10.80	2.55	0.125	5.33	1.418
11.12	2.55	0.125	5.47	1.333

It is observed that the values obtained do not vary much from the standard values [8].

The development of the theory and the reflection measurements are not carried out since they are quite in line with the transmission case.

2.5 Summary

A novel, non-contact, non-destructive method for determining the scattering characteristics of free waves from the samples in the planar form is developed. The novelty of this method is that the measurements are done using the ordinary pyramidal horns of nominal gain without incorporating any focusing mechanism. Necessary theoretical formulation required for the implementation of this method is done. To facilitate the measurements on scattering parameters, a microwave test bench is designed and constructed. TRL calibration is adopted for carrying out experiments in J (5-7 GHz) and X (8-12 GHz) bands. Solid planar samples like polystyrene, glass, glass epoxy and cement of various thickness are characterized using the method.

The existing theory for Non-Interactive Distributive (NID) dielectrics is modified for the free space method. Two dielectric sheets combined together is taken as the NID sample and the scattering parameters are experimentally determined using free waves and the effective dielectric constant is evaluated. The obtained values are then compared with the theoretically computed values. Measurements are done for the characterization of polystyrene-glass, polystyrene-glass epoxy and polystyrene-cement NID compounds.

The theory of free space method for material characterization is modified to adapt it for the case of liquids. Scattering from the four dielectric interfaces in the planar container containing the liquid sample is evaluated and used for determining the relative complex permittivity of the sample. The experimentally obtained transmission coefficient is utilized for computing the complex permittivity of the liquid. The permittivity values for Methanol, Ethanol, Oil and Water are evaluated using this method and are compared with the standard values.

Different accuracy conditions and limitations of the method are also discussed.

References

1. G. W. Chantry, "Infrared and Millimetre Waves", Vol.8, K.J. Button, Ed. New York:Academic Press, Chapter 1, pp. 1-49.
2. W. K. Tam and V. N. Tran, "Propagation modeling for indoor wireless communication", IEE Electronics and Communication Engineering Journal, Vol. 7, pp. 221-228, 1995.
3. Internet document: URL:
<http://www.cc.jyu.fi/~ngerman/HANNIBAL/NNIB/Papers/TP18.pdf>
4. W. W. Ho, "High temperature millimeter wave dielectric dielectric characterization of radome materials", Proc. SPIE Int. Soc. Opt. Eng., Vol. 362, pp. 190-195, 1982.
5. V. R. K. Murthy, S. Sundaram, B. Viswanathan (Editors), "Microwave Materials", Ch. 2, Narosa Publishing House, 1993.
6. M. N. Afsar, James R. Birch and R. N. Clarke, "The measurement of the properties of materials", Proc. of the IEEE, Vol. 74, No. 1, pp. 183-199, January 1986.
7. D. Glay, T. Lasri, A. Mamouni and Y. Leroy, "Free space moisture profile measurement", Proc. Electromagnetic wave Interaction with water and moist Substances, Weimar, Germany, pp. 235-242, 2001.
8. Musil and Zacek. Microwave measurements of complex permittivity by free space methods and their applications, Elsevier, 1986.
9. Y.Huang and M. Nakhkash, "Characterisation of layered dielectric medium using reflection coefficient", Electronics Letters, vol. 34, No. 12, pp. 1207-1208, June 1998.
10. D.K. Ghodgaonkar, V. V. Varadan and V. K. Varadan, "A Free-Space method for measurement of dielectric constants and loss tangents at microwave frequencies", IEEE Trans. on Instrumentation and Measurement, Vol. 37, No. 3, pp. 789-793, June 1989.
11. D. K. Ghodgaonkar, V. V. Varadan and V. K. Varadan, "Free-space measurement of complex permittivity and complex permeability of magnetic materials at microwave frequencies", IEEE Trans. on Instrumentation Measurement, Vol. 39, No. 2, pp. 387-394, April 1990.

12. Gerhard L. Friedsam and Erwin M. Biebl, "A Broadband Free-space dielectric properties measurement system at millimeter wavelengths", *IEEE Trans. on Instrumentation Measurement*, Vol. 46, No.2, pp.515-518, April 1997.
13. Neelakanta. P. S., Abeygunawardana. S and De Groff. D, "Free-Space method of measuring complex permittivity of fast-ion conductors at microwave frequencies using pelleted samples", *Conference Southcon*, pp. 224-225, 29-31 March 1994.
14. Juan Munoz, Marta Rojo, Alfredo Parreno and Jose Margineda, "Automatic measurement of permittivity and permeability at microwave frequencies using normal and oblique free-wave incidence with focused beam", *IEEE Trans. Instrumentation and Measurement*, Vol.47, No. 4, pp. 886-892, August 1998.
15. T. Lasri, D. Glay, A. Mamouni and Y. Leroy, "Non-destructive testing of materials by microwave systems", *Electronics letters*, Vol. 34, No. 5, pp. 470-471, March 1998.
16. H. Stuart Whitney and M.M.Z. Kharadly, "Some results on Low-level microwave treatment of the mountain pine beetle and the darkling beetle", *IEEE Trans. on Microwave Theory and Techniques*, Vol. 32, No. 8, pp. 798-802, August 1984.
17. Dion T. Fralick, "W-band Free Space Permittivity Measurement Setup for Candidate Radome Materials" *NASA Contractor Report 201720*, Contract NAS1-96014, August 1997.
18. Ferenc Volgyi, "Microwave NDT of Particleboards", *Proceedings of the 12th International Symposium on Nondestructive Testing of Wood University of Western Hungary, Sopron*, 13-15 September 2000.
19. Maher H. Umari, D.K. Ghodgaonkar, V. V. Varadan and V.K. Varadan, "A Free-Space Bistatic Calibration Technique for the measurement of parallel and perpendicular reflection coefficients of planar samples", *IEEE Trans. on Instrumentation and Measurement*, Vol. 40, No.1, pp. 19-24, February 1991.
20. P.G. Friederich and Rick L. Moore, "Free space EM measurement system", *Proc. URSI Radio Science Meeting*, Seattle, Washington. USA. p. 390. 1994.
21. Ding-Bing Lin and Tah-Hsiung Chu, "Polarization effects in bistatic microwave diversity imaging of two perfectly conducting cylinders", *Proc. APS-Int. Symp.*, Seattle, Washington, USA, pp. 1982-1985, June 1994.

22. Kaida Bin Khalid, "A portable microwave moisture meter for lossy liquids", Proc. Asia Pacific Microwave Conferene, Japan, pp. 477-481, 1994.
23. V.K. Varadan and V. V. Varadan, "Free Space measurement techniques for chiral composites", Proc. Progress in Electromagnetics Research Symposium (PIERS), Massachusetts, USA, 1991.
24. S.K. Sharma, P.K. Mukherjee and K. P. Singh, "Bistatic microwave remote sensing of gram at 9.5 GHz", Proc. IV International symposium on recent advances in microwave Technology, New Delhi, pp. 479-482, 1993.
25. A. W. Kraszewski, S. Trabelsi and S. O. Nelson, "Broadband Free-space microwave wheat permittivity measurements", Proc. Electromagnetic wave Interaction with water and moist Substances, Weimar, Germany, pp. 195-202, 2001.
26. S. Okamura and Y. Zhang, " New Method for Moisture Content Measurement Using Phase Shifts at Two Microwave Frequencies", J. of Microwave Power and Electromagnetic Energy, Vol. 35, No. 3, pp. 175-178, 2000.
27. K. A. Jose, V. K. Varadan, V. V. Varadan, "Wideband And Noncontact Characterization of The Complex permittivity Of Liquids", Microwave and Optical Technology Letters, Vol. 30, No. 2, pp. 75-79, July 2001.
28. Richard D. Hollinger, K. A. Jose, Anilkumar Tellakula, V. V. Varadan and V. K. Varadan, "Microwave Characterization Of Dielectric Materials From 8 To 110 GHz Using A Free-Space Setup", Microwave and Optical Technology Letters, Vol. 26, No. 2, pp. 100-105, July 2000.
29. C. A. Balanis, "Advaced Engineering Electromagnetics", John Wiley & Sons, 1989.
30. K.P. Thakur, K.J. Cresswell, M. Bogosanovich, and W.S. Holmes, "Non-interactive and distributive property of dielectrics in mixture", Electronics Letters, Vol.35, No.14, pp.1143-1144, 1999.

Appendix 2.1: Implementation of TRL calibration method

The process of implementing the TRL calibration method in a user-specified environment is defined in four steps

1. Selecting standards appropriate for the application
2. Defining the standards by modification of the internal calibration kit registers
3. Performing the calibration
4. Checking the performance

Requirements for TRL standards

Standard	Requirements
Zero Length THRU	<p>S_{21} and S_{12} are defined equal to 1 at 0 degrees (typically used to set the reference plane)</p> <p>S_{11} and S_{22} are defined equal to zero</p>
REFLECT	<p>Phase of Γ must be known within $\pm \frac{1}{4}$ wavelength.</p> <p>Must be the same Γ on both ports.</p> <p>May be used to set the reference plane if the phase response of the REFLECT is well known and specified.</p>
LINE	<p>Z_0 of the LINE establishes the reference impedance after error correction is applied.</p> <p>Insertion phase of the LINE must never be the same as that of the THRU.</p> <p>Optimal LINE length is $\pm \frac{1}{4}$ wavelength or 90 degrees relative to the THRU at the center frequency.</p> <p>Insertion phase or electrical length need only be specified within $\frac{1}{4}$ wavelength.</p>

Selection of Optimal LINE Length

Optimal LINE length is $\frac{1}{4}$ wavelength or 90 degrees relative to the THRU at the center frequency. Line Length is (LINE-THRU). If the lower and upper cut off frequencies of the bands are f_1 and f_2 GHz respectively, then the electrical length, 'l' is $\frac{15}{f_1(\text{GHz})+f_2(\text{GHz})}$. With this electrical length, insertion phase is to be calculated using the expression

$$\begin{aligned} \text{Phase (degrees)} &= \frac{360 \times f \times l}{c} \\ &= 12 \times f(\text{GHz}) \times l(\text{cm}) \end{aligned}$$

The insertion phase for f_1 and f_2 is to be calculated and it should be in between 20 and 160 degrees. If this condition is not satisfied, line length is to be slightly adjusted for getting the insertion phase with in the specified range.

Defining TRL standards

The standards selected should be entered into the calibration kit registers of the HP 8510C Network analyser. It can be done from the CAL menu and from the then sub menu MODIFY CAL1/2. THRU options are set in the calibration standard number 14, REFLECT in the 18 and LINE options in 15 and 16. Multiple LINE lengths can be incorporated using the two LINE standards. The corresponding offset delays and impedances should be set for each standards and saved.

Performing the calibration

To begin with, the fixture is connected to the coaxial test ports and desired stimulus conditions for measurements such as start frequency, stop frequency, number of points, power level, averaging are set in the network analyser. In the CAL menu, press TRL 2-PORT and this menu will give different options such as THRU, S11REFLECT, S22REFLECT, ISOLATION and LINE. This can performed in any convenient order. Pressing SAVE TRL CAL will enable to save the calibration coefficients in the desired calibration number. Error correction is automatically turned on.

Checking the Performance

Verification kits are available in the coaxial connector family. These kits contain devices whose characteristics are precisely and independently known. When these devices are measured, the difference between the displayed results and the known values indicate the level of measurement accuracy. In non-coaxial cases, these verification devices do not exist. However, there are some performance checks. Connection repeatability can be evaluated. Take a single S-parameter measurement and store its response into memory. Break the connection, reconnect the same device, and then re-measure. It will give the performance of the calibration.

GPR technique for Buried Object Detection

Ground Penetrating Radar (GPR) technique for detection of buried objects is carried out in this chapter. Theoretical simulations using Finite Difference Time Domain (FDTD) method for buried dielectric systems are done. Detection of various roots and other dielectric objects is carried out using time domain analysis of reflected signal. Experimental results for void detection and leak detection are also presented.

3.1 Introduction

The objects placed on top of a clear field are easily detectable. But if they are buried even a few centimeters under the soil, then the detection creates serious problems for an investigator. The detection and ranging of such systems is of immense importance in many fields of life and has been the subject of intensive research for the past few decades. The field 'Ground Penetrating Radar (GPR)' explores objects under ground using electromagnetic waves. Ground penetrating radar (sometimes called ground probing radar, georadar, subsurface radar, earth sounding radar) is a nondestructive and noninvasive method that produces a cross-sectional profile or record of subsurface features. These profiles give the information of the location of buried objects and is used for subsurface exploration, characterization and monitoring. It is widely used in locating lost utilities, environmental site characterization and monitoring, agriculture, archaeological and forensic investigation, unexploded ordnance and land mine detection, groundwater exploration, pavement and infrastructure characterization, mining, void and tunnel detection, sinkholes detection, and a lot of other applications [1-5]. The systems, which detect human subjects under earthquake rubble or debris, are developed by scientists [6].

The subsurface sensing and imaging problem is an information problem. ie, the information about a subsurface target from scattered and distorted waves received above the surface. Imaging techniques can be described by the properties of probe wave, the wave propagation characteristics of the medium and surface, and the nature of target/probe interaction. The technique is the same as that in other fields like underwater imaging, medical imaging inside the body, 3D biological microscopies inside a cell or collection of cells.

Ground penetrating radar operates by transmitting ultra high frequency radio waves down into the ground through a transducer or antenna. The transmitted energy is reflected from various buried objects or distinct contacts between different earth materials. The antenna then receives the reflected waves and stores them in the digital control unit. The antennas generally used are: simple dipoles, loaded dipoles, folded dipoles, bowtie, logarithmic spiral, end fire, slot, fractal, arrays etc.

Wavelength of the propagating electromagnetic wave determines the resolution of the system. Resolution increases with increasing frequency. The accessibility of sophisticated instruments operating with high dynamic range has enabled the scientists to use higher microwave frequencies [7]. Depth of investigation varies from less than a meter to more than kilo meters. It increases with decreasing frequency but only at the cost of resolution. Detectability of objects under ground depends on their size, shape, and orientation relative to the antenna, contrast with the host medium, as well as radiofrequency noise and interferences. Radiofrequency interference is mainly from radio, television, cellular phones, air traffic control, computers and geological noise.

In this chapter, some of the GPR applications are demonstrated at higher microwave frequencies (X and Ku bands). The experiment is conducted employing the versatile Vector Network Analyser (VNA), HP 8510C, which is having high dynamic range. An antenna kept in free space is used as a transmitter, and the same antenna receives the scattered power. The antenna used for the study is an ordinary pyramidal horn of nominal gain, which makes the study more appealing. Setting the network analyzer in the time domain mode and analyzing the obtained time domain response will give the information of the different discontinuities encountered in the path. The network analyzer does the measurement in the frequency domain, and it is then converted to time domain. The internal high-speed computer in the HP 8510C performs this calculation using Chirp-Z Fourier Transform computation techniques [8]. The time domain data will be displayed in the near real time.

Using the GPR method, different types of dielectric objects, roots, void and leakage are detected. The theoretical simulation of the scattered field from various objects is also carried out. The reflection coefficient from objects buried at different depths is derived from the simulation results. As the complex real situations could not be completely incorporated in the simulation, a close comparison between the experimental results and the simulated results is not possible. The simulation results are given in the first section of the chapter and the experimental results in the latter section. The factors to be included in the simulation for the near approximation to the real situation are also mentioned in the experimental section.

This chapter discusses the following categories of GPR applications:

- ❖ Theoretical analysis of the buried dielectric objects
- ❖ Detection of single and multiple dielectric blocks
- ❖ Roots detection
- ❖ Void detection
- ❖ Leakage detection

3.2 Review of the past work

Larsen and Jacobi [1], dedicates a chapter to video pulse radars and their application. Here the implementation of video pulse radar for the subsurface exploration is reviewed and the potentiality of it in the biological imaging is discussed.

Daniel [2] presents a detailed discussion on properties of materials at the frequencies usually used for GPR applications, different types of antennas used for GPR applications, modulation techniques, system design and different signal processing methods.

Many scientists [3-7] had been enthusiastically working in the different areas of GPR applications. Strongman [5] gives a detailed picture of the forensic applications of GPR. Chen et al. [6] describe the development of life-detection systems from debris.

Wang Xiande et al. [9] make an elaborate theoretical analysis on the scattering of electromagnetic wave by an object buried in ground. They prove the validity of the method by the numerical computations based on the moment method. They also discuss the effect of roughness of surface and bark layer on the scattering parameter of a target.

Kenneth Demarest et al. [10] calculated the fields scattered by the buried objects when the sources are close enough to the air/ground interface. Theoretical simulation of the scattered field is also done using FDTD technique. The authors show how a frequency-domain representation of the transmitted field can be used in

conjunction with the FDTD technique when the incident field is a plane wave generated by a distant antenna.

Degradation in performance of the buried mine detection by clutter is compensated by employing multi-static synthetic focusing from a 2-D real aperture [11]. The authors have described the implementation of the method, influence of different parameters such as clutter, ground condition etc. They have designed a system with an antenna array operating at a frequency of 1 GHz, which avoids clutters very well. The authors discuss different performance-limiting factors in detail and the steps to be taken to overcome these. Validation of the system was done by FDTD and they have done it using sandbox experiments with different objects like metal and plastic targets. They extended the experiments to outdoor environments also and developed Real-aperture synthetically organised radar (RASOR) system.

G. R. Olhoeft et al. [12] used a surface ground penetrating radar system to locate and measure the electromagnetic scattering different buried objects like pipes, wires, metal, plastic mines etc. This paper also presents the results of electrical and magnetic properties of a mixture and discusses the electromagnetic dispersion effects and the change of pulse shape due to the constructive and destructive interference, multipathing, multiple scattering etc. Different objects like steel and plastic mines, PVC pipe etc were buried at different depths and their position are found out for different frequencies. They employed HP 8753 network analyser for the characterisation of soil samples and GPR measurements were done by the SIR-10A+ GPR system, which is commercially available.

Ballard. N et al. discuss the details of the complex permittivity of the medium where the buried objects are deployed [13]. It enables one to predict the electrical delay for the electromagnetic wave to travel through the dielectric. The system consists of an electrically short monopole antenna backed by a ground plane and its performance is checked by immersing the antenna in the standard dielectrics such as pure water and salt water.

The scattering coefficient of an undulating surface is estimated by Calla and Sharma [14]. They report that the scattering coefficient increases with the soil moisture content and it is found that the value with vertical polarization is lower than that with horizontal polarization.

Jacqueline M. Bourgeois and Glenn S. Smith [15] describe a system composed of air, soil and buried land mine and is modeled using the FDTD method. They employ two parallel dipole antennas housed in corner reflectors tuned to a frequency of 790 MHz.

The electromagnetic scattering from buried land mines is discussed by Lawrence Carin et al [16]. They extensively study the conducting and plastic mines taking into account of the lossy, dispersive and potentially layered properties of soil. The theoretical model is used to predict wave phenomenology in various environments. They characterize the soil at different conditions before the mines (M20 anti-tank mine) are deployed.

Thomas P. Montoya and Glenn S. Smith [17] detect land mines using resistively loaded Vee Dipoles. They have developed 3D FDTD model and it is used to simulate the GPR land mine detection problem. In the study, they consider two types of land mines, the Italian TS-50 and VS-50. The properties of the pulse to be employed are also described in detail.

David Wong and Lawrence Carin [18] analyse the radar cross section of two types of mines using Ultra wide-band synthetic aperture radar (UWB SAR). In the paper, authors have shown the experimental and theoretical results in association with the two types of mines M20 and Valmara.

In a recent paper, M. B. Silevitch [19] discusses the possibility of application of Physics Based Signal Processing (PBSP) for the unification of subsurface sensing and other imaging techniques.

Maxwell's equations were replaced by a set of finite difference equations by K. S. Yee [20], which was a breakthrough in electromagnetics. Scattering of electromagnetic pulse by a perfectly conducting cylinder was demonstrated by him.

The paper described the grid size, boundary conditions and stability criterion. In the last part of the paper, the computed results using the present method were compared with the known results on diffraction of pulses by a wedge.

Gerrit Mur [21] presents highly absorbing boundary conditions for electromagnetic field equations that can be used for both two and three-dimensional configurations. Numerical results are proved considering the radiation pattern of an isotropic point source.

Numerical dispersion of the Time Average (TA) and Time-Forward (TF) schemes and their stability properties by the analytical methods are analysed by Jose A. Pereda et al. [22]. In the concluding remarks, they mention that for the treatment of lossy dielectrics using FDTD method, the TA scheme is better than the TF scheme.

R. J. Luebbers et al. [24] redefined Yee's FDTD equations incorporating the dispersive nature of the dielectrics. The accuracy of the extension was demonstrated by computing the reflection coefficient at an air-water interface over a wide frequency band. Later, the authors extended the work to N^{th} order dispersive media [25].

Jeffrey L. Young [26] describes the space-time profile of an electromagnetic wave in a Lorentz dielectric and a Debye medium. The effectiveness of the proposed numerical schemes is demonstrated by considering the one-dimensional slab problem. The results show that the dispersive nature of the medium significantly corrupts the original shape of the pulse.

William H. Weedon and C. M. Rappaport [27] generalise the dispersive nature of media and it is included in FDTD modelling of wave propagation. Two approaches are described in the paper: frequency-dependant complex permittivity and frequency dependant complex conductivity and the stability of these two approaches are also compared.

A method to efficiently and accurately compute a time-domain waveform from a network-analyser frequency-domain measurement is presented in a recent

paper [28]. The method is based on a robust interpolation technique to construct a pole-residue representation of the response of the device-under test and the validity is proved by considering some examples. This is more advantageous than the discrete Fourier transform.

Zoran A. Maricevic et al. [29] describe the enhancement of accuracy in the time domain measurements of the network analysers using Generalized Pencil of Function (GPOF) method (Matrix Pencil Method). This technique gives more accuracy than the conventional technique, Fourier transform that is employed in the network analysers.

J.T. Johnson et al. [30] discuss the detectability conditions of GPR systems. The detection of non-metallic anti-personal land mines are complicated due to low dielectric contrast. The methods to increase the dielectric contrast is discussed. In this paper, waveguide studies of target detection through a controlled depth of nitrogen penetration are reported, and it is shown that scattering from known depth targets can be significantly enhanced if an optimal amount of nitrogen is added.

3.3 Theoretical Analysis

The aim of the theoretical work is to simulate the scattering of waves by the buried objects and to obtain response of reflected signal from different objects placed at different depths.

Theoretical work is carried out on the model system as shown in *figure 3.1*. A dielectric medium is assumed to be filled in an area and the object(s) are buried in it. A wave/pulse signal is allowed to propagate from air and the scattered signal is obtained at different points of the system. Generally any type of wave (Gaussian pulse, Sine wave etc) can be assumed to be propagated from the source plane. In the present study, a gaussian pulse is considered to propagate from the source plane and the information about the buried object is obtained from the scattered field. The responses received at three test points P1, P2 and P3 at each time step are taken. Time domain response at P1 oriented in line with the buried object is compared with that from P2 and P3 and the information of the object is extracted.

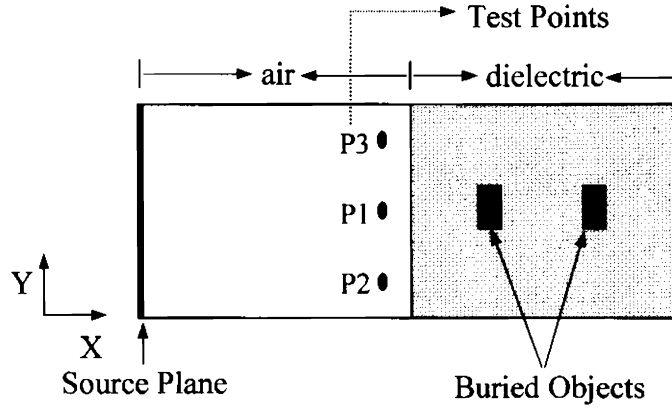


Figure 3.1 Schematic Diagram of the theoretical system

In the first set of simulation, a single rectangular object is assumed to be buried under ground at a depth of 8 cm from the air-dielectric interface. The dielectric medium is considered to be non-dispersive, linear, homogenous and isotropic. The discretized Maxwell's expressions [20] are the basis of the Finite Difference Time Domain (FDTD) method.

$$\text{Discretizing Maxwell's curl equations, } \nabla \times E = -\frac{\partial B}{\partial t} \text{ and } \nabla \times H = \frac{\partial D}{\partial t}$$

For a Transverse magnetic (TM) wave, $E_x = E_y = 0$ and $H_z = 0$

$$\frac{H_x(i, j, t+1) - H_x(i, j, t)}{dt} = -\frac{(E_z(i, j, t) - E_z(i, j-1, t))}{\mu_0 dy} \quad (3.1)$$

$$\frac{H_y(i, j, t+1) - H_y(i, j, t)}{dt} = \frac{(E_z(i, j, t) - E_z(i-1, j, t))}{\mu_0 dx} \quad (3.2)$$

$$\frac{E_z(i, j, t+1) - E_z(i, j, t)}{dt} =$$

$$\frac{(H_y(i+1, j, t) - H_y(i, j, t))}{\varepsilon dx} - \frac{(H_x(i, j+1, t) - H_x(i, j, t))}{\varepsilon dy} \quad (3.3)$$

In the real sense, both the buried objects and the surrounding medium are dispersive in nature. When the soil is wet, the dispersive nature becomes more prominent [1,2]. Incorporating the dispersive nature of the dielectric medium [23,24] in the constitutive FDTD equations, the electric and magnetic fields in a non-magnetic medium is given by

$$H_x(i, j, t+1) = H_x(i, j, t) - \frac{dt}{\mu_0 dy} (E_z(i, j, t) - E_z(i, j-1, t)) \quad (3.4)$$

$$H_y(i, j, t+1) = H_y(i, j, t) + \frac{dt}{\mu_0 dx} (E_z(i, j, t) - E_z(i-1, j, t)) \quad (3.5)$$

and

$$\begin{aligned} E_z(i, j, t+1) = & \frac{\epsilon_\infty}{\epsilon_\infty + \chi_0(i, j)} E_z(i, j, t) + \frac{1}{\epsilon_\infty + \chi_0(i, j)} \sum_{m=0}^{t-1} E_z(i, j, t-m) \Delta\chi_m(i, j) \\ & + \frac{dt}{(\epsilon_\infty + \chi_0(i, j))\epsilon_0 dx} (H_y(i+1, j, t) - H_y(i, j, t)) - \\ & \frac{dt}{(\epsilon_\infty + \chi_0(i, j))\epsilon_0 dy} (H_x(i, j+1, t) - H_x(i, j, t)) \quad (3.6) \end{aligned}$$

where

$$\chi_0(i, j) = (\epsilon_s - \epsilon_\infty) (1 - \exp(-dt/t_0)), \text{ time domain susceptibility function}$$

Above equation is obtained from complex frequency domain relative permittivity equation $\epsilon(\omega) = \epsilon_\infty + \frac{\epsilon_s - \epsilon_\infty}{1 + j\omega t_0}$ and frequency domain susceptibility function

$$\chi(\omega) = \frac{\epsilon_s - \epsilon_\infty}{1 + j\omega t_0}$$

$$\Delta\chi_m(i, j) = (\epsilon_s - \epsilon_\infty) \exp(-m dt/t_0) (1 - \exp(-dt/t_0))^2 ,$$

ϵ_s , the static permittivity of the dielectric, ϵ_∞ , the optical permittivity of the dielectric t_0 , the relaxation time of the dielectric and μ_0 , the permeability of free space.

Since the medium is assumed to be non-magnetic, the Yee equation for H field is kept unchanged.

The Gaussian pulse in time is given by

$$E_y(0,t) = E_0 e^{-(t-t_0)^2 / \tau^2} \quad (3.7)$$

In the Gaussian pulse, the parameter ' τ ' determines the width of the pulse. The time shift ' t_0 ' is chosen so that $t_0 \geq 2\tau$.

A Gaussian pulse with $dt = 16.667$ ps, $T_0 = 41.667$ ps was executed at the source plane. Yee cell was constructed from 140 grids in the X-direction and 80 grids in Y-direction with a grid spacing $dx = 0.005$ m and $dy = 0.005$ m respectively. Grid size is chosen so that the computational stability [18], $\sqrt{(dx)^2 + (dy)^2} \geq cdt$ (Courant-Friedrichs-Lewy condition) is satisfied.

Mur's absorbing boundary conditions [21] are applied at the boundaries. An object of dimensions 7cm x 3cm ($\epsilon_r = 3$) is placed at a distance of 8 cm from the air-dielectric interface inside the dielectric medium ($\epsilon_r = 2$). The response of the gaussian pulse with time is computed. The dielectric profiles of the theoretical system (in two orientations) are shown in *figures 3.2a & 3.2b*. Z-axis of the *figure 3.2a* represents the permittivity values. The movement of Gaussian pulse with respect to time is shown in the *figures 3.3a-3.3d*. In the *figures 3.3a and 3.3b*, the gaussian pulse is progressively moving along the X-direction. Z-axis of the *figures 3.3a-3.3d* represent the amplitude of the gaussian pulses. The situation after 150 time steps is depicted in *figure 3.3c*. It clearly shows the scattering of the pulse at the discontinuities. When the time step is increased to 220, many more reflections are found to occur from the different discontinuities. The comparison of the characteristics of the fields at different points gives the information of the region where the object is buried.

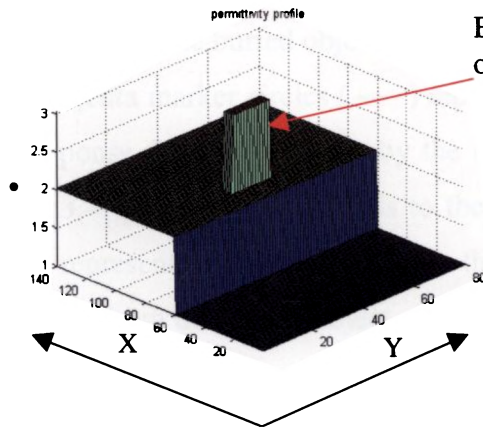


Figure 3.2a Dielectric profile of the system

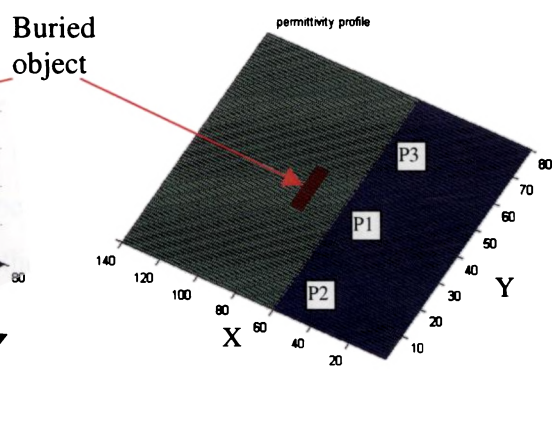


Figure 3.2b Top view of the system

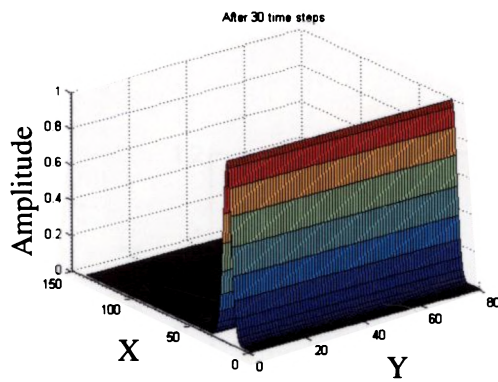


Figure 3.3a Position of gaussian pulse after 30 time steps

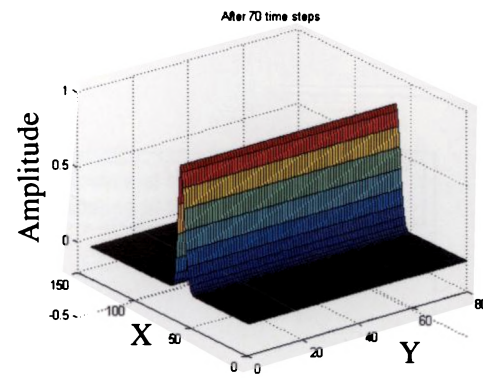


Figure 3.3b Position of gaussian pulse after 70 time steps

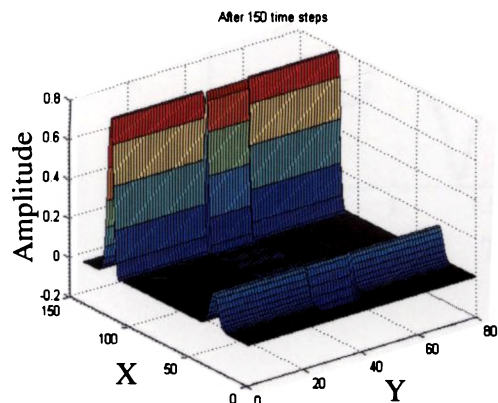


Figure 3.3c Scattered field after 150 time steps

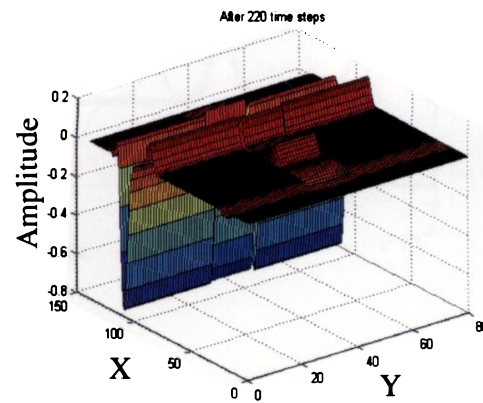


Figure 3.3d Scattered field after 220 time steps

The time domain responses from the three test points P1, P2 and P3 give the information of the buried object. This fact is explicit from *figure 3.4*. The green line with magenta marker circles ($\text{---}\circ\text{---}$) represents the response at the points P2 & P3 and the response from P1 is given by the red lines with blue cross markers ($\text{---}\times\text{---}$). In *figure 3.4*, peak R1 corresponds to the forward moving gaussian pulse. R2 in the figure represents the reflection from the air-dielectric interface. R3 represents the reflection from the buried object. R4 is the signal obtained from the back surface of the object. The reflected pulse from the air-dielectric interface will move towards source plane and it is again reflected back from the source plane(see *figure 3.1*). This can be considered as a secondary wave and is moving towards the dielectric and is recorded as R5. A small dip after the peak R5 corresponds to the reflected signal from the air-dielectric interface due to this second source.

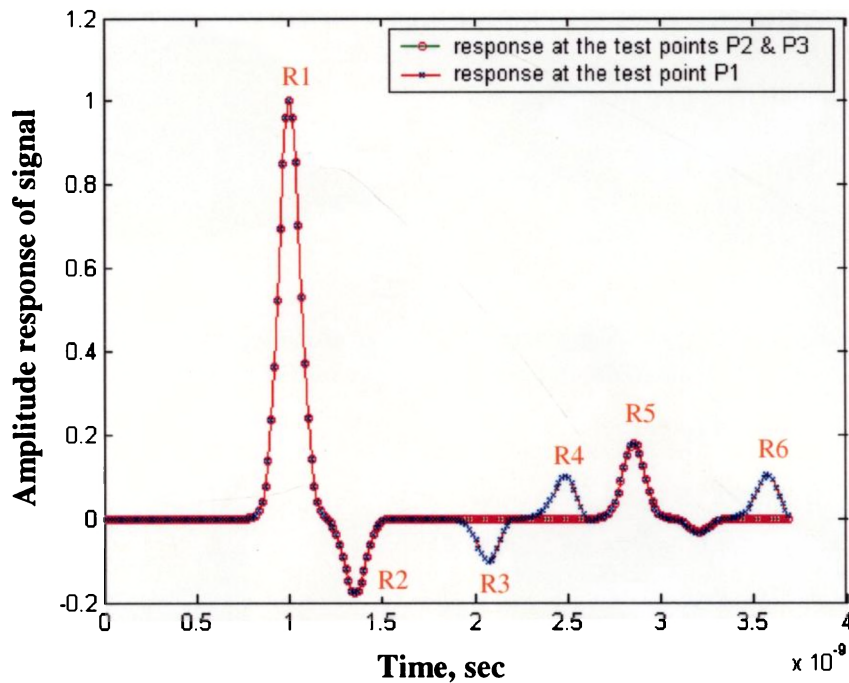


Figure 3.4 Theoretical time domain responses from the system with a buried object, $\epsilon_r = 3$

Figures 3.5a & 3.5b represent the theoretical system with two buried objects of same dielectric constant ($\epsilon_r = 3$) in a dielectric medium ($\epsilon_r = 2$). The buried objects considered are at a depth of 8 cm and 18 cm from the air-dielectric interface as shown in figures 3.5a & 3.5b. The scattered fields at different time steps are shown in the figures 3.6a-3.6d. The time domain response at three points P1, P2 and P3 are shown in the figure 3.7. In the response, peak R1 corresponds to the forward moving gaussian pulse, R2 is the reflection from the air-dielectric interface, R3 is the reflection from the front face of the first buried object, R4 is the signal obtained from the back surface of the object and R5 is the reflected signal from the source plane. In addition to these, dip R6 corresponds to the reflected signal from the second buried object. R7 is the signal reflected from the back end of the second object and R8 corresponds to the reflected signal from the end of the vessel.

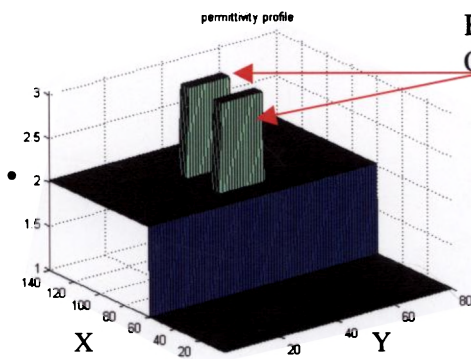


Figure 3.5a Permittivity profile of the system with two objects buried

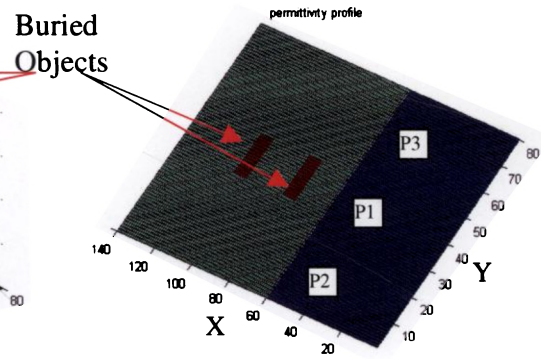


Figure 3.5b Top view of the system with two objects buried

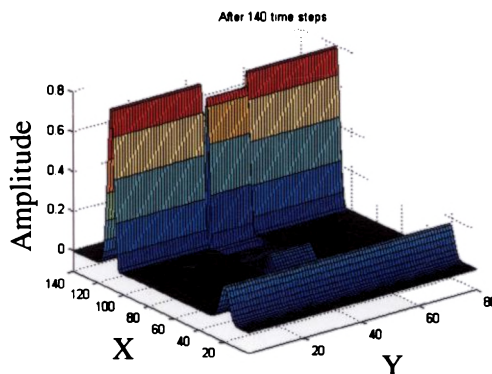


Figure 3.6a Scattered field after 140 time steps

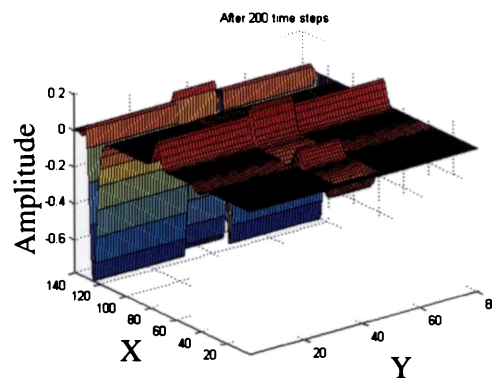


Figure 3.6b Scattered field after 200 time steps

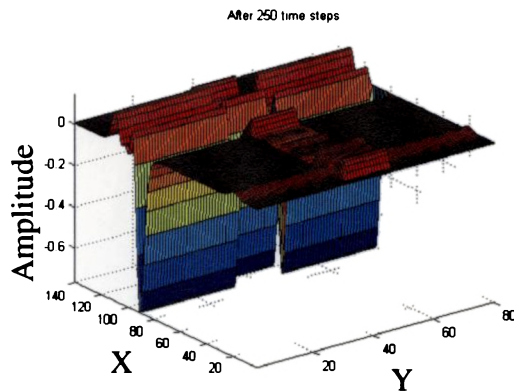


Figure 3.6c Scattered field after 250 time steps

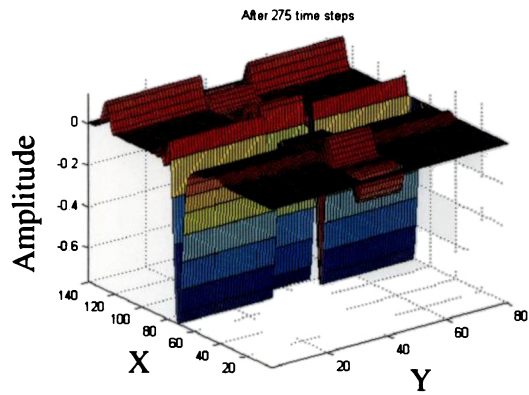


Figure 3.6d Scattered field after 275 time steps

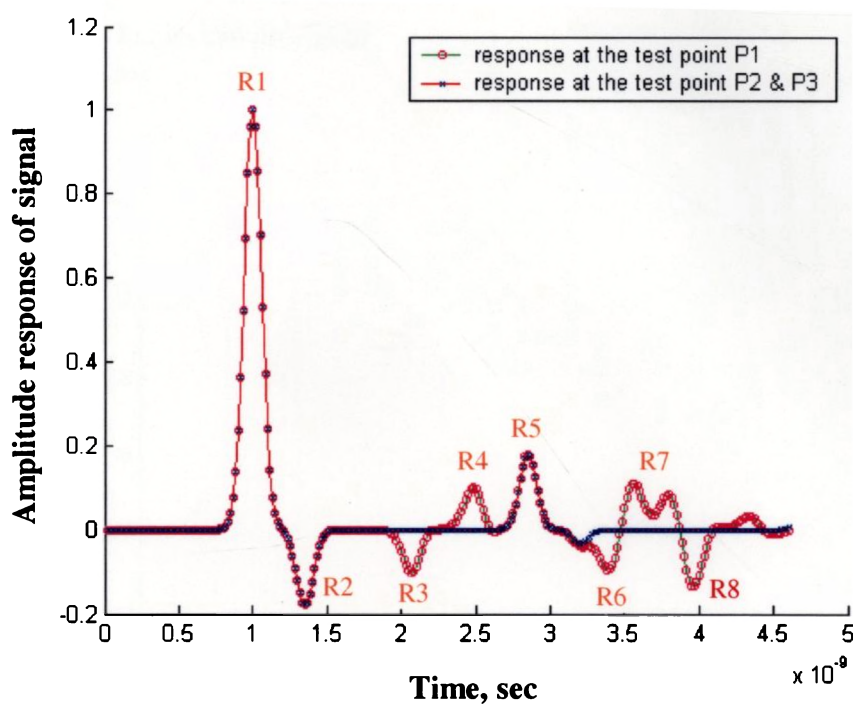


Figure 3.7 Theoretical time domain responses from the system with two buried objects ($\epsilon_r = 3$) in line

It is observed that the theoretical time domain responses in each case shows the signature of the buried object clearly.

3.3.1 Response from a Void

A void is simulated at a depth of 8 cm as shown in *figures 3.8a & 3.8b* and the response from this system is shown in *figure 3.9*.

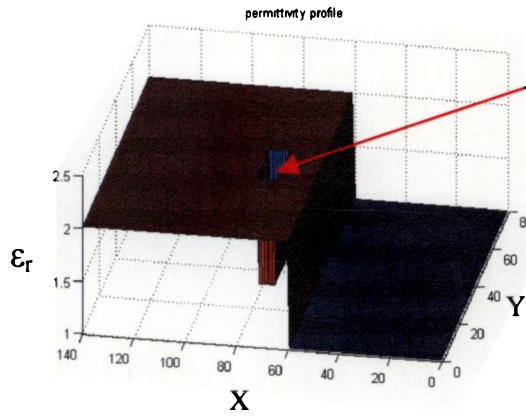


Figure 3.8a Dielectric profile of the void system

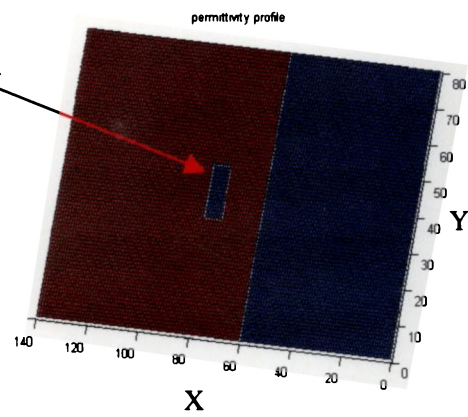


Figure 3.8b Top view of the void system

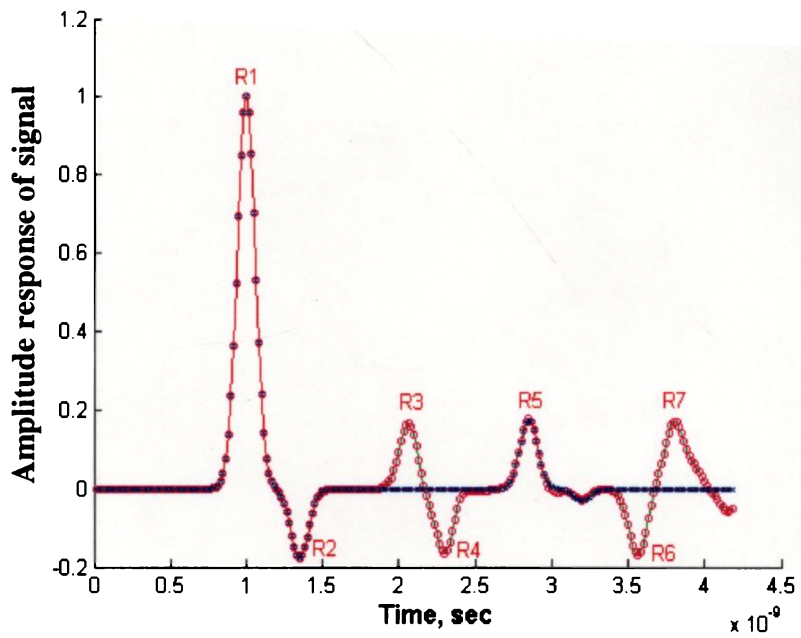


Figure 3.9 Theoretical time domain response from a void at 8 cm

From the comparison of *figures 3.4* and *3.9*, we can see that the points R3, R4 and R6 are reversed. It is because, in *figure 3.4*, the pulse is traveling from a medium of low dielectric constant to high one. But in this case, the pulse traverses from medium of high dielectric constant to low one. If one had considered the power pattern with respect to time instead of the field pattern as shown in *figures 3.4 & 3.9*, both the figures would have given the same response.

The response amplitudes of the reflected signals computed for various typical dielectric objects buried at different depths in different dielectric medium are tabulated in *tables 3.1, 3.2 & 3.3*. A successive reduction in magnitude of reflection coefficient with increase in depth occurs due to the incorporation of the complex part of the permittivity in the susceptibility function [24] and hence the attenuation is suffered by the pulse.

Table 3.1 Reflection coefficient (Γ) of different objects (assumed ϵ_r values) buried at different depths in a dielectric medium ($\epsilon_r = 2.56$, $\tan \delta = 0.00024$)

Dielectric constant of the buried objects	Depth of the buried object (cm)	$\Gamma_{\text{air-diel. interface}}$	$\Gamma_{\text{buried object}}$
3.2	5	-0.2520	-0.0549
	10		-0.0424
	15		-0.0334
	20		-0.0265
5	5	-0.2520	-0.1605
	10		-0.1186
	15		-0.0946
	20		-0.0762
10	5	-0.2520	-0.3297
	10		-0.2387
	15		-0.1907
	20		-0.1543
15	5	-0.2520	-0.4303
	10		-0.3076
	15		-0.2473
	20		-0.1991
20	5	-0.2520	-0.4988
	10		-0.3540
	15		-0.2863
	20		-0.2297
30	5	-0.2520	-0.5863
	10		-0.4195
	15		-0.3376
	20		-0.2698

Table 3.2 Reflection coefficient (Γ) of different objects (assumed ϵ_r values) buried at different depths in a dielectric medium ($\epsilon_r = 5$, $\tan \delta = 0.0003$)

Dielectric constant of the buried object	Depth of the buried object (cm)	$\Gamma_{\text{air-diel. interface}}$	$\Gamma_{\text{buried object}}$
3.2	5	-0.4076	00.0921
	10		00.0688
	15		00.0585
	20		00.0501
5	5	-0.4076	-0.0018
	10		-0.0088
	15		-0.0088
	20		-0.0088
10	5	-0.4076	-0.1523
	10		-0.1132
	15		-0.0941
	20		-0.0791
15	5	-0.4076	-0.2444
	10		-0.1811
	15		-0.1498
	20		-0.1257
20	5	-0.4076	-0.3093
	10		-0.2295
	15		-0.1892
	20		-0.1585
30	5	-0.4076	-0.4013
	10		-0.2962
	15		-0.2433
	20		-0.2050

Table 3.3 Reflection coefficient (Γ) of different objects (assumed ϵ_r values) buried at different depths in a dielectric medium ($\epsilon_r = 10$, $\tan \delta = 0.00191$)

Dielectric constant of the buried object	Depth of the buried object (cm)	$\Gamma_{\text{air-diel. interface}}$	$\Gamma_{\text{buried object}}$
3.2	5	-0.5652	0.1624
	10		0.1347
	15		0.1172
	20		0.1033
5	5	-0.5652	0.1019
	10		0.0846
	15		0.0741
	20		0.0658
10	5	-0.5652	-0.0069
	10		-0.0069
	15		-0.0069
	20		-0.0069
15	5	-0.5652	-0.0646
	10		-0.0524
	15		-0.0446
	20		-0.0395
20	5	-0.5652	-0.1115
	10		-0.0903
	15		-0.0771
	20		-0.0681
30	5	-0.5652	-0.1798
	10		-0.1446
	15		-0.1230
	20		-0.1084

3.3.2 Extraction of object details from the range profiles

Time domain signals are sometimes called *range profiles* because they give the information of the depth or range of the object. At the same time, the shape and span of the object can also be derived from range profiles at different locations.

In order to extract the object details, the amplitude of the time domain responses from the theoretical model is converted into power pattern. The range profiles in power domain from 11 different positions corresponding to a buried model object of rhombus shape ($\epsilon_r = 8.2$) are shown in *figure 3.10*. Knowledge of these positions and the corresponding range profiles will give the depth and shape of the object simultaneously. Data for each position can be stored in the computer and analysed with proper software to give the information of the buried object.

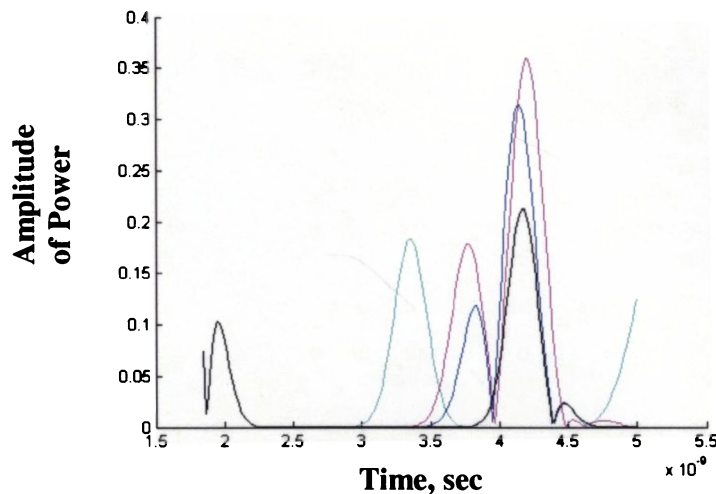


Figure 3.10 Range profiles at different positions

We can note that the peaks appearing in between 3 ns and 4 ns in *figure 3.10* are from the object. Using the Matlab programme, the cross sectional view of the image can be reconstructed as shown in *figures 3.11a* and *3.11b*.

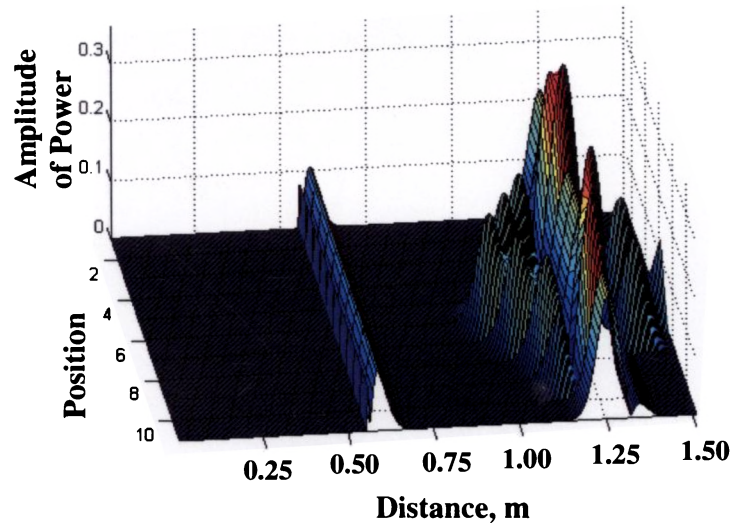


Figure 3.11a Reconstructed image from the range profiles

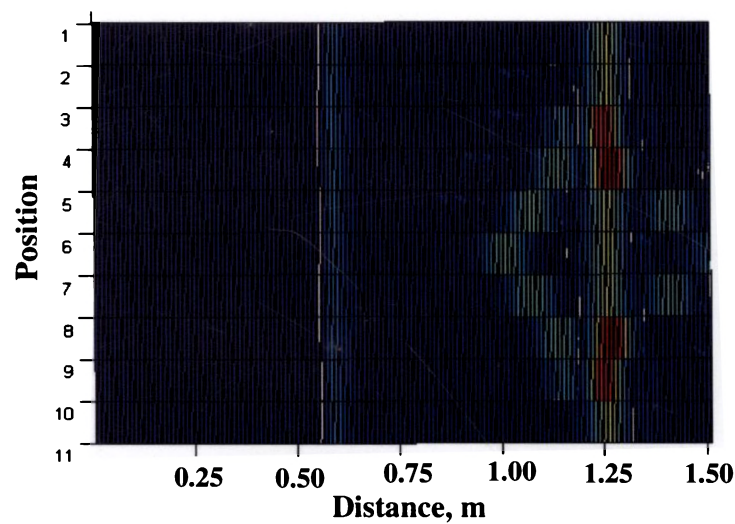


Figure 3.11b Top view of the reconstructed image

The velocity factor should be taken into consideration while calculating the actual depth of the object from the reconstructed image.

Another set of range profiles obtained from an object of rectangular cross section is shown in *figure 3.12*. The reconstructed images from these range profiles is shown in *figures 3.13a* and *3.13b*.

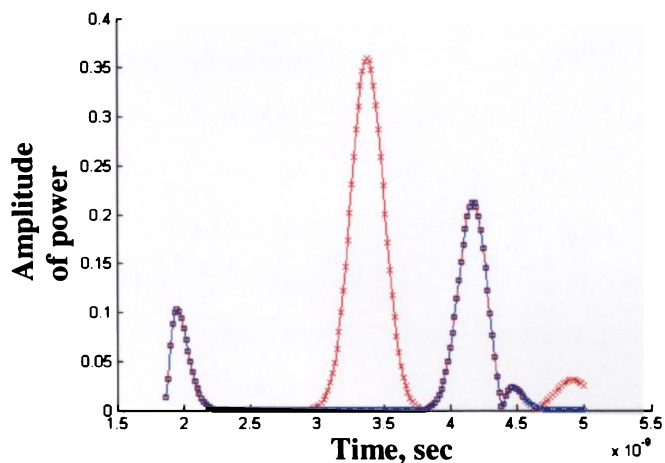


Figure 3.12 Range profiles from different positions

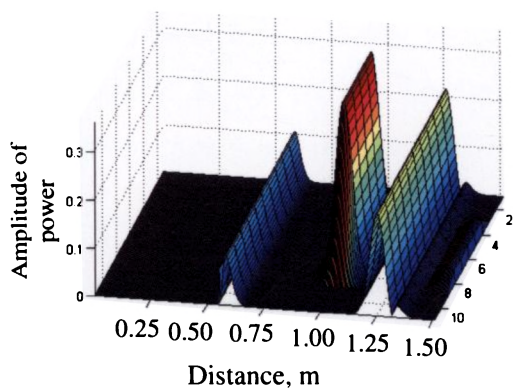


Figure 3.13a Reconstructed image from the range profiles

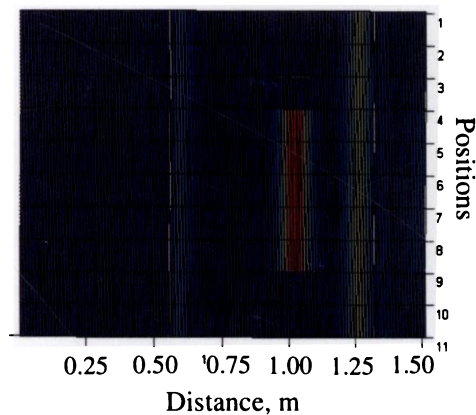


Figure 3.13b Top view of the reconstructed image

3.4 Experimental Results

3.4.1 Detection of Dielectrics

A vessel of dimension 40 cm x 40 cm x 35 cm filled with sand is used for the measurement and it acts as the simulated ground. The antenna is connected to one port of the S-parameter test-set and the S-parameter (S_{11} or S_{22}) corresponding to that port is set in the network analyzer. The reflected signals received by the pyramidal horn antenna at different locations of the vessel are analysed for the information of the buried object. The experimental set-up is as shown in *figure 3.14*. The advantage of the method is that it does not need any calibration. It is because the information is extracted only from the relative responses at different points.

Experiments are performed in X (8-12 GHz) and Ku (12-18 GHz) bands. The pyramidal horn antennas used are of approximately 15 dBi gain. Pyramidal horn antenna operating in X-band has a Half Power Beam Width (HPBW) 18° (E-plane) and 15.5° (H-plane) and aperture dimension 9.8 cm x 7.5 cm. The respective values for Ku-band horn antenna are 20° , 17° and 5.7 cm x 4.4 cm. The antenna is connected to HP 8514B S-parameter test set and interconnected to HP 8510C Network Analyser, HP 83651 B Sweep Oscillator and computer.

A dielectric object ($\epsilon_s = 5.5$, $\epsilon_\infty = 3.1$) of dimension 7 cm x 3 cm x 3 cm is placed at a depth of 8 cm from the front surface of the vessel as shown in *figure 3.14*. This object is considered because the plastic mines have a dielectric constant 3.2 [16]. For detecting the multiple objects, one more dielectric object is placed in line with the first object at a distance of 10 cm from the first object.

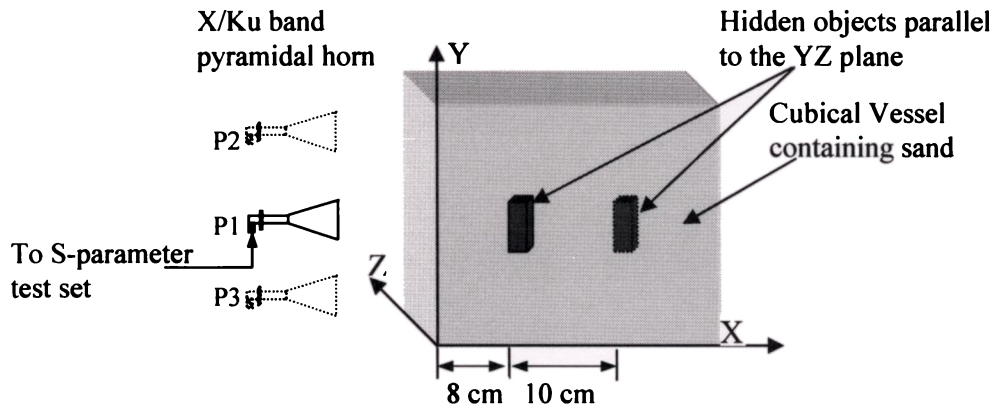


Figure 3.14. Experimental set-up for buried object detection

The response from an object buried in the container with an antenna operating in X-band is shown in *figure 3.15a*. The responses at three points P1, P2 and P3 are given in the figure.

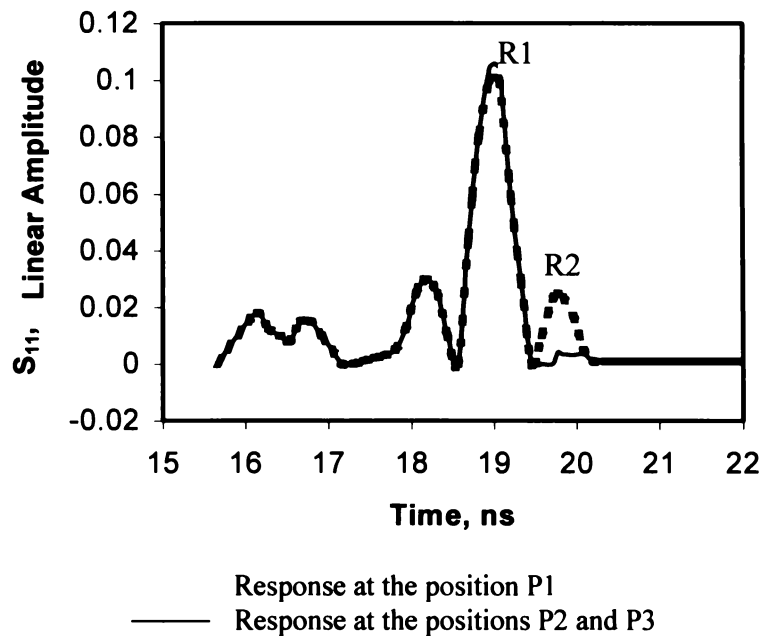


Figure 3.15a Time domain responses with one buried object (using X-band pyramidal horn)

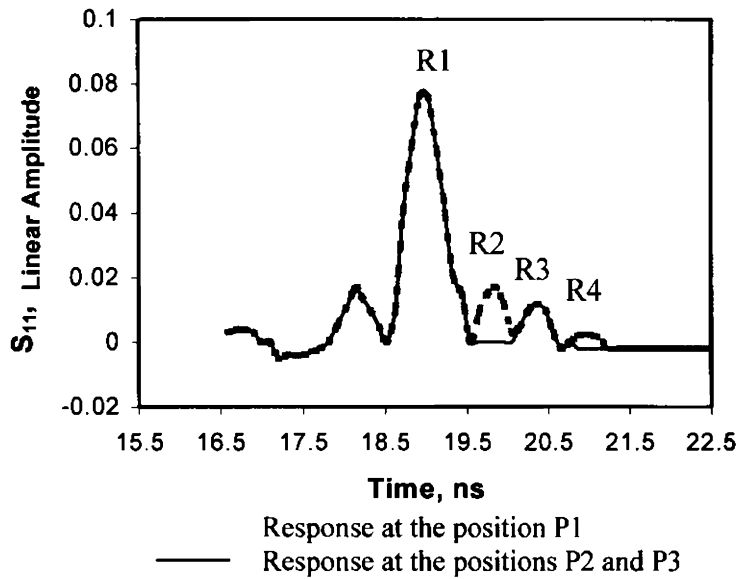


Figure 3.15b Time domain responses with two buried objects (using X-band pyramidal horn)

The response from the system after two dielectric objects buried is shown in figure 3.15b. It could be noted that in figure, the peak obtained at 20.35 ns is same for all the responses from P1, P2 & P3. It may be a reflection from any discontinuity, which is common to three test points or a cable discontinuity.

Figures 3.16a & 3.16b represent the responses of the single object and double objects buried system respectively in Ku-band.

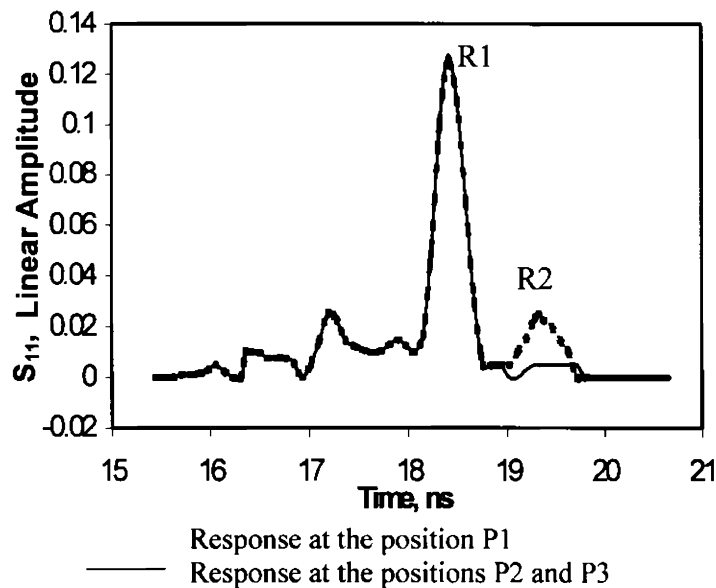


Figure 3.16a Time domain responses with one buried object (using Ku-band pyramidal horn)

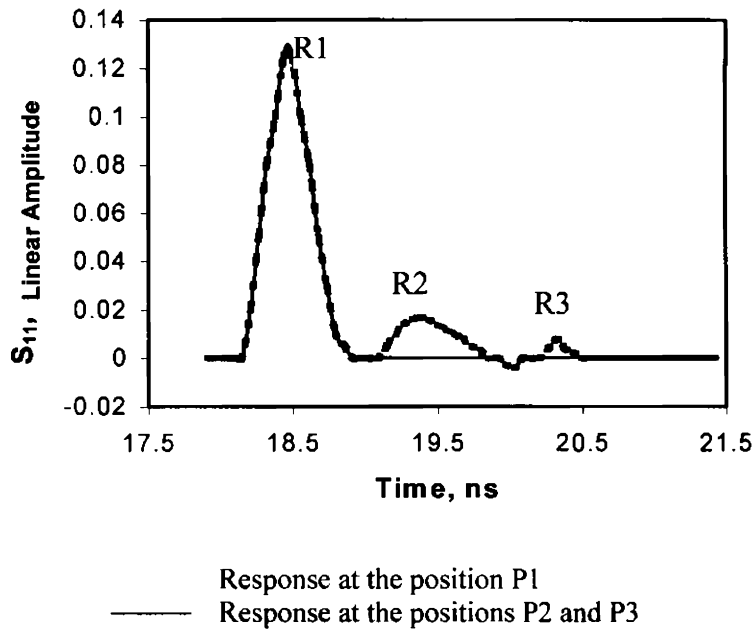


Figure 3.16b Time domain responses with two buried objects (using Ku-band pyramidal horn)

For the comparison of the amplitude of the reflected signal from the dielectric object, a metal pipe of the same size is placed at a distance of 8 cm from the surface and the response is noted. *Figures 3.17a* and *3.17b* give the response for X-band and Ku band.

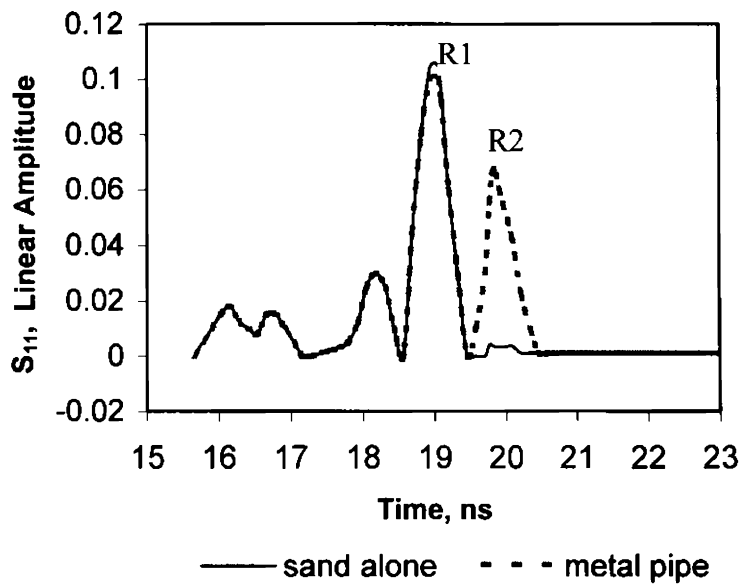


Figure 3.17a Time domain response with metal pipe (in X-band)

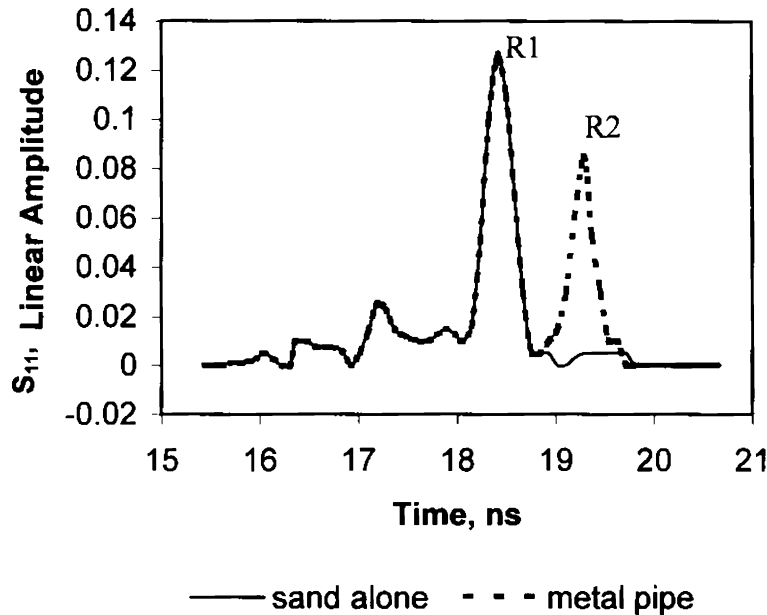


Figure 3.17b Time domain response with metal pipe (in Ku-band)

It can be observed that the metal pipe at a depth of 8 cm gives amplitudes of 67.5 milli Unit (mU) and 85 mU for the reflected signal in X and Ku bands, whereas the dielectric gives amplitudes of 23.5 mU and 25 mU at the same depth. ie, for the same depth, metal pipe gives nearly three to four times amplitude than the dielectric object.

3.4.2 Root detection

For the root detection, the same experimental methodology as explained in the previous section is employed. First of all, the time domain response of the ground without any sample material is noted. Then roots are put at a known depth and time domain responses are noted at different points and the experiment is repeated by placing the samples at different depths. The amplitude of reflected signal in each case is measured. Other dielectric objects like stone, wood etc are placed at the same depths and their corresponding responses are noted. These results help in differentiating the roots from other dielectric objects. It is observed that reflected signals from the roots have larger amplitude as they have more water content and hence high dielectric constant. Potato, onion, beet root, ash gourd and

carrot are used for this study. Wood and different types of stones are considered as other dielectric objects of the ground.

Potato and wood are placed at two locations at a depth of 20 cm from the front side of the container. The antenna is moved horizontally for detecting the two objects. The responses obtained for these materials are shown in *figure 3.18a*. Dotted line represents the response of the signal from potato, broken line that from wood and the solid line that from the empty ground. It can be seen that the peak appearing around 17.843 ns, indicates information about the position and nature of the root. The peak at 15.403 ns represents the reflection from the front surface of the container and it is the same in all cases. The magnitude of reflection obtained from the potato and the wood are 14.2 mU and 2.2 mU respectively. The peak obtained at 19.551 ns represents reflection from the back surface of the container.

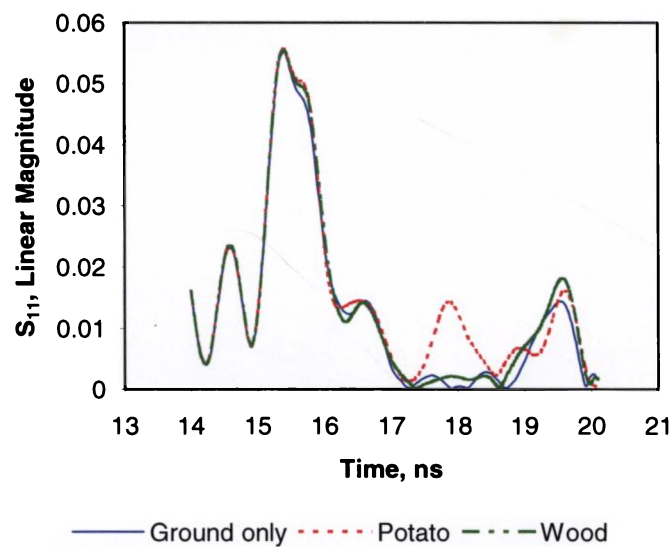


Figure 3.18a Range profile from potato and wood at a depth of 20 cm

The same potato sample is placed at a distance of 10 cm and the range profile from this system is shown in the *figure 3.18b*.

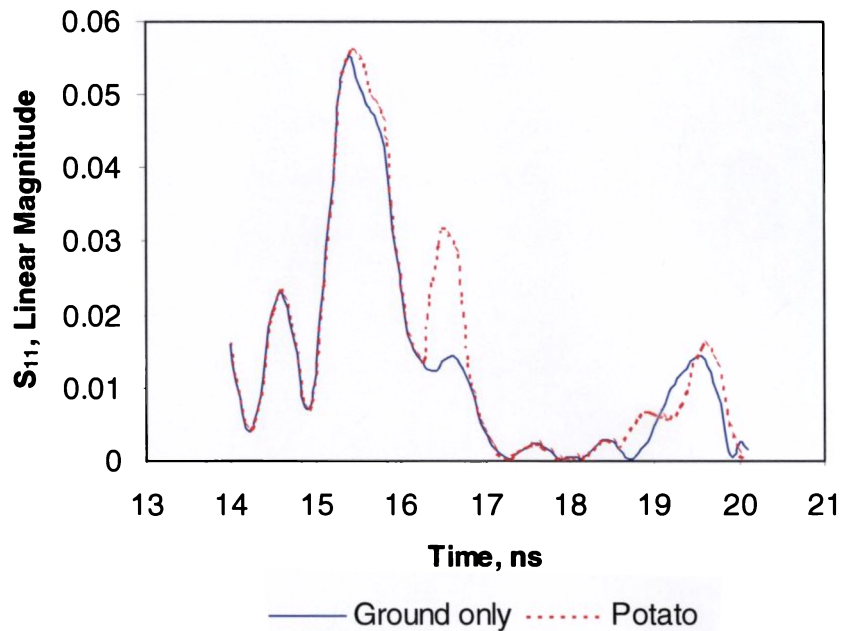


Figure 3.18b Range profile from potato at a depth of 10 cm

From the *figures 3.18a & 3.18b*, the amplitudes of reflected signal from potato at two depths 10 cm and 20 cm are obtained to be 32.3 mU and 14.2 mU respectively. Sharp decrease in the amplitude noted in the reflected signals can be attributed to the absorption in the soil.

Using this method, dielectric constant of the medium can be found out if we have the range profile and span of the container. The two responses obtained from the front surface and back surface of the vessel differ by 4.148 ns (15.403 ns ~ 19.551 ns). The actual distance between the two surfaces is 40 cm. From the time elapsed for the travel through a distance of 40 cm, we can find the dielectric constant of sand as 2.56.

The results obtained from carrot and the black stone (which contains traces of iron) when placed at a depth of 20 cm are as shown in *figure 3.19*. The dotted line is from the carrot and the broken line gives the response from the black stone. The raised amplitude for the black stone may be attributed to the presence of high content of iron.

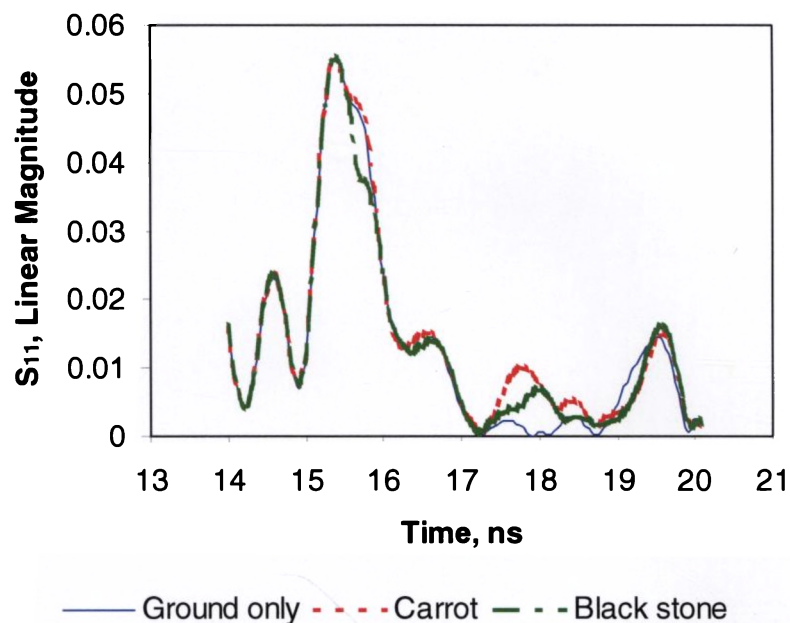


Figure 3.19 Range profile from carrot and black stone at a depth 20 cm

Figure 3.20 gives the reflected signal responses from beet root, onion and a group of potatoes when each of them are placed at a depth of 17 cm. The information of the object can easily be inferred around 18 ns.

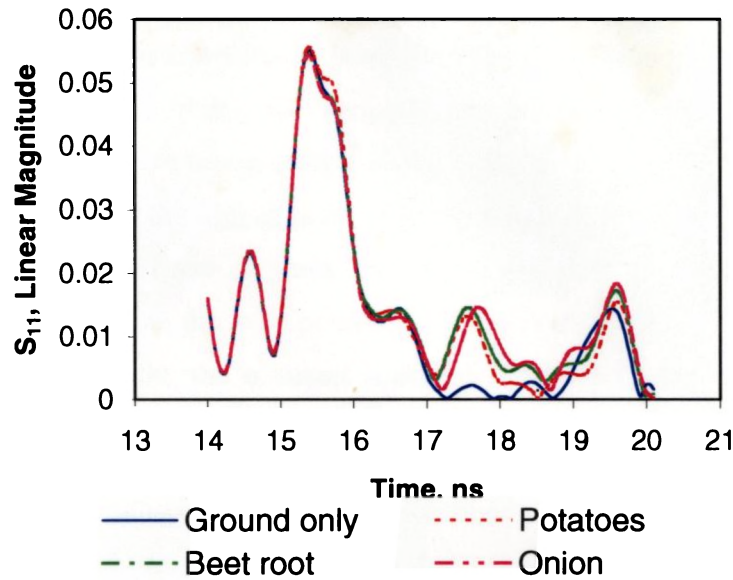


Figure 3.20 Range profile from potatoes, beet root and onion at a depth 17 cm

A typical response obtained from the vegetable ash guard is also given in *figure 3.21*. This is deliberately chosen for the study, even though this vegetable is not produced under the ground. The dependence of the shape of objects on the shape of the range profile is explored from this study.

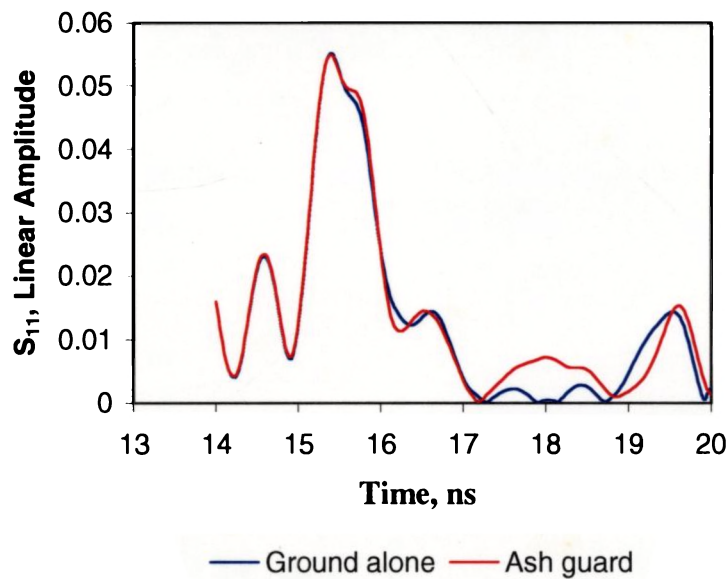


Figure 3.21. Range profile from ash guard at a depth of 20 cm

Ash guard has a large curved surface and size. It can be seen that the response from ash guard is near to 18 ns and the peak is broader than that of other peaks for samples shown in *figures 3.18, 3.19 & 3.20*. This indicates that the sample of larger planar area gives a sharp peak while a curved object a flat response/peak. This can be verified by considering the time domain reflected signal from the two objects: one with planar and the other with curved surface using FDTD simulation. Resultant of the scattered signals from different points of the object should be considered since the pyramidal horn picks the resultant scattered field rather than the individual gaussian pulses.

Consider a case, where an object of rectangular cross section is buried in a dielectric vessel as shown in *figures 3.22a & 3.22b* and the response at different points marked in *figure 3.22b* is shown in the *figure 3.23*.

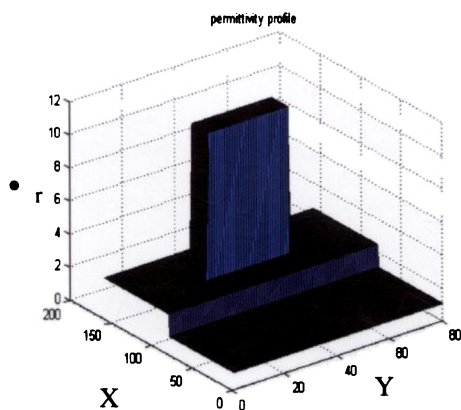


Figure 3.22a Dielectric profile of the system

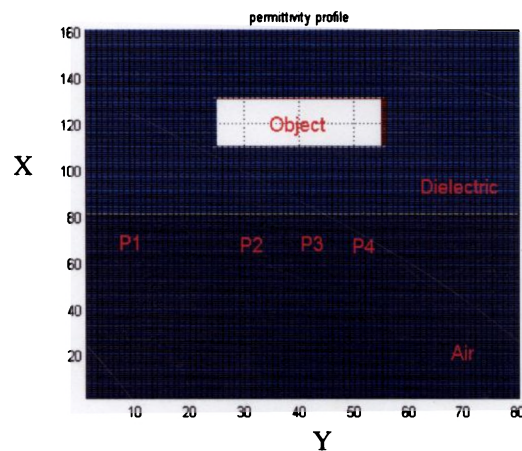


Figure 3.22b Elevated view of the system

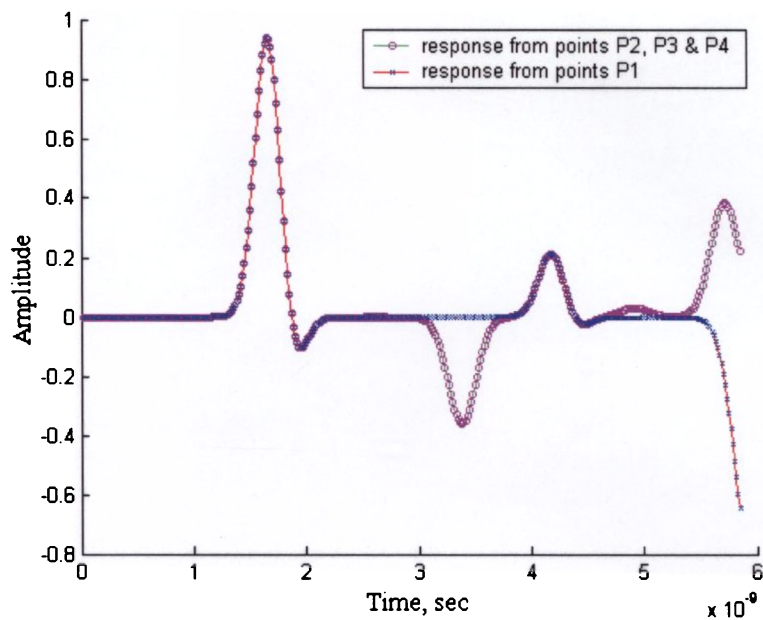


Figure 3.23 Response of the system in fig 3.22a

It can be seen that the responses from the points P2, P3 and P4 in *figure 3.22b* are the same. But if the object does not have a plane surface, the responses at different points will be different in the reference of time. Consider the case of an object having curved surface as shown in *figure 3.24a*. The reflected signals from different points P1, P2, P3 and P4 are shown in *figure 3.25a*. The points P2, P3 and P4 are in line with the object and the responses at these points show that they are different in time scale and having a slight time difference. If they are added to get resultant value, we get a broader dip as seen in *figure 3.25b*. It can be noted that the amplitude of resultant dip is less than the individual responses. Also, it can be inferred that the more the object curvature, more will be broadening of the resultant peak.

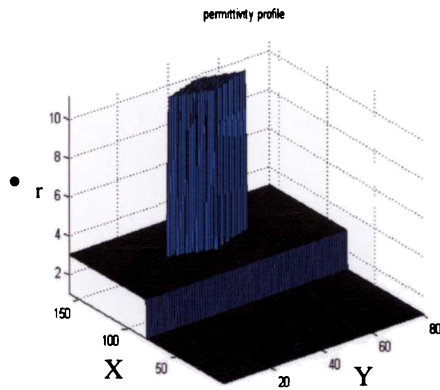


Figure 3.24a Range profile of the system

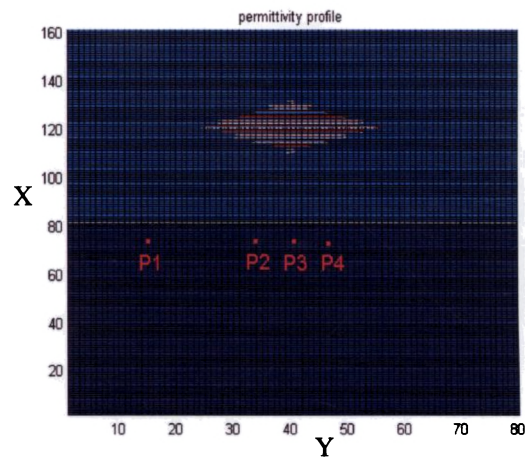


Figure 3.24b Elevated view of the system

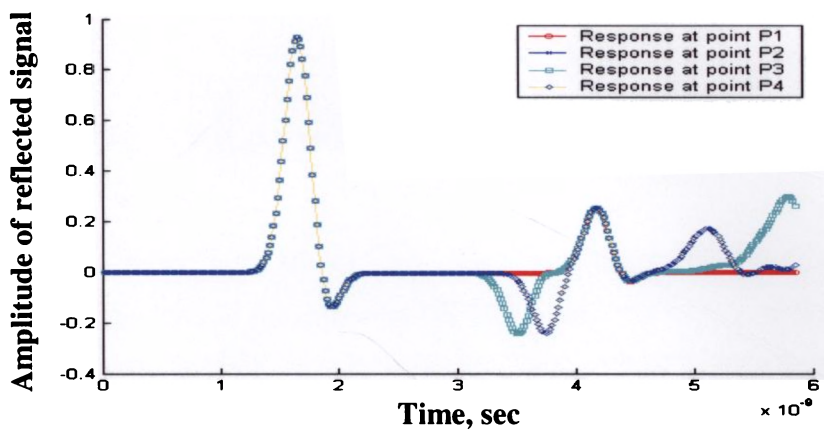


Figure 3.25a Time domain response from different region

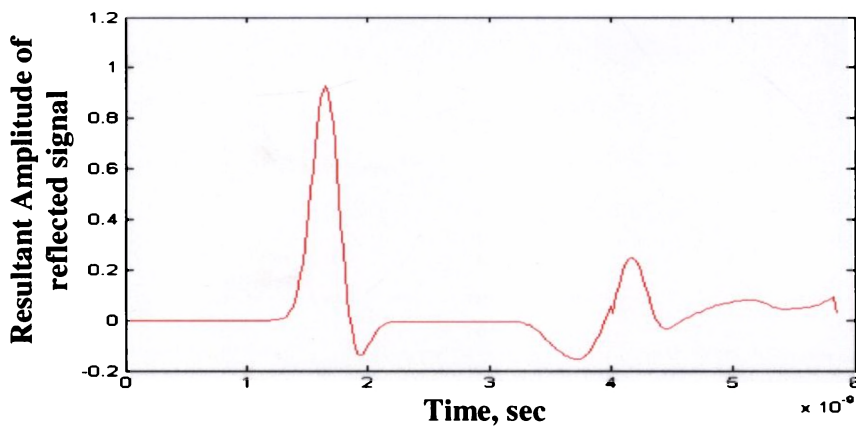


Figure 3.25b Resultant field of signals scattered from the object

To get a comparison of reflected amplitude, metal plate is kept at a depth of 20 cm and the response corresponding to this system is illustrated in *figure 3.26*.

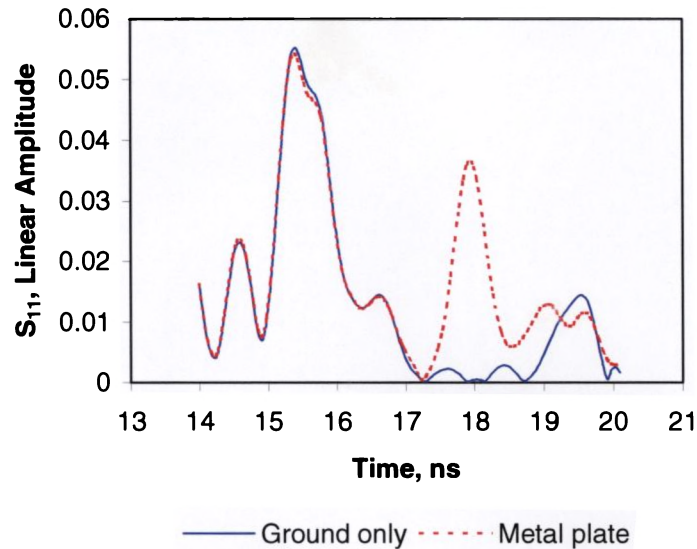


Figure 3.26. Range profile from a metal plate at a depth of 20 cm

Different roots and stones are placed at different depths and the corresponding time domain responses are plotted. A comparative evaluation of the amplitude of the reflected signal for different objects are consolidated in *table 3.4*.

Table 3.4 Amplitude of reflection for Potato, metal plate and two types of stone with distance

Depth (cm)	Amplitude of Reflected signal from roots (mU)	Amplitude of Reflected signal from Black stone (mU)	Amplitude of Reflected signal from concrete block (mU)	Amplitude of Reflected signal from metal (mU)
5	34.9	27.1	14.1	72.3
10	32.3	19.6	12.2	58.1
15	23.5	9.20	8.20	47.8
20	14.1	8.90	7.50	37.1

621.396.76
BIS

3.4.3. Void Detection

In the present study, void is generated by placing an empty ball of 12 cm diameter in sand. The air trapped in the ball provides a discontinuity. *Figure 3.27* shows the amplitude of response with the sand alone, void at depths of 12 cms and 18 cms.

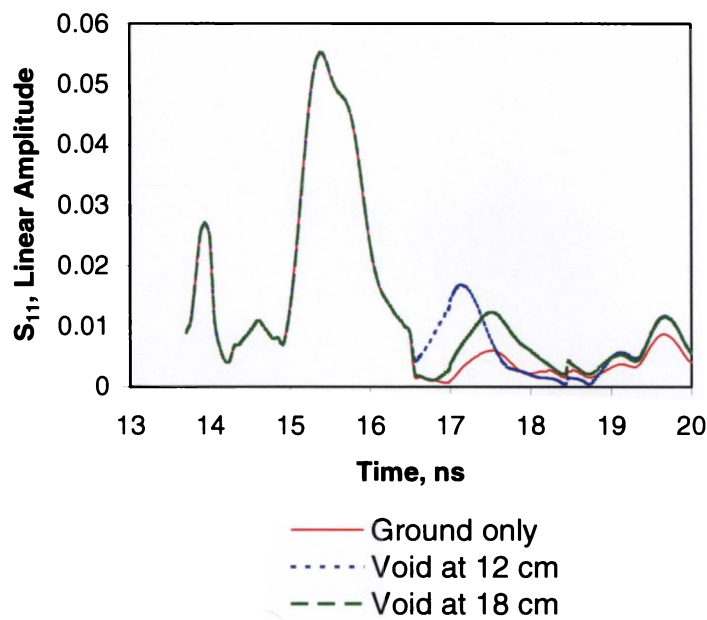
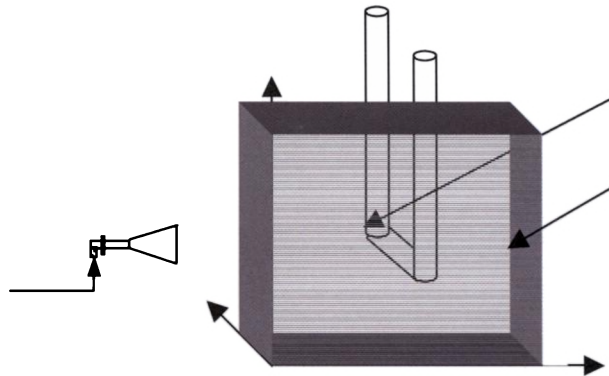


Figure 3.27 Response from a void at different depths

3.4.4 Leak Detection

For carrying out the leak detection of underground pipes, the set-up employed is as in *figure 3.28*. A U-shaped PVC pipe is placed at a depth of 15 cm in a vessel filled with sand. The response from this system is noted. Then the tube is filled with water and time domain signal is obtained. Known volume of water is allowed to flow out of the tube and the corresponding signal is also taken.



The responses plotted for different conditions mentioned above are shown in the

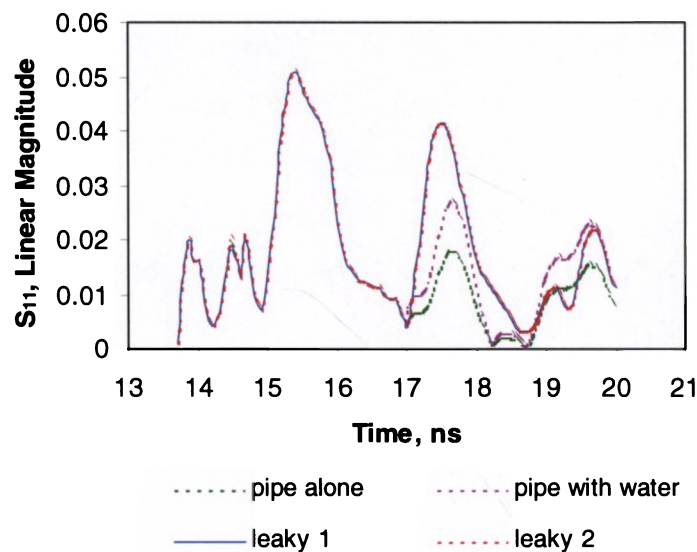


Figure 3.29 Response from an underground pipe at different conditions

figure 3.29.

From the graph, we can see that when pipe is filled with water, the amplitude of the response increases. Responses corresponding to two typical leaky conditions are shown in the graph: 600 ml of water and 1.2 litres of water is allowed to leak out. When it is made leaky, the response again increases and it can be noted that the response is slightly shifted towards left, which implies that water is spreading towards the front surface.

3.5 Summary

Some of the applications of the ground probing radar are discussed in the theoretical and experimental point of view. In the first section, theoretical simulation of the scattered field from buried objects is carried out. FDTD method is adopted for the implementation of the simulation incorporating the dispersive nature of the dielectrics. The amplitude of reflected signal (gaussian pulse) from various objects placed at different depths having different dielectric constant is computed and tabulated. The reconstruction of object details from the set of theoretical range profiles is also done in this section.

Experiments are conducted on a vessel filled with sand, which simulates the ground environment. Dielectric objects having dielectric constant same as that of plastic mines is buried in the vessel and are detected by analyzing the time domain reflected signal. The measurements in X and Ku bands are taken using ordinary pyramidal horn antennas placed in free space. Observations show that Ku band measurements do not contribute much in improving the accuracy. So further measurements are limited to X-band only. In the next part, root detection, which finds application in the field of crop/vegetable estimation, is carried out. Different types of roots are positioned in the vessel and the amplitudes of reflected signal from different depths are tabulated. It is observed that, these signals are easily differentiable from that of other naturally occurring dielectric objects such as stone, wood etc. It can also be seen that a root placed at a depth of 20 cm gives the same amplitude of reflected signal as that of a concrete block at a depth of 5 cm. Also, the relation between the shape of the range profile and the size of the object is established theoretically. The experiment is further extended to void detection. In the last part, leak detection from buried water pipe is carried out. It is noted that the amplitude of reflection increases with the leak. The reflection peak is found to be shifted towards that from air-solid interface.

References

1. Lawrence E. Larsen and John H. Jacobi, "Medical Applications of Microwave Imaging", IEEE Press, The Institute of Electrical and Electronics Engineers, Inc., New York, 1985.
2. D. J. Daniels, "Surface-Penetrating Radar", The Institution of Electrical Engineers, London, 1996.
3. Olhoeft, G.R., "Selected bibliography on ground penetrating radar", Proc. of the Symposium on the Applications of Geophysics to Engineering and Environmental Problems, Golden, CO, pp. 462-520, 1988.
4. Daniels D.J., "Surface-penetrating radar", Electron. and Commun. Eng. J., Vol. 8, No. 4, pp. 165-182, 1996.
5. Strongman K.B., "Forensic applications of ground penetrating radar", Geological Survey of Canada, Paper 90-4, pp.203-211, 1992.
6. Kun-Mu Chen, Yong Huang, Jianping Zhang and Adam Norman, "Microwave Life-Detection systems for searching human subjects under earthquake rubble or behind barrier", IEEE Trans. On Biomedical Engg., Vol.27, No.1, pp. 105-114, January2000.
7. S. Biju Kumar, C.K. Aanandan and K. T. Mathew, "Buried-object detection using Free-space Time-Domain Near-field measurements", Microwave and Optical Technology Letters, Vol. 31, No. 1, pp. 45-47, October 2000.
8. HP 8510B Network Analyser Operating and Programming Manual, Manual part no. 08510-90070, Hewlett Packard.
9. Wang Xiande, Luo Xianyun, Zhang Zhongzhi and Fu Junmei, "Electromagnetic scattering from target buried in layer of randomly distributed trunks", Microwave and Optical technology letter, vol. 24, no. 3, February 2000.
10. Kenneth Demarest, Richard Plumb and Zhubo Huang, "FDTD Modeling of scatterers in stratified media", IEEE Trans. On Antennas and Propagation, vol. 43, No. 10, pp. 1164-1168, October 1995.
11. R. Benjamin, I.J. Craddock, G. S. Hilton, S. Litobarski, E. McCutcheon, R. Nilavalan and G. N. Crisp, "Microwave detection of buried mines using non-contact, synthetic near-field focussing", IEE Proc.-Radar, Sonar Navig. Vol. 148, No. 4, pp. 233-240, August 2001.
12. Gary R. Olhoeft, Michael H. Powers and Dennis E. Capron, "Buried object detection with Ground Penetrating Radar", Proc. Of Unexploded Ordnance

- (UXO) detection and range remediation Conference, Golden, CO, pp. 207-233, May 1994.
13. Ballard. N., Langman. A., Inngs M. R., "On-line complex permittivity measurements for ground penetrating radar", Geoscience and Remote Sensing Symposium, IGARSS '94, Surface and Atmosphere Remote Sensing:Technologies, Data Analysis and Interpretation, Vol. 4, pp. 2513-2515, 1994.
 14. O. P. N. Calla and S. Sharma, "Study of scattering behaviour of dry and wet soil with undulating surface at microwave frequencies", Indian Journal of Radio & Space Physics, Vol. 30, pp. 332-336, December 2001.
 15. Jacqueline M. Bourgeois and Glenn S. Smith, "A complete electromagnetic simulation of the separated-aperture sensor for detecting buried land mines", IEEE Trans. On Antennas and Propagation, Vol.46, No.10, pp. 1419-1426, October 1998.
 16. Lawrence Carin, Norbert Geng, Mark McClure, Jeffrey Sichina and Lam Nguyen, "Ultra-Wide-Band Synthetic - Aperture Radar for Mine-field detection", IEEE Antennas and Propagation Magazine, Vol.41, No. 1, pp. 18-33, February 1999.
 17. Thomas P. Montoya and Glenn S. Smith, "Land mine detection using a Ground-Penetrating Radar based on Resistively loaded Vee dipoles", IEEE Trans. On Antennas and Propagation, Vol. 47, No. 12, pp. 1795-1806, December 1999.
 18. David Wong and Lawrence Carin " Analysis and processing of Ultra Wide-Band SAR Imagery for buried landmine detection", IEEE Trans. On Antennas and Propagation, Vol. 46, No. 11, pp. 1747-1748, November 1998.
 19. M. B. Silevitch, S. W. McKnight and C. Rappaport, " A Unified discipline of subsurface sensing and imaging systems", Subsurface Sensing Technologies and Applications, Vol. 1, No. 1, pp. 3-12, 2000.
 20. Kane S. Yee, "Numerical solution of initial boundary value problems involving Maxwell's equations in isotropic media", IEEE Trans. On Antennas and Propagation, Vol. 14, No. 8, pp. 302-307, May 1966.
 21. Gerrit Mur, "Absorbing Boundary conditions for the finite-difference approximation of the time-domain electromagnetic field equations", IEEE Trans. On Electromagnetic Compatibility, Vol. 23, No. 4, pp. 377-382, November 1981.
 22. Jose A. Pereda, Oscar Garcia, Angel Vegas and Andres Prieto, "Numerical dispersion and stability analysis of the FDTD technique in lossy dielectrics",

- IEEE Microwave and Guided Wave Letters, Vol. 8, No. 7, pp. 245-247, July 1998.
23. K. S. Cole and R. H. Cole, "Dispersion and absorption in dielectrics", *J. Chemical Physics*, Vol. 9, pp. 341-351, April 1941.
 24. Raymond J. Luebbers, Forrest Hunsberger, Karl S. Kunz, Ronald B. Standler and Michael Schneider, "A Frequency-dependant Finite-Difference Time-Domain Formulation for Dispersive Materials", *IEEE Trans. On Electromagnetic Compatibility*, Vol. 32, No. 3, pp. 222-227, August 1990.
 25. Raymond J. Luebbers and Forrest Hunsberger, "FDTD for Nth-order Dispersive Media", *IEEE Trans. On Antennas and Propagation*, Vol. 40, No. 11, pp. 1297-1301, November 1992.
 26. Jeffrey L. Young, "Propagation in Linear Dispersive Media: Finite Difference Time-Domain Methodologies", *IEEE Trans. On Antennas and Propagation*, Vol. 43, No. 4, pp. 422-425, April 1995.
 27. William H. Weedon, Carey M. Rappaport, "A General Method for FDTD modelling of wave propagation in arbitrary Frequency-dispersive media", *IEEE Trans. On Antennas and Propagation*, Vol. 45, No. 3, pp. 401-409, March 1997.
 28. Wendemagegnehu T. Beyene, "Improving Time-domain measurements with a network analyser using a robust rational interpolation technique", *IEEE Trans. On Microwave Theory and Techniques*, Vol. 49, No. 3, pp. 500-508, March 2001.
 29. Zoran A. Maricevic, Tapan K. Sarkar, Yingbo Hua and Antonije R. Djordjevic, "Time-Domain measurements with the Hewlett-Packard network analyzer HP 8510 using the Matrix Pencil Method", *IEEE Trans. On Microwave Theory and Techniques*, Vol.39, No.3, pp. 538-547, March 1991.
 30. Joel T. Johnson, Jatupum Jenwatanavet and Nan Wang, "Soil Modification Studies for Enhanced Mine Detection with Ground Penetrating Radar", *Proceedings of SPIE*, 1999.

Chapter 4
Biological Study

The electrical properties of some body tissues at microwave frequencies are studied. Cavity perturbation method is employed for the measurement. The results find applications in numerical simulation of cells, microwave imaging, Specific Absorption Rate (SAR) determination and other medical applications.

4.1 Introduction

Electrical properties of biological tissues and their interaction with electromagnetic waves have attracted the attention of researchers working in the field of medicine and electromagnetics. Extensive research had already been done in these fields and is still going on since its results have direct impact on human life [1-13]. In this modern world where microwaves are extensively utilized for communication, the study of the dielectric properties of tissues at these frequencies are of special interest. In order to understand the interaction of electromagnetic field with tissue, it is important to know its complex permittivity accurately [14]. Biological effects of microwaves and the application of microwaves in medicine represent two strongly developing areas of research. Availability of sophisticated microwave systems and components of smaller size at lower cost makes microwave applications in medicine more attractive. Microwaves are used in cancer therapy [15], hyperthermia treatment [16], diagnosis [17], clinical applications [18] and many more.

The invention of the non-invasive techniques of imaging of tissues, which are highly effective in revealing the conditions of the internal organs of the body, was a breakthrough in the field of medical diagnosis. Different tomographic techniques depending on the method of imaging and the object function imaged has been evolved. Electrical Impedance tomography (EIT), which conducts complex permittivity and/or conductivity [19-21] measurements in the radio spectrum, is one of those fields where the electrical properties are imaged. Recently, microwave imaging [22-28] has emerged as another field of great potentiality. The knowledge of the dielectric properties of various biological tissues at these frequencies is of much significance in deriving useful information in this kind of imaging. Any deviation from these standard values, obtained while imaging, lead to an indication of its physiological conditions [23,28]. Since the dielectric properties are highly dependant on temperature [24], the system that monitors the dielectric parameters of the biological tissues may also be able to determine the temperature distributions in the tissue.

There has been a recent increase in public concern over the exposure of humans to Radio Frequency (RF) Electromagnetic fields especially from mobile telephone handsets and associated devices. The most popular method for analyzing the dose of exposure is to determine the Specific Absorption Rate (SAR) of the device, which quantifies the amount of energy absorbed by biological tissue. SAR value is calculated using the following equation:

$$SAR = \frac{\sigma E_{rms}^2}{\rho}$$

where 'σ' is the conductivity of the medium in which the electric field measurement is made and 'ρ' is the density.

In this chapter, dielectric studies of some body fluids like bile, gastric juice, pancreatic juice, saliva, sweat and chicken bile in the microwave region have been carried out. The work is also extended to solid biological materials like pancreatic stone and bile stone. As many of the body fluids are available only in small quantities the cavity perturbation method is employed for its characterization. This method is well-accepted as it provides best results and requires only small amount of sample [29].

Dielectric properties such as conductivity, loss tangent, absorption coefficient and penetration depth are determined from the measured complex permittivity values. This information finds application in numerical simulation of cells [30], microwave imaging [22-28], Specific Absorption Rate (SAR) [31-34] determination and medical applications [35].

4.2 Review of the past work

The interaction of electromagnetic waves with biological objects is well known [1-13]. A pioneering work in the field of microwave dielectric properties of biological materials has been reported by H. F. Cook [1,2]. Schwan [3] has reported studies on electrical properties of some tissues and suspensions. Musil and Zacek

[4], consolidate the earlier results of dielectric properties of tissues. Polk and Postow [5] present the details of electromagnetic interaction with biological tissues.

C. Gabriel et al. and S. Gabriel et al. [6-8] determined the dielectric properties of many of the biological tissues in the range 10 Hz –100 GHz. The electrical parameters of any tissue at the desired frequency can be obtained from the table [13] provided.

Hornback et al [15] for the first time reported the clinical trials of microwave therapy for the treatment of cancer. Salcman [16] reported the trials of hyperthermia, feasibility of the method and the absence of secondary effects.

Naoya Hoshi et al. [17] present application of microwaves for the characterization of teeth. They analysed the transmission coefficient by placing the tooth to be tested in between the two waveguides and conducted the experiments in the range of 40 MHz-40 GHz. Dental carries are found to be more lossy than the healthy tooth and this could be used for dental diagnosis.

Masahiro Hiraoka et al. [18] present a review of the development of RF and Microwave heating equipment for hyperthermia and their clinical applications in detail. They describe the features of regional heating, inductive heating and thermal distribution in some of the tumors.

Impedance tomography was first proposed by Brown and Barber [19] for clinical applications. Since then, many scientists [20,21] are working intensively for the development of a complete system.

Larsen and Jacobi [22] compile the different areas related to biological applications of microwaves. Tissue permittivity measurements, microwave holography and coherent tomography, inverse methods in electromagnetic imaging, methods of microwave tomography, imaging system design etc are discussed in detail.

Bocquet et al [23] present a microwave radiometric system working at 3 GHz, which provides images for a square area about half a decimeter on a side.

[4], consolidate the earlier results of dielectric properties of tissues. Polk and Postow [5] present the details of electromagnetic interaction with biological tissues.

C. Gabriel et al. and S. Gabriel et al. [6-8] determined the dielectric properties of many of the biological tissues in the range 10 Hz – 100 GHz. The electrical parameters of any tissue at the desired frequency can be obtained from the table [13] provided.

Hornback et al [15] for the first time reported the clinical trials of microwave therapy for the treatment of cancer. Salcman [16] reported the trials of hyperthermia, feasibility of the method and the absence of secondary effects.

Naoya Hoshi et al. [17] present application of microwaves for the characterization of teeth. They analysed the transmission coefficient by placing the tooth to be tested in between the two waveguides and conducted the experiments in the range of 40 MHz-40 GHz. Dental carries are found to be more lossy than the healthy tooth and this could be used for dental diagnosis.

Masahiro Hiraoka et al. [18] present a review of the development of RF and Microwave heating equipment for hyperthermia and their clinical applications in detail. They describe the features of regional heating, inductive heating and thermal distribution in some of the tumors.

Impedance tomography was first proposed by Brown and Barber [19] for clinical applications. Since then, many scientists [20,21] are working intensively for the development of a complete system.

Larsen and Jacobi [22] compile the different areas related to biological applications of microwaves. Tissue permittivity measurements, microwave holography and coherent tomography, inverse methods in electromagnetic imaging, methods of microwave tomography, imaging system design etc are discussed in detail.

Bocquet et al [23] present a microwave radiometric system working at 3 GHz, which provides images for a square area about half a decimeter on a side.

They used multiprobe radiometer that improves their localization. Many scientists [24-27] are independently and collectively working on the improvement of this type of imaging.

Paul M. Meaney et al [28] discussed in detail the prototype for active microwave imaging of the breast. They have observed that electromagnetic properties of breast malignancy are significantly different from normal breast tissues at frequency near 900 MHz.

The numerical modeling of head [30] is performed from the conductivity and dielectric constant of the tissues. The effect of microwave absorption in human head due to the hand held portable radios and transceivers are also reported by Cleveland Jr. et al [32], O.P Gandhi et al. [33], and Klaus Meier et al [34].

An exhaustive data is presented by Thuery [35] on the medical applications of microwaves. Interaction of e.m. waves with the organism, biological effects and effects on nervous system due to microwaves, safety standards of exposure to e.m. radiation and different biomedical applications are discussed in detail.

Linfeng Chen et al [30] describe that resonant methods, mainly resonator methods and resonant perturbation methods have relatively higher accuracy than nonresonant methods. In the paper they discuss the amendment of cavity perturbation method for permittivity measurement of extremely low-loss dielectrics. They have also compared the results obtained before and after the amendment.

The earliest treatment on cavity perturbation theory is given by Bethe and Schwinger [36]. According to them the perturbation is caused (i) by the insertion of small dielectric sample into a cavity and (ii) by a small deformation of the boundary surface of the cavity.

A detailed perturbation formula with necessary approximations is given by Waldron [37]. He concludes that the high accuracy perturbation formula will only be realised if the specimen is suitably shaped and positioned in the cavity. Harrington [38] gives a detailed description of perturbation due to cavity walls and the insertion of the material into the cavity field region. Many types of cavities and

modifications are proposed by the researchers [39,40]. The accuracy conditions of the cavity resonator measurements are also discussed by many researchers [29,41].

4.3 Sample collection and method of measurement

The biological samples are collected from a Digestive Disease Center. In this center research, diagnosis and treatment of diseases connected to the digestive system are done using the advanced medical technology, the Endoscopy. The internal organs are examined using the modern Endoscope named Videotoscope (see figure 4.1), which consists of an Endoscope, CPU and a Monitor. A charge-coupled device at the tip of the shaft transmits the magnified image into TV screen. The handle of the Endoscope has control knobs for maneuvering the tip and also buttons to regulate irrigation water, air insufflation and suction for removing air and secretions. Also there is an instrument channel allowing the passage of biopsy forceps, snares for removing polyps and devices to control bleeding.

In routine Upper Gastro Intestinal (UGI) Endoscopy, entire esophagus, stomach and the proximal duodenum are examined. Some of the common conditions that are routinely diagnosed by endoscopy include Gastro esophageal reflux disease, Peptic ulcer and cancer of Upper Gastro Intestinal tract. During this investigation, bile samples and bile stones are collected. Usually bile stones are removed by ERCP (Endoscopic Retrograde Cholangio Pancreatography) surgery. This is a variation of UGI endoscopy, combining Endoscopic and Radiologic techniques to visualise biliary and pancreatic duct systems. A side-viewing instrument after being placed into the descending duodenum, the papilla of Vater (where bile duct and pancreatic duct opens into GIT) is cannulated and contrast medium injected, thus visualising pancreatic duct and hepato biliary tree radiographically. It is useful in the diagnosis of stones and cancer of bile duct and also pancreatic disorders like chronic pancreatitis and pancreatic malignancy. Therapeutic potentials include removal of bile duct stones and palliation of obstructive jaundice by placing stents to bypass obstructing lesions. Bile, pancreatic juice, pancreatic stone and gastric juice are collected in this way. All the biological samples were preserved in freezing temperature to avoid the possibility of decay. However the dielectric measurements were done at 25°C.

Because of many constraints such as high dielectric loss and faster decay rate of biological materials, the studies on the dielectric properties on these materials are seen very seldom in the literature. Also, much care should be taken in handling the infected biological samples.



Figure 4.1 Video endoscope: Pentax ED-3440T

The dielectric characterization of biological samples is performed using the cavity perturbation technique. It is one of the most accurate methods available [29].

The main attractive feature of this method is that it requires only a small volume of sample.

The basic principle of the cavity perturbation technique is that the field is perturbed by the introduction of the sample. The dielectric parameters can be determined from the cavity parameters such as resonant frequency and quality factor. The basic criterion in the method is that field perturbation should be small. This is satisfied when the perturbing sample is of small volume compared to that of cavity. Normally the biological fluids like bile, gastric juice, pancreatic juice etc are available only in small quantities. So the cavity perturbation method is most suitable.

The cavity resonator is constructed with a portion of a transmission line (waveguide or coaxial line) with two ends closed. The cavity resonator employed for the study is a transmission type one. There is a coupling device, which is usually called as iris, to couple the microwave power to the resonator and from the resonator. The principle of the resonant cavity perturbation method is discussed in detail by many scientists [36-40].

Dielectric study of biological liquids is carried out in two bands, S (2-4 GHz) and C (4-8 GHz). Three cavities are constructed and the physical dimensions are given in the *table 4.1*. S-band cavity resonator is constructed from the section of the standard rectangular waveguide WR-284. In the case of C-band, a WR-159 waveguide is used.

For the accommodation of solid samples like bile stone and pancreatic stone, a special type of S-band cavity is designed. It is constructed with a provision for inserting the solid samples. A rectangular opening of 4 cm x 3 cm is cut at the non-radiating wall of the cavity resonator. Metallic cover of the same dimension is put back so that there is no leakage of energy from the opening. The resonating frequencies and the corresponding quality factors of the cavity, before and after the opening, show no substantial difference in the quality factor. This indicates that there is no much leakage through the metal cover. The schematic diagram of this cavity is shown in *figure 4.2*. The inner side of the cavity and the position of the

sample holder, which accommodates the solid samples, are shown in the figure through a window. The sample holder is in the form of a small cup made of low-loss polystyrene. It rests on a rod of the same material and can slide along the slot.

The cavity resonator is connected to the two ports of S-parameter test set and it is excited in the TE_{10p} mode. The length of the resonator determines the number of resonant frequencies. Typical resonant frequency spectrum of the cavity resonators are shown in *figures 4.3a & 4.3b* and the cavity parameters are given in the *table 4.2*.

Table 4.1 Physical dimensions of the cavity resonators

Type of cavity	Length, d (mm)	Breadth, a (mm)	Height, b (mm)
S-band1	353	72.0	33.5
S-band2	224	72.0	33.5
C-band	165	34.5	15.5

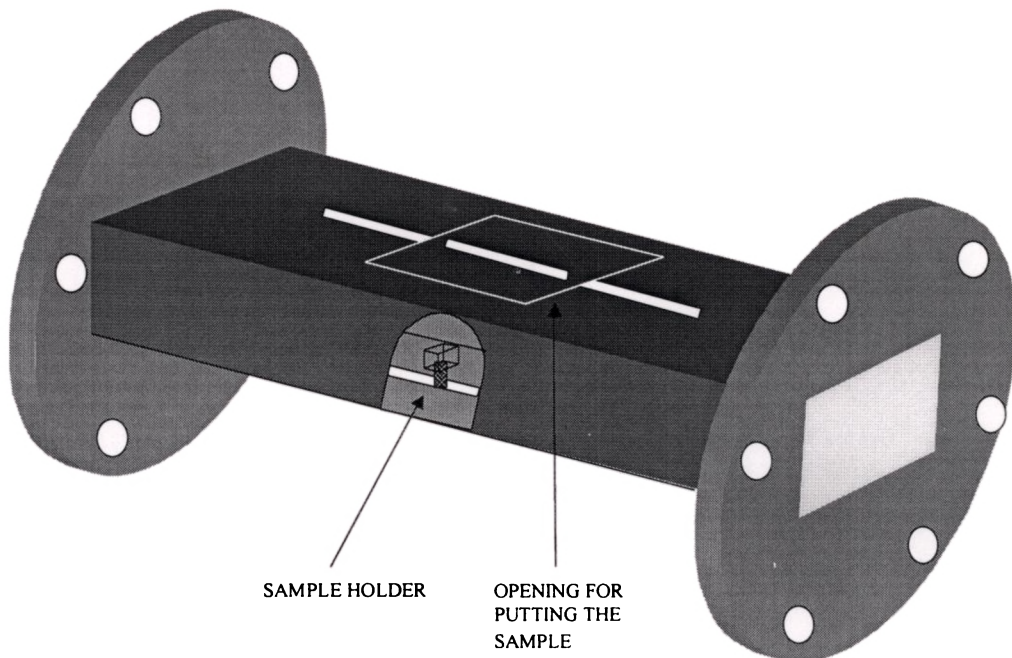


Figure 4.2 Schematic diagram of cavity resonator for bile stone measurement

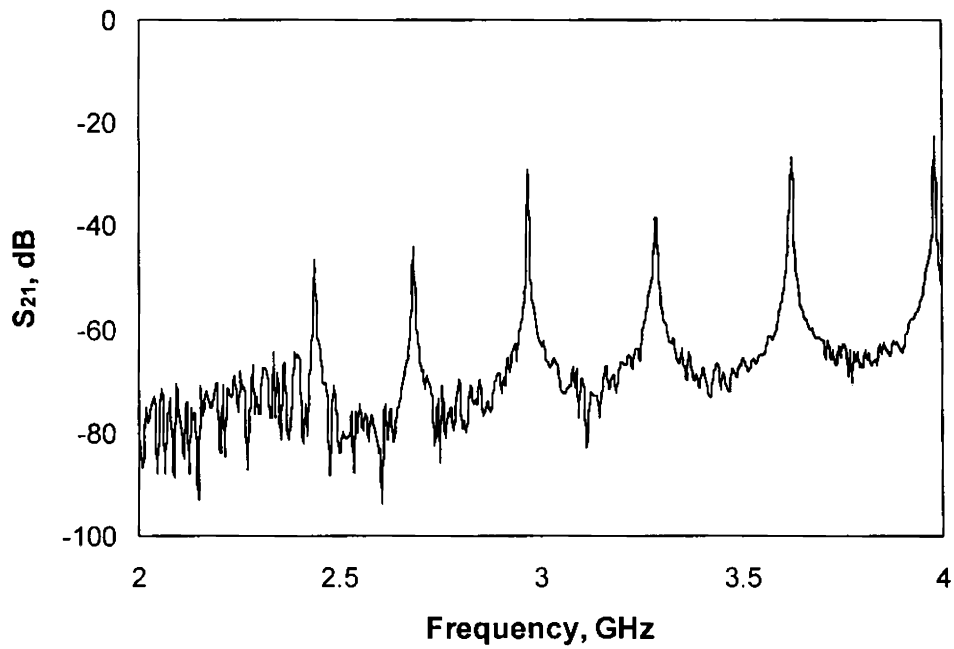


Figure 4.3a. Resonant frequency spectrum of S-band cavity resonator

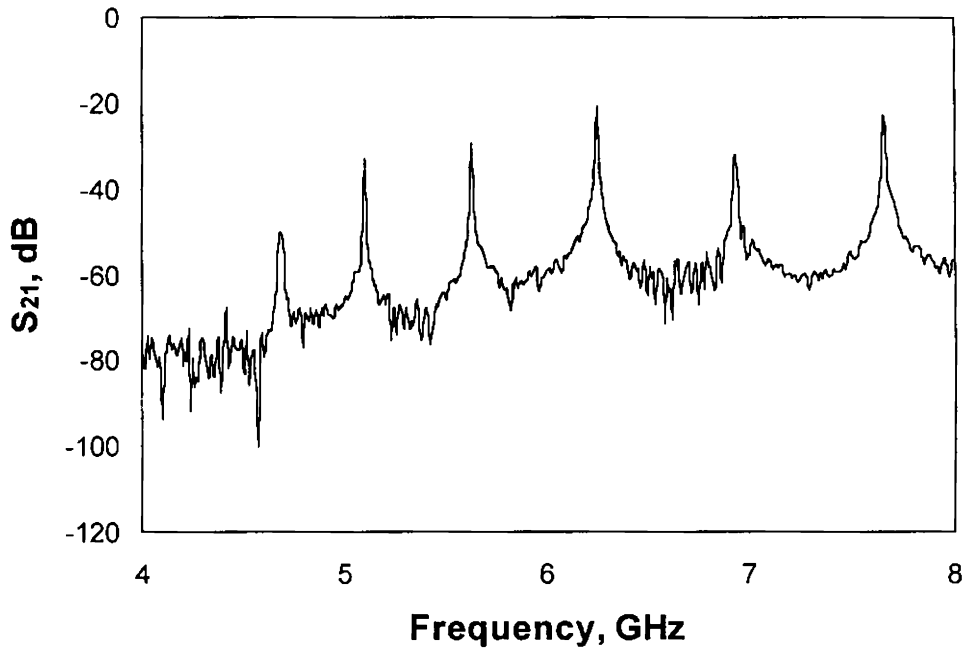


Figure 4.3b. Resonant frequency spectrum of C-band cavity resonator

Table 4.2 The characteristic features of rectangular cavity resonators

Type of cavity	Resonant Frequency (GHz)	Unloaded Q-factor
S-band Cavity 1 (TE ₁₀₃ – TE ₁₀₇)	2.4397	6870
	2.6833	6323
	2.9692	5716
	3.2853	4954
	3.6237	4289
S-band Cavity 2 (TE ₁₀₃ – TE ₁₀₆)	2.4615	2019
	2.8748	2100
	3.3713	1995
	3.9165	1743
C-band Cavity (TE ₁₀₃ - TE ₁₀₇)	5.0992	4391
	5.6335	5165
	6.2497	3017
	6.9282	2801
	7.6580	2750

4.4 Theoretical considerations

The determination of the complex permittivity and conductivity is based on the theory of perturbation. When a dielectric material is introduced in a cavity resonator at the position of maximum electric field, the contribution of magnetic field for the perturbation is minimum. The field perturbation due to the introduction of dielectric sample at the position of maximum electric field [40] is related by

$$-\frac{d\Omega}{\Omega} \approx \frac{(\bar{\epsilon}_r - 1) \int_{V_s} \mathbf{E} \cdot \mathbf{E}_0^* \max dV}{2 \int_{V_c} |\mathbf{E}_0|^2 dV} \quad (4.1)$$

where $d\Omega$ is the complex frequency shift.

E_0 is the electric field inside the unperturbed cavity and E is the electric field in the perturbed state, $\bar{\epsilon}_r$ is the relative complex permittivity of the sample. But $\bar{\epsilon}_r = \epsilon_r' - j\epsilon_r''$. where ϵ_r' is the real part of the complex permittivity, which is usually known as dielectric constant and ϵ_r'' is the imaginary part of the complex permittivity, which is associated with dielectric loss of the material. V_s and V_c are the volumes of the sample and the cavity resonator respectively.

Complex frequency shift is related to the Quality factor as

$$\frac{d\Omega}{\Omega} = \frac{d\omega}{\omega} + \frac{j}{2} \left(\frac{1}{Q_s} - \frac{1}{Q_t} \right) \quad (4.2)$$

Q_s and Q_t are the quality factors of cavity resonator with and without the sample respectively.

Quality factor Q is given by, $Q = \frac{f}{\Delta f}$

where f is the resonant frequency and Δf is the corresponding 3dB bandwidth.

For small sample, we assume that $E = E_0$.

For dominant TE_{10p} mode in rectangular wave guide,

$$E_0 = E_{0_{\max}} \sin \frac{\pi x}{a} \sin \frac{p\pi z}{d}, \quad p = 1, 2, 3, \dots \quad (4.3)$$

$E_{0_{\max}}$ is the peak value of E_0 . 'a' is the broader dimension and 'd', the length of the waveguide cavity resonator respectively.

From equations (4.1), (4.2) and (4.3), we get

$$\epsilon_r' - 1 = \frac{f_t - f_s}{2f_s} \left(\frac{V_c}{V_s} \right) \quad (4.4)$$

$$\epsilon_r'' = \frac{V_c}{4V_s} \left(\frac{Q_t - Q_s}{Q_t Q_s} \right) \quad (4.5)$$

Loss tangent is given by the expression

$$\tan \delta = \frac{\epsilon_r''}{\epsilon_r'} \quad (4.6)$$

The complex conductivity can be found out from the dielectric constant.

$$\sigma_e^* = j\omega \epsilon^* \quad (4.7)$$

But $\epsilon^* = \epsilon_0 (\epsilon_r' - j\epsilon_r'')$ is the complex absolute permittivity.

$$\sigma_e^* = \omega \epsilon_0 (j\epsilon_r' + \epsilon_r'') \quad (4.8)$$

The physical idea of conductivity is given by the real part of (4.8). The effective conductivity is written as

$$\sigma_e = \omega \epsilon_0 \epsilon_r'' \quad (4.9)$$

Materials can be classified in terms of their transparency to e.m. wave through it. The transparency is defined by the parameter, absorption coefficient [42], given by

$$\alpha = \frac{\pi \epsilon_r'' f}{nc} \quad (4.10)$$

where n is the real part of the complex refractive index $\sqrt{\epsilon^*}$, c is the velocity of light.

4.5 Measurement Procedure

For the measurements of complex permittivity of biological liquids, a capillary tube (radius less than 0.5 mm) made of low loss fused silica is used. The empty tube is cleaned, dried and inserted in the cavity resonator. One of the resonant frequencies is selected and the tube is adjusted for the position of maximum perturbation where the resonant frequency and 3dB bandwidth are determined. The empty tube is then taken out and filled with the biological liquid and the measurement is repeated to determine the new resonant frequency and 3dB bandwidth. The procedure is repeated for all other resonant frequencies. Measurements are made for different samples of bile, gastric juice, saliva, pancreatic juice, sweat and chicken bile.

For the measurement of cavity parameters with the solid samples (bile stones, pancreatic stone) the specially designed cavity resonator is used. Because of large sample size, the measurements are done in the S band only. When these samples are inserted in C-band, the perturbation condition - the perturbation should be small - fails. The sample is usually irregular and can be shaped by applying low pressure. The cup is placed in the cavity resonator through the rectangular slot of the waveguide. The rectangular slot is closed with a metal piece of correct size to form a part of the waveguide. As in the case of measurement of liquids, the resonant frequency and 3dB bandwidth of the cavity resonator with empty cup are determined. Then the experiment is repeated after placing the sample in the cup.

4.6 Accuracy conditions

Since all biological materials are high loss dielectrics, the volume of samples should be small in order to satisfy the perturbation conditions. Hence, capillary tubes of small diameter should be used. To satisfy the perturbation condition, the relative resonance frequency shift $\left(\frac{\delta f}{f}\right)$ should be of the order of 0.001. This means that the big samples, which will give a change of more than 0.001 GHz in the resonance frequency, may contribute some error in the determination of the permittivity. Similarly the shift in the quality factor should be only upto a fraction of 10-15% from

the unloaded condition. Also, the material of the capillary tube should be low loss ($\tan\delta$ should be of the order of 0.0001). Another very important point to be taken care is the very precise measurement of the radius of the capillary tube. The radius should be measured at different cross sections of the capillary tube and average value should be considered for the calculation. A slight error in the diameter measurement makes drastic changes in the results. The sample should be vertically placed inside the cavity. The inner side of the cavity resonator should be routinely cleaned and silvered to reduce the wall losses [29] as silvering improves the quality factors of the frequencies.

4.7 Experimental Results

4.7.1 Bile

The complex permittivities of normal and infected bile are found to differ. The dielectric constant of normal bile varies from 61 to 53 (± 2) in the frequency range from 2 GHz to 8 GHz. Depending on the nature of the disease, the infected bile has a dielectric constant greater or less than that of normal bile. But it is observed that most of the infected bile samples have high dielectric loss and conductivity than the normal bile. Eight samples were collected from the following patients with various diseases who were undergoing different types of treatment.

1. a patient suffering from a stone in the gall bladder and the bile duct (Cholelithiasis and Choledocholithiasis). Gall bladder and Common bile duct stones were removed by ERCP (sample 1)
2. a patient suffering from a bile duct stone (Choledocholithiasis) alone (sample 2)
3. a patient suffering from Cholestatic Jaundice (Primary Sclerosing Cholangitis), which is an inflammatory bowel disease. As a result, the bile ducts become narrowed and irregular. The gall bladder of this patient was removed by laproscopic cholecystectomy (sample 3).
4. a patient suffering from biliary obstruction and jaundice. (sample 4)

5. a patient suffering from Carcinoma Head Pancreas. He underwent stenting with the video endoscope. (sample 5)
6. a patient suffering from obstructive jaundice due to carcinoma of the Ampulla of Vater. (sample 6)
7. a patient suffering from acute calculus cholecystectomy. (sample 7)
8. a patient suffering from the same disease as in sample 7. But this patient got affected by the disease very recently. (sample 8)

Three samples of normal bile were collected and their average value is shown in the tables and figures as normal value for comparison. Real parts of complex permittivity of infected bile samples and normal bile are shown in *figure 4.4a & 4.4b* and the imaginary parts of complex permittivity of different samples in *figure 4.4c & 4.4d*.

Other dielectric parameters such as loss tangent $\tan \delta$, conductivity σ_c , absorption coefficient α and penetration depth δ for different samples are shown in the *tables 4.3a & 4.3b*.

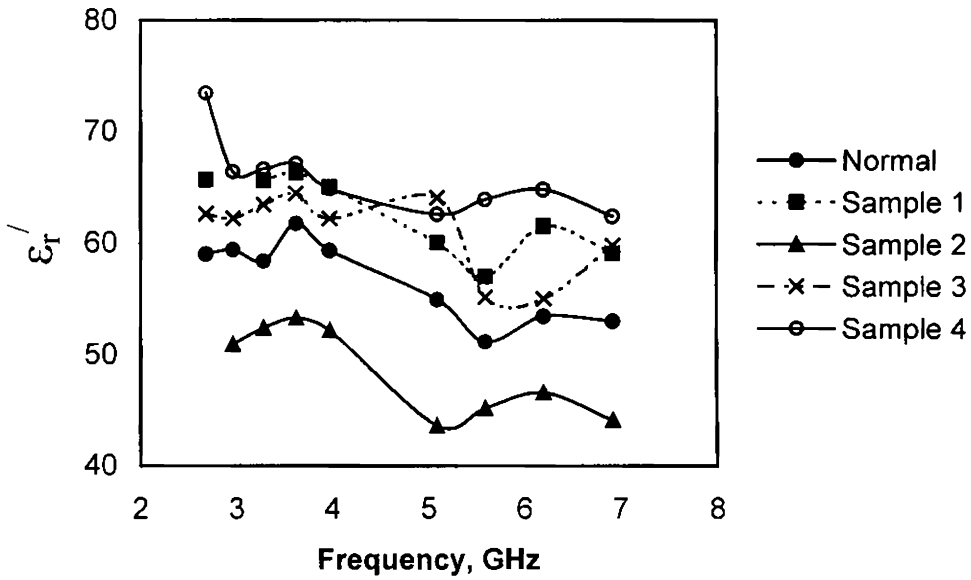


Figure 4.4a Real part of complex permittivity of bile samples with frequency

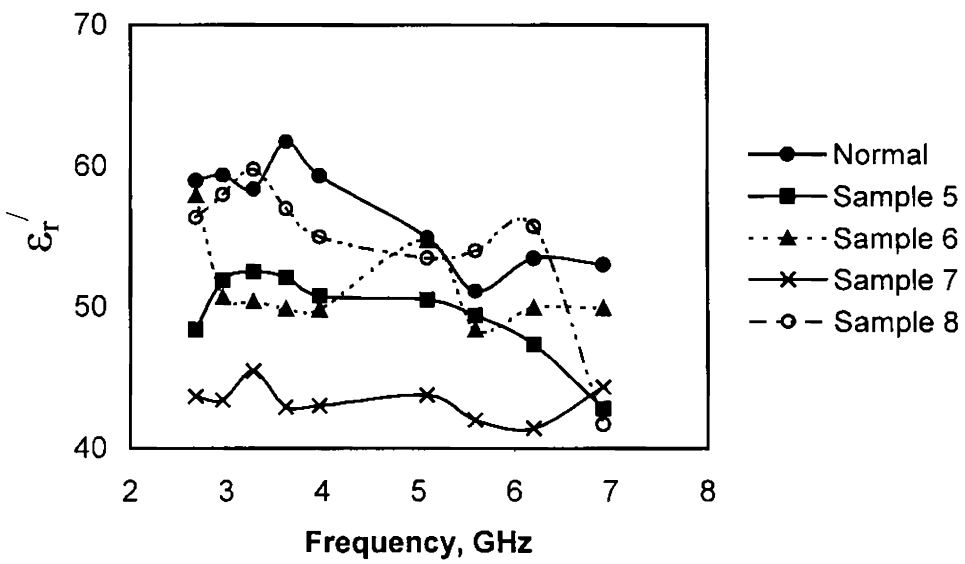


Figure 4.4b Real part of complex permittivity of bile samples with frequency

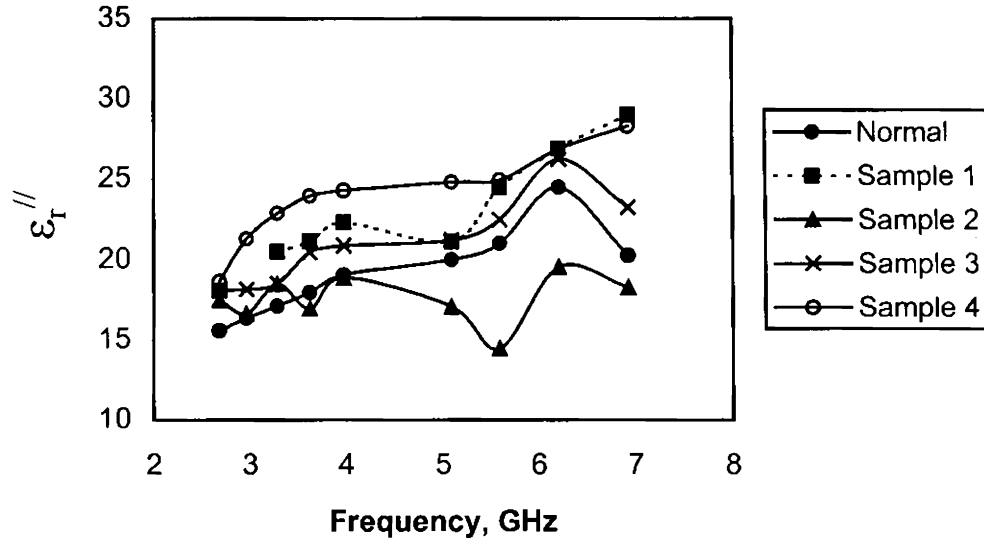


Figure 4.4c Imaginary part of complex permittivity of bile samples with frequency

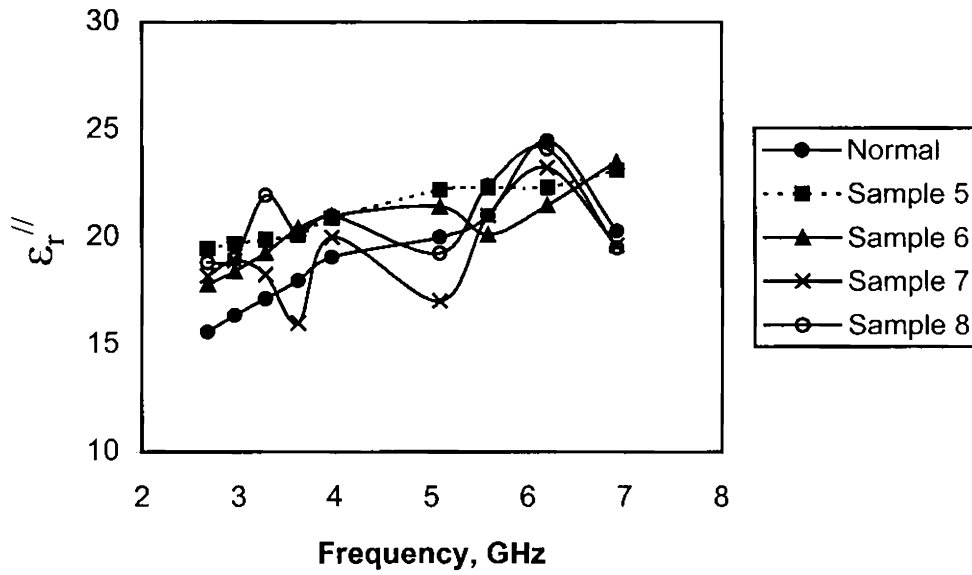


Figure 4.4d Imaginary part of complex permittivity of bile samples with frequency

Table 4.3a Loss tangent $\tan \delta$, conductivity σ_e , absorption coefficient α and penetration depth δ for different bile samples

	f (GHz)	$\tan \delta$	σ_e (S/m)	α (m ⁻¹)	δ (cm)
Normal	2.68	0.264	2.322	56.440	1.771
	3.28	0.293	3.122	76.160	1.312
	3.97	0.321	4.207	101.59	0.984
	5.09	0.364	5.660	141.59	0.706
	6.20	0.457	8.435	212.04	0.471
	6.92	0.382	7.799	198.27	0.504
Sample 1	2.68	0.275	2.694	62.056	1.611
	3.28	0.312	3.737	85.870	1.164
	3.97	0.343	4.924	113.42	0.881
	5.09	0.352	5.977	143.19	0.698
	6.20	0.437	9.272	217.75	0.459
	6.92	0.490	11.153	265.76	0.376
Sample 2	2.96	0.326	2.737	71.320	1.402
	3.28	0.353	3.372	86.440	1.156
	3.97	0.362	4.170	107.04	0.934
	5.09	0.391	4.834	135.40	0.738
	6.20	0.419	6.736	182.06	0.549
	6.92	0.414	7.038	195.59	0.511
Sample 3	2.68	0.289	2.694	63.500	1.574
	3.28	0.292	3.376	79.020	1.265
	3.97	0.335	4.604	108.510	0.921
	5.09	0.331	6.002	139.430	0.717
	6.20	0.476	9.038	223.53	0.447
	6.92	0.388	8.938	213.89	0.467
Sample 4	2.68	0.254	2.780	60.627	1.649
	3.28	0.343	4.170	94.881	1.053
	3.97	0.374	5.361	123.310	0.810
	5.09	0.396	7.015	163.981	0.609
	6.2	0.414	9.255	212.243	0.471
	6.92	0.453	10.884	253.347	0.394

Table 4.3b Loss tangent $\tan \delta$, conductivity σ_e , absorption coefficient α and penetration depth δ for different bile samples

	f (GHz)	$\tan \delta$	σ_e (S/m)	α (m^{-1})	δ (cm)
Normal	2.68	0.264	2.322	56.44	1.771
	3.28	0.293	3.122	76.16	1.312
	3.97	0.321	4.207	101.59	0.984
	5.09	0.364	5.660	141.59	0.706
	6.20	0.457	8.435	212.04	0.471
	6.92	0.382	7.799	198.27	0.504
Sample 5	2.68	0.402	2.898	76.987	1.298
	3.28	0.378	3.625	92.655	1.079
	3.97	0.411	4.604	119.308	0.838
	5.09	0.439	6.277	162.616	0.614
	6.2	0.471	7.697	205.343	0.486
	6.92	0.539	8.884	247.447	0.404
Sample 6	2.68	0.307	2.651	64.846	1.542
	3.28	0.382	3.513	91.606	1.091
	3.97	0.421	4.633	121.098	0.825
	5.09	0.391	6.060	151.489	0.660
	6.2	0.430	7.401	193.018	0.518
	6.92	0.470	9.038	234.826	0.425
Sample 7	2.68	0.416	2.710	75.708	1.320
	3.28	0.401	3.326	91.173	1.096
	3.97	0.465	4.412	123.595	0.809
	5.09	0.389	4.817	134.713	0.742
	6.2	0.560	8.004	226.070	0.442
	6.92	0.442	7.542	208.487	0.479
Sample 8	2.68	0.333	2.803	69.378	1.441
	3.28	0.367	3.999	95.867	1.043
	3.97	0.381	4.633	115.644	0.864
	5.09	0.359	5.445	138.085	0.724
	6.2	0.432	8.304	204.941	0.487
	6.92	0.467	7.499	213.199	0.469

4.7.2 Bile Stone

Hard biological materials deposited in the gall bladder or the bile duct are generally known as bile stones (Cholithiasis and Choledocholithiasis). Such materials deposited in the pancreas are known as pancreatic stones. The complex permittivity of bile stones collected from these patients were also studied. The real and imaginary parts of the complex permittivity are shown in the *figures 4.5a & 4.5b*. *Table 4.4* shows other dielectric parameters derived from the complex dielectric constant.

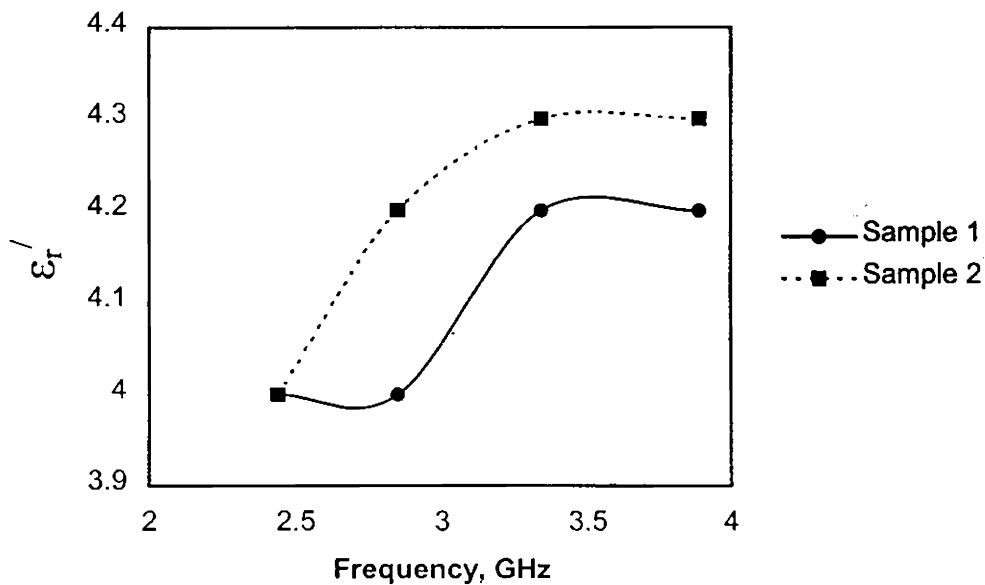


Figure 4.5a Real part of complex permittivity of bile stone samples with frequency

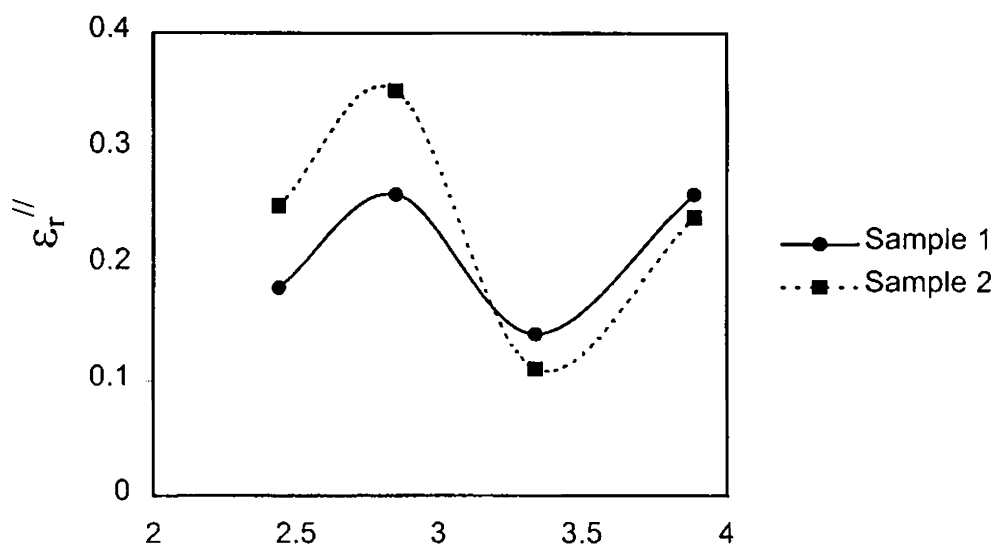


Figure 4.5b Imaginary part of complex permittivity of bile stone samples with frequency

Table 4.4 Loss tangent $\tan \delta$, conductivity σ_e , absorption coefficient α and penetration depth δ for different bile stone samples

	f (GHz)	$\tan \delta$	σ_e (S/m)	α (m ⁻¹)	δ (cm)
Sample 1	2.44	0.045	0.0244	2.298	43.518
	2.85	0.065	0.0412	3.876	25.800
	3.34	0.033	0.0256	2.388	41.879
	3.89	0.061	0.0562	5.163	19.368
Sample 2	2.44	0.063	0.0339	3.191	31.340
	2.85	0.083	0.0554	5.090	19.646
	3.34	0.026	0.0204	1.854	53.929
	3.89	0.056	0.0518	4.710	21.229

The dielectric constant of these samples is found to be almost the same as that of fat [4]. Slight variations in the real and imaginary parts of the complex permittivity of different bile stones were observed.

4.7.3 Gastric Juice

Gastric juices of two persons were collected and complex permittivities of these samples were determined. The two persons were suffering from gall stone disease and artral erosion. They underwent the removal of the gall bladder, which contained multiple mixed stones. The dielectric constant and dielectric loss of gastric juice varies from patient to patient. *Figures 4.6a & 4.6b* describe the variation of complex permittivity of the samples and *table 4.5* gives other dielectric parameters.

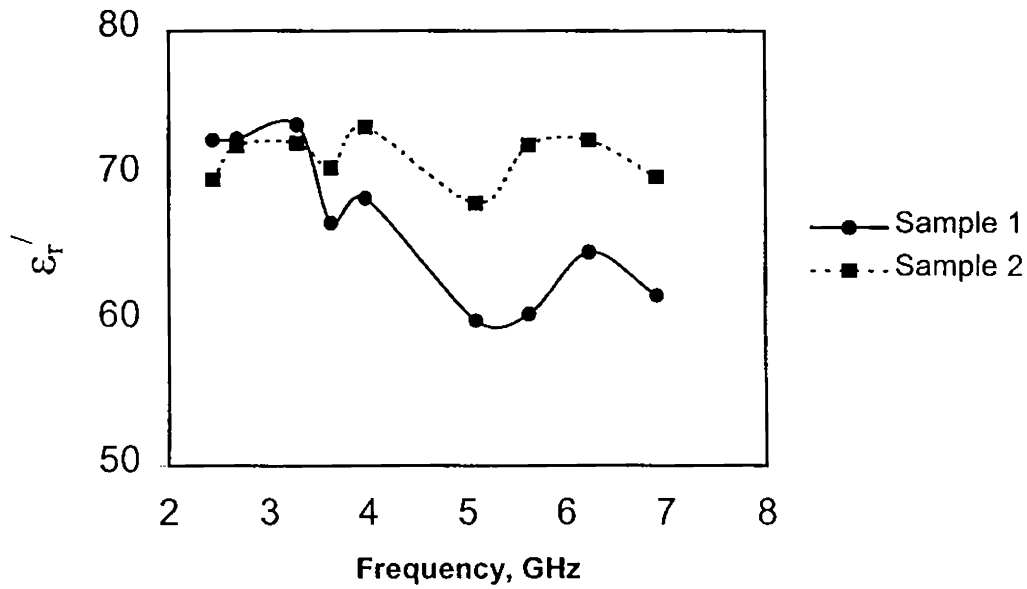


Figure 4.6a Real part of complex permittivity of gastric juice samples with frequency

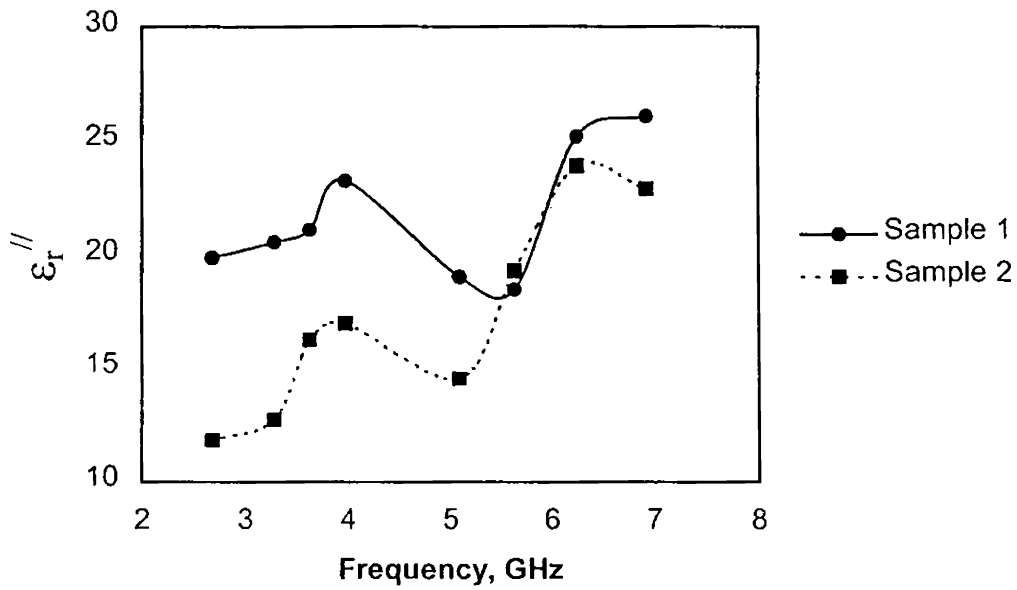


Figure 4.6b Imaginary part of complex permittivity of gastric juice samples with frequency

Table 4.5. Loss tangent $\tan \delta$, conductivity σ_e , absorption coefficient α and penetration depth δ for different gastric juice samples

	f (GHz)	$\tan \delta$	σ_e (S/m)	α (m ⁻¹)	δ (cm)
Sample 1	2.44	0.242	2.371	52.114	1.919
	2.68	0.274	2.959	64.851	1.542
	3.28	0.279	3.748	81.557	1.226
	3.62	0.316	4.243	96.664	1.034
	3.97	0.339	5.127	115.158	0.868
	5.09	0.317	5.380	129.241	0.773
	5.63	0.305	5.779	138.394	0.722
	6.24	0.389	8.732	200.790	0.498
	6.92	0.422	10.026	235.368	0.425
Sample 2	2.44	0.136	1.285	28.935	3.456
	2.68	0.164	1.763	39.001	2.564
	3.28	0.177	2.324	51.316	1.948
	3.62	0.230	3.273	72.941	1.371
	3.97	0.231	3.748	81.907	1.229
	5.09	0.213	4.113	93.363	1.071
	5.63	0.267	6.035	132.707	0.753
	6.24	0.329	8.285	180.991	0.552
	6.92	0.327	8.803	195.812	0.511

4.7.4 Saliva

Both saliva and gastric juice have many similar functions. It is observed that there is a slight variation in the dielectric properties for these two biological materials. Saliva was collected from two healthy persons. *Figures 4.7a & 4.7b* show the variation of real and imaginary parts of the complex permittivity with frequency and the derived dielectric parameters are tabulated in *table 4.6*.

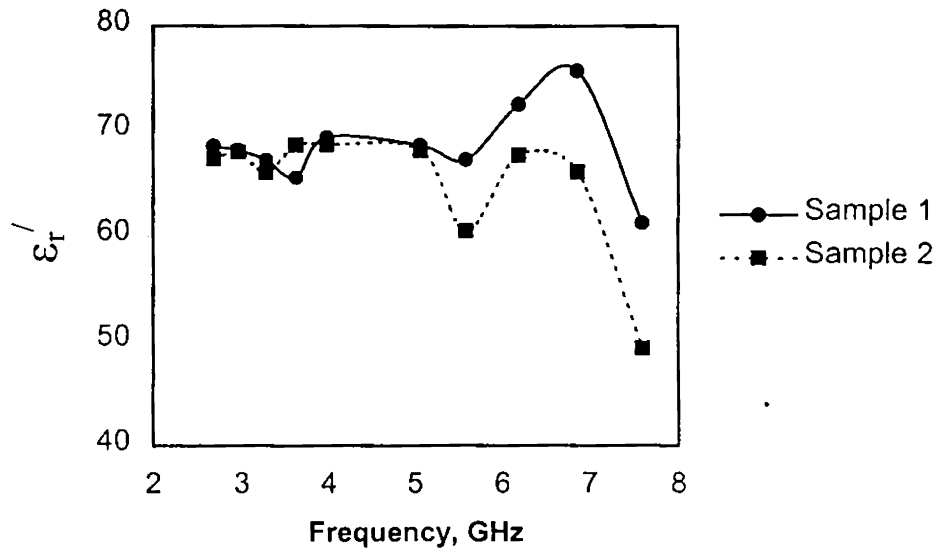


Figure 4.7a Real part of complex permittivity of gastric juice samples with frequency

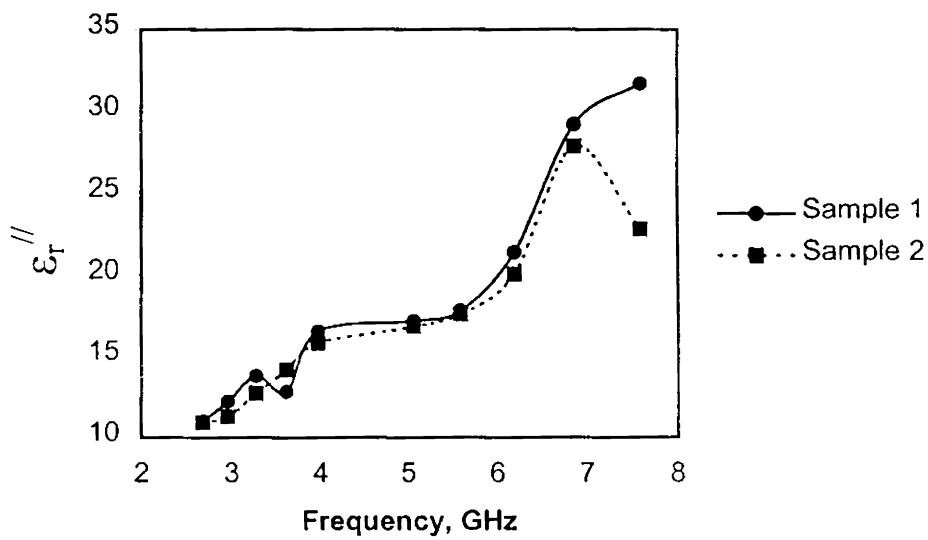


Figure 4.7b Imaginary part of complex permittivity of gastric juice samples with frequency

Table 4.6 Loss tangent $\tan \delta$, conductivity σ_e , absorption coefficient α and penetration depth δ for different saliva samples

	f (GHz)	$\tan \delta$	σ_e (S/m)	α (m ⁻¹)	δ (cm)
Sample 1	2.68	0.160	1.635	37.09	2.696
	2.96	0.179	2.008	45.65	2.190
	3.28	0.205	2.514	57.46	1.740
	3.62	0.195	2.573	59.61	1.677
	3.97	0.238	3.645	81.86	1.221
	5.06	0.250	4.823	108.87	0.918
	5.58	0.264	5.520	125.74	0.795
	6.19	0.295	7.351	160.91	0.621
	6.86	0.385	11.125	236.61	0.422
	7.6	0.517	13.381	312.41	0.320
Sample 2	2.68	0.162	1.626	37.22	2.687
	2.96	0.165	1.855	42.25	2.367
	3.28	0.193	2.324	53.64	1.864
	3.62	0.206	2.848	64.44	1.552
	3.97	0.230	3.484	78.68	1.270
	5.06	0.246	4.722	106.96	0.935
	5.58	0.291	5.455	130.81	0.764
	6.19	0.296	6.890	156.14	0.640
	6.86	0.422	10.618	241.03	0.415
	7.6	0.462	9.622	251.74	0.397

4.7.5 Pancreatic Stone

Complex Permittivity of pancreatic stone collected from a patient was studied. These stones are harder than bile stones and have the same physical nature of kidney stone. *Figures 4.8a & 4.8b* show the variation of real and imaginary parts of the complex permittivity with frequency and the derived dielectric parameters are tabulated in *table 4.7*.

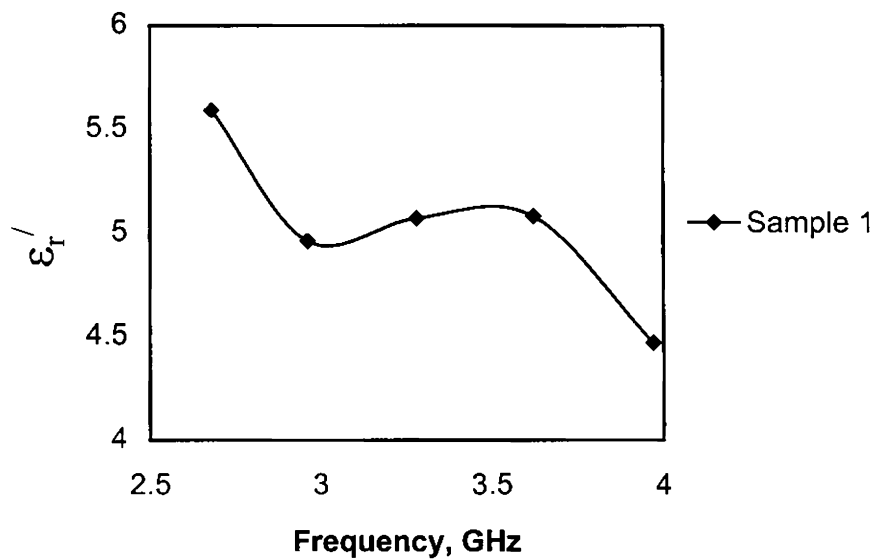


Figure 4.8a Real part of complex permittivity of pancreatic stone sample with frequency

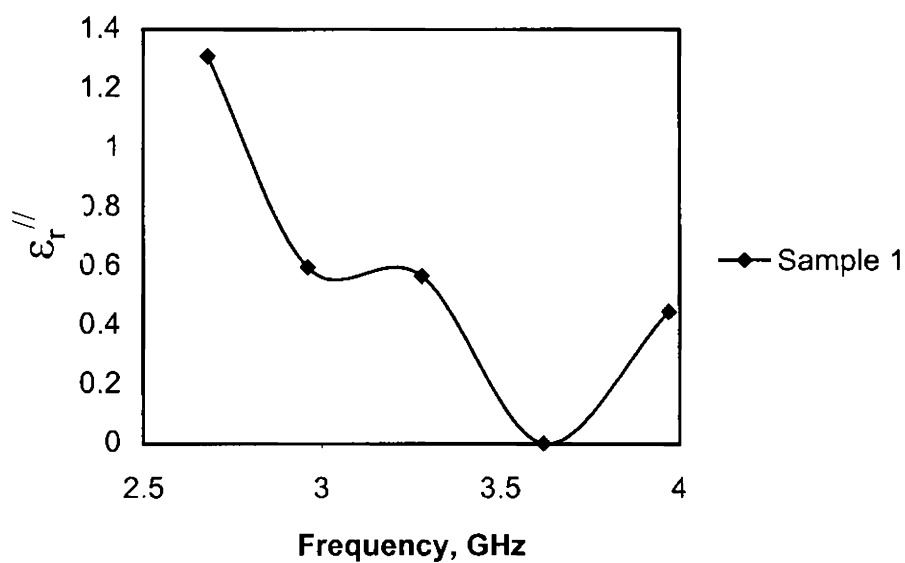


Figure 4.8b Imaginary part of complex permittivity of pancreatic stone sample with frequency

Table 4.7 Loss tangent $\tan \delta$, conductivity σ_e , absorption coefficient α and penetration depth δ for pancreatic stone sample

f (GHz)	$\tan \delta$	σ_e (S/m)	α (m^{-1})	δ (cm)
2.68	0.2343	0.1951	15.438	6.477
2.96	0.1204	0.0983	8.298	12.050
3.28	0.1120	0.1035	8.646	11.565
3.62	0.0002	0.0002	0.018	5407.82
3.97	0.1002	0.0988	8.794	11.372

4.7.6 Pancreatic Juice

Complex permittivity of pancreatic juice collected from two persons was determined. The two persons were suffering from gal stone disease and artral erosion. They underwent surgery for the removal of gall bladder, which contained multiple mixed stones. The pancreas of these persons was normal. Dielectric constant and dielectric loss of pancreatic juice were determined. *Figures 4.9a & 4.9b* show the real and imaginary parts of the average complex permittivity of pancreatic juice and *table 4.8* gives other dielectric parameters such conductivity, loss tangent, absorption coefficient and penetration depth.

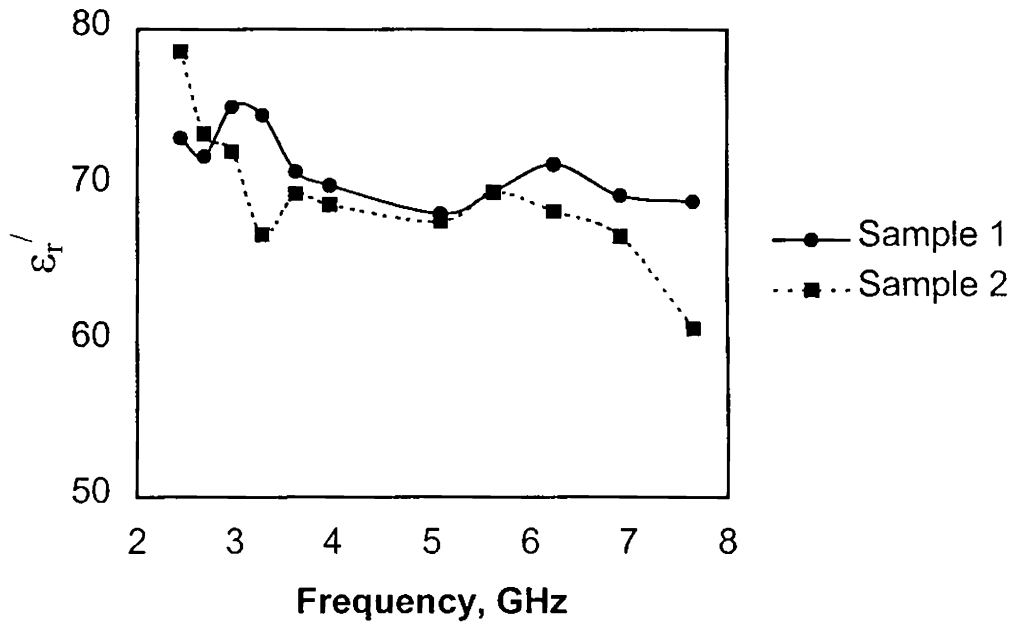


Figure 4.9a. Real part of complex permittivity of pancreatic juice samples with frequency

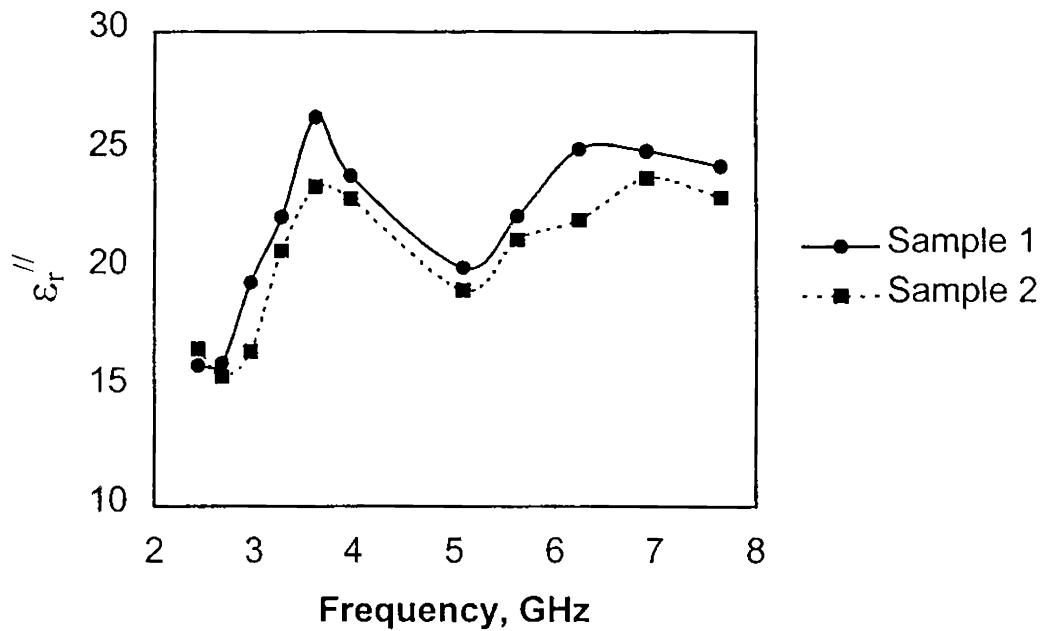


Figure 4.9b. Imaginary part of complex permittivity of pancreatic juice samples with frequency

Table 4.8 Loss tangent $\tan \delta$, conductivity σ_e , absorption coefficient α and penetration depth δ for different pancreatic juice samples

	f (GHz)	$\tan \delta$	σ_e (S/m)	α (m ⁻¹)	δ (cm)
Sample 1	2.44	0.218	2.160	47.328	2.112
	2.68	0.223	2.387	52.731	1.896
	2.97	0.259	3.207	69.175	1.445
	3.28	0.298	4.050	87.449	1.143
	3.62	0.372	5.315	116.952	0.855
	3.97	0.342	5.288	117.385	0.851
	5.09	0.294	5.680	128.194	0.780
	5.63	0.319	6.968	155.373	0.643
	6.24	0.351	8.697	191.089	0.523
	6.92	0.360	9.614	214.061	0.467
	7.65	0.353	10.352	231.296	0.432
Sample 2	2.44	0.211	2.255	47.647	2.098
	2.68	0.211	2.302	50.386	1.984
	2.97	0.229	2.728	60.106	1.663
	3.28	0.310	3.786	86.200	1.160
	3.62	0.338	4.728	105.364	0.949
	3.97	0.334	5.074	113.716	0.879
	5.09	0.282	5.411	122.678	0.815
	5.63	0.306	6.656	148.671	0.672
	6.24	0.323	7.667	172.481	0.579
	6.92	0.357	9.180	208.391	0.479
	7.65	0.378	9.800	232.617	0.429

4.7.7 Sweat

Sweat was collected from two person and the dielectric constant was determined. The result shows that the real part of the complex permittivity of sweat is almost the same as that of urine [43]. Frequency dependency of the complex permittivity is shown in the *figures 4.10a & 4.10b*. *Table 4.9* gives the variation of other parameters with frequency and sample.

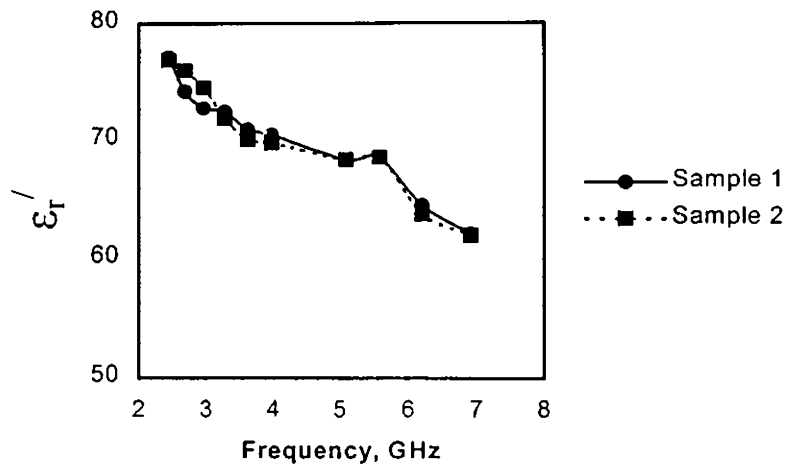


Figure 4.10a Real part of complex permittivity of sweat samples with frequency

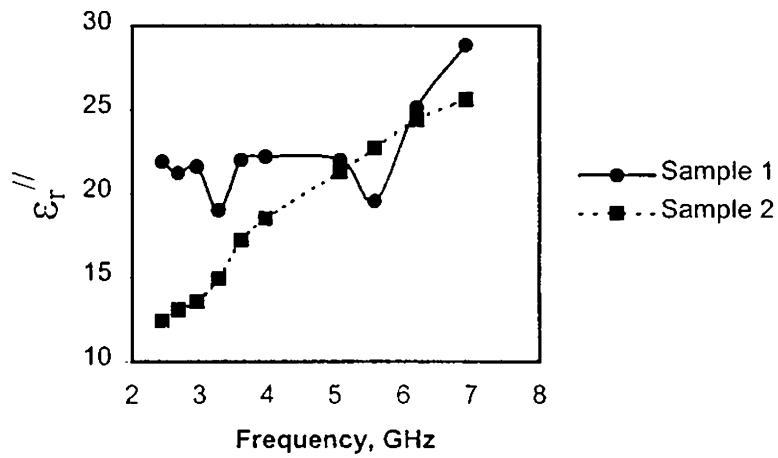


Figure 4.10b Imaginary part of complex permittivity of sweat samples with frequency

Table 4.9 Loss tangent $\tan \delta$, conductivity σ_e , absorption coefficient α and penetration depth δ for different sweat samples

	f (GHz)	$\tan \delta$	σ_e (S/m)	α (m ⁻¹)	δ (cm)
Sample 1	2.44	0.284	2.970	63.076	1.585
	2.68	0.286	3.161	68.410	1.462
	2.96	0.297	3.555	77.645	1.288
	3.28	0.262	3.464	75.968	1.316
	3.62	0.310	4.426	97.786	1.023
	3.97	0.315	4.898	108.559	0.921
	5.09	0.322	6.224	139.962	0.714
	5.59	0.285	6.074	136.749	0.731
	6.2	0.389	8.659	199.379	0.502
	6.92	0.464	11.092	258.469	0.387
Sample 2	2.44	0.161	1.682	36.003	2.778
	2.68	0.172	1.944	41.837	2.390
	2.97	0.182	2.231	48.461	2.064
	3.28	0.207	2.716	60.008	1.666
	3.62	0.245	3.461	77.266	1.294
	3.97	0.265	4.082	91.228	1.096
	5.09	0.311	6.026	135.611	0.737
	5.63	0.331	7.052	158.260	0.632
	6.24	0.382	8.408	194.824	0.513
	6.92	0.413	9.846	230.805	0.433

4.7.8 Chicken Bile

Complex permittivity of chicken bile is studied with an intention to get a comparison of the value of human bile. It is collected in a capillary tube and inserted in to the cavity resonator. As before the measurement is performed. The dielectric nature of this sample is illustrated in *figures 4.11a & 4.11b* and in *table 4.10*.

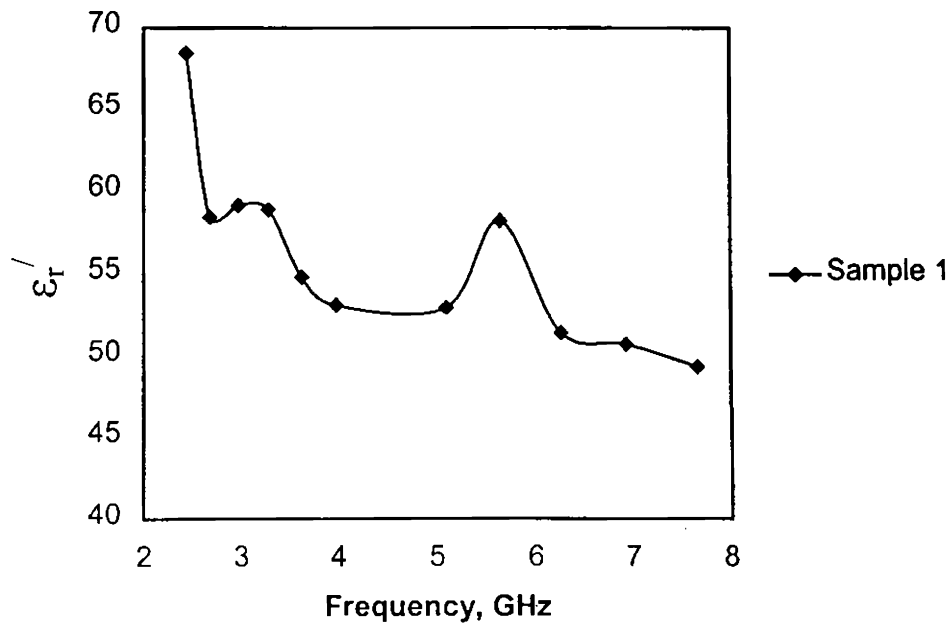


Figure 4.11a Real part of complex permittivity of chicken bile with frequency

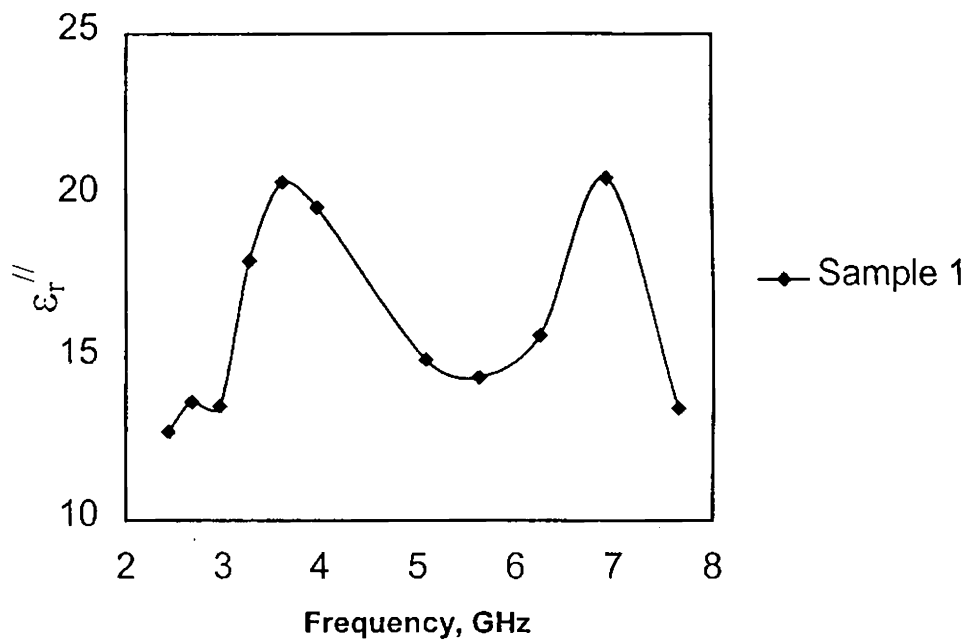


Figure 4.11b Imaginary part of complex permittivity of chicken bile with frequency

Table 4.10 Loss tangent $\tan \delta$, conductivity σ_e , absorption coefficient α and penetration depth δ for chicken bile sample

f (GHz)	$\tan \delta$	σ_e (S/m)	α (m^{-1})	δ (cm)
2.44	0.1858	1.725	39.100	2.557
2.68	0.2337	2.033	49.774	2.009
2.97	0.2285	2.230	54.276	1.842
3.28	0.3058	3.281	79.647	1.255
3.62	0.3725	4.106	102.764	0.973
3.97	0.3700	4.333	110.214	0.907
5.09	0.2825	4.229	108.429	0.922
5.63	0.2478	4.512	110.578	0.904
6.25	0.3061	5.464	141.939	0.704
6.92	0.4053	7.904	205.025	0.488
7.65	0.2728	5.723	152.064	0.657

The comparison of the *figures 4.4 & 4.11* and *tables 4.3 & 4.10* shows that the complex permittivity and other derived quantities of chicken bile does not vary much with that of human bile except for some slight random variations.

4.8 Dielectric contrast of fluids with water

As the body fluids are having aqueous base, the dielectric parameters of the samples are compared with the reference values of water obtained by the same method. The complex permittivity of water is given in *table 4.11*. The comparison will give the idea of the percentage of water in the samples. The dielectric contrast of different samples with respect to water is given in *figures 4.12-4.17*.

Table 4.11. Complex permittivity of water

Frequency, GHz	ϵ_r'	ϵ_r''
2.68	76.42	7.92
2.96	75.61	9.20
3.28	74.32	11.93
3.62	74.26	14.86
3.97	72.74	16.20
5.09	72.06	16.41
5.59	70.91	17.68
6.20	69.43	20.1
6.92	67.73	21.5

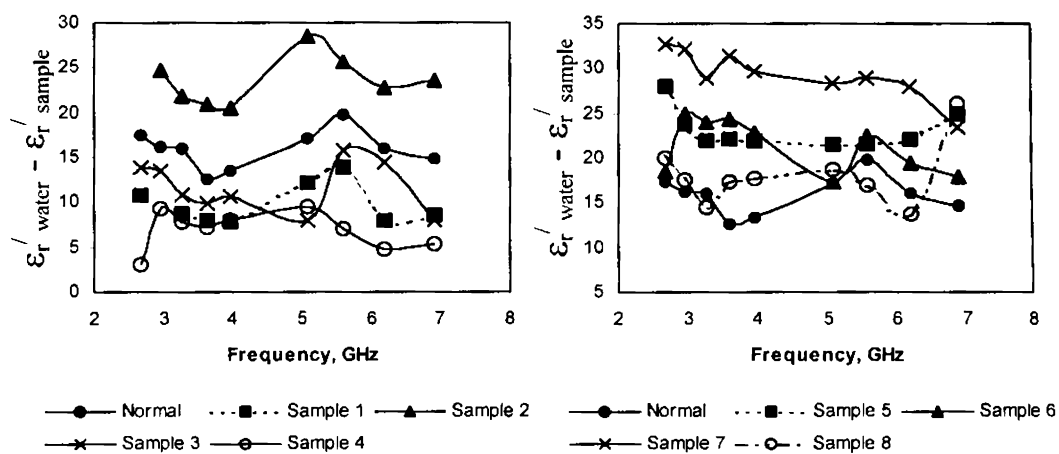


Figure 4.12a Dielectric contrast of bile samples (Real part)

From the figures 4.12a & 4.12b, it is observed that all the bile samples are having dielectric constant less than that of water but the imaginary part is higher than the corresponding value for water.

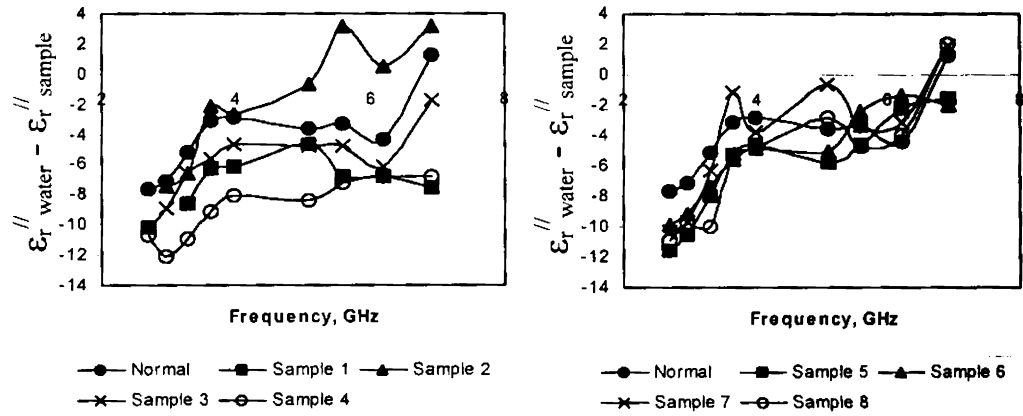


Figure 4.12b Dielectric contrast of bile samples (Imaginary part)

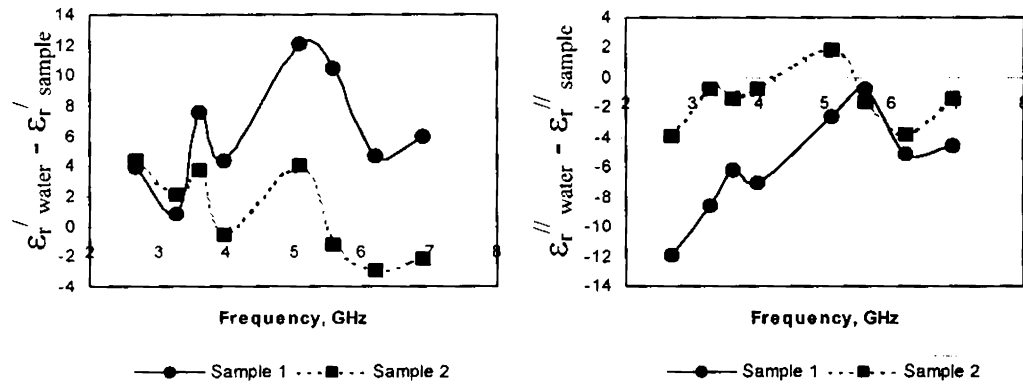


Figure 4.13 Dielectric contrast of Gastric Juice

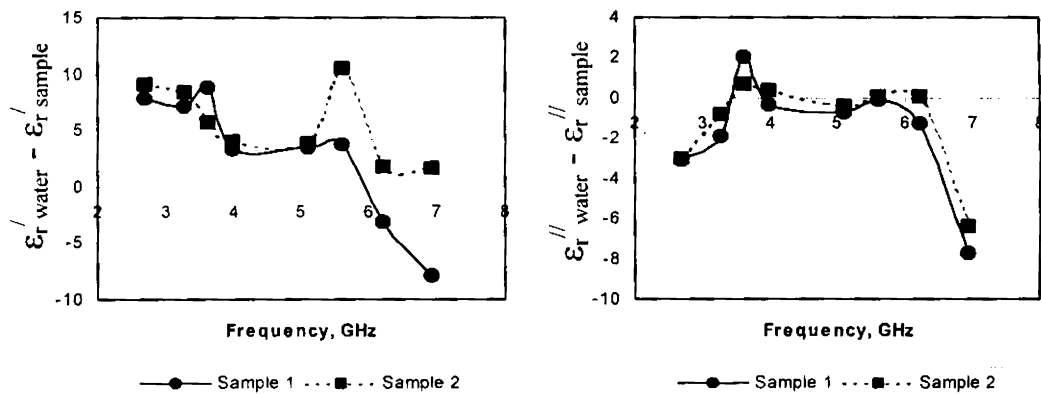


Figure 4.14 Dielectric contrast of saliva

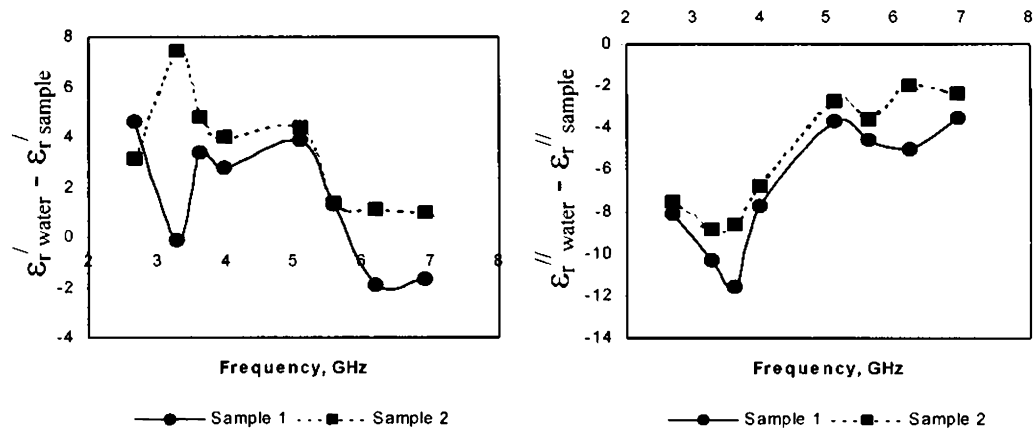


Figure 4.15 Dielectric contrast of Pancreatic Juice

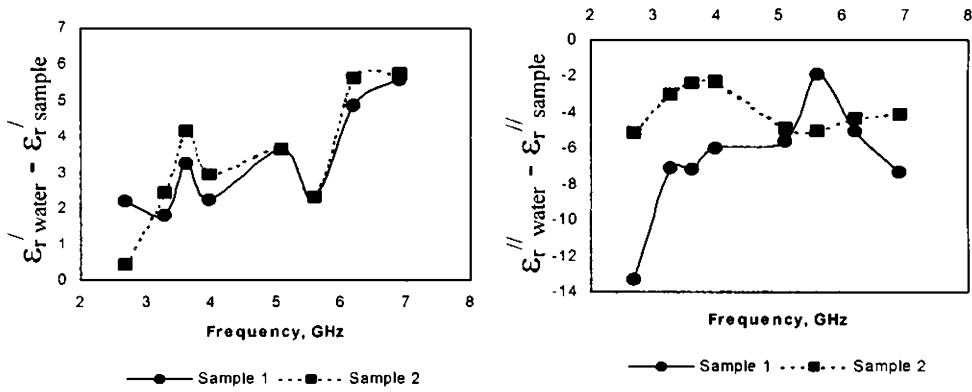


Figure 4.16 Dielectric contrast of Sweat

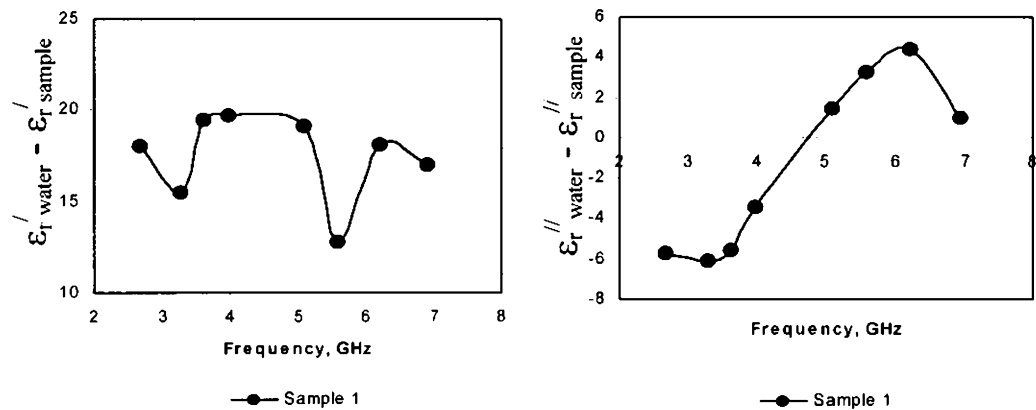


Figure 4.17 Dielectric contrast of Chicken bile

4.9 Summary

Dielectric characterization of biological tissues at microwave frequencies is done. Different biological samples are collected from a digestive disease center. The samples subjected for the study include: bile, bile stone, gastric juice, pancreatic juice, pancreatic stone, saliva, sweat and chicken bile. As the samples are available only in small quantities, the cavity perturbation technique is most suited for the study. Special type S-band cavity resonator with the provision for inserting the solid samples is designed, fabricated and used for the measurement of samples like pancreatic stone and bile stone. The measurement is limited only to S-band for these samples to satisfy the perturbation condition. The fluid samples are characterized in the S and C band frequencies. Variation of relative complex permittivity values of the samples with frequency are shown graphically and other derived dielectric properties such as loss tangent, conductivity, absorption coefficient and penetration depth are given in tables. As the body fluids have aqueous base, the dielectric parameters of the samples are compared with the reference values of water.

The dielectric nature of normal bile sample is found to be exactly the same as reported in [13]. The real parts of complex permittivity of malignant bile samples do not show a consistent nature of variation with respect to the corresponding normal sample. But the imaginary part of most of the bile samples are noticed to be high compared to that of normal bile. Conductivities of the malignant bile samples are also high. The dielectric constant of bile stone is found to be nearly the same as that of fat.

Comparison with standard values in the case of other fluids is not done as the values are not available in literature.

References

1. H.F.Cook, "The dielectric behaviour of human blood at microwave frequencies", *Nature*, vol.168, pp.247-248, 1951.
2. H.F.Cook, "The dielectric behaviour of some types of human tissues at microwave frequencies", *Brit. J. Appl. Phys.*, vol.2, pp.295-304, 1951.
3. H.P. Schwan, "Electrical Properties of tissue and cell suspensions", *Adv. Biol. Med. Phys.* Vol. 5, pp.147-209, 1957.
4. Musil, J. and Zacek, F., "Microwave measurements of complex permittivity by free space methods and their applications", *Studies in Electrical and Electronic Engineering 22*, Elsevier Science Publishers. Amsterdam, 1986.
5. C. Polk and E. Postow, "CRC Handbook of Biological Effects of Electromagnetic Fields", CRC Press. Second Edition, 1995.
6. C.Gabriel, S.Gabriel and E.Corthout: "The dielectric properties of biological tissues: I. Literature survey", *Phys. Med. Biol.*, Vol.41, pp.2231-2249, 1996.
7. S.Gabriel, R.W.Lau and C.Gabriel: "The dielectric properties of biological tissues: II. Measurements in the frequency range 10 Hz to 20 GHz", *Phys. Med. Biol.*, Vol. 41, pp.2251-2269, 1996.
8. S.Gabriel, R.W.Lau and C.Gabriel: "The dielectric properties of biological tissues: III. Parametric models for the dielectric spectrum of tissues", *Phys. Med. Biol.*, Vol.41, pp.2271-2293, 1996.
9. U.Raveendranath, Biju Kumar.S, Sebastian Mathew and K.T.Mathew, "Microwave diagnosis of diabetes in human beings using cavity perturbation technique", *Proc. On International Conference Microwave and Millimeterwave Technology-98*, Beijing, China, pp. 803-806, August 1998.
10. Biju Kumar.S, U.Raveendranath, Philip Augustine and K.T.Mathew, "The Study Of The Dielectric Behaviour of Human Bile At Microwave Frequencies", *Proc. On Third Workshop on Electromagnetic Wave Interaction With Water and Moist Substances*, Athens, Georgia, pp.235-238. 1999.
11. Biju Kumar. S, U. Raveendranath, Philip Augustine and K. T. Mathew, "Dielectric Properties Of Certain Biological Materials At Microwave Frequencies", *J. Microwave Power*, Vol. 36, No.3, pp.67-75, 2001.

12. Biju Kumar.S, Philip Augustine and K.T.Mathew, "Dielectric properties of certain biological materials at microwave frequencies", Proceedings on Fourth Conference on Electromagnetic Wave Interaction With Water and Moist Substances, May 13-16, Weimar, Germany, pp. 73-78, 2001.
13. Internet document: URL: <http://niremf.iroec.fcnr.it/tissprop/>
14. Katie F. Staebell and Devendra Misra, "An experimental technique for In Vivo permittivity measurement of Materials at microwave frequencies" IEEE Trans. on Microwave Theory and Techniques, Vol. 38, No. 3, pp. 337-339, March 1990.
15. Hornback N., Shupe R., Shidnia H., Joe B., Sayoc E., George R. and Marshall C., "Radiation and microwave therapy in the treatment of advanced cancer", Radiology, Vol. 130, pp. 459-464, 1978.
16. Salcman M., "Clinical hyperthermia trials: design principles and practice" J. Microwave power, Vol.16, No. 2, pp. 171-177, 1981.
17. Naoya Hoshi, Yoshio Nikawa, Keiji Kawai and Shigeyuki Ebisu, "Application of Microwaves and Millimeter waves for the characterization of teeth for dental diagnosis and treatment", IEEE Trans. on Microwave Theory and Tech., Vol. 46, No.6, pp, 834-838, June 1998.
18. Masahiro Hiraoka, Michihide Mitsumori, Naotoshi Hiroi, Shinji Ohno, Yoshiaki Tanaka, Youji Kotsuka and Keizo Sugimachi, "Development of RF and Microwave Heating Equipment and clinical applications to Cancer treatment in Japan", IEEE Trans. on Microwave Theory and Tech., Vol. 48, No.11, pp, 1789-1799, November 2000.
19. B.H.Brown and B.C. Barber, "Applied potential tomography-A new in vivo medical imaging technique" Clin. Phys. Physiol. Meas. Vol. 4, No. 1, 1982.
20. Peter M. Edic, Gary J. Saulnier, Jonathan C. Newell and David Isaacson, "A Real-Time Electrical Impedance Tomograph", IEEE Trans. on Biomedical Engg., Vol. 42, No. 9, pp. 849-859, September 1995.
21. Jean-Francois Chateaux and Mustapha Nadi, "Comparison of performances of electrical impedances tomography evaluated with 2-D and 3-D models", IEEE Trans. on Microwave Theory and Techniques. Vol. 48, No.11, pp. 1874-1878, November 2000.
22. Lawrence E. Larsen and John H. Jacobi, "Medical Applications of Microwave Imaging", IEEE Press, The Institute of Electrical and Electronics Engineers, Inc., New York, 1985.
23. B.Bocquet, VAN DE Velde, A. Mamouni, Y.Leroy. G. Glaux. J. Delannoy and D. Delvallee, "Microwave Radiometric Imaging at 3 GHz for the

- exploration of Breast Tumors”, *IEEE Trans. on Microwave Theory and Techniques*, Vol. 38, No. 6, pp.791-793, June 1990.
24. Paul M. Meaney, Keith D. Paulsen, Alexander Hartov and Robert K. Crane, “An Active Microwave Imaging system for reconstruction of 2-D Electrical property distribution”, *IEEE Trans. on Biomedical Engg.*, Vol. 42, No. 10, pp. 1017-1026, October 1995.
 25. R.D. Murch and T.K.K. Chan, “Improving microwave imaging by enhancing diffraction tomography” *IEEE Trans. on Microwave Theory and Techniques*, Vol. 44, pp. 379-388, 1996.
 26. Ann Franchois and Christian Pichot, “Microwave Imaging-Complex Permittivity Reconstruction with a Levenberg-Marquardt method”, *IEEE Trans. on Antennas and Propag.*, Vol. 45, No. 2, pp. 203-215, February 1997.
 27. Serguei Y. Semenov et al., “Three Dimensional Microwave Tomography: Experimental prototype of the system and Vector Born Reconstruction method”, *IEEE Trans. on Biomedical Engg.*, Vol. 46, No. 8, pp. 937-946, August 1999.
 28. Paul M. Meaney, Margaret W. Fanning, Dun Li, Steven P. Poplack and Keith D. Paulsen, “A Clinical prototype for active microwave imaging of the breast”, *IEEE Trans. on Microwave Theory and Techniques*, Vol. 48, No.11, pp. 1841-1853, November 2000.
 29. Linfeng Chen, C. K. Ong and B. T. G. Tan, “Amendment of Cavity Perturbation method for Permittivity measurement of extremely low-loss dielectrics”, *IEEE Trans. on Instrumentation and Measurement*, Vol.48, No.6, pp. 1031-1037, December 1998.
 30. Internet document; URL: <http://www-ibt.etec.uni-karlsruhe.de/people/mag/frames/papers/EMC99-MD/node3.html>
 31. William D. Hurt, John M. Zirix and Patrick A. Mason, “Variability in EMF Permittivity values: Implications for SAR calculations”, *IEEE Trans. on Biomedical Engg.*, Vol. 47, No. 3, pp. 396-401, March 2000.
 32. R.F. Cleveland Jr and T.W. Athey, “Specific Absorption rate (SAR) in models of the human head exposed to hand-held UHF portable radios”. *Bioelectromagn.*, Vol.10, pp.173-186, 1989.
 33. O.P. Gandhi and J.Y. Chen, “Electromagnetic absorption in the human head from experimental 6 GHz handheld transceivers” *IEEE Trans. Electromag. Compat.*, Vol.37, 1995, pp.547-558.
 34. Klaus Meier, Volker Hombach, Ralf Kastle, Roger Yew-Siow Tay and Niels Kuster, “The dependance of electromagnetic energy absorption upon human-

- head modeling at 1800 MHz”, IEEE Trans. on Microwave Theory and Techniques, Vol. 45, No.11, November 1997, pp. 2058-2062.
35. Jacques Thuery, “MICROWAVES: Industrial, Scientific and Medical Applications”, Artech House, 1992.
 36. H.A.Bethe and J.Schwinger, NRDC Report D1-117, Cornell University, March 1943.
 37. R.A.Waldron, "Perturbation theory of resonant cavities", Proc. IEE, Vol.107C, pp. 272-274,1960.
 38. R.F.Harrington, “Time - Harmonic Electromagnetic Fields”, McGraw-Hill, New York, p. 317, 1961.
 39. U.Raveendranath and K.T.Mathew, " New cavity perturbation technique for measuring the complex permeability of ferrite materials ", Microwave and Optical Tech.Lett., vol.18, pp.241-243, 1998.
 40. H. Baltes, W. Gopel and J. Hesse (Editors), “Sensors Update Volume 7”, Wiley-VCH, Germany, pp.185-210, 2000.
 41. Richard G. Carter, “Accuracy of microwave cavity perturbation measurements”, IEEE Trans. on Microwave Theory and Techniques, Vol. 49, No.5, pp. 918-923, May 2001.
 42. Bradford L. Smith and M. Carpentier, “The Microwave Engineering Handbook”, Vol.3, Chapman and Hall, 1993.
 43. U. Raveendranath, “The study of the dielectric and magnetic properties of materials using modified cavity perturbation techniques”, Ph.D Dissertation, Mahatma Gandhi University, Kottayam, India, May 1996.

Conclusions and Future Scope

The thesis mainly focuses on material characterization in different environments: freely available samples taken in planar form, biological samples available in small quantities and buried objects. Each of these studies is given in separate chapter.

Free space method, which is described in chapter 2, finds many applications in the fields of industry, medicine and communication. As it is a non-contact method, it can be employed for monitoring the electrical properties of materials moving through a conveyor belt in real time. Also, measurement on such systems at high temperature is possible. NID theory can be applied to the characterization of thin films. Dielectric properties of thin films deposited on any dielectric substrate can be determined. In chemical industry, the stages of a chemical reaction can be monitored online. Online monitoring will be more efficient as it saves time and avoids risk of sample collection.

Chapter 3 deals with the applications of GPR in the detection of buried objects. Dielectric contrast is one of the main factors, which decides the detectability of a system. It could be noted that the two dielectric objects of same dielectric constant 3.2 (ϵ_r of plastic mine) placed in a medium of dielectric constant 2.56 (ϵ_r of sand) could even be detected employing the time domain analysis of the

reflected signal. This type of detection finds strategic importance as it provides solution to the problem of clearance of non-metallic mines. The demining of these mines using the conventional techniques had been proved futile. The studies on the detection of voids and leakage in pipes find many applications.

A rare study on some of the biological tissues is presented in the chapter 5. The determined electrical properties of tissues can be used for numerical modeling of cells, microwave imaging, SAR test etc. All these techniques need the accurate determination of dielectric constant. In the modern world, the use of cellular and other wireless communication systems is booming up. At the same time people are concerned about the hazardous effects of microwaves on living cells. The effect is usually studied on human phantom models. The construction of the models requires the knowledge of the dielectric parameters of the various body tissues. It is in this context that the present study gains significance. The case study on biological samples shows that the properties of normal and infected body tissues are different. Even though the change in the dielectric properties of infected samples from that of normal one may not be a clear evidence of an ailment, it is an indication of some disorder.

In medical field, the free space method may be adapted for imaging the biological samples. This method can also be used in wireless technology. Evaluation of electrical properties and attenuation of obstacles in the path of RF waves can be done using free waves. An intelligent system for controlling the power output or frequency depending on the feed back values of the attenuation may be developed.

The simulation employed in GPR can be extended for the exploration of the effects due to the factors such as the different proportion of water content in the soil, the level and roughness of the soil etc on the reflected signal. This may find applications in geological explorations. In the detection of mines, a state-of-the art

technique for scanning and imaging an active mine field can be developed using GPR. The probing antenna can be attached to a robotic arm capable of three degrees of rotation and the whole detecting system can be housed in a military vehicle. In industry, a system based on the GPR principle can be developed for monitoring liquid or gas through a pipe, as pipe with and without the sample gives different reflection responses. It may also be implemented for the online monitoring of different stages of extraction and purification of crude petroleum in a plant.

Since biological samples show fluctuation in the dielectric nature with time and other physiological conditions, more investigation in this direction should be done. The infected cells at various stages of advancement and the normal cells should be analysed. The results from these comparative studies can be utilized for the detection of the onset of such diseases. Studying the properties of infected tissues at different stages, the threshold of detectability of infected cells can be determined.

APPENDIX:REPRINTS OF PUBLISHED PAPERS

tremely sharp peaks at the lateral spectral frequencies that coincide with the real parts of the surface-wave poles. Therefore a more sophisticated method should be utilized for accurate integration, such as a 20-point Gaussian quadrature. Besides, the original finite integration limits effectively may be replaced by $k_x/k_0 = -20.0$ and $+20.0$ without causing noticeable errors since a significant variation concentrates between the two points. Similarly, remarkable peaks exist in the low spectral range for the off-diagonal spectral matrix elements, and a major amplitude variation resides between $k_x/k_0 = -40.0$ and $+40.0$, which are recommended to replace the original infinite limits as well.

REFERENCES

1. N.K. Das and D.M. Pozer, Full-wave spectral-domain computation of material, radiation and guided wave losses in infinite multilayered printed transmission lines, *IEEE Trans Microwave Theory Tech* 39 (1991), 54–63.
2. H. Shigesawa, M. Tsuji, and A.A. Oliner, Dominant mode power leakage from printed-circuit waveguides, *Radio Sci* 26 (1991), 559–564.
3. D. Nghiem, J.T. Williams, D.R. Jackson, and A.A. Oliner, Proper and improper dominant mode on stripline with a small air gap, *Radio Sci* 28 (1993), 1163–1180.
4. D. Nghiem, J.T. Williams, D.R. Jackson, and A.A. Oliner, Existence of a leaky dominant mode on microstrip line with an isotropic substrate: Theory and measurements, *IEEE Trans Microwave Theory Tech* 44 (1996), 1710–1715.
5. R.E. Collin, *Field theory of guided waves*, IEEE Press, New York, 1991, 2nd ed., chap. 5.
6. T. Itoh (Editor), *Numerical techniques for microwave and millimeter-wave passive structures*, Wiley, New York, 1989, chap. 5.
7. K.C. Gupta, R. Garg, and I. Bahl, *Microstrip lines and slotlines*, Artech House, Norwood, MA, 1996, 2nd ed., chap. 2.
8. H.P. Hsu, *Outline of Fourier analysis*, Unitech, 1967.
9. R.V. Churchill, J.W. Brown, and R.F. Verhey, *Complex variables and applications*, McGraw-Hill, New York, 1974, 3rd ed., chap. 5.
10. D. Hanselman and B. Littlefield, *Mastering Matlab™ 5: A comprehensive tutorial and reference*, Prentice-Hall, Englewood Cliffs, NJ, 1996.
11. G.J. Borse, *Numerical methods with Matlab™*, PWS Publishing, New York, 1997.
12. S. Nam and T. Itoh, Calculation of accurate complex resonant frequency of an open microstrip resonator using the spectral domain method, *Electromag Waves Appl* 2 (1988), 635–651.

© 2000 John Wiley & Sons, Inc.

A SIMPLE FREE-SPACE METHOD FOR MEASURING THE COMPLEX PERMITTIVITY OF SINGLE AND COMPOUND DIELECTRIC MATERIALS

S. Biju Kumar,¹ U. Raveendranath,¹ P. Mohanan,¹ K. T. Mathew,¹ M. Hajian,² and L. P. Ligthart²

¹Department of Electronics
Cochin University of Science and Technology
Cochin-682 022, Kerala, India

²Department of Electrical Engineering
Technical University of Delft
2628 CD Delft, The Netherlands

Received 27 January 2000

ABSTRACT: A simple and efficient method for determining the complex permittivity of dielectric materials from both reflected and transmitted

Contract grant sponsor: IRCTR, Delft University, The Netherlands
Contract grant number: Project Agreement TU Delft IS 980077

signals is presented. It is also novel because the technique is implemented using two pyramidal horns without any focusing mechanisms. The dielectric constant of a noninteractive and distributive (NID) mixture of dielectrics is also determined. © 2000 John Wiley & Sons, Inc. *Microwave Opt Technol Lett* 26: 117–119, 2000.

Key words: free-space method; complex permittivity; compound materials

INTRODUCTION

Many papers have been published on the free-space measurement of the permittivity and permeability of materials [1–3]. Although the basic principles involved and parameters measured are the same, each method has its own novelty, uniqueness, and limitations. Free-space measurement of the dielectric constant of concrete [1] gives only the real part of the complex permittivity at very low frequency. The permittivity and permeability measurement with a focused beam for normal and oblique incidence [2] uses an ellipsoidal reflector. An elaborate free-space method using highly focused electromagnetic waves with spot-focused antennas [3] measures the complex permittivity and permeability. In this method, ϵ and μ are chosen from the multivalued solutions by properly selecting the sample thickness. The authors propose a simple free-space measurement technique for determining the complex permittivity of sample materials over a wide range of frequencies.

EXPERIMENTAL SETUP AND MEASUREMENT TECHNIQUE

The experimental setup consists of a vector network analyzer (VNA), an S -parameter test set, a sweep oscillator, an interfacing computer, and a microwave test bench. The test bench is made up of low-loss polystyrene materials in order to minimize unwanted reflection. The schematic diagram of the experimental setup is shown in Figure 1. Two identical antennas are mounted on the test bench, and the sample material in the form of a flat sheet is kept positioned at the reference plane. The measurements are carried out in the J - and X -bands. For J -band measurement, pyramidal horns of a half-power beam width (HPBW) of 22.5° (E -plane) and 21.5° (H -plane) and aperture dimensions $14\text{ cm} \times 10.5\text{ cm}$ are used. For X -band, the antennas have an HPBW of 18° (E -plane) and 15.5° (H -plane) and aperture dimensions of $9.8\text{ cm} \times 7.5\text{ cm}$. To minimize unwanted reflection from the surroundings, the test bench is situated in the anechoic chamber.

To begin, the system is calibrated using the thru-reflect-line (TRL) technique. For J - and X -band measurements, calibration standards in the TRL option should be modified separately. To increase the accuracy of measurement, a gating option is also applied. In order to minimize the edge diffraction, the sample size should be more than 5λ . S_{11} and S_{21} are measured after fixing the sample sheet at the reference plane. The effective dielectric constant of a noninteractive distributive (NID) mixture of dielectrics also can be found from the S -parameter measurements. Sample sheets are kept together at the sample holder for the measurement. This method can be extended to any number of samples of known thickness and surface area.

THEORETICAL ANALYSIS

Consider a dielectric slab of thickness d placed in free space. Using the ray-tracing model, the total input reflection coefficient can be written in a geometric series that takes the

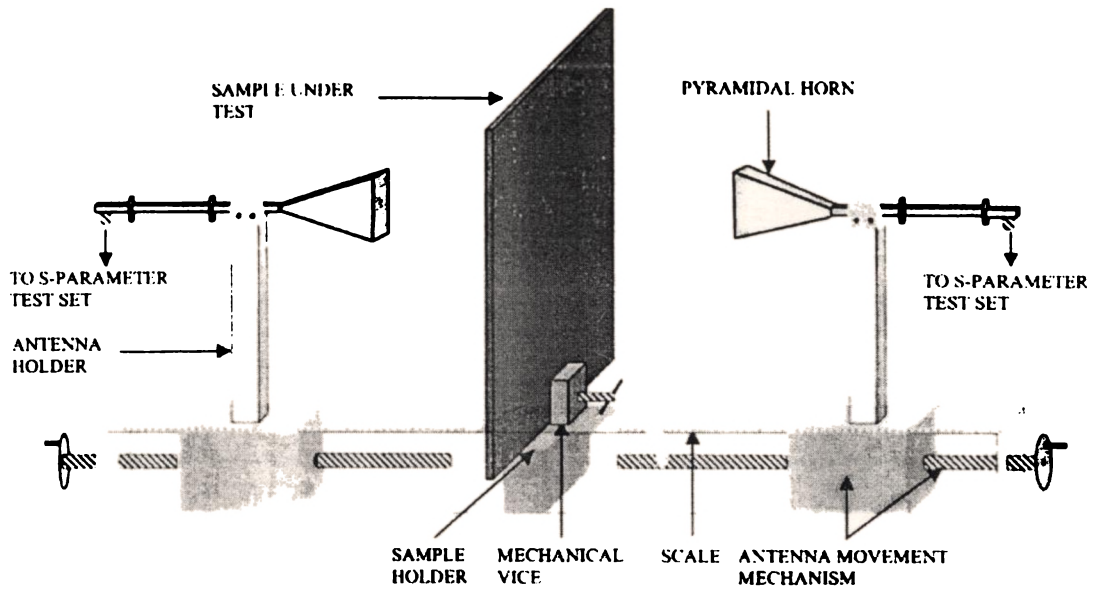


Figure 1 Schematic diagram of microwave test bench with the sample

form [4]

$$\Gamma_{in} = \Gamma_{12} + \frac{T_{12}T_{21}\Gamma_{21}e^{-2j\beta d}}{1 - \Gamma_{21}^2e^{-2j\beta d}} \quad (1)$$

Γ_{12} is the intrinsic reflection coefficient of the initial reflection, and $(T_{12}T_{21}\Gamma_{21}e^{-2j\beta d})$ is the contribution due to the first bounce within the slab. $\beta d = (2\pi d/\lambda) = (2\pi d\sqrt{\mu_r\epsilon_r}/\lambda_0)$, where λ is the wavelength in the medium, λ_0 is the free-space wavelength, and μ_r and ϵ_r are the complex relative permeability and permittivity of the medium, respectively. We also know that $\Gamma_{21} = -\Gamma_{12}$, $T_{12} = 1 + \Gamma_{12}$, and $T_{21} = 1 + \Gamma_{21} = 1 - \Gamma_{12}$. The indexes 1 and 2 represent the air and the medium, respectively. Rearranging Eq. (1),

$$\Gamma_{in} = S_{11} = \frac{[1 - e^{-2j(\omega d/c)x}]}{[1 - \Gamma_{12}^2e^{-2j(\omega d/c)x}]} \Gamma_{12} \quad (2)$$

Usually for a dielectric medium, μ_r is taken as unity, and $\sqrt{\mu_r\epsilon_r}$ is reduced to $\sqrt{\epsilon_r} = \sqrt{\epsilon_r' - j\epsilon_r''} = x$.

Similarly, the total transmission coefficient T_{12} is evaluated as

$$T_{12} = S_{21} = \frac{[(1 - \Gamma_{12}^2)e^{-j(\omega d/c)x}]}{[1 - \Gamma_{12}^2e^{-2j(\omega d/c)x}]} \quad (3)$$

The reflection coefficient Γ_{12} at the air-medium interface is related to the impedances Z_0 and Z_1 of the air and

dielectric slab, respectively, as $\Gamma_{12} = (Z_1 - Z_0)/(Z_1 + Z_0)$. But $Z_0 = 120\pi$ and $Z_1 = (Z_0/x)$. Solving S_{11} and S_{21} independently, x can be found, and hence, the complex dielectric constant ϵ_r . The exponentials in Eqs. (2) and (3) should be expanded to a sufficient number of terms for the convergence of the required solution.

The effective dielectric constant of a compound of different noninteracting and distributive materials [5] is given by the expression

$$\epsilon_{r\text{ eff}} = \frac{\sum_{i=1}^n \epsilon_{ri}t_i}{\sum_{i=1}^n t_i} \quad (4)$$

where ϵ_{ri} and t_i are the dielectric constant and the thickness of samples of the same cross-sectional area, respectively. Equation (4) can be used to verify the results obtained by the present method for the NID mixtures.

EXPERIMENTAL RESULTS

The complex permittivity and loss tangent of the different dielectric materials are determined from the measured values of S_{11} and S_{21} . It is observed that the complex permittivity calculated from S_{11} is identical to that from S_{21} . The results are in good agreement with the standard values [3]. Tables 1

TABLE 1 Complex Permittivity of Different Samples from the Reflection Measurement

Frequency (GHz)	NID Mixture (Polystyrene-Glass)									
	Glass		Polystyrene		Glass Epoxy		Free Space		Theory [5]	
	ϵ_r'	$\tan \delta$	ϵ_r'	$\tan \delta$	ϵ_r'	$\tan \delta$	ϵ_r'	$\tan \delta$	ϵ_r'	$\tan \delta$
5.4	4.85	0.147	2.65	0.064	3.49	0.272	3.9	0.174	3.84	0.122
5.8	4.56	0.144	2.55	0.050	3.44	0.238	3.52	0.210	3.63	0.113
6.2	4.41	0.156	2.47	0.040	3.36	0.208	3.54	0.104	3.52	0.118
6.6	4.32	0.178	2.40	0.033	3.26	0.193	3.26	0.082	3.43	0.133

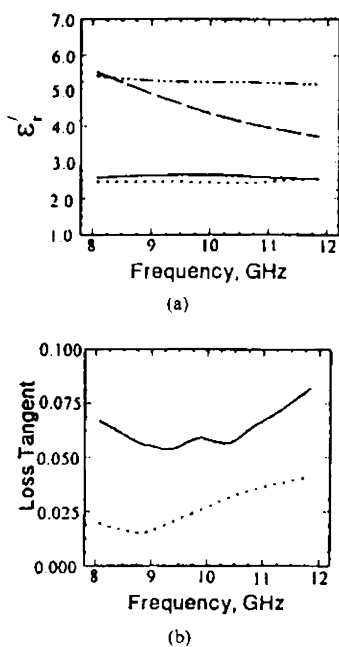


Figure 2 (a) Variation of ϵ' with frequency. — polystyrene (from S_{11} measurement), polystyrene (from S_{21} measurement), ---- glass (from S_{11} measurement), - · - · - glass (from S_{21} measurement). (b) Variation of loss tangent with frequency. — average of values measured from S_{11} and S_{21} for polystyrene, average of values measured from S_{11} and S_{21} for glass

and 2 show the complex permittivity of polystyrene (thickness = 4 mm), glass (thickness = 4.76 mm), glass epoxy (thickness = 1.56 mm), and NID mixtures of polystyrene-glass (thickness = 8.76 mm) and polystyrene-glass epoxy (thickness = 5.56 mm). Figure 2(a) shows the variation of ϵ' versus frequency, and Figure 2(b) shows the variation of average loss tangent versus frequency for glass and polystyrene in the X-band. From Tables 1 and 2, it can be seen that the effective dielectric constant obtained for NID mixtures by the present method is identical to that obtained from [5]. Thus, the determination of the effective dielectric constant is a clear support to the theory of NID mixture.

CONCLUSIONS

A novel free-space method of measuring the complex permittivity using two ordinary pyramidal horn antennas of sufficient flaring is presented. Measurement of reflection and transmission coefficients can be simultaneously done, and the complex permittivity is computed from both of the data. The absence of a focusing mechanism does not adversely affect

the accuracy of S_{11} and S_{21} . It is observed that the sum of the reflected and transmitted power from a perfect dielectric polystyrene sheet is nearly equal to unity, and the energy loss due to nonfocusing is less than 1.2%. The complex permittivity measurement of compound materials has wide applications in industry. If the NID mixture is made up of layers of different constituents and the thickness of each layer and the effective dielectric constant are known, the unknown dielectric constant of a particular constituent can be determined.

REFERENCES

1. Y. Huang and M. Nakhkash, Characterisation of layered dielectric medium using reflection coefficient, *Electron Lett* 34 (1998), 1207-1208.
2. M. Juan, M. Rojo, A. Parreno, and J. Margineda, Automatic measurement of permittivity and permeability at microwave frequencies using normal and oblique free-wave incidence with focused beam, *IEEE Trans Instrum Meas* 47 (1998), 886-892.
3. D.K. Ghodgaonkar, V.V. Varadan, and V.K. Varadan, Free-space measurement of complex permittivity and complex permeability of magnetic materials at microwave frequencies, *IEEE Trans Instrum Meas* 39 (1990), 387-394.
4. C.A. Balanis, *Advanced engineering electromagnetics*, Wiley, New York, 1989, p. 223.
5. K.P. Thakur, K.J. Cresswell, M. Bogosonovich, and W.S. Holmes, Non-interactive and distributive property of dielectrics in mixture, *Electron Lett* 35 (1999), 1143-1144.

© 2000 John Wiley & Sons, Inc.

A FINITE-ELEMENT 3-D METHOD FOR THE DESIGN OF TWT COLLECTORS

Stefano D'Agostino¹ and Claudio Paoloni²

¹ Department of Electronic Engineering
University of Roma "La Sapienza"
00184 Roma, Italy

² Department of Electronic Engineering
University of Roma "Tor Vergata"
00133 Roma, Italy

Received 9 February 2000

ABSTRACT: This letter discusses the basic philosophy of a fully three-dimensional finite-element method for collector design together with its main features. In particular, attention is focused on the dedicated mesh generator and the strategy followed for the solution of the coupled electromagnetic and motional problem within the same finite-element discretization context. An example of simulation is carried out, and indications of future applications are also provided. © 2000 John Wiley & Sons, Inc. *Microwave Opt Technol Lett* 26: 119-122, 2000.

Key words: traveling-wave tubes; collector; efficiency

TABLE 2 Complex Permittivity of Different Samples from the Transmission Measurement

Frequency (GHz)	Glass		Polystyrene		Glass Epoxy		NID Mixture (Polystyrene-Glass Epoxy)			
	ϵ'	$\tan \delta$	ϵ'	$\tan \delta$	ϵ'	$\tan \delta$	Free Space		Theory [5]	
	ϵ'	$\tan \delta$	ϵ'	$\tan \delta$	ϵ'	$\tan \delta$	ϵ'	$\tan \delta$	ϵ'	$\tan \delta$
5.4	5.26	0.296	2.64	0.081	3.77	0.082	2.94	0.024	2.96	0.080
5.8	5.24	0.288	2.76	0.047	3.70	0.078	2.90	0.021	3.03	0.056
6.2	5.15	0.295	2.83	0.017	3.65	0.074	2.88	0.017	3.06	0.036
6.6	5.01	0.297	2.85	0.015	3.61	0.078	2.85	0.014	3.06	0.036

BURIED-OBJECT DETECTION USING FREE-SPACE TIME-DOMAIN NEAR-FIELD MEASUREMENTS

S. Biju Kumar,¹ C. K. Aanandan,¹ and K. T. Mathew¹

¹ Department of Electronics
Cochin University of Science and Technology
Cochin-682 022, Kerala, India

Received 18 April 2001

ABSTRACT: The detection of buried objects using time-domain free-space measurements was carried out in the near field. The location of a hidden object was determined from an analysis of the reflected signal. This method can be extended to detect any number of objects. Measurements were carried out in the X - and Ku -bands using ordinary rectangular pyramidal horn antennas of gain ~ 15 dB. The same antenna was used as the transmitter and receiver. The experimental results were compared with simulated results by applying the two-dimensional finite-difference time-domain (FDTD) method, and agree well with each other. The dispersive nature of the dielectric medium was considered for the simulation. © 2001 John Wiley & Sons, Inc. *Microwave Opt Technol Lett* 31: 45–47, 2001.

Key words: free-space measurements; mine detection; FDTD; near-field measurements

1. INTRODUCTION

One of the major hurdles for the peacekeepers of war is the extensive use of the most dangerous land mines planted by foes. Extensive research has been ongoing in land-mine detection. A mine with a nonmetallic covering makes it impossible for conventional metal detectors to detect it, so there is a need to develop new techniques for land-mine detection, which should be very effective in detecting mines even with low loss and low-contrast dielectric materials. Many researchers have concentrated their attention in this field. Montoya and Smith [1] detected land mines using resistively loaded vee dipoles. Demarest, Plumb, and Huang [2] calculated the fields scattered by buried objects when the sources are close enough to the air-ground interface. A novel method of detecting buried objects like underground pipes, voids, cables, etc., using ordinary pyramidal horns both in the X - and Ku -bands is presented by the authors.

2. THEORETICAL ANALYSIS

Theoretical work was carried out on the system as shown in Figure 1. The dielectric medium ($\epsilon_s = 2.5$) is assumed to be dispersive, linear, homogeneous, and isotropic. The discretized Maxwell's expressions for space and time were given by Yee [3]. Incorporating the dispersive nature of the dielectric medium [4] in the constitutive FDTD equations, the expression for the H -field is kept unchanged as the medium is assumed to be nonmagnetic, and is given by

$$H_x(i, j, t + 1) = H_x(i, j, t) - \frac{dt}{\mu_0 dy} (E_z(i, j, t) - E_z(i, j - 1, t)) \quad (1)$$

S. Biju Kumar (Young Collaborator Programme) and C. K. Aanandan (Associate Scheme) are thankful to the International Centre for Theoretical Physics (ICTP), Trieste, Italy, for financial assistance to visit ICTP and to carry out the theoretical work on FDTD.

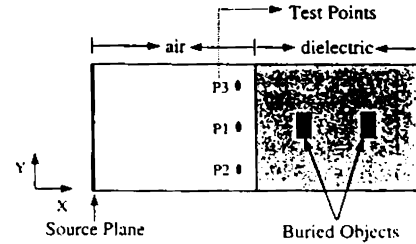


Figure 1 Schematic diagram of the theoretical system

$$H_y(i, j, t + 1) = H_y(i, j, t) + \frac{dt}{\mu_0 dx} (E_z(i, j, t) - E_z(i - 1, j, t)) \quad (2)$$

Because of the dispersive nature of the dielectric medium, the electric field is modified. The expression for the E -field is given by

$$E_z(i, j, t + 1) = \frac{\epsilon_x}{\epsilon_x + \chi_0(i, j)} E_z(i, j, t) + \frac{1}{\epsilon_x + \chi_0(i, j)} \sum_{m=0}^{t-1} E_z(i, j, t - m) \Delta \chi_m(i, j) + \frac{dt}{(\epsilon_x + \chi_0(i, j)) \epsilon_0 dx} (H_y(i + 1, j, t) - H_y(i, j, t)) - \frac{dt}{(\epsilon_x + \chi_0(i, j)) \epsilon_0 dy} (H_x(i, j + 1, t) - H_x(i, j, t)) \quad (3)$$

where $\chi_0(i, j) = (\epsilon_s - \epsilon_x) \chi 1 - \exp(-dt/t_0)$ is the susceptibility function, $\Delta \chi_m(i, j) = (\epsilon_s - \epsilon_x) \exp(-mdt/t_0) \chi 1 - \exp(-dt/t_0))^2$, ϵ_s is the static permittivity of the dielectric, ϵ_x is the optical permittivity of the dielectric, t_0 is the relaxation time of the dielectric, and μ_0 is the permeability of free space.

A Gaussian pulse with $dt = 16.667$ ps, $T_0 = 41.667$ ps was executed at the source plane. A Yee cell was constructed from 140 grids in the X -direction and 80 grids in the Y -direction with a grid spacing $dx = 0.5$ cm and $dy = 0.5$ cm, respectively. Mur's boundary conditions [5] were applied at the boundaries. A dielectric object ($\epsilon_s = 4$) of dimensions 3 cm \times 3 cm was placed at a distance of 8 cm from the air-dielectric interface, as shown in figure 1. The response of the Gaussian pulse with time was noted. The same procedure was repeated with one more object placed at a distance of 18 cm away from the front surface, in line with the first object.

$P1$, $P2$, and $P3$ were three test points selected for study. The time-domain response from these points gives information on the buried object. This is explicit from Figure 2(a), (b). Figure 2(a) is the response obtained with a single object buried in the vessel, and Figure 2(b) is that when two objects are in a line. The dotted line represents the response at point $P1$, and the solid line that at $P2$ and $P3$. Peak $R1$ corresponds to the forward-moving Gaussian pulse, and $R2$ the

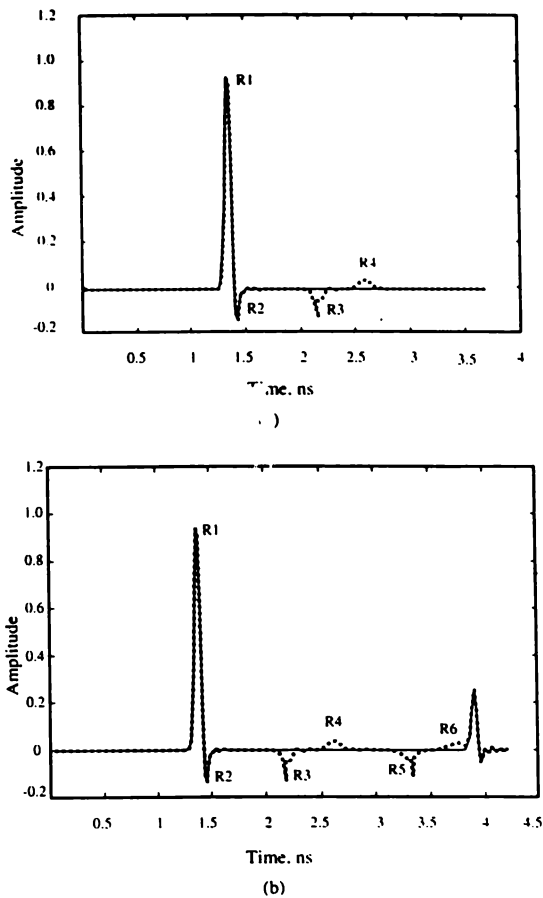


Figure 2 Theoretical time-domain responses. (a) With one buried object. (b) With two buried objects in line. ----- response at test point P_1 , — response at points P_2 and P_3

reflection from the air–dielectric interface. R_3 represents the reflection from the first buried object, and R_5 that from the second object. R_4 and R_6 are the signals obtained due to the smaller dimensions of the objects. This can be avoided if the sample dimension is greater than the width of the Gaussian pulse. In Figure 2(b), the response after peak R_6 is the repetition of the reflections.

3. EXPERIMENTAL SETUP AND RESULTS

Experiments were performed in the X - and Ku -bands. A cubical vessel of dimensions $40\text{ cm} \times 40\text{ cm} \times 35\text{ cm}$ was filled with dry sand ($\epsilon_r = 2.5$). The pyramidal horn antenna which was connected to one port of the S -parameter test set transmitted 10 mW power, and the same antenna received the reflected power from the vessel. The X -band horn antenna has a half-power beamwidth (HPBW) of 18° (E -plane) and 15.5° (H -plane) and aperture dimensions $9.8\text{ cm} \times 7.5\text{ cm}$. The respective values for the Ku -band horn antenna are 20° , 17° , and $5.7\text{ cm} \times 4.4\text{ cm}$. Both of the antennas have a gain of $\sim 15\text{ dB}$. A dielectric block ($\epsilon_r = 4$) of dimensions $7\text{ cm} \times 3\text{ cm} \times 3\text{ cm}$ was buried at a distance of 8 cm from the front surface of the vessel. Then the pyramidal horn antenna was set at each position P_1 , P_2 , and P_3 (near-field points), as shown in Figure 3. The time-domain response was plotted with an HP 8510 C vector network analyzer. The same procedure was repeated, with one more object buried at a distance of 10 cm behind the first object. The results obtained are shown in Figure 4.

Figure 4(a), (b) represents the response obtained for single object in the X - and Ku -bands, respectively, and Figure 4(c) gives the response of two objects in the Ku -band. In the figures, R_1 is the reflection from the front surface of the vessel. R_2 corresponds to the reflection from the first object, and R_3 that from the second object. The dotted line represents the time-domain response of the Gaussian pulse corresponding to point P_1 , and the solid lines corresponding to P_2 and P_3 . The minor peaks appearing in front of R_1 may be due to the discontinuities in the cables and connectors. A comparison of the theoretical and experimental results is shown in Table 1.

4. CONCLUSION

A simple and accurate method of detecting buried objects in the time domain has been presented. The results are compared with FDTD simulation results. An ordinary pyramidal horn with moderate aperture and nominal gain is used for the measurement. This technique finds wide applications in the detection of buried objects like land mines, pipes, voids, etc. The work can be extended to determine the dielectric parameters of hidden objects.

ACKNOWLEDGMENT

The authors express their appreciation for the constructive suggestions and discussions rendered by Dr. P. Mohanan, Department of Electronics, Cochin University of Science and Technology, during the course of this work.

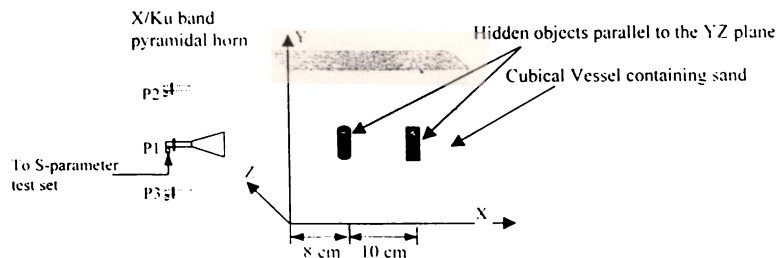


Figure 3 Experimental setup

TABLE 1 Comparison of Results from Theory and Experiment

Actual Depth	Theoretical Results (from Fig. 2)	Experimental Results (from Fig. 3)
8 cm (first object)	$(R2-R3)/2 \rightarrow 0.3705$ ns (7.125 cm) ^a	$(R1-R2)/2 \rightarrow 0.4117$ ns, 0.465 ns (8.42 cm)(average) ^a
18 cm (second object)	$(R2-R5)/2 \rightarrow 0.92855$ ns (17.86 cm) ^a	$(R1-R3)/2 \rightarrow 0.9254$ ns (17.79 cm) ^a

^aThe velocity factor in the dielectric is incorporated.

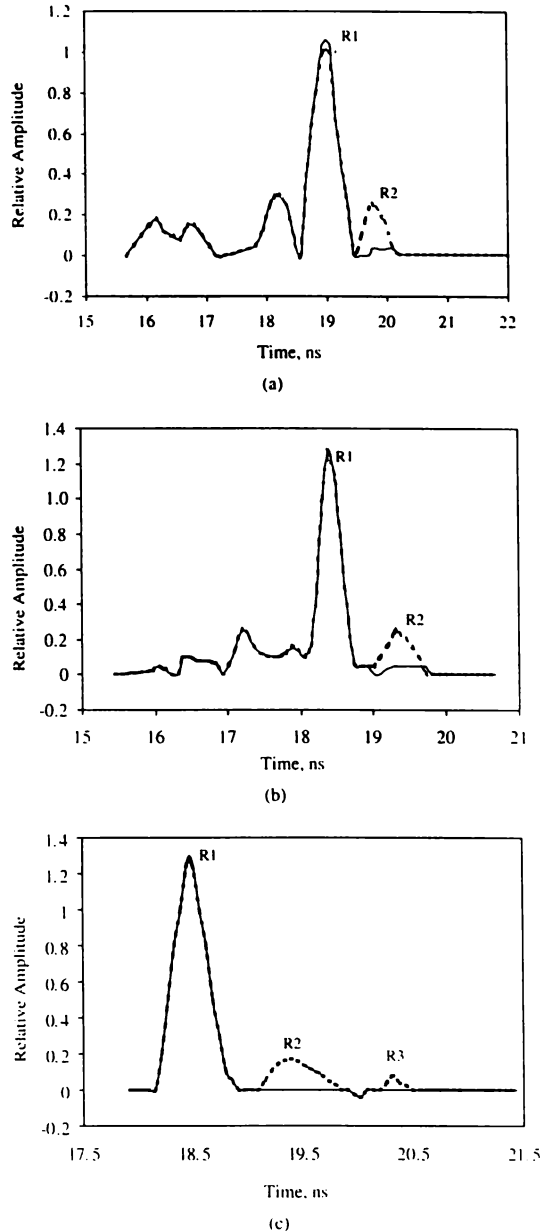


Figure 4 Experimental time-domain responses. (a) With one buried object (*X*-band response). (b) With one buried object (*Ku*-band response). (c) With two buried objects (*Ku*-band response). ----- response at test point *P*₁, — response at points *P*₂ and *P*₃

REFERENCES

1. T.P. Montoya and G.S. Smith, Land mine detection using a ground-penetrating radar based on resistively loaded vee dipoles, *IEEE Trans Antennas Propagat* 47 (1999), 1795-1806.
2. K. Demarest, R. Plumb, and Z. Huang, FDTD modeling of scatterers in stratified media, *IEEE Trans Antennas Propagat* 43 (1995), 1164-1168.
3. K.S. Yee, Numerical solution of initial boundary value problems involving Maxwell's equations in isotropic media, *IEEE Trans Antennas Propagat* AP-14 (1966), 302-307.
4. R. Luebbers, F.P. Hunsberger, K.S. Kunz, R.B. Standler, and M. Schneider, A frequency-dependent finite-difference time-domain formulation for dispersive materials, *IEEE Trans Electromag Compat* 32 (1990), 222-227.
5. G. Mur, Absorbing boundary conditions for the finite-difference approximation of the time-domain electromagnetic-field equations, *IEEE Trans Electromag Compat* EMC-23 (1981), 377-382.

© 2001 John Wiley & Sons, Inc.

FAR-FIELD PATTERN CALCULATION IN BODY-OF-REVOLUTION FINITE-DIFFERENCE TIME-DOMAIN (BOR-FDTD) METHOD

Wenhua Yu,¹ Nader Farahat,¹ and Raj Mittra¹
¹Electromagnetic Communication Laboratory
 The Pennsylvania State University
 University Park, Pennsylvania 16802

Received 23 April 2001

ABSTRACT: In this paper, we present a far-field pattern calculation technique in the body-of-revolution finite-difference time-domain (BOR-FDTD) method. Because the BOR-FDTD solves two- and half-dimensional problems, it has different features from the three-dimensional FDTD method in the far-field pattern calculation. A monopole antenna fed by a coax is used to validate the technique described in this paper. © 2001 John Wiley & Sons, Inc. *Microwave Opt Technol Lett* 31: 47-50, 2001.

Key words: BOR; FDTD; near-to-far field transformation; monopole antenna

I. INTRODUCTION

The numerical techniques based on the finite-difference time-domain (FDTD) algorithm applicable to general electromagnetic problems have grown in importance [1-5]. The BOR-FDTD has a great advantage over the three-dimensional FDTD for a rotationally symmetric problem [6-11]. It is well known that the three-dimensional near-to-far-field transformation technique has been widely used to compute the far-field pattern in the FDTD simulations [4, 5]. Because

DIELECTRIC PROPERTIES OF CERTAIN BIOLOGICAL MATERIALS AT MICROWAVE FREQUENCIES

S. Biju Kumar, K.T. Mathew,
U. Raveendranath and P. Augustine

In the medical field, microwaves play a larger role for treatment than diagnosis. For the detection of diseases by microwave methods, it is essential to know the dielectric properties of biological materials. For the present study, a cavity perturbation technique was employed to determine the dielectric properties of these materials. Rectangular cavity resonators were used to measure the complex permittivity of human bile, bile stones, gastric juice and saliva. The measurements were carried out in the S and J bands. It is observed that normal and infected bile have different dielectric constant and loss tangent. Dielectric constant of infected bile and gastric juice varies from patient to patient. Detection and extraction of bile stone with possible method of treatment is also discussed.

Key Words: Biological materials, Permittivity, Cavity Resonators, Perturbation Technique

ABOUT THE AUTHORS:

S. Biju Kumar and K. T. Mathew are affiliated with the Department of Electronics, Cochin University of Science and Technology, Cochin, Kerala, India. U. Raveendranath is affiliated with the ALD, NAL, Bangalore, India. Philip Augustine is affiliated with the Digestive Disease Centre, P.V.S Memorial Hospital, Cochin, Kerala, India.

© International Microwave Power Institute 2001.

The great affinity of microwaves for absorption in biological objects is well known [Schwan, 1957; Tran and Stuchly, 1987; Gandhi and Chen, 1995; David Dunn et al., 1996]. Biological effects of microwaves and the application of microwaves in medicine represent strongly developing areas of research. Availability of sophisticated microwave systems and components of smaller size at lower cost makes microwave applications in medicine more attractive. Microwaves are used in cardiac therapy, cancer therapy and hyperthermia treatment.

Detailed studies on the medical application and the effects of microwaves on tissues have been reported by a number of researchers [Livesay and Chen, 1974; Anderson et al., 1984; Teng et al., 1995]. Different types of applicators have been used for microwave prostatic hyperthermia [David Despretz et al., 1972]. Distribution of maximum microwave power for heating off-centre tumors was described by Rappaport and Morgenthaler [1987]. Various methods of analysing focussed pulse-modulated microwave signals inside the biological tissues were described by Konstantina et al. [1996] and Najafabadi and Peterson [1996]. The effect of microwave absorption in the human head from handheld portable radio and mobile telephones were also reported [Gandhi et al., 1996; Cleveland and Athey, 1989]. Polk and Postow [1995] give a comprehensive background on investigations of the interaction of microwaves with the nervous system. Microwave imaging in medical applications is an emerging area of recent research [Murch and Chan, 1996; Souvorov et al., 2000].

For any type of microwave treatment, initial conditions of the object under treatment should be known. This involves determination of the complex permittivity and conductivity of the object. Because of many constraints such as high dielectric loss and faster decay rate of biological materials, the studies on the dielectric properties on these materials are seen very seldom in the

literature. Also, much care should be taken in handling the infected biological samples like bile, bile stones etc. Though various methods are available for permittivity measurement, the cavity perturbation technique has unique advantages and is the most accurate method.

Sample Collection

Biological samples were collected from the Digestive Disease Centre of P.V.S Memorial Hospital, Cochin, India. In this center, research, diagnosis and treatment are done. Internal organs were examined with an advanced medical technology, endoscopy. The modern endoscope, Videoendoscope, has an endoscope, CPU and a monitor. A charge-coupled device at the tip of the shaft transmits the image data to a TV monitor. The handle of the endoscope has control knobs for maneuvering the tip and also controls to regulate irrigation water, air insufflation and suction for removing air and secretions. Also, there is an instrument channel allowing the passage of biopsy forceps, snares for removing polyps and foreign bodies or devices to control bleeding. In routine Upper Gastro Intestinal (UGI) Endoscopy, the entire esophagus, stomach and the proximal duodenum are examined. Some of the common conditions that are routinely diagnosed by endoscopy include Gastroesophageal reflux disease, Peptic ulcer and cancer of the UGI tract. During this investigation, biles and bile stones are collected. Usually bile stones are removed by ERCP (Endoscopic Retrograde Cholangio Pancreatography) surgery. This is a variation of UGI endoscopy, combining endoscopic and radiological techniques to visualize biliary and pancreatic duct systems. With a side-viewing instrument, after being placed into the descending duodenum, the papilla of Vater (where bile duct and pancreatic duct opens into GIT) is cannulated and contrast medium injected, thus visualizing the pancreatic duct and the hepato biliary tree radiographically. It is useful in the diagnosis of stones and cancer of bile duct and also pancreatic disorders like chronic pancreatitis and pancreatic malignancy. Therapeutic potentials include removal of bile

duct stones and palliation of obstructive jaundice by placing stents to bypass obstructing lesions. Pancreatic juice, pancreatic stone and gastric juice can be collected in this way. All the biological samples were preserved at freezing temperature to avoid the possibility of deterioration. The dielectric measurements were done at 25°C.

Experimental Setup and Method of Measurement

The principles and resonant cavity perturbation method were described previously [Raveendranath and Mathew, 1995]. However, the experimental setup was modified to accommodate different types of samples. The basic principle in the cavity perturbation technique is the field perturbation by the samples and the determination of the resonant frequencies and 3dB bandwidths of the cavity resonator. The cavity resonator is constructed with a portion of a transmission line (waveguide or coaxial line) with one or both ends closed. The cavity resonator can be either transmission or reflection type. There is a coupling device to couple the microwave power to the resonator. The cavity resonator is connected to a HP 8510C Network Analyzer, HP 83651B Sweep Oscillator and HP 8514B S-parameter test set as shown in Figure 1. For this study, S and J band rectangular cavity resonators were used. The length of the resonator determines the number of resonant frequencies. The cavity resonator is excited in the TE_{10p} mode. A typical resonant frequency spectrum of the cavity resonator is shown in Figure 2. The field within the cavity resonator is perturbed by the introduction of the dielectric samples. For the measurements of complex permittivity of biological liquids, a capillary tube (radius less than 0.5 mm) made of low loss fused silica is used. The empty tube is cleaned, dried and inserted in the cavity resonator. One of the resonant frequencies is selected and the tube is adjusted for the position of maximum perturbation where the resonant frequency and 3dB bandwidth are determined. The empty tube is then taken out and filled with the biological liquid and the measurement is repeated to determine the

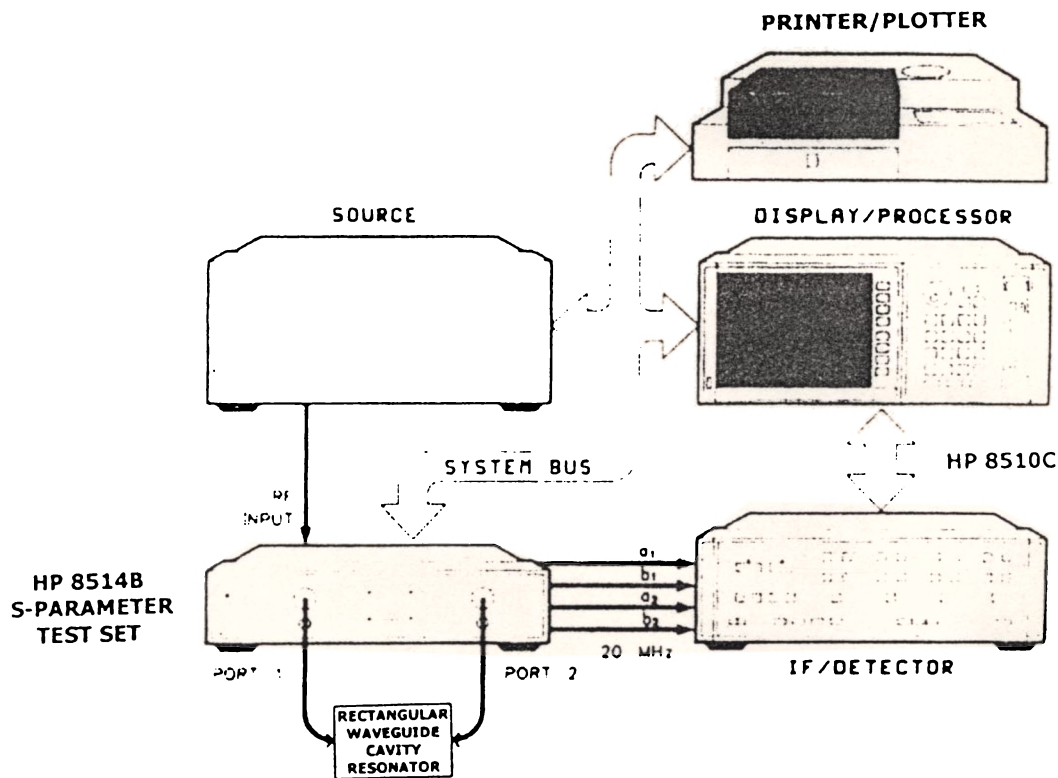


FIGURE 1: Schematic diagram of the experimental setup.

new resonant frequency and 3dB bandwidth. The procedure is repeated for all other frequencies. Measurements were made for different types of bile, gastric juice and saliva.

For the measurement of resonant frequency and 3dB bandwidth of solid samples (bile stones) a specially designed cavity resonator was constructed. Because of large sample size, the measurements were done in the S band only. A rectangular slot of size 4 cm x 3 cm was cut at the top of the cavity resonator for the introduction of the sample and a slot of sufficient length was made at the bottom of the cavity resonator to permit movement of the sample for maximum perturbation. The opening was made on the non-radiating wall of the waveguide and this was exactly fit when the metal cover was put back. It was ex-

perimentally observed that there was practically no shift in resonant frequency or quality factor due to the rectangular opening. The sample is usually irregular and can be shaped by applying low pressure. A small cup made of low-loss polystyrene rests on a rod of the same material and can slide along the slot. After placing the cup in the cavity resonator, the rectangular slot of the waveguide is closed with a metal piece of correct size so that it forms a part of the waveguide. As before, the resonant frequency and 3dB bandwidth of the cavity resonator with empty cup were determined. Then the experiment was repeated with a sample in the cup. The schematic diagram of the cavity resonator for measurement of bile stone is shown in Figure 3.

For S and J bands, different types of cavities

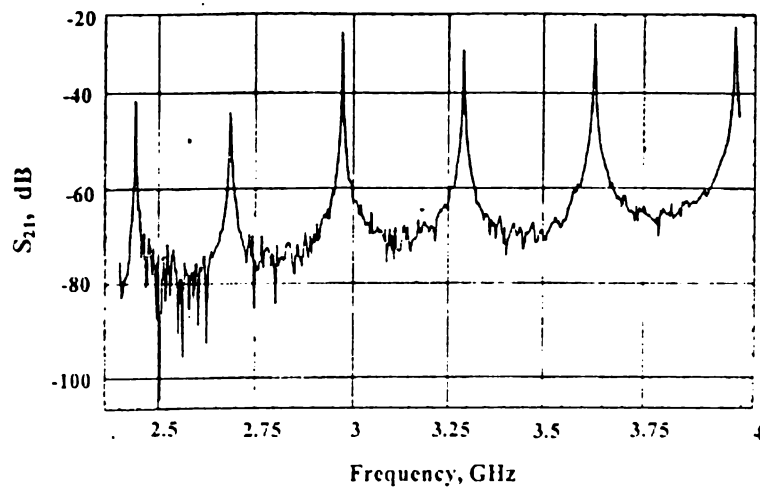


FIGURE 2a: Resonant frequency spectrum of S-band cavity resonator.

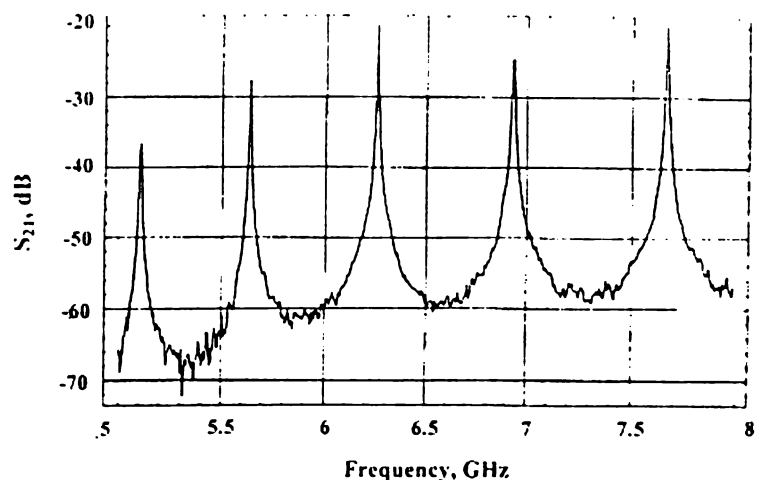


FIGURE 2b: Resonant frequency spectrum of J-band cavity resonator.

were constructed. Since all biological materials are high loss dielectrics, the volume of samples should be small in order to satisfy the requirements for the perturbation measurements. Hence, capillary tubes of small diameter were used. Another very important point is the very precise measurement of the radius of the capillary tube. A slight error in the diameter measurement makes drastic changes in the results.

Theory

The real and imaginary parts of the relative complex permittivity of the biological samples are given by [Raveendranath and Mathew, 1995; Mathew and Raveendranath, 1999]

$$\epsilon_r' - 1 = \frac{f_t - f_s}{2f_s} \left(\frac{V_c}{V_s} \right) \quad (1)$$

$$\epsilon_r'' = \frac{V_c}{4V_s} \left(\frac{Q_t - Q_s}{Q_t Q_s} \right) \quad (2)$$

Here, $\bar{\epsilon}_r = \epsilon_r' - j\epsilon_r''$ is the relative complex permittivity of the sample, ϵ_r' is the real part of the relative complex permittivity, which is usually known as dielectric constant and ϵ_r'' , the imaginary part of the relative complex permittivity, which is associated with the dielectric loss of

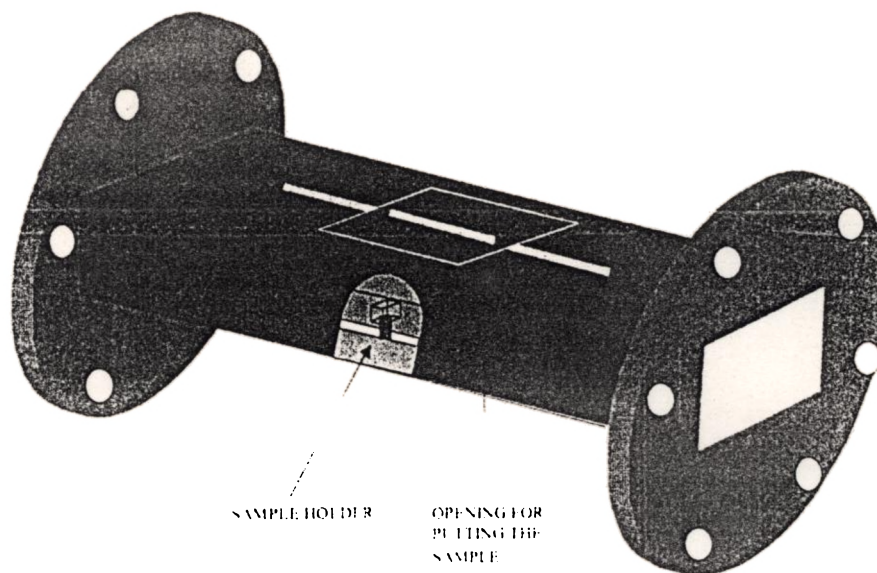


FIGURE 3: Schematic diagram of cavity resonator for bile stone measurement.

the material. V_s and V_c are the volumes of the sample and the cavity resonator respectively. From equations 1 and 2, it is observed that the real part of complex permittivity depends on the resonant frequency shift and the imaginary part depends on the quality factors.

Results and Discussion

Bile

The complex permittivities of normal and infected biles were found to differ. The dielectric constant of normal bile varies from 61 to 53 (± 2) in the frequency range from 2 GHz to 8 GHz. Depending on the nature of the disease, the infected bile has a dielectric constant greater or less than that of normal bile. Infected bile with high dielectric constant indicates that it has more water content than normal bile. Three infected samples were collected from the following and the respective complex permittivity was measured:

1. a patient suffering from a stone in the gall bladder and the bile duct (Cholelithiasis and Cho-

ledocholithiasis). Gall bladder and Common bile duct stones were removed by ERCP (sample 1)

2. a patient suffering from a bile duct stone (Choledocholithiasis) alone (sample 2)
3. a patient suffering from Cholestatic Jaundice (Primary Sclerosing Cholangitis), which is an inflammatory bowel disease. As a result, the bile ducts become narrowed and irregular. The gall bladder of this patient was removed by laproscopic cholecystectomy (sample 3).

Real and imaginary parts of the relative complex permittivity of infected biles of these persons are shown in Figure 4.

Bile Stone

Hard biological materials deposited in the gall bladder or the bile duct are generally known as bile stones (Cholithiasis and Choledocholithiasis). Such materials deposited in the pancreas are known as pancreatic stones. Bile stone is a fat like material. The complex permittivities of bile stones

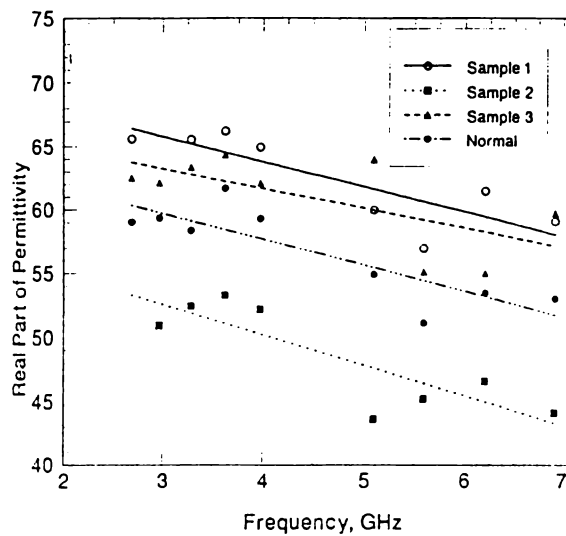


FIGURE 4a: Real part of relative complex permittivity of infected and normal biles at different frequencies.

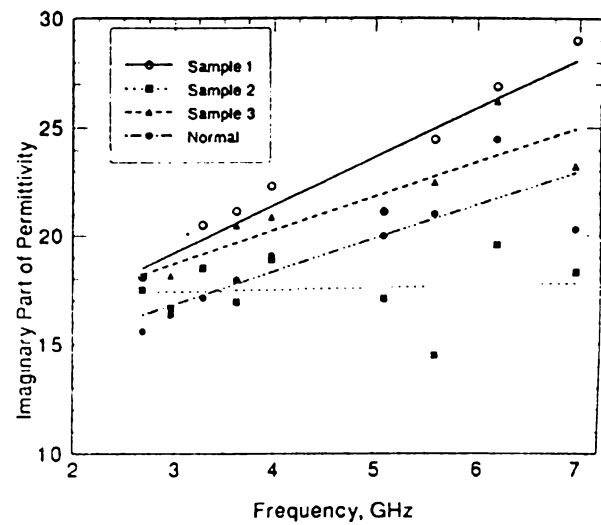


FIGURE 4b: Imaginary part of relative complex permittivity of infected and normal biles at different frequencies.

	Frequency (GHz)	ϵ'_r	ϵ''_r
Sample 1	2.44	4.0	0.18
	2.85	4.0	0.26
	3.34	4.2	0.14
	3.89	4.2	0.26
Sample 2	2.44	4.0	0.25
	2.85	4.2	0.35
	3.34	4.3	0.11
	3.89	4.3	0.24

TABLE 1: Complex Permittivity of Bile Stones.

collected from these patients were also studied. Its dielectric constant is found to be same as that of fat. Slight variations in the real and imaginary parts of the complex permittivity of different bile stones were observed. Table 1 shows the complex dielectric constant of bile stones collected from two patients.

Gastric Juice

Gastric juices of two persons were collected and complex permittivities of these samples were determined. The two persons were suffering from gall stone disease and artral erosion. They underwent the removal of the gall bladder, which con-

tained multiple mixed stones. The dielectric constant and dielectric loss of gastric juice varies from patient to patient. This is clear from Figure 5.

Saliva

Both saliva and gastric juice have many similar functions. There is slight variation in the dielectric properties for these two biological materials. Saliva

was collected from two healthy persons. Figure 6 shows the variation of real and imaginary parts of the complex permittivity with frequency.

Conclusions

The dielectric properties of tissue from human bodies, including bile, bile stone, gastric juices and saliva are presented. This is particularly impor-

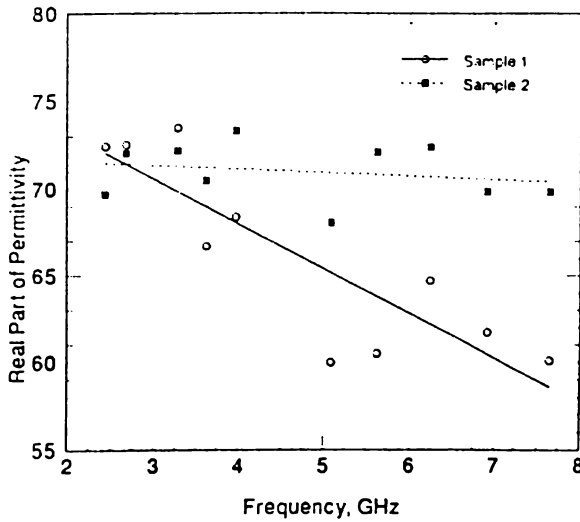


FIGURE 5a: Real part of relative complex permittivity of gastric juices at different frequencies.

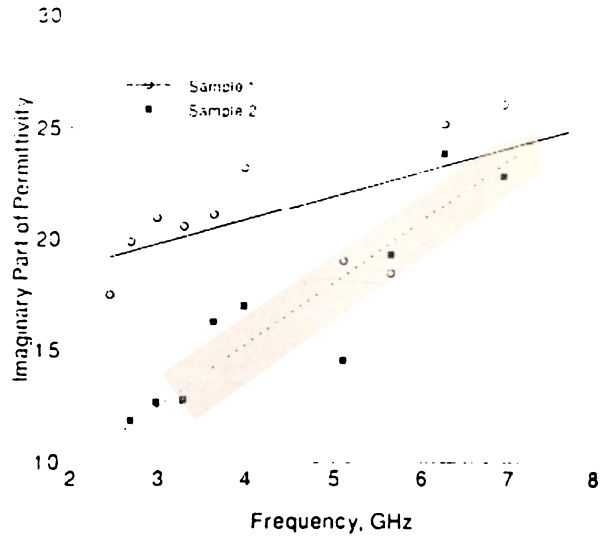


FIGURE 5b: Imaginary part of relative complex permittivity of gastric juices at different frequencies.

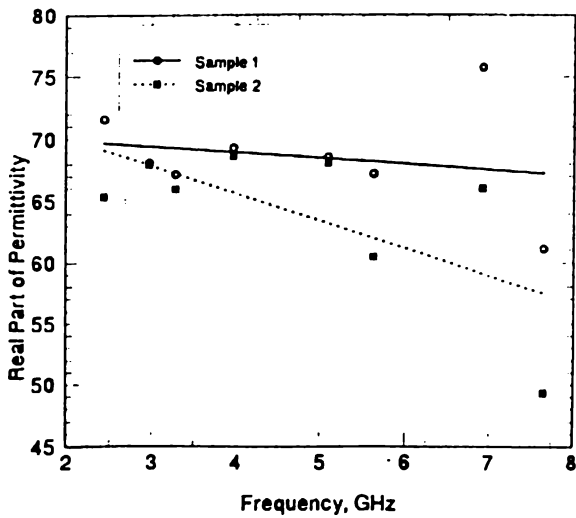


FIGURE 6a: Real part of relative complex permittivity of saliva at different frequencies.

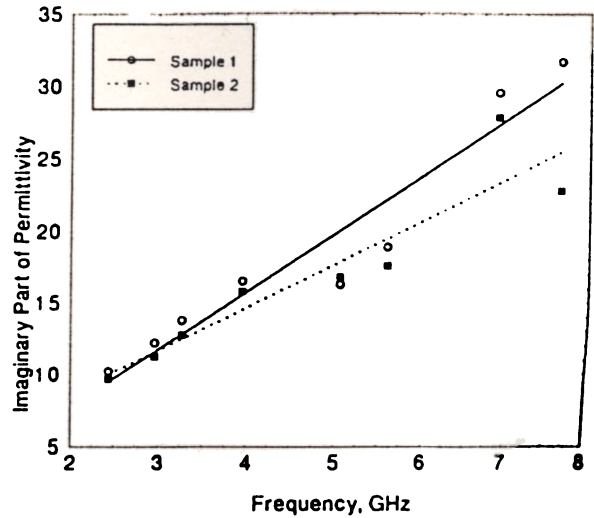


FIGURE 6b: Imaginary part of relative complex permittivity of saliva at different frequencies.

tant since the samples are collected from the internal organs of human beings and are not easily available. Because these samples are available only in small quantities, the cavity perturbation technique is suitable for their dielectric properties determination. This study suggests that the deviation of dielectric properties for different tissues of a healthy person and a patient may be related to the presence of disease in the patient. More study is needed to establish the differences and their significance.

Acknowledgements

The authors are thankful for the cooperation extended by Dr. Ajith Tharakan, Dr. Aneesh and other staff of the PVS Memorial Hospital, Cochin, India.

References

- Alexandre E. Souvorov, Alexander E. Bulyshev, Serguei Y. Semenov, Robert H. Svenson, and George P. Tatsis. 2000. Two-Dimensional computer analysis of a microwave flat antenna array for breast cancer tomography. *IEEE Trans. on Microwave Theory and Techniques* 48: 1413-1415.
- Anderson, J.B. et al. 1984. A hyperthermia system using a new type of inductive applicator. *IEEE Trans. Biomed. Eng.* 31: 212-227.
- Cleveland Jr, R.F. and Athey, T.W. 1989. Specific Absorption Rate (SAR) in models of the human head exposed to hand-held UHF portable radios. *Bioelectromagn.* 10: 173-186.
- David Despretz, Jean-Christophe Camart, Christophe Michel, Jean-Jacques Fabre, Bernard Prevost, Jean-Pierre Sozanski and Maurice Chive. 1996. Microwave prostatic hyperthermia: Interest of urethral and rectal applicators combination-theoretical study and animal experimental results. *IEEE Trans. on Microwave Theory and Techniques* 44: 1762-1768.
- David Dunn, Rappaport, C. and Andrew J. Terzuoli, Jr. 1996. FDTD verification of deep-set brain tumor hyperthermia using a spherical microwave source distribution. *IEEE Trans. on Microwave Theory and Techniques* 44: 1769-1777.
- Gandhi, O.P. and Chen, J.Y. 1995. Electromagnetic absorption in the human head from experimental 6 GHz handheld transceivers. *IEEE Trans. Electromag. Compat.* 37: 547-558.
- Gandhi, O.P., Lazzi, G. and Furse, C.M. 1996. Electromagnetic absorption in the human head and neck for mobile telephones at 835 and 1900 MHz. *IEEE Trans. on Microwave Theory and Techniques* 44: 1884-1897.
- Konstantina .S. Nikita. and Uzonoglu, N.K. 1996. Analysis of focussing of pulse modulated microwave signals inside a tissue medium. *IEEE Trans. on Microwave Theory and Techniques* 44: 1788-1798.
- Livesay, D.E. and Chen, K.M. 1974. Electromagnetic fields induced inside arbitrarily shaped biological bodies. *IEEE Trans. on Microwave Theory and Techniques* 22: 1273-1280.
- Mathew, K.T. and Raveendranath, U. 1999. *Sensors Update Vol. 7.* Wiley VCH Publications. Germany.
- Murch, R.D. and Chan, T.K.K. 1996. Improving microwave imaging by enhancing diffraction tomography. *IEEE Trans. on Microwave Theory and Techniques* 44: 379-388.
- Musil, J. and Zacek, F. 1986. *Microwave measurements of complex permittivity by free space methods and their applications.* Studies in Electrical and Electronic Engineering 22, Elsevier Science Publishers. Amsterdam.
- Polk, C. and Postow, E. 1995. *CRC Handbook of Biological Effects of Electromagnetic Fields.* CRC Press. Second Edition
- Rappaport, C. and Morgenthaler, F. 1987. Optimal source distribution for hyperthermia at the center of a sphere of muscle tissue. *IEEE Trans. on Microwave Theory and Techniques* 35: 1322-1327.
- Raveendranath, U. and Mathew, K.T. 1995. Microwave technique for water pollution study. *J. Microwave Power and Electromagnetic Energy* 30: 187-195.
- Reza M. Najafabadi and Peterson, A.F. 1996. Focussing and impedance properties of conformable phased array antennas for microwave hyperthermia. *IEEE Trans. on Microwave Theory and Techniques* 44: 1799-1802.

-
- Schwan, H.P. 1957. Electrical properties of tissue and cell suspensions. *Advances in Biological and Medical Physics*. Vol. 5. Academic Press.
- Teng, J., Carton de Tournai, D., Duhamel, F. and Vander Vorst, A. 1995. Variations of the somatosensory evoked potentials due to microwave fields in the spinal cord. *IEEE MTT-S Microwave Symp.*: 295-298.
- Tran, V.N. and Stuchly, S.S. 1987. Dielectric properties of beef, beef liver, chicken and salmon at frequencies from 100 to 2500 MHz. *J. of Microwave Power* 22: 29-33.

Complex permittivity and conductivity of poly aniline at microwave frequencies

S. Biju Kumar^a, Honey Hohn^b, Rani Joseph^b, M. Hajian^c,
L.P. Lighthart^c, K.T. Mathew^{a,*}

^aDepartment of Electronics, Cochin University of Science and Technology, Cochin-682 022, Kerala, India

^bDepartment of Polymer Science and Rubber Technology, Cochin University of Science and Technology, Cochin-682 022, Kerala, India

^cDepartment of Electrical Engineering, Technical University of Delft, 2628 CD Delft, The Netherlands

Abstract

Dielectric properties of polyaniline at different frequencies were studied. Cavity perturbation technique was employed for the study. Poly aniline in the powder and pelletised forms were prepared under different environmental conditions. Different samples of poly aniline exhibit high conductivity. However, the conductivity of samples prepared under different environmental conditions is found to vary. All the samples in the powder form have high conductivity irrespective of the method of preparation. The high conductivity at microwave frequency makes it possible to be used for developing microwave components like filters. © 2001 Elsevier Science Ltd. All rights reserved.

Keywords: Complex permittivity; Perturbation technique; Polyaniline

1. Introduction

All dielectric materials are characterised by their dielectric parameters such as dielectric constant, conductivity and polarisation^{1,2}. These parameters differ with frequency, temperature, pressure etc. Among a large variety of conducting polymers, polyaniline has very important place. It has wide applications in industry, defense and scientific field.^{3,4} Poly aniline samples were prepared at different conditions and each sample was studied.

2. Method of preparation of samples

Chemical oxidative polymerization of aniline was carried out using ammonium per sulphate as initiator in the presence of 1 M HCl and would take about 4 h at room temperature to complete the process. It was then filtered, washed and dried under three different conditions. The different conditions are given below

1. Room temperature drying for 48 h. It was observed that 48 hours drying at room temperature is sufficient to eliminate water content of the

sample and further drying does not change the mass of the sample, showing drying is complete.

2. Oven drying (50–60 °C) under vacuum for 8 h. Very high temperature may affect the quality of polymer. Thus for a safer side, temperature is limited to 60 °C.
3. Vacuum drying for 16 h at room temperature. Vacuum drying for 16 h gives the same amount of drying as at 48 h room temperature drying.

The poly aniline thus prepared is in fine powder form. Measurements were carried out for the samples in powder and pellet forms. Fine powder is pelletised by applying pressure. The density of the pellet is different for different pressure. Diameter of all pellets is 2.5 mm but volume varies slightly.

3. Theory and measurement technique

Dielectric parameters were measured using cavity perturbation technique. Rectangular Cavity operating at S-band (2–4GHz) was used. The block diagram of the experimental arrangement is shown in Fig. 1 and the schematic diagram of the rectangular cavity is shown in Fig. 2. Pelletised samples can be inserted into the cavity through the opening as shown in the figure. Powder samples can

* Corresponding author. Tel.: +91-484-532161; fax: +91-484-532800.

E-mail address: mathew@doe.cusat.edu (K.T. Mathew).

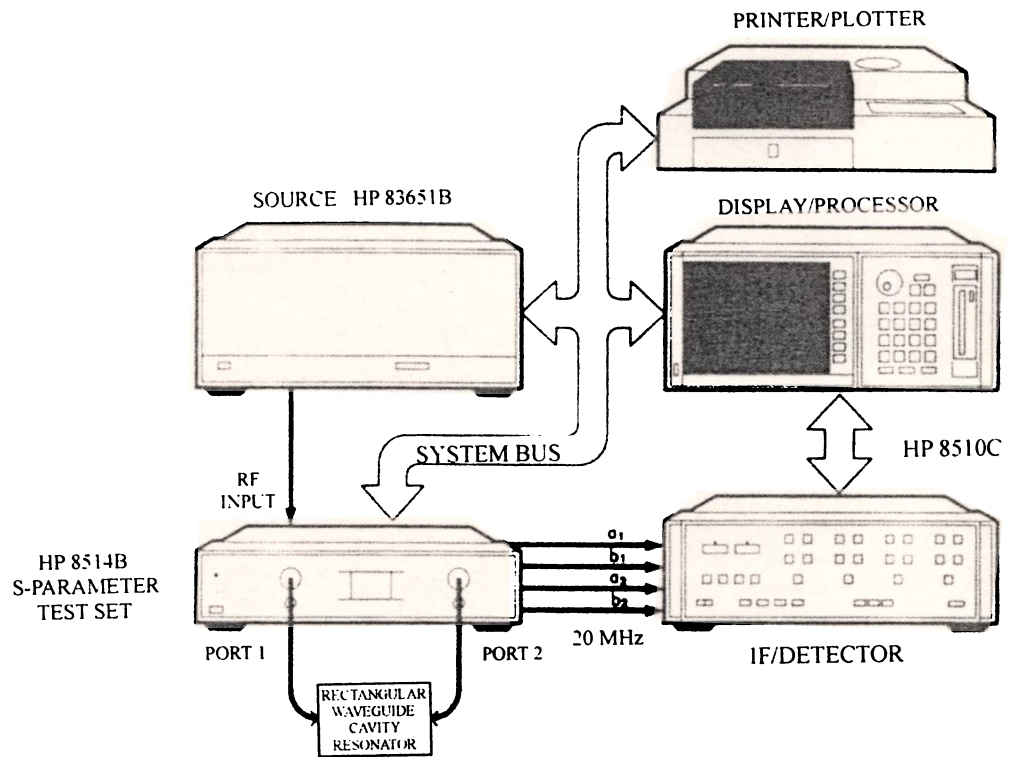


Fig. 1. Block diagram of the experimental set-up.

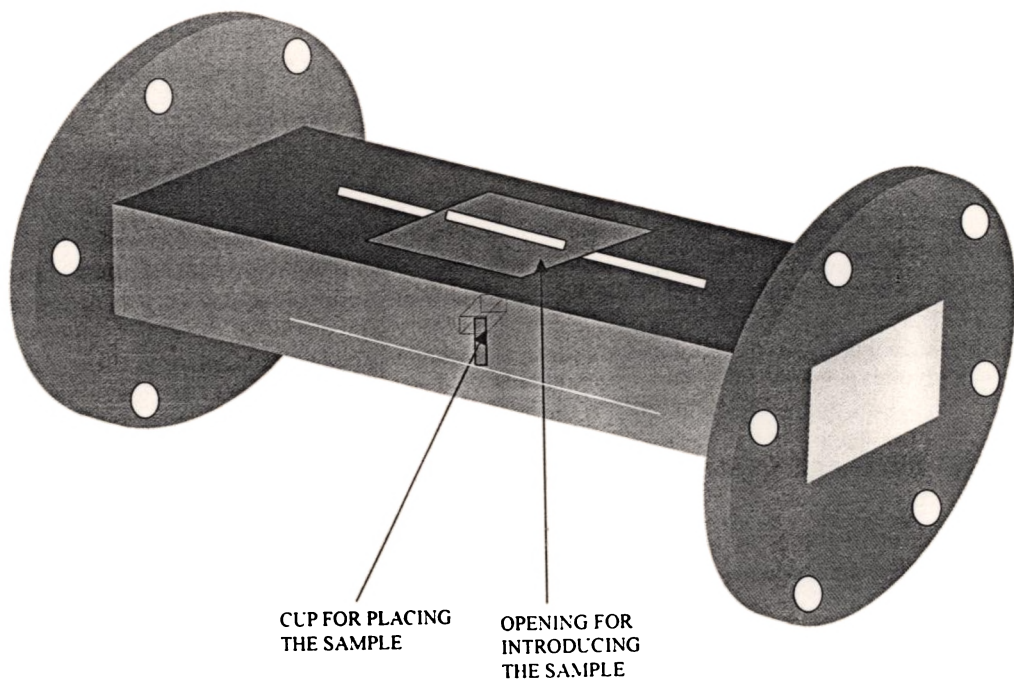


Fig. 2. Schematic diagram of the rectangular cavity resonator.

also be studied using the same cavity. For the complex permittivity measurement of powder, it is taken in the capillary tube of low loss silica of small bore (less than 0.5 mm radius) and wall thickness. The weight fraction of the powder samples is almost the same in all cases.

The determination of the complex permittivity and conductivity is based on the theory of perturbation. When the sample is introduced into the cavity, the relative complex frequency shift of the resonator is given by Waldron⁵ as

$$\frac{d\Omega}{\Omega} \approx \frac{(\bar{\epsilon}_r - 1)\epsilon_0 \int_{V_s} E \cdot E_0^* dV + (\bar{\mu}_r - 1)\mu_0 \int_{V_c} H \cdot H_0^* dV}{\int_{V_c} (D_0 \cdot E_0^* + B_0 \cdot H_0^*) dV} \quad (1)$$

E_0 is the electric field in the unperturbed cavity, E is the electric field in the perturbed cavity and D is the displacement current density. H_0 , H and B are the respective magnetic quantities. $\bar{\epsilon}_r$ is the relative complex permittivity of the sample. But $\bar{\epsilon}_r = \epsilon_r' - j\epsilon_r''$ where ϵ_r' is the real part of the complex permittivity and ϵ_r'' is the imaginary part of the complex permittivity. μ is the magnetic parameter.

The numerator of Eq. (1) represents the total energy stored in the sample and the denominator represents the total energy stored in the cavity. When a dielectric material is introduced in a cavity resonator at the position of maximum electric field, the contribution of magnetic field for the perturbation is minimum. The field perturbation due to the introduction of dielectric sample at the position of maximum electric field is related by Kupfer et al.⁶

$$\frac{d\Omega}{\Omega} \approx \frac{(\bar{\epsilon}_r - 1) \int_{V_s} E \cdot E_{0\max}^* dV}{2 \int_{V_c} |E_0|^2 dV} \quad (2)$$

where $d\Omega$ is the complex frequency shift. V_s and V_c are the volumes of the sample and the cavity resonator respectively. Complex frequency shift is related to the quality factor, Q as

$$\frac{d\Omega}{\Omega} = \frac{d\omega}{\omega} + \frac{j}{2} \left(\frac{1}{Q_s} - \frac{1}{Q_t} \right) \quad (3)$$

Q_s and Q_t are the quality factors of cavity resonator with and without the sample.

Quality factor Q is given by, $Q = \frac{f}{\Delta f}$ where f is the resonant frequency and Δf is the corresponding 3 dB bandwidth.

For small sample, we assume that $E = E_0$ which is one of the assumptions taken in the theory of perturbation. For dominant TE_{10p} mode in rectangular wave guide,

$$E_0 = E_{0\max} \sin \frac{\pi x}{a} \sin \frac{p\pi z}{d}, \quad p = 1, 2, 3 \dots \quad (4)$$

$E_{0\max}$ is the peak value of E_0 , a is the broader dimension and d the length of the waveguide cavity resonator, respectively.

From Eqs. (2)–(4), we get

$$\epsilon_r' - 1 = \frac{f_t - f_s}{2f_s} \left(\frac{V_c}{V_s} \right) \quad (5)$$

$$\epsilon_r'' = \frac{V_c}{4V_s} \left(\frac{Q_t - Q_s}{Q_t Q_s} \right) \quad (6)$$

The real part, ϵ_r' of the complex permittivity is usually known as dielectric constant. The imaginary part, ϵ_r'' of the complex permittivity is associated with dielectric loss of the material.

For a dielectric material having non-zero conductivity, we have Maxwell's curl equation

$$\begin{aligned} \nabla \times H &= (\sigma + j\omega\epsilon)E \\ &= (\sigma + \omega\epsilon'')E + j\omega\epsilon'E \end{aligned}$$

The loss tangent

$$\tan \delta = \frac{\sigma + \omega\epsilon''}{\omega\epsilon'}$$

Here $\sigma + \omega\epsilon''$ is the effective conductivity of the medium.

When σ is very small, the effective conductivity is reduced to

$$\sigma_e = \omega\epsilon'' = 2\pi f\epsilon_0\epsilon_r'' \quad (7)$$

4. Results and discussion

It is observed that the polyaniline exhibits high conductivity. However the complex permittivity and conductivity of the samples prepared at different environmental conditions vary. The samples in the powder form have greater conductivity than that in the pellet form irrespective of the method of preparation. The conductivity measurement of poly aniline at static electric field indicates that it has the property of insulator. All measurements were done at 25 °C. The results are shown in Table 1. An exhaustive study of the complex permittivity and conductivity of the poly aniline in the powder and pellet forms shows interesting results. The conductivity is less than that of a conductor but greater than that of an insulator at microwave frequencies. Because of this property, poly aniline can be used to construct microwave components like filters. An anomaly observed in the dielectric behaviour of poly aniline is that its conductivity drops to a very low value when it is pelletised from the powder form. ϵ'' And hence σ_e is small means that $(Q_t - Q_s)$ is very small [Eq. (6)]. Due to experimental

Table 1
Dielectric parameters of different samples of poly aniline

	Sample	Frequency (GHz)	ϵ'	ϵ''	σ_c (S/m)
Room temperature drying for 48 h	Powder	2.43	13.04	9.84	1.336
	Powder	2.97	12.53	8.65	1.43
	Pellet	2.86	6.88	0.0059	0.00094
	Pellet	3.9	5.68	0.0953	0.0207
Oven drying 50–60 °C for 8 h under vacuum	Powder	2.43	10.03	2.18	0.2958
	Powder	2.97	9.70	2.05	0.338
	Pellet	2.86	7.27	−0.1558	−0.0249
	Pellet	3.9	8.86	0.0087	0.0019
Vacuum drying for 16 h at room temperature	Powder	2.68	13.73	6.66	0.9939
	Powder	3.97	9.72	4.97	1.098
	Pellet	2.86	11.18	0.941	0.1496
	Pellet	3.36	11.52	−0.4425	−0.0825

error, sometimes, Q_2 may be slightly greater than Q_1 and hence the negative values for ϵ'' and σ_c . The effect of external field on the dielectric behaviour of poly aniline at microwave frequencies is under investigation.

References

1. Martinelli, M., Rolla, P. A. and Tombari, E., A method for dielectric loss measurements by a microwave cavity in fixed resonance condition., *IEEE Trans. Microwave Theory and Techniques*, 1985, **33**, 779–783.
2. Xu, Y., Ghannouchi, F. M. and Bosisio, R. C., Theoretical and experimental study of measurement of microwave permittivity using open-ended elliptical coaxial line probes. *IEEE Trans. Microwave Theory and Techniques*, 1992, **40**, 143–150.
3. Lee, C. Y., Song, H. G., Jang, K. S., Oh, E. J., Epstein, A. J. and Joo, J., Electromagnetic interference shielding efficiency of poly-aniline mixtures and multilayer films. *Synthetic Metals*, 1999, **102**, 1346–1349.
4. Joo, J., MacDiarmid, A. G. and Epstein, A. J., Control of dielectric response of polyanilines: applications to EMI Shielding. *Proc. Annual Technical Conference of Soc. of Plastics Engineers*, Boston, MA, 7–11 May 1995, **2**, pp. 1672–1677.
5. Waldron, R. A., Perturbation theory of resonant cavities. In *Proceedings of IEE.*, 1960, **107C**, pp. 272–274.
6. Kupfer, K., Kraszewski, A. and Knöchel, R., *Sensors Update Vol. 7- RF & Microwave Sensing of Moist Materials, Food and other Dielectrics*. Wiley-VCH, Germany, 2000, pp. 186–209.

Broadband Coaxial Cavity Resonator for Complex Permittivity Measurements of Liquids

U. Raveendranath, S. Bijukumar, and K. T. Mathew

Abstract—A novel cavity perturbation technique using coaxial cavity resonators for the measurement of complex permittivity of liquids is presented. The method employs two types of resonators (Resonator I and Resonator II). Resonator I operates in the frequency range 600 MHz–7 GHz and resonator II operates in the frequency range 4 GHz–14 GHz. The introduction of the capillary tube filled with the sample liquid into the coaxial resonator causes shifts in the resonance frequency and loaded Q -factor of the resonator. The shifts in the resonance frequency and loaded Q -factor are used to determine the real and imaginary parts of the complex permittivity of the sample liquid, respectively. Using this technique, the dielectric parameters of water and nitrobenzene are measured. The results are compared with those obtained using other standard methods. The sources of errors are analyzed.

I. INTRODUCTION

A THOROUGH knowledge of the dielectric properties of a material is essential for its proper use in industrial, scientific, and medical applications. Various techniques in frequency as well as in time domain have been adopted to measure the complex permittivity of materials. Among the available methods, the cavity perturbation technique has a unique place due to many attractive features. The earliest treatment of cavity perturbation theory was given by Bethe and Schwinger [1]. According to them the perturbation was caused 1) by the insertion of small dielectric sample into a cavity and 2) by a small deformation of the boundary surface of the cavity. It was Birnbaum and Franau [2] who developed a measurement technique based on cavity perturbation theory for the first time. In their experimental arrangement, a small cylindrical sample was placed in a rectangular cavity. Slater [3] discussed the applications of cavity perturbation technique. Casimir [4] extended the cavity perturbation theory for the determination of the magnetic parameters of small sphere. Artman and Tannenwald [5] proposed an experimental technique for measuring the magnetic susceptibility tensor components in microwave cavities. General expressions for the perturbation of microwave cavities by the ferrite materials were developed. Waldron [6] modified Casimir's treatment to suit its application to the anisotropic magnetic materials namely ferrites. Artman [7] considered the effect of sample size on the apparent properties of ferrites observed by using cavity perturbation methods. Perturbation effects associated with propagation of electromagnetic waves within the specimen were also considered. Spencer *et al.* [8] suggested a criterion

for the applicability of cavity perturbation theory for measuring dielectric constants and permeabilities of materials. Kohane *et al.* [9] suggested cavity perturbation techniques for material characterization. None of the researchers mentioned above gave the derivation for perturbation formula in detail. A detailed perturbation formula with necessary approximations was given by Waldron [10]. He concluded that the high accuracy perturbation formula would only be realized if the specimen is suitably shaped and positioned in the cavity. Estlin and Bussey [11] suggested correction factors for sample insertion holes for cavity perturbation technique. Harrington [12] gave a detailed study of perturbation due to cavity walls and the insertion of the material into the cavity field region. Champlin and Krongard [13] developed a cavity perturbation technique for the measurement of conductivity and permittivity of small spherical samples. Roussy and Felden [14] suggested a cavity perturbation method for studying the dielectric properties of powders under controlled pressure. Waldron [15] showed that the uncertainty principle leads to errors in the cavity perturbation methods. Ho and Hall [16] measured the dielectric properties of sea water and NaCl solutions using a cylindrical cavity in the TM_{010} mode. Cavities of special shapes with strong fields in some regions have also been used to increase the sensitivity of measurement. Blume [17] studied the dielectric properties of polluted water with reflection type cavity. For the measurements of losses of small samples, Martinelli *et al.* [18] suggested a cavity perturbation technique. Chao [19] reviewed the theory and technique of cavity perturbation method. For measuring the complex permittivity of thin substrate materials, Dube *et al.* [20] suggested a cavity perturbation technique. Henry *et al.* [21] studied the polymer latex coalescence by dielectric measurements at microwave frequencies using cavity perturbation technique. Akyel *et al.* [22] suggested a cavity perturbation technique in which high temperature measurements can be conducted. For the measurement of complex permittivity of highly polar liquids like water, Mathew *et al.* [23] proposed a new cavity perturbation method. Raveendranath *et al.* [24] suggested a novel cavity perturbation technique for the complex permeability measurement of ferrite materials. Generally cavity perturbation techniques are used for low-loss and medium-loss materials. But the present technique based on cavity perturbation theory gives good results even for high-loss liquid like water.

Recently, broadband coaxial probe techniques [25]–[27] have been employed for complex permittivity measurement. Though these methods give good results, they require elaborate calibration procedures, and significant errors may occur due to improper contact at the probe-material interface for solids. In an

Manuscript received November 15, 1998; revised September 21, 2000.

The authors are with the Department of Electronics, Cochin University of Science and Technology, Cochin 682 022, Kerala, India (e-mail: mathew@doe.cusat.edu).

Publisher Item Identifier S 0018-9456(00)10945-3.

earlier paper [28], the authors suggested a coaxial cavity resonator technique. This paper discusses in detail the theoretical and experimental aspects of this technique.

II. DESIGN AND FABRICATION OF THE COAXIAL RESONATOR

Coaxial cavity resonators are sections of coaxial lines with both or one end shorted by a good conductor. Electromagnetic fields excited in the resonator are reflected from the ends and the waves add in phase. For resonance the total phase shift in the propagating waves must be 2π or its multiple. If ϕ_1 and ϕ_2 are the phases introduced due to the reflections at the two ends and " d " is the length of the resonator, then the condition for resonance will be

$$\phi_1 + \phi_2 + 2\beta d = 2n\pi \quad \text{where } n = 1, 2, 3, \dots \quad (1)$$

For an open-end resonator,

$$\phi_1 = 0, \quad \phi_2 = \pi,$$

so

$$2\beta d = (2n - 1)\pi \quad \lambda_r = \frac{4d}{(2n - 1)} \quad (2)$$

where λ_r is the resonant wavelength. β is the phase shift constant. Thus, the coaxial line section with one end open acts as a resonator in the vicinity of the frequency for which its length is an odd multiple of a quarter wavelength. Various modes are possible for a resonator of given length. The field configurations of these modes may easily be inferred from the propagating TEM mode in a coaxial line. However, care must be taken that higher order TE and TM modes are not excited in such a resonator. The basic condition is $\lambda_r > (\pi/2(b+a))$ where " a " is the radius of the inner conductor and " b " is the inner radius of the outer conductor. In an open-end resonator, there is a possibility of radiation loss from the open end, resulting in poor quality factor. In order to overcome this, the outer conductor is extended beyond the end of the inner conductor such that it forms a cylindrical waveguide operating below cutoff in the TM_{01} mode.

The cutoff frequencies for circular waveguide can be calculated from the separation equations [12].

For TM mode

$$\left[\frac{X_{np}}{b} \right]^2 + k_z^2 = k^2. \quad (3)$$

For TE mode

$$\left[\frac{X'_{np}}{b} \right]^2 + k_z^2 = k^2 \quad (4)$$

where

- k wave number;
- k_z wavenumber in the propagation direction;
- X_{np} and X'_{np} p th order zero of the Bessel functions of the first kind and order n .

In the present investigation, the basic coaxial resonator consists of a circular waveguide with a removable center conductor located along its axis. From Table I, it is clear that comparatively wide range of frequencies can be covered by using the

TABLE I
CHARACTERISTIC FEATURES OF COAXIAL RESONATORS

Type of cavity	Length of centre conductor (mm)	Characteristics of resonators	
		Resonance Frequency (GHz)	Loaded Q-factor (Q_0)
Resonator I	168	0.424	342
		1.399	1104
		2.171	1342
		3.035	1011
		3.340	728
		4.760	682
		5.620	814
		6.483	2401
		6.622	1363
	113	1.888	1279
		3.147	1128
		4.396	1150
		5.983	658
		7.301	428
		8.661	312
	88	2.360	468
		4.024	1216
		5.364	2683
6.341		4365	
7.279		2426	
8.630		582	
Resonator II	120	1.380	678
		3.130	406
		4.360	794
		5.632	826
		6.880	625
		9.265	1100
		10.495	2409
		12.951	4531
		14.177	2200
	100	0.748	688
		2.256	741
		3.684	323
		5.260	454
		6.80	772
		8.083	1283
		9.565	6547
		11.051	1223
		13.934	1624

center conductors of different lengths. The TEM mode propagates up to the end of the center conductor. The resonator is fed by a rectangular feed loop. The coupling mechanism will generate spurious higher order modes, which are usually cut off and have an evanescent nonpropagating nature. Since the energy is coupled into or out of the cavity through the same coupling mechanism, the resonator is one-port reflection type. The physical dimensions of the coaxial cavity resonators are shown in Table II. Resonator I has TM_{01} mode cutoff at 6.96 GHz and TE_{11} mode cut off at 5.3 GHz. For resonator II, the values are 19.1 GHz and 14.6 GHz, respectively. Table I shows the characteristic features of resonators I and II. The schematic diagram of the resonator is shown in Fig. 1.

III. THEORETICAL ANALYSIS

In the cavity perturbation technique, the "perturbation"—a gradual disturbance—of the field inside the cavity is generated by changing the dielectric medium inside the cavity. If ϵ_1 is the dielectric constant of the medium inside the empty cavity and ϵ_2 that of the medium after the introduction of a small sample, the change in dielectric constant is $\epsilon_1 \sim \epsilon_2 = \Delta\epsilon$. If $E_{\rho n}^0$ and $E_{\rho n}$ are the fields inside the cavity before and after the introduction of sample in the cavity, theory of perturbation states that $E_{\rho n} \rightarrow E_{\rho n}^0$ when $\Delta\epsilon \rightarrow 0$. This is the fundamental and very reasonable assumption [12] of the theory of perturbation. This

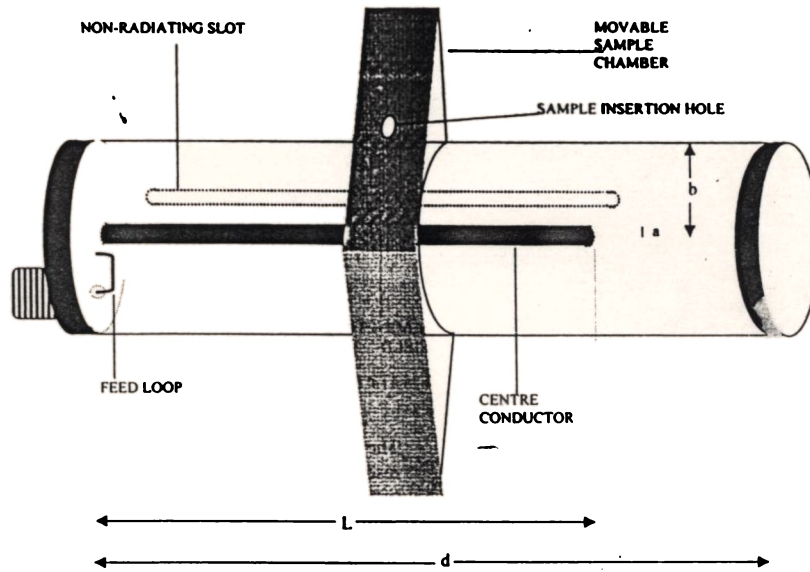


Fig. 1. Schematic diagram of the coaxial cavity resonator.

TABLE II
DESIGN PARAMETERS OF COAXIAL TRANSMISSION LINE RESONATORS

Dimension (mm)	Resonator I	Resonator II
Length of the resonator (<i>d</i>)	250	140
Lengths of the centre conductors (<i>L</i>)	168 113 88	120 100
Inner radius of the resonator (<i>b</i>)	16.25	6.64
Radius of the centre conductor (<i>a</i>)	3.0	1.36
Distance from the centre conductor to feed loop (<i>c</i>)	3.0	0.75
Feed loop, inner dimension (<i>h</i> x <i>l</i>)	2 x 8	1 x 2

fundamental assumption is applied in the theory of coaxial resonator.

The coaxial transmission line resonator consists of a circular waveguide which operates below cutoff for the TM_{01} mode. Along the axis of the waveguide there is a removable center conductor. Thus the TEM mode can propagate upto the end of the center conductor.

The standing wave field components of the resonant TEM mode are obtained by combining the forward and backward propagating waves (in cylindrical coordinate system $\{\rho, \phi, z\}$) as [12], [29]

$$E_{\rho s}^0 = \frac{Ae^{j\beta z}}{\rho} + \frac{Be^{-j\beta z}}{\rho} \tag{5}$$

$$H_{\phi s}^0 = -\frac{Ae^{j\beta z}}{\eta\rho} + \frac{Be^{-j\beta z}}{\eta\rho} \tag{6}$$

where η is the free space impedance and A and B are constants. The boundary conditions require that $E_{\rho s}^0$ must vanish

at $z = 0$ which is the fixed end of the center conductor. At $z = L$, (where L is the length of the center conductor) the maximum field corresponding to resonance occurs. The first condition gives $A = -B$, while the second gives the resonance condition. Now, (5) and (6) become

$$E_{\rho s}^0 = 2j\frac{A}{\rho} \sin \beta z = jE_{av} \sin \beta z \tag{7}$$

$$H_{\phi s}^0 = -2\frac{A}{\eta\rho} \cos \beta z = -\frac{E_{av}}{\eta} \cos \beta z. \tag{8}$$

Since " ρ " varies from " a " to " b " (from the surface of the center conductor to the inner radius of the resonator) the average field acting on the sample may be considered. Thus E_{av} is the average electric field. The electrical energy stored in the cavity is

$$W_e = \frac{\epsilon_0}{2} \int_{V_c} E_{\rho s}^0{}^2 dV. \tag{9}$$

On substituting the value of $E_{\rho s}^0$ from (7) in (9) we get

$$W_e = \frac{\epsilon_0}{2} \int_0^{2\pi} \int_a^b \int_0^L E_{av}^2 \sin^2 \beta z \rho d\rho d\phi dz. \tag{10}$$

Here " b " is the inner radius of the outer conductor and " a " is the radius of the center conductor.

When the sample is introduced into the cavity, the relative complex frequency shift of the resonator is given by Waldron [10] as shown in (11) at the bottom of the next page. The numerator of (11) represents the total energy stored in the sample and the denominator represents the total energy stored in the cavity.

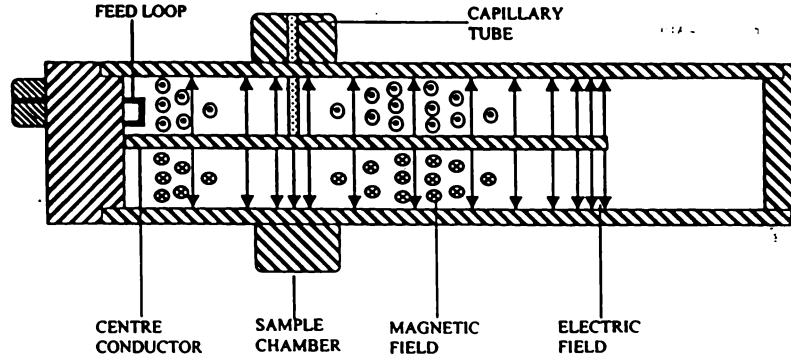


Fig. 2. Cross-sectional view of the coaxial cavity resonator.

The total energy stored in the cavity is

$$\int_{V_c} (D_0 \cdot E_0^* + B_0 \cdot H_0^*) dV = 4W_e. \quad (12)$$

When the dielectric sample is introduced at the position of maximum electric field (Fig. 2) the relative frequency shift is given by

$$-\frac{d\Omega}{\Omega} \approx \frac{(\bar{\epsilon}_r - 1) \int_{V_s} \epsilon_0 E_{\rho s \max} \cdot E_{\rho s \max}^0 dV}{4W_e}. \quad (13)$$

Substituting for W_e from (10), (13) becomes

$$-\frac{d\Omega}{\Omega} \approx \frac{(\bar{\epsilon}_r - 1) \int_{V_s} E_{\rho s \max} \cdot E_{\rho s \max}^0 dV}{2 \int_0^{2\pi} \int_a^b \int_0^L E_{av}^2 \sin^2 \beta z \rho d\rho d\phi dz} \approx \frac{(\bar{\epsilon}_r - 1)V_s}{\pi L(b^2 - a^2)}. \quad (14)$$

For small volume of the sample, $E_{\rho s \max} = E_{\rho s \max}^0 = E_{av}$. $V_s = \pi r^2(b - a)$ where r is the inner radius of the capillary tube. However, $\bar{\epsilon}_r = \epsilon_r' - j\epsilon_r''$. Then, (14) becomes

$$\frac{d\Omega}{\Omega} \approx -\frac{(\epsilon_r' - 1)r^2}{L(b + a)} + \frac{j\epsilon_r''r^2}{L(b + a)}. \quad (15)$$

The relative complex frequency shift is related to the shifts in resonance frequency and loaded Q -factor by the standard equation [10]

$$\frac{d\Omega}{\Omega} \approx \frac{(f_s - f_0)}{f_s} + j \left[\frac{1}{Q_s} - \frac{1}{Q_0} \right] \quad (16)$$

where f_s and f_0 are the resonant frequencies of the cavity with and without the sample. Q_s and Q_0 are the corresponding Quality factors. From (15) and (16), we can write

$$(\epsilon_r' - 1) = \frac{L(b + a)}{r^2} \frac{(f_0 - f_s)}{f_s} \quad (17)$$

$$\epsilon_r'' = \frac{L(b + a)}{2r^2} \left[\frac{1}{Q_s} - \frac{1}{Q_0} \right]. \quad (18)$$

If the frequency shift is measured from the resonance frequency f_t of the cavity loaded with empty tube rather than that of the empty cavity alone, the above equations become

$$(\epsilon_r' - 1) = \frac{L(b + a)}{r^2} \frac{(f_t - f_s)}{f_s} \quad (19)$$

$$\epsilon_r'' = \frac{L(b + a)}{2r^2} \left[\frac{1}{Q_s} - \frac{1}{Q_t} \right] \quad (20)$$

where Q_t is the quality factor of the cavity loaded with empty tube, f_s and Q_s are the resonance frequency and quality factor of the cavity loaded with capillary tube containing the sample liquid, respectively.

The effective conductivity of the sample under test is given by

$$\sigma_e = \omega \epsilon_r'' = 2\pi f \epsilon_0 \epsilon_r''. \quad (21)$$

$$-\frac{d\Omega}{\Omega} \approx \frac{(\bar{\epsilon}_r - 1)\epsilon_0 \int_{V_s} E \cdot E_0^* dV + (\bar{\mu}_r - 1)\mu_0 \int_{V_s} H \cdot H_0^* dV}{\int_{V_c} (D_0 \cdot E_0^* + B_0 \cdot H_0^*) dV}. \quad (11)$$

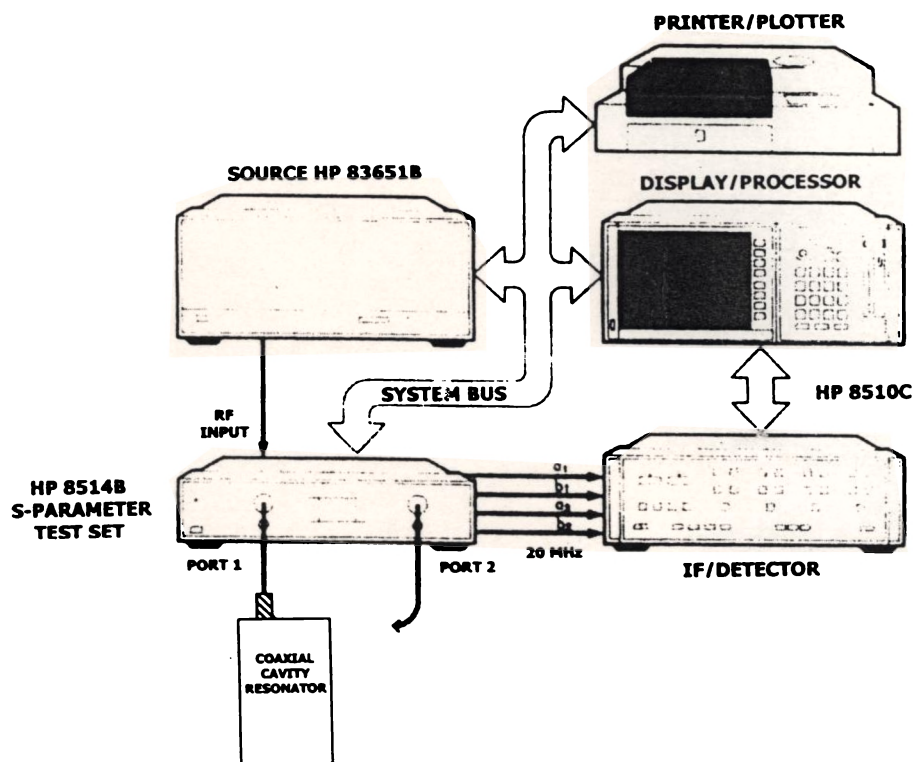


Fig. 3. Block diagram of the experimental setup.

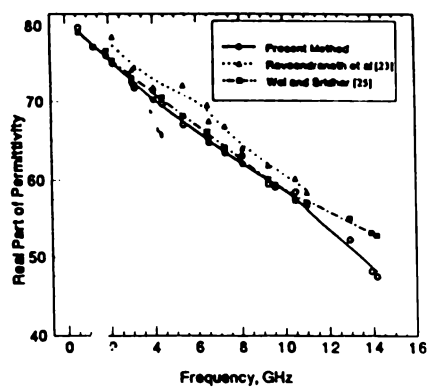
IV. EXPERIMENTAL SETUP AND MEASUREMENTS

The experimental setup consists of HP 8510B network analyzer, S -parameter test set, sweep oscillator, and instrumentation computer (Fig. 3). The resonator is connected to one port of the S -parameter test set. A movable sample chamber is attached around the resonator and a small hole is drilled in it for inserting the sample into the cavity field region. On the wall of the resonator, there is a long narrow slot to facilitate the movement of the sample along the cavity (Fig. 1). This narrow slot is nonradiating and there is negligible field redistribution due to its presence. An empty capillary tube made of low loss fused silica ($\tan \delta = 0.0002$) is introduced into the cavity at the position of maximum electric field corresponding to each resonance frequency, by sliding it along the slot, as shown in Fig. 2. Resonance frequency and Q -factor of the cavity loaded with empty capillary tube are determined. The liquid whose dielectric parameters are to be determined is placed in the capillary tube both ends of which are sealed. The measurements are repeated. From the shifts in the resonance frequencies and Q -values, the real and imaginary parts of complex permittivity can be calculated. For the resonator I, sharp resonance peaks are available from 600 MHz to 7 GHz. Resonance peaks are not very sharp at low frequencies for the resonator II. Hence resonator II is used for measurements in the frequency range 4 GHz–14 GHz.

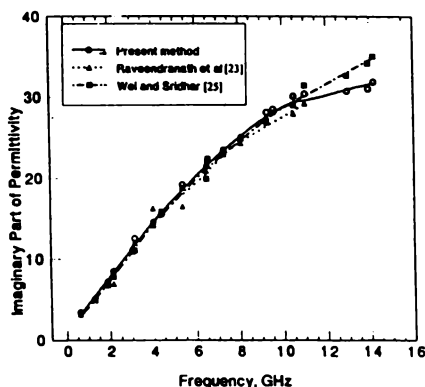
From Table I, it is noted that for a given center conductor, loaded Q -factors are considerably low at certain resonance frequencies. Therefore, the measurements are performed at those frequencies where Q -values are high. All the measurements in this work are performed at constant temperature 27 °C.

V. SOURCES OF ERROR AND ACCURACY CONDITIONS

Though accuracy of measurement is the most attractive feature of perturbation techniques, care should be taken to eliminate all possible sources of error. In the present study HP 8510B Network Analyzer was used. Accuracy of the instrument is 0.001 dB for the power measurement, 1 Hz for frequency measurement, 0.01° in the phase measurement, and 0.01 ns for time domain measurement [30]. Main sources of experimental error are 1) high relative resonance frequency shift ($\delta f_r/f_r$); 2) nonuniformity of cross section of tube; 3) high loss tangent of capillary tube; 4) mismatch of coupling loop; and 5) axis tilt of center conductor. To satisfy the perturbation condition, relative resonance frequency shift ($\delta f_r/f_r$) should be of the order of 0.001. So the size of the capillary tubes is properly chosen to give a frequency shift of the order of 0.001 GHz and a decrease in the Q -factor of the cavity from Q_0 by a factor of 10–15%. With these criteria in mind, sample tubes of different diameters



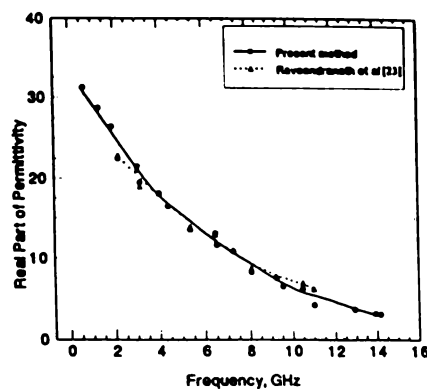
(a)



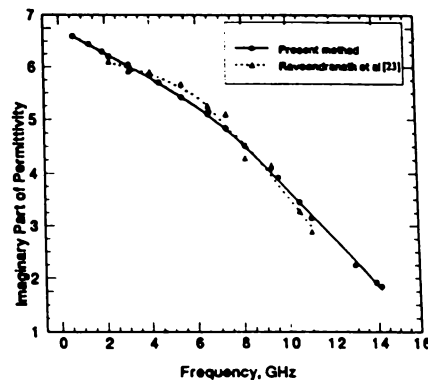
(b)

Fig. 4. (a) Real part of permittivity of water versus frequency. (b) Imaginary part of permittivity of water versus frequency.

are selected for different materials (polar, nonpolar, etc.) to enhance the sensitivity of measurement. The significant error that usually occurs in the complex permittivity measurement is due to the nonuniformity of cross-section of the tube. It causes error in the value of V_s . So the diameter of the tube should be accurately measured at different cross-sections of the tube and average value should be taken. An error in the diameter measurement of a capillary tube by a least count of 0.001 mm causes less than 1% variation in the complex permittivity. An error of five least count causes 2.5% variation in the complex permittivity. The thickness of the wall of the tube should be negligibly small and the loss tangent of the material of the tube be very low ($\tan \delta = 0.0002$). Hence, the resonance frequency and Q -factor of the cavity loaded with empty sample tube is almost the same as that of the empty cavity alone. The coupling loop of the resonator must be properly designed for maximum impedance matching. This can be judged from the return loss of the resonator without the sample. Care should be taken to see whether the center conductor remains coaxially. Inclination of the center conductor by 10° and 15° make 2% and 3.5% errors, respectively, in the permittivity measurements.



(a)



(b)

Fig. 5. (a) Real part of permittivity of nitrobenzene versus frequency. (b) Imaginary part of permittivity of nitrobenzene versus frequency.

VI. RESULTS AND DISCUSSION

Coaxial cavity resonator technique offers an accurate method for measuring the dielectric parameters of all types of liquids. In the present study, water and nitrobenzene were considered. These liquids are polar in nature and consequently have high complex permittivity. As expected, the real part of the complex permittivity of water and nitrobenzene is found to be decreasing with frequency. The imaginary part of complex permittivity of these liquids also varies with frequency. The results are shown in Figs. 4 and 5. Conductivity of water and nitrobenzene are also determined and plotted in Figs. 6(a) and (b).

The technique developed by Wei and Sridhar [25] gives very accurate results in the determination of dielectric parameters of water. A comparative study of the results obtained with the methods suggested by Von Hippel [31], E. H. Grant *et al.* [32], and J. B. Hasted [33] show that their results are not in good agreement with those of Wei and Sridhar [25]. In this context, the present technique is very significant as the dielectric parameters of water measured agree well with the results of Wei and Sridhar. In the case of nitrobenzene, the results are compared with that of rectangular cavity method [23]. The attractive fea-

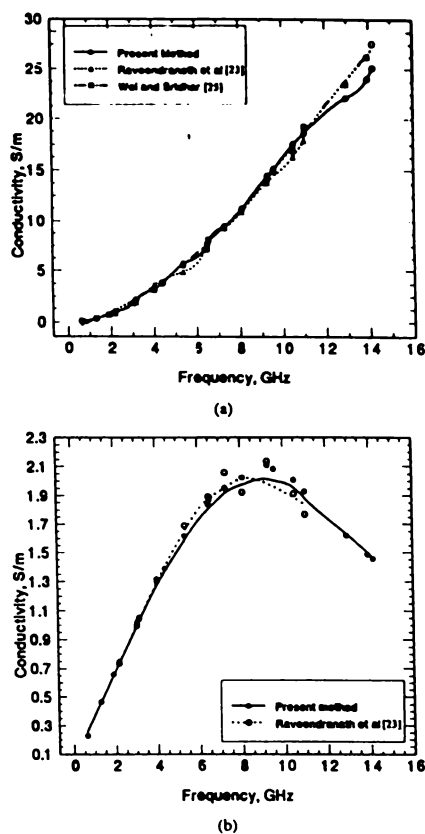


Fig. 6. (a) Conductivity of water versus frequency. (b) Conductivity of nitrobenzene versus frequency.

ture of this method is that the measurement of the dielectric parameters over a wide range of frequencies can be performed. Since the volume of the sample required for the measurement is very small (<0.5 ml), precious liquids available in very small quantities can be studied using the present technique. Thus it finds applications in the fields like Biotechnology and Biochemistry. The present method is very well suited for the measurement of dielectric parameters of low loss and medium loss liquids. This technique may be extended for solids and vapors.

REFERENCES

- [1] H. A. Bethe and J. Schwinger, Cornell Univ., Ithaca, NY, NRDC Rep. DI-117, Mar. 1943.
- [2] G. Birnbaum and J. Franau, "Measurement of the dielectric constant and loss of solids and liquids by a cavity perturbation method," *J. Appl. Phys.*, vol. 20, pp. 817-818, 1949.
- [3] J. C. Slater, *Microwave Electronics*. New York: Van Nostrand, 1950, pp. 80-81.
- [4] H. B. G. Casimir, "On the theory of electromagnetic waves in resonant cavities," *Philips Res. Rep.* 6, 1951.
- [5] J. O. Artman and P. E. Tannenwald, "Measurement of susceptibility tensor in ferrites," *J. Appl. Phys.*, vol. 26, pp. 1124-1132, 1955.
- [6] R. A. Waldron, "Theory of the measurement of the elements of the permeability tensor of a ferrite by means of a resonant cavity," *Proc. Inst. Elect. Eng. B*, vol. 104, p. 307, 1956.
- [7] J. O. Artman, "Effects of size on the microwave properties of ferrite rods, discs and spheres," *J. Appl. Phys.*, vol. 20, pp. 92-98, 1957.
- [8] E. G. Spencer, R. C. LeCraw, and L. A. Ault, "Note on cavity perturbation theory," *J. Appl. Phys.*, vol. 28, pp. 130-132, 1957.
- [9] T. Kohane and H. M. Sirvetz, "The measurement of microwave resistivity by eddy current loss in small spheres," *Rev. Sci. Instrum.*, vol. 30, pp. 1059-1060, 1959.
- [10] R. A. Waldron, "Perturbation theory of resonant cavities," *Proc. Inst. Elect. Eng.*, vol. 107-C, pp. 272-274, 1960.
- [11] A. J. Estlin and H. E. Bussey, "Errors in dielectric measurements due to a sample insertion hole in a cavity," *IRE Trans. Microwave Theory Tech.*, vol. 6, pp. 650-653, 1960.
- [12] R. F. Harrington, *Time-Harmonic Electromagnetic Fields*. New York: McGraw-Hill, 1961, p. 317.
- [13] K. S. Champlin and R. R. Krongard, "The measurement of conductivity and permittivity of semiconductor spheres by an extension of the cavity perturbation method," *IRE Trans. Microwave Theory Tech.*, vol. MTT-9, pp. 545-551, 1961.
- [14] G. Roussy and M. Felden, "A sensitive method for measuring complex permittivity with a microwave resonator," *IEEE Trans. Microwave Theory Tech.*, vol. MTT-14, pp. 171-175, 1966.
- [15] R. A. Waldron, "Errors due to the uncertainty principle in swept frequency cavity measurements of properties of materials," *IEEE Trans. Microwave Theory Tech.*, vol. MTT-16, pp. 314-315, 1968.
- [16] W. Ho and W. F. Hall, "Measurement of the dielectric properties of seawater and sodium chloride solutions at 2.65 GHz," *J. Geophys. Res.*, vol. 78, pp. 6301-6315, 1973.
- [17] H.-J. C. Blume, "Measurement of dielectric properties and determination of microwave emissivity of polluted waters," *IEEE Trans. Instrum. Meas.*, vol. IM-29, pp. 281-291, 1980.
- [18] M. Martinelli, P. A. Rolla, and E. Tombari, "A method for dielectric loss measurements by a microwave cavity in fixed resonance condition," *IEEE Trans. Microwave Theory Tech.*, vol. MTT-33, pp. 779-783, 1985.
- [19] S. H. Chao, "Measurements of microwave conductivity and dielectric constant by the cavity perturbation method and their errors," *IEEE Trans. Microwave Theory Tech.*, vol. MTT-33, pp. 519-526, 1985.
- [20] D. C. Dube, M. T. Lanagan, J. H. Kim, and S. J. Jang, "Dielectric measurements on substrate materials at microwave frequencies using a cavity perturbation technique," *J. Appl. Phys.*, vol. 63, pp. 2466-2468, 1988.
- [21] F. Henry, F. Cansell, J. L. Guillaume, and C. Pichot, "Study of the polymer latex coalescence by dielectric measurements at microwave frequency—Feasibility of the method," *Colloid Polym. Sci.*, vol. 267, pp. 167-178, 1989.
- [22] C. Akyel and R. G. Bosio, "Permittivity measurements of granular food products suitable for computer simulations of microwave cooking process," *IEEE Trans. Instrum. Meas.*, vol. 39, pp. 497-500, 1990.
- [23] K. T. Mathew and U. Raveendranath, "Waveguide cavity perturbation method for measuring complex permittivity of water," *Microwave Opt. Tech. Lett.*, vol. 6, pp. 104-106, 1993.
- [24] U. Raveendranath and K. T. Mathew, "New cavity perturbation technique for measuring the complex permeability of ferrite materials," *Microwave Opt. Tech. Lett.*, vol. 18, pp. 241-243, 1998.
- [25] Z. Wei and S. Sridhar, "Radiation corrected open-ended coax-line technique for dielectric measurements of liquids up to 20 GHz," *IEEE Trans. Microwave Theory Tech.*, vol. 39, pp. 526-531, 1991.
- [26] Y. Xu, F. M. Ghannouchi, and R. C. Bosio, "Theoretical and experimental study of measurement of microwave permittivity using open-ended elliptical coaxial line probes," *IEEE Trans. Microwave Theory Tech.*, vol. 40, pp. 143-150, 1992.
- [27] D. M. Xu, L. P. Liu, and Z. Y. Jiyang, "Measurement of dielectric properties of biological substances using an improved open-ended coaxial line resonator method," *IEEE Trans. Instrum. Meas.*, vol. IM-35, pp. 13-18, 1986.
- [28] U. Raveendranath, J. Jacob, and K. T. Mathew, "Complex permittivity measurement of liquids with coaxial cavity resonators using a perturbation technique," *Electron. Lett.*, vol. 32, pp. 988-990, 1996.
- [29] M. L. Sisodia and G. S. Raghuvanshi, *Microwave Circuits and Passive Devices*. New Delhi, India: Wiley Eastern, 1991, p. 265.
- [30] *HP 8510B Network Analyzer Operating and Programming Manual*: Hewlett-Packard, Apr. 1988.
- [31] A. R. Von Hippel, Ed., *Dielectric Materials and Applications*. New York: Wiley, 1954.
- [32] E. H. Grant, T. J. Buchanan, and H. F. Cook, "Dielectric behavior of water at microwave frequencies," *J. Chem. Phys.*, vol. 26, pp. 156-161, 1957.
- [33] J. B. Hasted, *Aqueous Dielectrics*. London, U.K.: Chapman & Hall, 1973.



U. Raveendranath received the M.S. degree in physics and the Ph.D. degree in microwave electronics from the School of Pure and Applied Physics, Mahatma Gandhi University, India, in 1989 and 1997, respectively.

He was a Lecturer with the Department of Electronics, Cochin University of Science and Technology, Cochin, India, from 1997 to 1999. He is a Scientist with the Aerospace Electronics and Systems Division, National Aerospace Laboratory (NAL), Bangalore, India. His fields of interest include microwave techniques for material characterization, microwave antennas and computational electromagnetics. He co-authored *Sensors Update, Vol. 7* (New York: Wiley). He also was a Researcher in the collaboration project sponsored by the IRCTR, Delft University, The Netherlands.



S. Bijukumar received the M.Sc. degree in physics from Kerala University, India, in 1997 and is currently pursuing the Ph.D. degree at Department of Electronics, Cochin University of Science and Technology, India.

He is a Researcher in the "Measurement of complex permittivity in the frequency domain" Project, IRCTR, Delft University, The Netherlands. He has visited the Abdus Salam International Centre for Theoretical Physics (ICTP), Trieste, Italy, under the Young Student Programme, where he worked in the field of FDTD techniques. His fields of interest are free space complex permittivity measurements, microwave material study, and microwave antennas.



K. T. Mathew received the B.Sc. and M.Sc. degrees in physics from Kerala University, India, in 1968 and 1970, respectively, and the Ph.D. degree from Cochin University, India, in 1978.

From 1970 to 1986, he was with St. Teresa's College, Ernakulam, India. In 1987, he joined the Mahatma Gandhi University, India, and in 1990, was appointed to the Cochin University of Science and Technology, where he is now Professor of electronics. He has published more than 50 papers. In 1998, he was with the Technical University of Delft (TU Delft), The Netherlands, and later, in a collaboration project between Cochin University and TU Delft. He is the Principal Investigator of a major research project for microwave imaging for medical applications funded by the government of India and the co-author of *Sensors Update Vol. 7* (New York: Wiley). His research interests are antennas, microwave materials study, aquametry, and microwave imaging.

Dr. Mathew is a Fellow of the Institution of Electronics and Telecommunications Engineers, India and a member of the Expert Committee, DOEACC Society, Government of India.

Effect of Drying Conditions on Microwave Conductivity of Polyaniline

HONEY JOHN,¹ S. BIJU KUMAR,² K. T. MATHEW,² RANI JOSEPH¹

¹ Department of Polymer Science and Rubber Technology, Cochin University of Science and Technology, Cochin 682 022, Kerala, India

² Department of Electronics, Cochin University of Science and Technology, Cochin 682 022, Kerala, India

Received 7 September 2000; accepted 21 June 2001

Published online 19 December 2001

ABSTRACT: Polyaniline was synthesized by using ammonium persulfate initiator in the presence of 1M HCl. It was dried under different drying conditions like room temperature drying (for 48 h), oven drying (at 50–60°C for 8 h under a vacuum), and vacuum drying (at room temperature for 16 h). The conductivities of these samples were measured at microwave frequencies. These samples were also pelletized and the measurements were repeated. The cavity perturbation technique was used for the study. © 2002 John Wiley & Sons, Inc. *J Appl Polym Sci* 83: 2008–2012, 2002

Key words: polyaniline; conductivity; frequency

INTRODUCTION

Conducting polymers have been proved to be excellent replacements for metals and semiconductors in electrochemical applications, notably for the energy storage process, corrosion protection, electrochromic devices, electrochemical sensors, and so forth and above all as a strong electromagnetic imaging material.^{1,2} These uses have recently attracted significant attention from all branches of polymer research with a growing interdisciplinary trend. Electrically conducting polymers differ from inorganic crystalline semiconductors in two ways: they are molecular in character and lack long-range orders. With a large variety of conducting polymers, polyaniline (PAN) is a relatively stable, electrically conducting polymer resulting from the oxidative polymerization of aniline, which is easy to prepare. Also, the environmental stability of PAN appears to be

extremely good compared to a number of other conducting polymers. For this reason it is one of the most potentially useful conducting polymers.

Recently, La Croix and Diaz³ proposed that the thermal decomposition of the material occurs in two stages, although the thermal stability of PAN has been reported up to 400°C. Two studies^{4,5} subsequently reported a three-step decomposition process for the HCl protonated conducting form: the initial loss is due to volatilization of water molecules, the second loss is related to loss of dopant moiety, and the third loss is related to degradation of the polymer backbone due to production of gases such as acetylene and ammonia. The present article reports the effect of drying conditions on microwave conductivity of PAN at various frequencies.

EXPERIMENTAL

Materials

Reagent grade aniline was distilled prior to use. The HCl and ammonium persulfate were used as received.

Correspondence to: R. Joseph.

Journal of Applied Polymer Science, Vol. 83, 2008–2012 (2002)
© 2002 John Wiley & Sons, Inc.
DOI 10.1002/japp.10155

Table I Results of Pure Polyaniline Powder

Frequency (GHz)	Room Temp. Drying (48 h)	Oven Drying (8 h at 50–60°C)	Vacuum Drying (16 h at 28°C)
2.6S	Real = 12.3128	Real = 8.7712	Real = 12.7267
	Imag = 9.8054	Imag = 1.9812	Imag = 6.6646
	Cond = 1.4628	Cond = 0.2955	Cond = 0.9939
3.2S	Real = 11.5464	Real = 9.2441	Real = 9.6073
	Imag = 9.1273	Imag = 2.4281	Imag = 6.5399
	Cond = 1.6671	Cond = 0.4435	Cond = 1.1942
3.62	Real = 13.8470	Real = 8.3815	Real = 8.4765
	Imag = 8.9477	Imag = 2.2015	Imag = 7.9897
	Cond = 1.8013	Cond = 0.4435	Cond = 1.6090

Real, real part of complex permittivity; Imag, imaginary part of complex permittivity; and Cond, conductivity of the sample (S/m).

Table II Results of Pure Polyaniline Pellets

Frequency (GHz)	Room Temp. Drying (48 h)	Oven Drying (8 h at 50–60°C Under Vacuum)	Vacuum Drying (16 h at 28°C)
2.86	Real = 10.3276	Real = 7.0903	Real = 10.1776
	Imag = 0.4517	Imag = 0.1707	Imag = 0.9401
	Cond = 0.0719	Cond = 0.0272	Cond = 0.1496
3.9	Real = 11.8709	Real = 6.9380	Real = 10.0244
	Imag = 1.7346	Imag = 0.8693	Imag = 0.7891
	Cond = 0.3757	Cond = 0.1888	Cond = 0.1712

Preparation of PAN

Chemical oxidative polymerization of aniline was carried out using ammonium persulfate as an initiator in the presence of 1M HCl. The polymer formed was dried under different conditions like room temperature (for 48 h), under a vacuum (under a 1 kg/cm² vacuum for 16 h), and in a vacuum oven (at 50–60°C for 8 h). The dielectric properties and the conductivities of these samples were measured using the cavity perturbation technique.

The experimental setup consists of a HP8510 vector network analyzer, a sweep oscillator, a S-parameter test set, and a rectangular cavity resonator. The resonant frequency and quality (Q) factor of the cavity resonator with and without the samples in the cavity were measured and the dielectric parameters were evaluated. All the measurements were done in S band (2–4 GHz) at 25°C. The PAN samples were pelletized and the microwave conductivity of these samples was also measured using the same technique. In the mi-

crowave studies the conductivity (σ) is expressed in terms of the loss or imaginary part of the complex permittivity:

$$\sigma = 2 \prod f \epsilon_0 \epsilon''$$

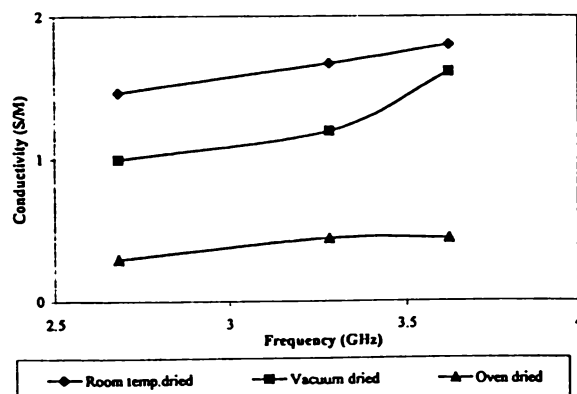


Figure 1 Variation of conductivity of PAN powder with frequency at different drying conditions.

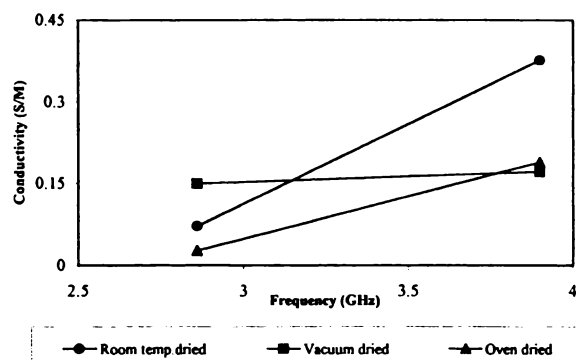


Figure 2 Variation of conductivity of PA pellet with frequency at different drying conditions.

where ϵ_0 is the permittivity of free space or a vacuum, ϵ_r'' is the imaginary part of the complex permittivity, and

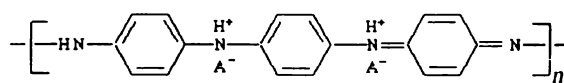
$$\epsilon_r'' = V_c/4V_s(1/Q_s - 1/Q_t)$$

where V_c is the volume of the cavity, V_s is the volume of the sample, Q_s is the quality factor of the cavity loaded with the sample, and Q_t is the quality factor of the cavity with the empty sample holder.

RESULTS AND DISCUSSION

Tables I and II show the conductivity values for PAN powder and pellet samples, respectively, under different drying conditions. The dielectric loss in all cases is found to increase with an increase in frequency.

Protonation in PAN leads to the formation of a radical cation by an internal redox reaction, which causes reorganization of the electronic structure to give semiquinone radical cations. The degree of protonation and the electronic conductivity thus become a function of the dopant concentration.



Structure of Conducting Polyaniline

At low frequencies the dipoles synchronized their orientation with the field. However, as the frequency increases, the inertia of the molecule and the binding forces become dominant and it is the basis for dielectric heating or dielectric loss. Figures 1 and 2 show that the conductivity increases with the frequency in all cases, and it may

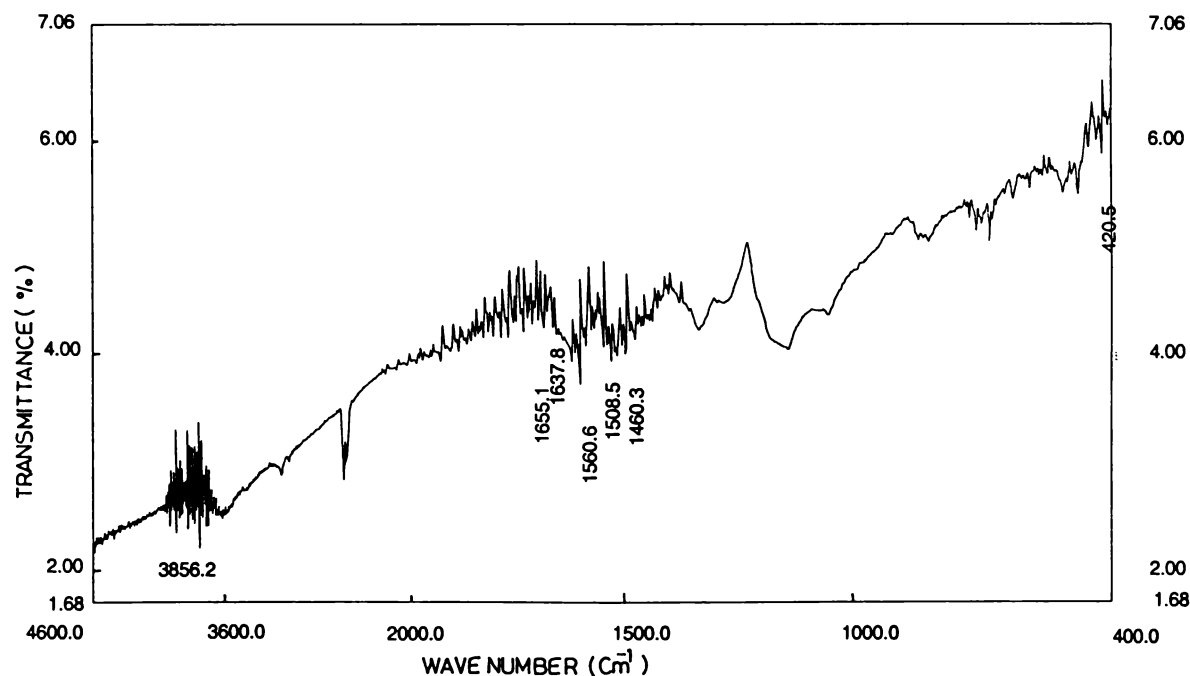


Figure 3 IR spectrum of room temperature dried PAN powder.

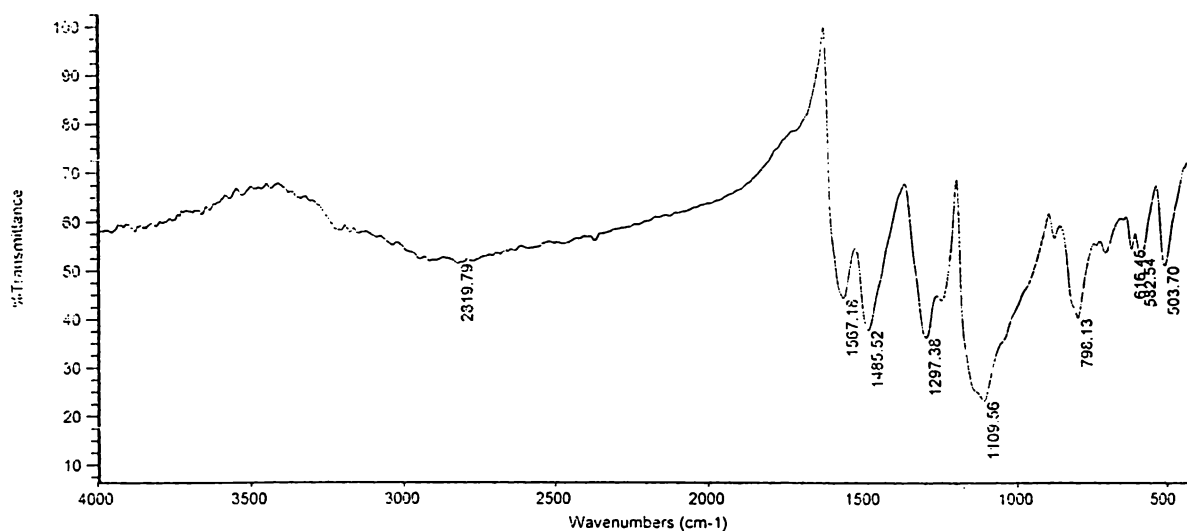


Figure 4 IR spectrum of vacuum dried PAN powder.

be due to the increase in the dielectric loss with the increase in frequency.

Tables I and II also show that the microwave conductivity of the room temperature dried powder form of PAN is greater compared to a vacuum dried sample, which is superior to the oven dried sample. Similarly, when the powder sample is converted to a pellet by applying pressure, the conductivity is reduced, irrespective of the drying conditions.

It is evident from the experiment that there is a loss of dopant molecules under a vacuum and

during high temperature drying, which will reduce the dielectric loss, which in turn reduces the conductivity. This is confirmed by the IR spectra of the various samples. Figures 3–5 show the IR spectra of powder samples that were room temperature dried, vacuum dried, and oven dried, respectively. In the IR spectra of the room temperature dried sample the principal absorption at 1150 cm^{-1} indicates the presence of PAN-HCl.⁶ The absorptions at 1325, 1275, 1150, and 1050 cm^{-1} shift to 1297, 1250, 1109.56, and 890 cm^{-1} , respectively, in the vacuum dried sample. It is

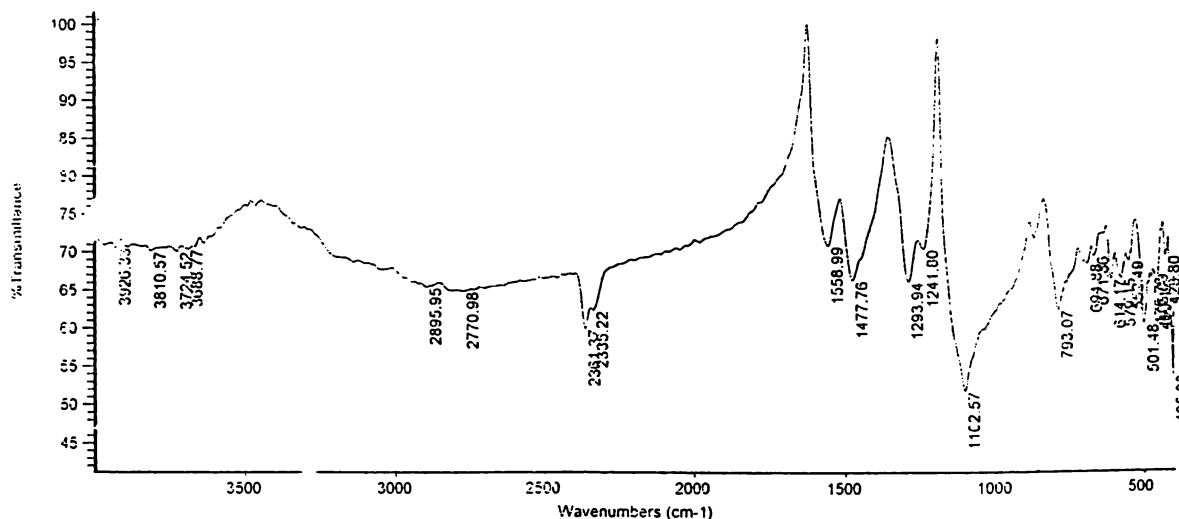


Figure 5 IR spectrum of oven dried PAN powder.

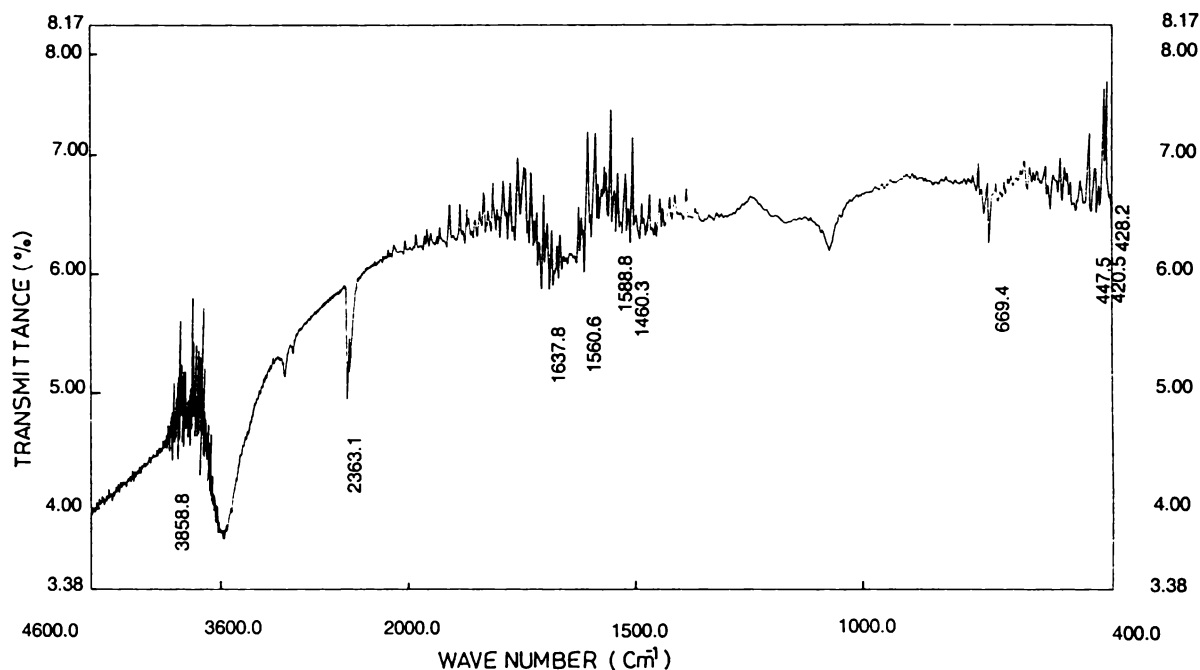


Figure 6 IR spectrum of room temperature dried PAN pellet.

shifted to 1293.94, 1241.8, 1102.57, and 862 cm^{-1} , respectively, in the oven dried sample. The low frequency shifts can be attributed to the deprotonation of the PAN salt.⁷

The same reason applies to the reduced conductivity of the pellet samples. The pellets are made by applying pressure, which may cause the loss of dopant molecules. Figure 6 shows the IR spectra of the room temperature dried pellet sample. In the IR spectra of the pellet sample the absorption peaks are shifted to 1315, 1160, 1075, and 1025 cm^{-1} , respectively, from that of the powder sample.

CONCLUSION

The microwave conductivity of PAN is found to be related to the dopant concentration. The conductivity is decreased when the amount of dopant molecules is decreased. The conductivity is found

to increase with the increase in frequency. The drying condition is found to affect the dopant concentration in PAN.

REFERENCES

1. Lee, N. Li; Ong, L. H. *J Appl Electrochem* 1992, 22, 512.
2. Trinidal, M. F.; Montemayer, C.; Falas, E. *J Electrochem Soc* 1991, 138, 3186.
3. La Croix, J. C.; Diaz, A. F. *J Electrochem Soc* 1988, 135, 1457.
4. Patil, S. F.; Bedaker, A. G.; Agastic, C. *Mater Lett* 1992, 14, 307.
5. Chan, H. S. O.; Hopok, H.; Khor, E.; Tan, M. M. *Synth Met* 1995, 31, 95.
6. Saravanan, V.; Palaniappan, S.; Seetharamu, S. *Macromol New Frontiers* 1995, 1, 344.
7. Anand, J.; Swapna Rao, P.; Palaniappan, S.; Sathyanarayana, D. N. *Macromol New Frontiers* 1998, 1, 374.

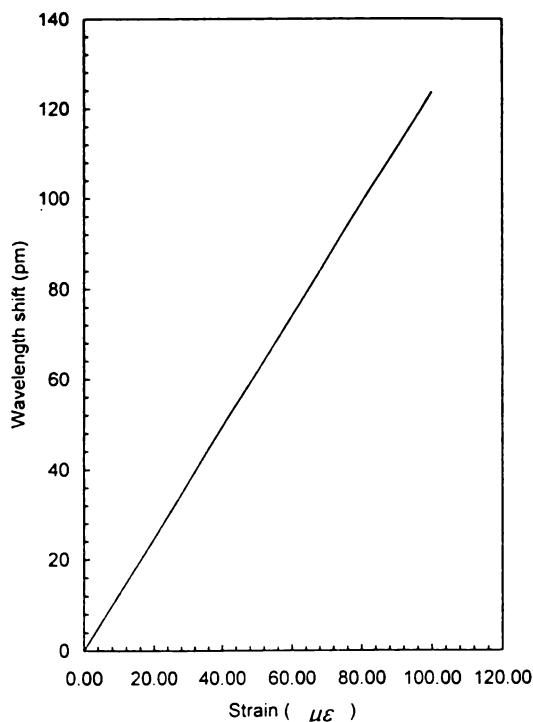


Figure 5 Transmission dip displacement as function of a static applied strain

REFERENCES

1. K.O. Hill, Y. Fujii, D.C. Johnson, and B.S. Kawasaki, Photosensitivity in optical waveguides: Application to reflection filter fabrication, *Appl Phys Lett* 32 (1978), 647-649.
2. R. Kashyap, *Fiber Bragg gratings*, Academic, San Diego, CA, 1999.
3. H.A. Haus and C.V. Shank, Anti-symmetric type of distributed feedback lasers, *IEEE J Quantum Electron* QE-12 (1976), 532-539.
4. H. Assch, H. Storoy, J.T. Kringlebotn, W. Margulis, B. Sahlgren, and S. Sandgren, 10 cm long Yb⁺ DFB fibre laser with permanent phase shifted grating, *Electron Lett* 31 (1995), 969-970.
5. R. Kashyap, P.E. McKee, and D. Armes, UV written reflection grating structures in photosensitive optical fibres using phase-shifted phase masks, *Electron Lett* 30 (1994), 1977-1978.
6. J. Canning and M.G. Sceats, π -phase shifted periodic distributed structures in optical fibers by UV post-processing, *Electron Lett* 30 (1994), 1244-1245.
7. L. Wei and W.Y. Lit, Phase-shifted Bragg grating filters with symmetrical structures, *J Lightwave Technol* 15 (1997), 1405-1410.
8. H.T. Hattori, V.M. Schneider, and O. Lisboa, Cantor set fiber Bragg grating, *J Optical Soc Amer A* 17 (2000), 1548-1589.
9. M. Yamada and K. Sakuda, Analysis of almost-periodic distributed feedback slab waveguides via a fundamental matrix approach, *Appl Opt* 26 (1987), 3474-3478.
10. P. Yeh, *Optical waves in layered media*, Wiley, New York, 1988.

© 2001 John Wiley & Sons, Inc.

STRIP-LOADED HOLLOW DIELECTRIC H-PLANE SECTORAL HORN ANTENNAS FOR SQUARE RADIATION PATTERN

V. P. Joseph,¹ S. Biju Kumar,¹ and K. T. Mathew¹

¹ Department of Electronics
Cochin University of Science and Technology
Cochin 682 022, Kerala, India

Received 29 September 2000

ABSTRACT: The radiation characteristics of a new type of hollow dielectric H-plane sectoral horn antenna are presented. Metallic strips of optimum length are loaded on the H-walls of the sectoral horns. The effects of strip loading for producing square patterns in the H plane are discussed. © 2001 John Wiley & Sons, Inc. *Microwave Opt Technol Lett* 29: 45-46, 2001.

Key words: antennas; dielectric horn antennas; square radiation patterns

1. INTRODUCTION

Dielectric antennas are of great importance because of their low loss, high gain, light weight, the feasibility of obtaining shaped beams, ease of fabrication, etc. [1]. Solid and hollow dielectric horn antennas have received special attention due to their increased directivity and high gain compared to metallic horns [2-4]. Only a few attempts were noted in the literature on the study of rectangular hollow dielectric horn antennas. In this letter, we present a new hollow dielectric horn antenna capable of producing a flat-top radiation pattern with low sidelobe levels and cross polarization in the H-plane.

2. ANTENNA DESIGN AND EXPERIMENTAL SETUP

A schematic diagram of the strip-loaded hollow dielectric H-plane horn antenna is shown in Figure 1. The horn is fabricated using low-loss dielectric (polystyrene of dielectric constant $\epsilon_r = 2.56$), and is fixed at the end of an open metallic waveguide. A properly tapered dielectric rod (launcher) is placed at the throat of the antenna for reducing the feed end discontinuity. The tapering length inside the waveguide is optimized for minimum VSWR. Two thin metal strips of length l are placed on the H-walls of the horn. This modifies the aperture field of the horn, changing the radiation pattern considerably. The sidelobe levels and half-power beamwidth (HPBW) of the E- and H-plane patterns can be adjusted by changing the strip length. An HP 8341B synthesized sweeper, HP 8510B network analyzer, and a plotter with the antenna under test in the receiving mode constitute the experimental setup.

3. EXPERIMENTAL RESULTS

E- and H-plane radiation patterns of H-plane sectoral horns of different flare angles and strip lengths were analyzed for different frequencies in the X-band. The H-plane patterns are found to be very broad, and the E-plane patterns are narrow. By adjusting the strip length and frequency, it is possible to produce flat-top (square) patterns with high HPBW in the H-plane. The sidelobe levels of these patterns are very low. Figure 2 shows a typical radiation pattern for a horn of flare angle 20° with a strip of length of 2λ at 10.4 GHz. The variation of HPBW with frequency and strip length is shown in Figure 3. The VSWR of the horn is very low for the entire

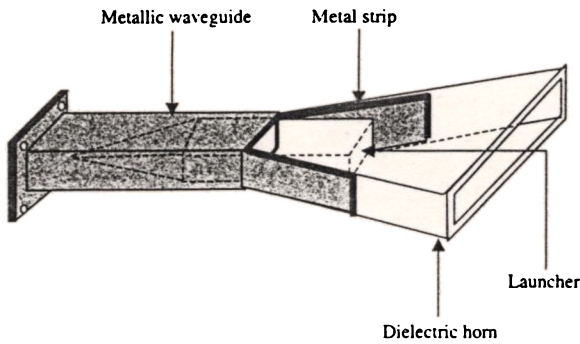


Figure 1 Schematic diagram of strip-loaded hollow dielectric *H*-plane sectoral horn antenna

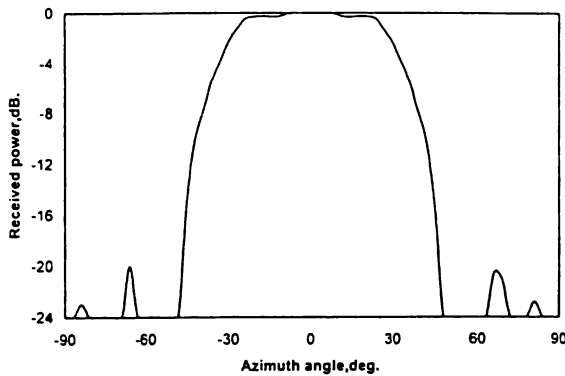


Figure 2 Square radiation pattern in the *H*-plane of the horn

TABLE 1 Radiation Characteristics of the Test Horn

Flare Angle (deg.)	Strip Length (λ)	Frequency (GHz)	HPBW (deg.)		Sidelobe Level (dB)		VSWR
			<i>H</i>	<i>E</i>	<i>H</i>	<i>E</i>	
10	1	8.5	41	31	-24	-16	1.06
	3	10.5	68	18	-20	-8.5	1.18
20	2	8.5	43	26	-30	-12	1.08
	3	10.4	51	22	-28	-10	1.1
30	1	8.5	65	23	-35	-11.5	1.17
	3	9.5	50	21	-32	-8	1.25
45	1	8.5	70	25	-28	-16	1.09
	2	9.5	58	27	-17	-20	1.1

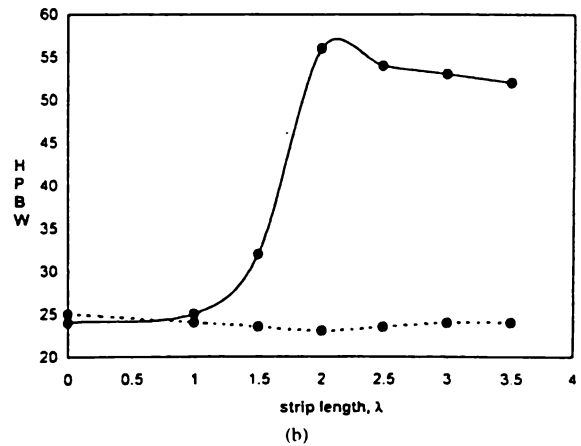
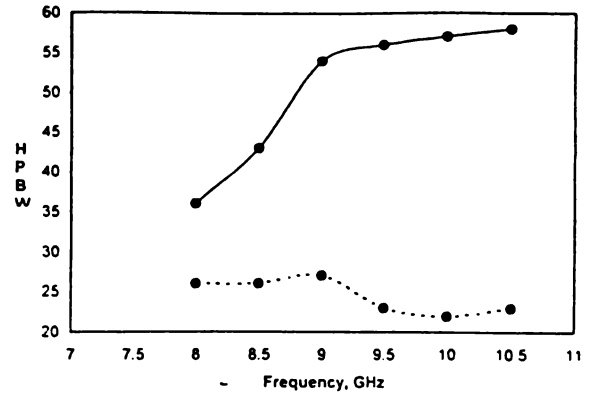


Figure 3 (a) HPBW against frequency for strip length $l = 2\lambda$. —●— *H*-plane 20°, - -●- *E*-plane 20°. (b) HPBW against strip length at frequency 9.5 GHz. —●— *H*-plane 20°, - -●- *E*-plane 20°

X-band. The radiation characteristics of the test horn are tabulated in Table 1.

4. CONCLUSIONS

The performance of a strip-loaded hollow dielectric *H*-plane sectoral horn antenna is presented. The study shows that the new horn is capable of producing a broad square pattern in the *H*-plane and a narrow pattern in the *E*-plane. It has high gain and low VSWR, sidelobe levels, and cross-polar levels. It may be an ideal feed for reflector antennas.

REFERENCES

1. R. Chatterji, Dielectric and dielectric loaded antennas. Research Studies Press Ltd., U.K. and Wiley, New York. 1985.
2. N. Brooking, P.J.B. Clarricoats, and A.D. Oliver. Radiation pattern of pyramidal dielectric waveguide, *Electron Lett* 10 (1974), 33-34.
3. J.R. James, Engineering approach to the design of tapered dielectric rod and horn antennas, *Radio Electron Eng* 42 (1972), 251-259.
4. V.P. Joseph, S. Mathew, J. Jacob, U. Ravindranath, and K.T. Mathew, Radiation characteristics of strip loaded hollow dielectric *E*-plane sectoral horn antennas, *Electron Lett* 33 (1997), 2002-2004.

© 2001 John Wiley & Sons, Inc.

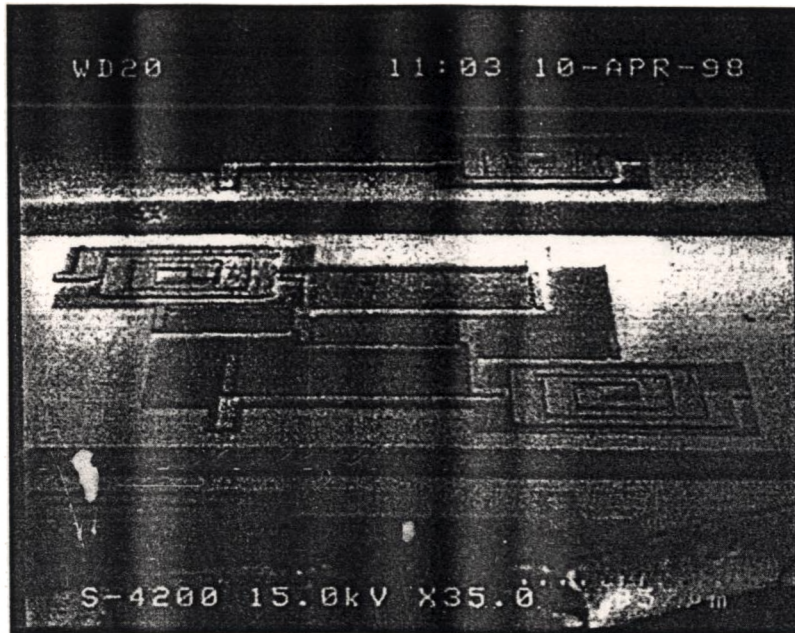


Figure 6 SEM photograph of a 2.4 GHz bandpass filter (2 mm × 2 mm)

V. CONCLUSIONS

High Q -value inductors were fabricated on high-resistivity Al_2O_3 substrates for MIC application. The measured results of these passive components were predicted well according to EM simulation, and equivalent circuit models were also extracted. A 2.4 GHz MIC bandpass filter was realized by these components to verify the inductor performance and the model accuracy.

REFERENCES

1. L. Zu, Y. Lu et al., High Q -factor inductors integrated on MCM Si substrates, *IEEE Trans Comp, Packag, Manufact Technol* 19 (1996), 635–643.
2. SONNET user's manual—EM user's manual, 1995, pp. 1–3.
3. S. Chaki et al., Experimental study on spiral inductors, *IEEE MTT-S Tech Dig*, 1995, pp. 753–756.
4. Y.C. Shih et al., A broadband parameters extraction technique for the equivalent circuit of planar inductors, *IEEE MTT-S Tech Dig*, 1992, pp. 1345–1348.
5. G.L. Matthaei, L. Young, and E.M.T. Jones, *Microwave filters, impedance-matching networks and coupling structures*, McGraw-Hill, New York, 1980, pp. 481–485.

© 1999 John Wiley & Sons, Inc.
CCC 0895-2477/99

A NEW CORNER REFLECTOR ANTENNA WITH PERIODIC STRIP SUBREFLECTORS

Sebastian Mathew,¹ Joe Jacob,¹ V. P. Joseph,² S. Bijukumar,² U. Raveendranath,² and K. T. Mathew²

¹ School of Pure and Applied Physics
Mahatma Gandhi University
Kottayam, Kerala, India

² Department of Electronics
Cochin University of Science and Technology
Cochin, Kerala, India

Received 7 August 1998

ABSTRACT: This paper presents the design of a new type of corner reflector (CR) antenna and the experimental investigation of its radiation characteristics. The design involves the addition of planar parallel periodic strips to the two sides of a CR antenna. The position, angular orientation, and number of strips have a notable effect on the H -plane radiation characteristics of the antenna. Certain configurations of the new antenna are capable of producing very sharp axial beams with gain on the order of 5 dB over the square corner reflector antenna. A configuration that can provide symmetric twin beams with enhanced gain and reduced half-power beam width (HPBW) is also presented. © 1999 John Wiley & Sons, Inc. *Microwave Opt Technol Lett* 20: 326–328, 1999.

Key words: antennas; reflector antennas; gain

INTRODUCTION

In the class of reflector antennas, CR antenna is a favorite choice where a moderate gain is required, due to the simplicity of its design. Since its introduction by Kraus [1], several researchers have performed much work on modifying the radiation characteristics of CR antennas, both experimentally and theoretically [2–6]. A recent paper by Mathew et al. [7]

reported the modification of CR antenna characteristics by adding two supplementary reflectors.

This letter presents the design of a CR antenna with periodic parallel planar metallic strips attached to the two reflecting sides and the resulting improvement in the radiation characteristics. It is seen that the gain of the antenna increases and the HPBW decreases. The performance of the antenna for different dimensions of the strip structures is analyzed. There are configurations that can provide axial gains on the order of 5 dB over the square corner reflector antenna. Also, cases providing sharp symmetrical twin beams with gain enhancement are noted. In this type of antenna, the primary corner angles above 90° are very effective, whereas acute angles require large antenna dimensions.

ANTENNA DESIGN AND EXPERIMENTAL SETUP

The schematic diagram of the new CR antenna is given in Figure 1. It is constructed by attaching two metallic strip structures S_1 and S_2 to the two sides of a CR at a distance l from the apex. The structure consists of n metallic strips of width w and length h kept at a periodicity of d . α and β are the primary and secondary corner angles, respectively. The distance l , angle β , and the number of strips n can be varied. An HP 8350B sweep oscillator, together with an HP 8410B network analyzer, were used for studying the radiation characteristics. The antenna under test (AUT) was used as the receiver, and a standard pyramidal horn was used as the transmitter. The VSWR was measured using an HP 8510B

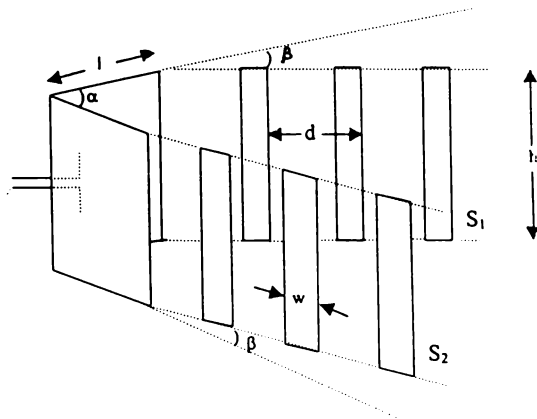


Figure 1 Schematic diagram of the new CR antenna

network analyzer. The experiment was conducted in the X-band (at 8.5 GHz).

EXPERIMENTAL DETAILS AND RESULTS

After arranging a particular configuration, the radiation patterns were plotted for different values of β . The value of β for which the axial power is maximum is taken as β_{opt} . This is repeated for different values of n , and the effect is studied. The experiment is repeated for various fixed values of l , and corresponding patterns are plotted. h is optimized as 1.5λ through experimental iterations. w was varied, and it was seen that a width of 0.3λ is sufficient to provide the maximum gain observed. The effect of variation in d was studied, and it was optimized as 1λ .

Now, α is changed to other fixed values, and the whole experiment is repeated. It is seen that β_{opt} also depends on α , and increases with it. This is shown in Figure 2.

The results obtained from the experimental study are tabulated in Table 1. The gain of the antenna is seen to be increasing with the number of strips. In all cases, it is seen that when the axial gain increases, the HPBW decreases. A typical normalized radiation pattern of a configuration ($\alpha = 120^\circ$, $\beta = 45^\circ$, $n = 5$, and $l = 1\lambda$) is given in Figure 3 in comparison with that of a square corner reflector of equivalent dimensions. Contrary to ordinary CR antennas, this type of antenna with obtuse primary angles produces sharp fan

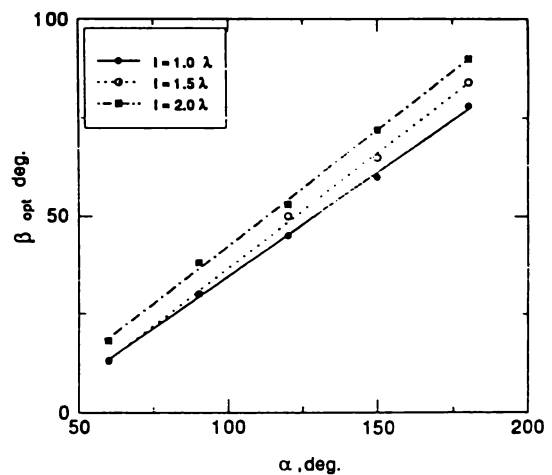


Figure 2 β_{opt} versus α for different values of l when $n = 5$

TABLE 1 Radiation Characteristics of Selected Configurations of the New Antenna

α	Antenna Parameters	$l = 1\lambda$				$l = 2\lambda$			
		$n = 2$	$n = 3$	$n = 4$	$n = 5$	$n = 2$	$n = 3$	$n = 4$	$n = 5$
90°	β_{opt}	30°	30°	30°	30°	38°	38°	38°	38°
	Relative gain	1.6	2.2	3.4	4.0	2.4	3.6	4.2	4.6
	HPBW	18°	16°	11°	11°	13°	12°	10°	10°
	VSWR	1.52	1.58	1.49	1.29	1.92	1.83	1.85	1.85
120°	β_{opt}	45°	45°	45°	45°	60°	60°	55°	53°
	Relative gain	3.6	4.8	5.4	5.6	2.2	3.8	4.4	4.8
	HPBW	16°	14°	13°	11°	22°	10°	9°	9°
	VSWR	1.99	1.81	1.79	1.54	2.08	2.07	2.03	1.99

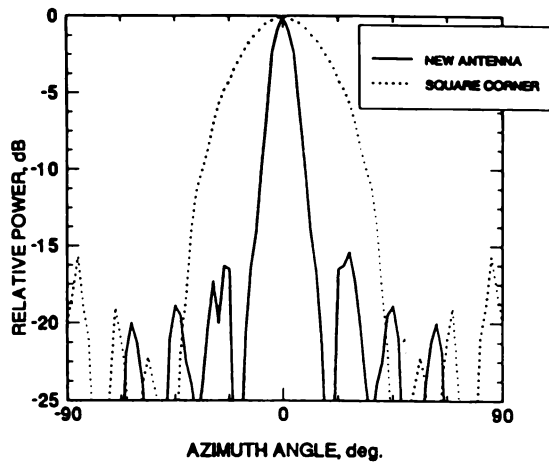


Figure 3 Normalized H -plane radiation pattern of a typical configuration ($\alpha = 120^\circ$, $\beta = 45^\circ$, $n = 5$, and $l = \lambda$) at 8.5 GHz along with that of a square corner reflector

beams with large axial gains. When α , l , and β are fixed at certain particular values, the main beam splits into two with a very deep null along the axis. A typical radiation pattern is shown in Figure 4.

No appreciable deterioration in the VSWR could be observed due to the strip attachment of the corner reflector antenna when l is small. But for large l , the VSWR goes high. The VSWR chart for a typical configuration ($\alpha = 90^\circ$, $\beta = 30^\circ$, $n = 5$, and $l = 1\lambda$) is given in Figure 5. It is seen that the cross-polar level is below -18 dB. The sidelobe level is seen to be below -13 dB in most cases.

CONCLUSION

The design and experimental analysis of a new type of corner reflector antenna has been carried out. The configurations of the antenna offering enhanced performance were studied,

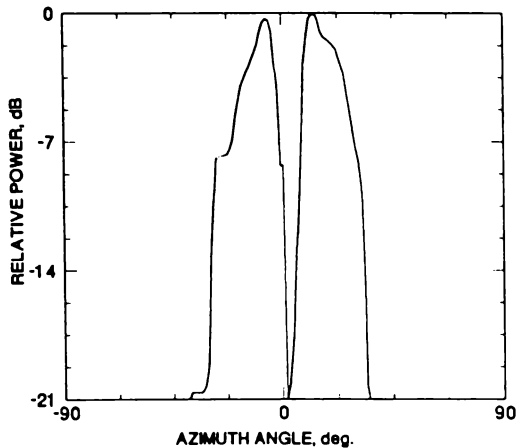


Figure 4 Radiation pattern of a configuration providing symmetric twin beams ($\alpha = 180^\circ$, $\beta = 60^\circ$, $n = 3$, and $l = \lambda$) at 8.5 GHz

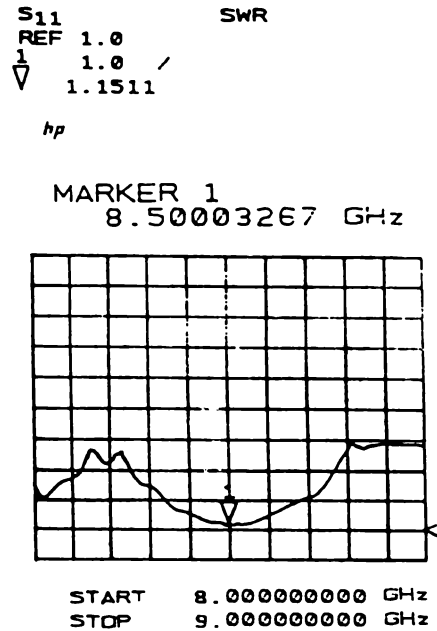


Figure 5 Variation of VSWR with frequency for the configuration with $\alpha = 90^\circ$, $\beta = 30^\circ$, $n = 5$, and $l = \lambda$

and the characteristics were compared with those of a square corner reflector antenna. An axial gain enhancement on the order of 5 dB, and hence a reduction in the HPBW, are observed. It is also possible to get two very sharp beams symmetrically on either side of the axis with a sharp null at the center.

REFERENCES

1. J.D. Kraus, The corner reflector antenna. Proc IRE 28 (1940), 513-519.
2. J.R. Wait, On the theory of an antenna with an infinite corner reflector. Can J Phys 32 (1954), 365-371.
3. A.C. Wilson and H.V. Cottony, Radiation patterns of finite size corner reflector antennas, IRE Trans Antennas Propagat AP-8 (1960), 144-157.
4. D. Proctor, Graphs simplify corner reflector antenna design. Microwaves 14 (1975), 48-52.
5. K. Vasudevan and K.G. Nair, A corrugated corner reflector system, IEEE Trans Antennas Propagat 30 (1982), 524-526.
6. V.P. Joseph and K.T. Mathew, Dual corner reflector antenna for better performance. Indian J Radio Space Phys 21 (1992), 192-194.
7. K.T. Mathew, J. Jacob, S. Mathew, and U. Raveendranath, Triple corner reflector antenna and its performance in the H -plane. Electron Lett 32 (1996), 1432.

© 1999 John Wiley & Sons, Inc.
CCC 0895-2477/99

Improved Loaded Quality Factor of Cavity Resonators with Cross Iris Coupling

U RAVEENDRANATH, S BIJU KUMAR AND K T MATHEW, FIETE

Department of Electronics, Cochin University of Science and Technology, Cochin 682 022, India.

The performance of circular, rectangular and cross irises for the coupling of microwave power to rectangular waveguide cavity resonators is discussed. For the measurement of complex permittivity of materials using cavity perturbation techniques, rectangular cavities with high Q -factors are required. Compared to the conventional rectangular and circular irises, the cross iris coupling structure provides very high loaded quality factor for all the resonant frequencies. The proposed cross iris coupling structure enhances the accuracy of complex permittivity measurements.

ELECTROMAGNETIC scattering through apertures is of great importance in microwave technology. Large number of theoretical and experimental investigations have been done in this field^[1-5]. Modification of coupling mechanism of microwave power to the cavities is essential for improving the loaded quality factor of cavity resonators. Different coupling techniques such as probe (electric coupling), loop (magnetic coupling) and open guide (electric coupling) are used to couple power to the cavities. The simplest among them is the open guide coupling. In this category, generally circular/rectangular irises are employed. When a resonant cavity is coupled to an external load, its characteristics are considerably modified by the coupling element. For the investigation of the dielectric and magnetic properties of materials, microwave cavity resonator techniques are widely used^[6,7]. Resonators of high Q -factor are used for the measurements. Hence the coupling mechanism of a cavity resonator has important role in improving the loaded Q -value. In the present investigation different types of iris coupling structures are analysed. A new coupling mechanism - cross iris coupling - for enhancing the loaded quality factor of the cavity resonator is proposed.

THEORETICAL ASPECTS

A cavity is considered to be a closed volume. The coupling system radiates power and this lowers the loaded Q -value of the resonator. The losses that usually occur in a cavity resonator are (1) dielectric loss (2) wall loss and (3) coupling loss. Let P_{Ld} , P_{Lw} and P_{Lc} are the time average power losses of a resonator, the total quality factor of the resonator is given by

$$Q_t = \omega_r \frac{W_s}{P_{Ld} + P_{Lw} + P_{Lc}} \quad (1)$$

or

$$\frac{1}{Q_t} = \frac{1}{Q_d} + \frac{1}{Q_w} + \frac{1}{Q_c} \quad (2)$$

Where ω_r is the resonant frequency and W_s is the energy stored in the cavity. The unloaded Q -value is given by

$$\frac{1}{Q_0} = \frac{1}{Q_d} + \frac{1}{Q_w} \quad (3)$$

For a cavity with given medium, Q_0 is constant. So the total loaded quality factor Q_t depends on the value of Q_c . The total loaded quality factor Q_t and unloaded quality factor Q_0 are related by the coupling parameter^[8]

$$K = \left[\frac{Q_t - Q_0}{Q_t + Q_0} \right]^2 \quad (4)$$

The lower the value of K , the higher is the loaded Q -factor

From (2) and (3)

$$\frac{1}{Q_c} = \frac{1}{Q_t} - \frac{1}{Q_0} \quad (5)$$

Also the coupling coefficient^[9]

$$k = \frac{Q_0}{1 + Q_t} \quad (6)$$

From (4) and (6) we get

$$K = \left[\frac{k}{2 + k} \right]^2 \quad (7)$$

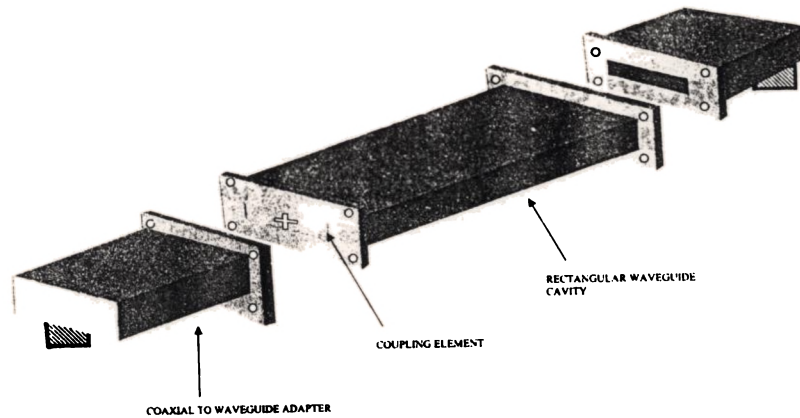


Fig 1 Rectangular waveguide resonator with iris coupling structure

In order to get higher loaded quality factor, coupling parameter K and hence coupling coefficient k should be low. The motivation of the present work is to design a coupling iris which will give higher loaded quality factor for all the resonant frequencies of a resonator.

EXPERIMENTAL DETAILS AND RESULTS

X-band transmission type rectangular waveguide cavity of length 13.5 cm is employed for the study. The iris is made on conducting metallic sheets. Since thick irises adversely affect input impedance and Q -value power should be coupled into or out of the cavity through irises in thin conducting sheets. In the present case sheets of thickness 0.1 mm are used for the fabrication of iris coupling elements. The iris coupling structure is held between the coaxial to waveguide adapter and the cavity (Fig 1). The cavity is connected to the two ports of the S -parameter Test Set and is excited in the TE_{10n} mode. Fig 2 shows the experimental set-up.

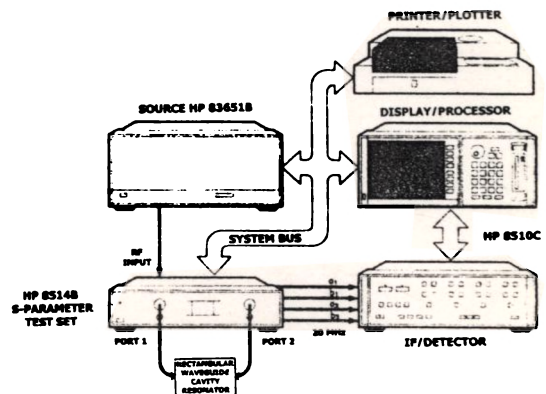


Fig 2 Experimental set-up

Different types of irises designed for the study are shown in Fig 3. Loaded Q -factor of the cavity with each coupling structure is determined from the amplitude response of the cavity ($Q_l = f_r / \Delta f$, where f_r is the resonance frequency and Δf is the 3dB bandwidth). Table 1 shows the loaded quality factor of the cavity with different iris structures. Rectangular irises of width 1 mm and lengths 5 mm, 6mm, 7mm, 8mm, and 9mm are selected for the study. The loaded quality factor of the cavity for each rectangular iris is measured. It is observed that, for each resonant frequency, the Q -factor varies with the length of the rectangular iris. Thus rectangular iris of 7 mm length gives comparatively high Q -factors.

Most commonly used type of iris structure is circular. Circular irises of diameters 5mm, 6mm, 7mm, 8mm and 9mm are taken for the measurement. From the Table 1, it can be seen that circular iris of 6 mm diameter gives high loaded quality factor at the resonance

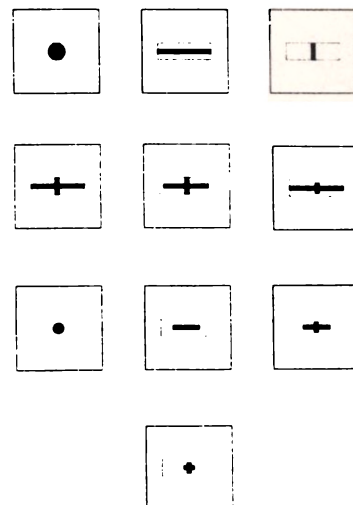


Fig 3 Different types of irises

TABLE 1 Loaded quality factor of cavity resonator for different types of irises

Frequency (GHz)	Diameter of Circular Iris						Length of Rectangular iris (width 1 mm)						Length of Cross iris (width 1 mm)					
	5mm	6mm	7mm	8 mm	9 mm	10 mm	5mm	6mm	7mm	8mm	9mm	10mm	5mm	6mm	7mm	8mm	9mm	10mm
8.5	1930	2525	720	550	425	392	452	212	1185	1015	1004	932	1912	2795	424	452	485	542
9.3	1150	1640	198	210	225	317	314	442	227	362	572	796	1805	2724	510	324	238	195
10.1	1142	925	475	368	374	288	610	598	817	646	485	302	1120	2010	185	177	162	150
10.9	810	472	342	295	285	310	525	488	785	578	394	206	1085	1740	845	589	378	246
11.8	515	1085	520	475	365	308	135	1115	792	515	265	102	1192	1362	592	410	265	192

TABLE 2 Coupling parameters and coupling coefficients of different types of irises

Frequency (GHz)	Coupling coefficient k			Coupling parameter K		
	Cross	Circular	Rectangular	Cross	Circular	Rectangular
8.5	1.6	2.1	22.3	0.05	0.13	0.84
9.3	1.8	3.1	11.1	0.08	0.25	0.69
10.1	2.6	5.7	9.4	0.19	0.49	0.65
10.9	3.1	13.2	12.1	0.25	0.74	0.72
11.8	4.5	6.1	5.5	0.41	0.52	0.48

TABLE 3 Impedance of various types of irises

Frequency (GHz)	Cross iris						Circular iris						Rectangular iris					
	5 mm		6 mm		7 mm		5mm		6 mm		7 mm		5 mm		6 mm		7 mm	
	R(Ω)	X(Ω)	R(Ω)	X(Ω)	R(Ω)	X(Ω)	R(Ω)	X(Ω)	R(Ω)	X(Ω)	R(Ω)	X(Ω)	R(Ω)	X(Ω)	R(Ω)	X(Ω)	R(Ω)	X(Ω)
8.5	53.16	0.487	53.93	0.488	55.13	0.712	55.47	0.719	56.78	0.642	58.19	0.814	51.96	0.361	52.79	0.412	55.31	0.704
9.3	50.76	3.668	51.03	4.467	51.21	5.963	51.30	6.197	51.55	7.542	52.06	9.261	50.49	2.304	50.71	3.295	51.46	6.089
10.1	46.90	3.354	46.14	4.255	45.06	5.391	44.98	5.492	44.14	6.692	42.93	8.267	48.04	2.141	47.15	3.006	44.61	5.687
10.9	44.90	0.176	43.64	0.293	41.90	0.618	42.01	0.557	40.37	0.914	38.52	1.469	46.80	0.031	45.36	0.072	41.36	0.478
11.8	45.21	-3.22	43.85	-3.66	41.95	-4.74	42.31	-4.56	40.45	-5.09	38.43	-5.68	47.10	-2.14	45.64	-3.01	41.20	-4.98

frequencies 8.5 GHz, 9.3 GHz and 11.8 GHz. For 10.1 GHz and 10.9 GHz, circular iris with 5 mm diameter gives better performance.

Symmetric and asymmetric cross iris coupling elements are designed for the study. It is found that

asymmetric structures show very low *Q*-factors and they are not taken into consideration. Symmetric cross iris of width 1 mm and lengths 5 mm, 6mm, 7mm, 8mm and 9mm are designed used as coupling elements. Cross iris with 6 mm length provides highest loaded quality factor.

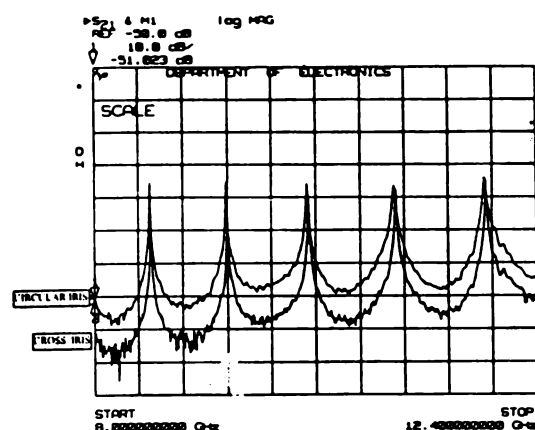


Fig 4 Amplitude response of the cavity for circular (diameter 6 mm) and cross (length 6 mm) irises

The coupling coefficient, k and coupling parameter, K of different types of irises are shown in Table 2. K and k values are lowest for symmetric cross irises, which result high loaded quality factor.

Table 3 shows the impedance variation of different irises for different resonant frequencies. It shows that the irises with different dimensions have comparatively good impedance matching with the 50Ω source. The Q -factors are highest for cross iris compared to other irises. Figure 4 shows the amplitude response of the rectangular cavity resonator for circular iris (diameter 6 mm) and symmetric cross iris (length 6 mm). The improved loaded Q -factor may be due to the fact that the spurious modes generated at the aperture are suppressed by the peculiar structure of the cross iris. Change in the waveguide height causes field distortion and a set of non-propagating TM_{1n} modes is generated along with the dominant TE_{10} mode^[10]. Similarly, the change in the waveguide width produces field distortion causing a set of non-propagating TE_{m0} modes with dominant TM mode. The cross iris may be considered as the combination of vertical and horizontal slits obtained by reducing the width and height of the waveguide. So it is reasonable to believe that the cross iris suppresses the spurious modes without perturbing the dominant mode (TE_{10}). This argument is in line with the mode suppression technique developed by Sequeria^[11].

CONCLUSION

An extensive experimental study shows that cross iris coupling improves the loaded Q -factors of a cavity resonator considerably. In the case of rectangular and circular irises, highest loaded quality factor for different frequencies are obtained with different iris dimensions. But the symmetric cross iris of particular dimension provides the highest loaded Q -factor for all resonant frequencies of the given resonator. Thus the cross iris is found to be an excellent coupling element over the conventional types of irises.

REFERENCES

1. H A Bethe, Theory of diffraction by small holes, *Phys Rev*, vol 66, pp 163-182, 1944.
2. S B Cohn, The electric polarizability of apertures of arbitrary shape, *Prof IRE*, vol 40, pp 1069-1071, 1952.
3. S B Cohn, Microwave coupling by large apertures, *Proc IRE*, vol 40, pp 696-699, June 1952.
4. H A Wheeler, Coupling holes between resonant cavities or waveguides evaluated in terms of volume ratios, *IEEE Trans Microwave Theory Tech*, vol 12, pp 231-234, March 1964.
5. U Raveendranath, K T Mathew & K G Nair, Cross iris coupling for improving the loaded quality factor of cavity resonators, *IEEE AP-S symposium Digest*, vol 2, pp 1082-1085, June 1994.
6. Anand Parkash, J K Vaid & Abhai Mansigh, Measurement of dielectric parameters at microwave frequencies by cavity perturbation method, *IEEE Trans Microwave Theory Tech*, vol 27, pp 791-794, 1979.
7. K T Mathew & U Raveendranath, Waveguide cavity perturbation method for measuring complex permittivity of water, *Microwave and Optical Technology Letters*, vol 6, pp 10-106, October 1993.
8. W Ho & W F Hall, Measurement of the dielectric properties of sea water and NaCl solutions at 2.65 GHz, *J Geoph Research*, vol 78, pp 6301-6315, 1973.
9. Samuel Y Liao, *Microwave devices and circuits*, Prentice-Hall, p 106, 1987.
10. Peter A Rizzi, *Microwave engineering - passive circuits*, Prentice - Hall, New Jersey, 1988.
11. H B Sequeria, Extracting ϵ_r and μ_r of solids from one-port phaser network analyser measurements, *IEEE Trans Instrum Meas*, vol 39, pp 621-627, 1990.

Authors

Raveendranath U, received the MSc (Physics) and PhD (Microwave Electronics) degrees from the School of Pure and Applied Physics, Mahatma Gandhi University, Kerala in 1989 and 1997 respectively. He worked as a lecturer in Electronics in the Department of Electronics, Cochin University of Science and Technology, Cochin, Kerala from 1997 November to 1999 September. He is currently working as Scientist 'C' in the Aerospace Electronics and Systems Division, National Aerospace Laboratory (NAL), Bangalore. His fields of interests include microwave techniques for material characterisation, microwave antennas and computational electromagnetics.



Permittivity in the Frequency Domain' sponsored by the IRCTR, Delft University, The Netherlands as a part of GPR Program.

K T Mathew, received BSc and MSc degrees in 1968 and 1970 from Kerala University. He took PhD in Microwave Electronics from Cochin University of Science and Technology (CUSAT) in 1978. He has published 45 research papers in International national journals and conferences and is guiding students for PhD. He worked as a visiting scientist in the Technical University (TU Delft), The Netherlands in 1998. He is the Chief Investigator of an International Collaboration Project between CUSAT and TU Delft.



He is the co-author of a book "Sensors Update, Vol 7" published by the Wiley-VCH publishers. His research interests are Microwave Antennas, Microwave Material Characterisation, Microwave Imaging in medical applications etc. At present he is a Professor in the Department of Electronics, CUSAT. He is a life fellow of IETE and member of expert committee of DOEACC Society, Government of India.

S Biju Kumar, got his MSc (Physics with Electronics Specialisation) Degree from Kerala University in 1997. In the same year he joined in the Department of Electronics, Cochin University of Science and Technology for PhD and the work is still continuing. The fields of interests are Microwave Antennas, Material Characterisation using Cavity Perturbation Technique, Free Space Complex Permittivity Measurements. He is the student member of IEEE. He is a researcher of the project entitled 'Measurement of Complex



Index

- Absorbing Boundary conditions, 104
- Bile, 111, 120, 126, 145, 156, 161
- Carcinoma Head Pancreas, 121
- Chicken Bile, 138, 161
- Chirp-Z Fourier Transform, 66
- Cholecholithiasis, 120, 126
- Cholelithiasis, 120
- Cholestatic Jaundice, 120
- Courant-Friedrichs-Lewy condition, 74
- ERCP, 111, 120
- FDTD, 68, 69, 70, 72, 73, 96, 102, 103, 105
- Finite Difference Time Domain, 14, 72
- Gall bladder, 120
- Gastric juice, 128
- Gaussian pulse, 71, 73, 74
- Ground Penetrating Radar, 65, 104, 105
- Half Power Beam Width, 27, 87
- Industrial Application, 3, 160
- LINE, 18, 27, 28, 33, 39, 61, 62, 161
- Loss tangent, 118, 124, 125, 127, 130, 132, 134, 136, 138, 140
- MATHEMATICA, 40, 54, 159
- Medical Application, 103, 146, 148
- Microwave Imaging, 103, 146, 147
- Non-Interactive Distributive, 36, 57
- Open Resonators, 16
- REFLECT, 27, 33, 61, 62
- Resonant cavities, 10, 160
- Root detection, 91, 161
- Saliva, 130, 161
- S-parameter, 20, 27, 36, 63, 87, 114
- Specific Absorption Rate, 108
- Sweat, 136, 161
- THRU, 18, 33, 55, 61, 62
- THRU-REFLECT-LINE, 33
- Transverse magnetic, 72
- TRL calibration, 33, 39, 57, 61, 161
- Vector Network Analyser, 27, 66
- Videoendoscope, 111
- Void detection, 67
- WR-159, 113
- WR-284, 113
- Yee cell, 74

LIST OF PUBLICATIONS OF THE CANDIDATE

INTERNATIONAL JOURNALS

1. Raveendranath.U, **Biju Kumar.S**, and K.T.Mathew, "Broad Band Coaxial Resonator For Complex Permittivity Measurements Of Liquids", **IEEE Trans. on Instrumentation and Measurement**, Vol. 49, No. 6, December 2000, pp. 1305-1312.
2. **Biju Kumar. S**, U. Raveendranath, P.Mohanan, K.T. Mathew, M.Hajian and L.P. Lighthart, "A Simple Free Space Method for measuring the Complex Permittivity of Single and Compound Dielectric Materials", **Microwave and Optical Technology Letters (USA)**, vol.26, No.2, **July 2000**, pp. 117-119.
3. Sebastian Mathew, Joe Jacob, V.P.Joseph, **Biju Kumar.S**, Raveendranath.U and K.T.Mathew, " A New Corner Reflector Antenna With Periodic Strip Sub Reflectors", **Microwave and Optical Technology Letters (USA)**, vol.20, No.5, **March 1999**, pp. 326-328.
4. V.P. Joseph, **S. Biju Kumar** and K.T. Mathew, "Strip loaded hollow dielectric H-plane sectoral horn antennas for square radiation pattern", **Microwave and Optical Technology Letters (USA)** , vol.29, No.1, **April 2001**, pp. 45-46.
5. Honey John, **Biju Kumar.S**, Rani George and K.T.Mathew, "Effect of drying conditions on microwave conductivity of poly aniline", **Journal of Applied Polymer Science(USA)**, Vol. 83, No. 9, pp. 2008-2012, 2002.
6. **Biju Kumar.S**, K.T.Mathew, U.Raveendranath and Philip Augustine "Dielectric Behaviour of certain human fluids at Microwave Frequencies", **Microwave Power and Electromagnetic Energy**, Vol.36, No. 2, 2001, pp. 67-75
7. **Biju Kumar.S**, Honey John, Rani George, K.T.Mathew, M. Hajian and L. P. Lighthart, "Dielectric Properties of Poly Aniline in different forms at microwave frequencies", **Journal of European Ceramics Society**, Vol. 21/15, November 2001, pp. 2677-2680.
8. Raveendranath.U, **Biju Kumar.S**, and K.T.Mathew, " Improved Loaded Quality factor of Cavity Resonators with Cross Iris coupling", **Technical Review, Institution of Electronics and Telecommunication Engineers (IETE), India**, vol.16, No.5&6, **September-December 1999**, pp. 481-485.
9. **Biju Kumar. S**, C.K. Aanandan and K.T. Mathew, "Buried Object Detection using Time Domain Free Space Near Field Measuremnets", **Microwave and Optical Technology Letters (USA)** , Vol.31, No.1, October 2001, pp. 45-47.
10. K. T. Mathew, **S. Biju Kumar**, Anil Lonappan, Joe Jacob, Jacob Samuel, Thomas Kurian, "Dielectric properties of ionomers at microwave frequencies", Accepted for publication in **Material Letters**.

SEMINARS/SYMPOSIA PAPERS

1. **Biju Kumar.S**, U.Raveendranath, Philip Augustine and K.T.Mathew, "The Study Of The Dielectric Behaviour of Human Bile At Microwave Frequencies", Proceedings on **Third Workshop on Electromagnetic Wave Interaction With Water and Moist Substances**, April 11-13, Athens, Georgia, pp.235-238, 1999.
2. Raveendranath.U, **Biju Kumar.S**, Sebastian Mathew and K.T.Mathew, " Microwave Diagnosis Of Diabetes In Humanbeings Using Cavity Perturbation Technique", **Proceedings on International Conference on Microwave and Millimeter Technology (ICMMT-98)**, August 18-20, Beijing, pp.803-806, 1998.
3. **Biju Kumar.S**, U.Raveendranath, P. Mohanan and K.T.Mathew, "Hazards due to Microwaves-General Aspects", Proceedings of the **International Symposium on Safety (SAFE-99)** , Cochin, November 1999.
4. **Biju Kumar.S**, Honey John, Rani George, M. Hajian, L. P. Lighthart and K.T.Mathew, "Dielectric Properties of Poly Aniline in different forms at microwave frequencies", **Proceedings of International Conference on Microwave Materials and Applications 2000(MMA-2000)**, September 2000, Bled, Slovenia.
5. **Biju Kumar.S**, Joe Jacob and K.T.Mathew, "Free Space measurement techniques for leak detection of underground pipes and vegetable detection", Proceedings on **Fourth Conference on Electromagnetic Wave Interaction With Water and Moist Substances**, May 13-16, Weimar, Germany, pp. 390-394, 2001.
6. **Biju Kumar.S**, Philip Augustine and K.T.Mathew, "Dielectric properties of certain biological materials at microwave frequencies", Proceedings on **Fourth Conference on Electromagnetic Wave Interaction With Water and Moist Substances**, May 13-16, Weimar, Germany, pp. 73-78, 2001.
7. **Biju Kumar.S**, Joe Jacob, Anil Lonappan and K.T.Mathew, "Microwave Study on the Electrical Properties of Human Tissues at Different Pathological Conditions", Accepted for **Electromagnetic Methods in Pharmacy and Medicine Conference**, IOP Conference, UK
8. **Biju Kumar.S**, Jacob George, P.Mohanan and K.T.Mathew, "A Study On Rectangular Microstrip Antenna", Proceedings on National Symposium on Antennas and Propagation(APSVM-98), 15-16 December, Cochin, pp.258-261, 1998.
9. Sebastian Mathew, Joe Jacob, V.P.Joseph, **Biju Kumar.S**, U.Raveendranath and K.T.Mathew, "Periodic Strips Attached Corner Reflector Antenna For Enhanced Performance", Proceedings on National Symposium on Antennas and Propagation(APSVM-98), 15-16 December, Cochin, pp.166-169, 1998.

10. V.P.Joseph, Joe Jacob, Sebastian Mathew, **Biju Kumar.S**, U.Raveendranath and K.T.Mathew, "Strip Loaded H-Plane Hollow Dielectric Sectoral Horn Antennas", Proceedings on National Symposium on Antennas and Propagation(APSYM-98), 15-16 December, Cochin, pp.170-172, 1998.
11. **S. Biju Kumar**, C.K. Aanandan, P. Mohanan & K.T. Mathew, "Free Space Measurements for Material Characterisation and Buried Object Detection" Proceedings on National Symposium on Antennas and Propagation(APSYM-2000), 6-8 December, Cochin, pp.227-229, 2000.
12. **S. Biju Kumar**, Philip Augustine and K. T. Mathew, " Dielectric behaviour of certain biological materials and bile at microwave frequencies using cavity perturbation method", Presented in the National Symposium on Medical, Plant and Industrial Biotechnology, 1-2 December, 2000, Cochin.
13. **S. Biju Kumar**, V. K. Shine and K. T. Mathew, "Automated Cavity Resonator for Complex Permittivity Measurement at Microwave Frequencies", Presented in National Symposium on Instrumentation, Chandigarh, 29-31 January 2001.
14. **S. Biju Kumar**, Joe Jacob and K. T. Mathew, "Detection Of Roots And Leak In Underground Pipes Using Microwaves", Proc. of 14th Kerala Science Congress, Cochin, 29-31 January 2002, pp. 502-505.

COMMUNICATED PAPERS

1. Honey John, **Biju Kumar.S**, Rani George and K.T.Mathew, "Studies on polyaniline-polyvinyl chloride composites", Communicated to **Rubber, Plastics and Composites**.
2. K. T. Mathew, Anil Lonappan, **S. Biju Kumar**, Joe Jacob "Microwave studies of certain surgical gloves", Communicated to **International Journal of Natural Rubber Research**.
3. K.T. Mathew, **S. Biju Kumar**, Anil Lonappan, Joe Jacob, Jacob Samuel, Thommachan Xavier, Thomas Kurian "Microwave Studies of ZnS:HSR ionomers", Communicated to **Material Chemistry and Physics Journal**.
4. Thommachan Xavier, Jacob Samuel, Thomas Kurian, K.T. Mathew, **S. Biju Kumar**, Anil Lonappan, Joe Jacob, "Microwave Investigations of the Dielectric and conductivity behaviors in novel thermoplastic ionomers based on radiation induced styrene grafted natural rubber (SGNR) using Cavity Perturbation Technique", Communicated to **Macromolecules, USA**.
5. **Biju Kumar. S**, Joe Jacob and K. T. Mathew, "Free space measurement for complex permittivity measurement of liquids" (To be submitted to **IEEE Sensors**)

RESUME OF THE CANDIDATE: BIJU KUMAR S.

Permanent Address

Sreedharamandiram
Ayiroor, Perumkadavila.P.O.
Trivandrum – 695 124
Kerala, India

Phone : 91 471 275627
E.mail : bijukumar_98@yahoo.com

Present Address

Senior Research Fellow, Department of
Electronics, Cochin University of Science
and Technology, Kochi-682 022, Kerala,
India

Phone: 91 484 532161
Fax: 91 484 532800
E-mail: biju@doe.cusat.edu

Objective: *To involve in Research and Development activities in the field of Microwave Propagation, Material Characterisation, Microwave Devices, Buried Object Detection and biomedical applications of microwaves and Numerical modelling*

EDUCATION

- a) **Ph.D in Microwave Electronics**- Thesis submitted in March, 2002
- b) **Master of Science in Physics**- Kerala University, Kerala, India (July 1997).
- c) **Bachelor of Science in Physics**- Kerala University, Kerala, India (July 1995).



COMPUTER PROFICIENCY

Operating Systems DOS, WINDOWS 95/NT, LINUX
General Applications Axum, Sigma Plot, MS OFFICE.
Technical Applications MATHEMATICA, MATLAB, PUFF, IE3D, FIDELITY
Languages C, HP BASIC

AWARDS OBTAINED

- ❖ **Young Scientist Award** by Government of India. As the part of award, participated in the Nobel Laureates meeting in Lindau, Germany held during 25-29 June, 2001. Continuing the meeting, Indian team visited different German Universities and research centres, as per the invitation from DFG (Deutsche Forschungsgemeinschaft).
- ❖ Visited International Centre for Theoretical Physics (ICTP), Italy for three months in a **Young Collaborator Programme**.
- ❖ Council for Scientific and Industrial Research, Government of India, awarded direct **Senior Research Fellowship** in October 2000.